FACULTY OF SCIENCE AND TECHNOLOGY

MASTER THESIS

Study programme / specialisation:

Mechanical and Structural Engineering and Materials Science / Civil Engineering Structures

The spring semester, 2021

Open / ~~Confidential~~

Author: Martin Severin Gullaksen

Martin S. Gullaksen

(signature author)

Course coordinator:

Jasna Bogunovic Jakobsen

Supervisor(s):

Jasna Bogunovic Jakobsen

Thesis title: Wind and Vibrations Measurements on the Lysefjord Bridge

Credits (ECTS): 30

Keywords:

Wind

Vibrations

Frequencies

Accelerations

Acceleration spectra

Pages: 97

+ appendix: 37

Stavanger, 29.06.22

Approved by the Dean 30 Sep 21
Faculty of Science and Technology

Wind and Vibrations Measurements on the Lysefjord Bridge

Martin Severin Gullaksen

University of Stavanger

Department of Mechanical and Structural Engineering and Materials Science

March-June, 2022

Preface

This thesis marks the end of my two-year master's degree in Engineering Structures and Materials at the University of Stavanger. I spent the autumn semester on exchange in Portugal and did not return to Norway before March 2022. Consequently, the work with this thesis has been conducted from mid-March to June 2022.

The idea for this thesis comes from my supervisor, Jasna Bogunovic Jakobsen, whom I wish to thank for all help, guidance and MATLAB code that I could never have written on my own.

A special thanks to my good friends and fellow students at Ivar Langens Hus, who made these two years memorable in many ways.

Lastly, I would like to thank my family for their unconditional support during these two years.

Martin S. Gullaksen

Martin Severin Gullaksen

Abstract

The Lysefjord Bridge is a suspension bridge located in the western part of Norway. Since 2013 it has been used as a full-scale wind engineering laboratory and is fitted with sonic anemometers, tri-axial accelerometers, pressure probes and a GNSS based displacement sensor.

The objective of this thesis is to gain knowledge about the wind effects a suspension bridge is exposed to, and try to link some of these wind effects to the vertical accelerations of the bridge deck.

Large quantities of wind data is aquired from four different time-series originating during the fall of 2021. These data was processed, analysed and visualised mainly by the use of MATLAB, and compared to results of previous research on the bridge.

The results showed that the horizontal wind velocity and the vertical wind velocity from the four different time-series had little impact regarding the vertical accelerations of the bridge deck. The wind direction seemed to have a miniscule impact on the horizontal velocity, but looked to have a larger impact on both the vertical wind velocity and the vertical angle-of attack.

The general conclusion was that for lower wind velocities, traffic had larger impact on the vertical accelerations. The noticeable accelerations registered by the accelerometers was seen regardless of measured wind velocity from the surrounding anemometers at the same timestamps.

Sammendrag

Lysefjordbrua er en hengebru som ligger i den vestlige delen av Norge. Siden 2013 har den blitt brukt som et fullskala vindteknisk laboratorium og er utstyrt med soniske anemometere, tri-aksiale akselerometere, trykkmålere og en GNSS-basert forskyvningssensor.

Målet med denne avhandlingen er å få kunnskap om vindeffektene en hengebro utsettes for, og forsøke å knytte noen av disse vindeffektene til de vertikale akselerasjonene på brodekket.

Store mengder vinddata er hentet fra fire ulike tidsserier med opprinnelse fra høsten 2021. Disse dataene ble behandlet, analysert og visualisert hovedsakelig ved bruk av MATLAB og sammenlignet med resultater fra tidligere forskning på broen.

Resultatene viste at den horisontale vindhastigheten og den vertikale vindhastigheten fra de fire forskjellige tidsseriene hadde liten innvirkning på de vertikale akselerasjonene til brodekket. Vindretningen så ut til å ha en liten innvirkning på den horisontale hastigheten, men så ut til å ha større innvirkning på både den vertikale vindhastigheten og den vertikale angrepsvinkelen.

Den generelle konklusjonen var at for lavere vindhastigheter hadde trafikken større innvirkning på de vertikale akselerasjonene. De merkbare akselerasjonene ble registrert uavhengig av målt vindhastighet fra de omkringliggende anemometrene på de samme tidspunktene.

Contents

Table of Figures

List of Tables

1.0 Introduction

This chapter will introduce the reader to the main topics in this thesis, the problem description and the scope of the thesis.

1.1 Lysefjord Bridge

The Lysefjord Bridge is a suspension bridge located in the county of Rogaland, in the western part of Norway, just outside the city of Stavanger. The bridge has a main span of 446 meters. It is the main crossing of the long and narrow fjord Lysefjorden. Since 2013 the bridge has been fitted with various instruments to monitor and research the wind and the structural health of the bridge, so-called Wind and Structural Health Monitoring systems (WASHMS) [1].

The aim of the WASHMS is to identify modal parameters such as eigen-frequencies and mode shapes and allow a direct study of the wind-induced vibrations [1]. A further description of the instruments installed on the bridge is found in chapter 2.2 and 3.2.

Figure 1: The Lysefjord Bridge [32]

1.2 Problem description

This thesis will look at the horizontal and vertical wind velocity, the correlation of anemometers, the turbulence intensity and the wind direction at the Lysefjord Bridge, and link some of these factors with the vertical accelerations of the bridge deck measured by the three pairs of accelerometers installed at different hangars. The goal is to gain knowledge about the wind effects on a suspension

bridge and to see whether the different wind data can be linked to each other and to the vertical accelerations or not.

1.3 Scope

The data that is analysed and discussed in this thesis comes from four different 10-minute time periods of continuous wind measurement extracted from the main server where a master data logging unit stores all the data from the different instruments on the bridge. The four time periods originate at different times during the fall of 2021. Further details of this can be found in chapter 2.3.

The data of horizontal and vertical wind velocity, wind direction, vertical angle, turbulence intensity and correlation between the anemometers from the four time periods is analysed and the results is presented in chapter 4. The vertical accelerations of the bridge deck will also be presented during this chapter, along with the vertical acceleration spectra of each pair of accelerometers.

These results are then discussed further in chapter 5 and connections between the different factors are found, before a conclusion and suggestions for further research is presented in chapter 6.

Horizontal accelerations and accelerations due to torsion is not the focus in this thesis and will not be discussed. As the main point is to gain knowledge about the different wind effects on the bridge, calculations of the wind loading due to the wind effects will not be presented.

2.0 Method

This chapter will include a short description of the methods used in this thesis, as a foundation for the results and the conclusions of the work.

2.1 Qualitative and quantitative method

Qualitative studies rely on the acquisition and analysis of non-numerical data such as audio or video and can be achieved in several different ways, e.g., through observations, interviews or focus groups. Qualitative studies gather knowledge from human experience to find answers and conclusions to problems. Quantitative studies on the other hand, rely on hard data such as numbers and graphs to gather information about a problem and/or solving an issue [2].

To gather information about the behaviour of the Lysefjord Bridge when exposed to wind, it is necessary to accumulate large quantities of precise data and analyse this data using appropriate tools. Comparing the analysed data to other researchers` findings will help validate the subsequent results and confirm whether the data can be used to make accurate assumptions about the bridge behaviour. Based on this, a quantitative method is the natural choice of methodology

As part of this quantitative method, signal processing will also be used. Signal processing is used to "model and analyse analog and digital representations of physical events" [3]. In this case, the signals that are processed are discrete-time samples of continuous sizes from the real-world physical event that is wind.

2.2 The instruments installed on the Lysefjord Bridge

Since November 2013, the Lysefjord bridge has been used as a full-scale wind engineering laboratory and has been equipped with a wind and structural health monitoring system. As of 22.03.2022, the bridge is instrumented with eleven 3D sonic anemometers, three pressure probes, four pairs of tri-axial accelerometers inside the bridge deck and a GNSS based displacement sensor [1 Every instrument installed does however have limitations to them with regards to precision and accuracy, as it is difficult to get exact measurements of real-world events.

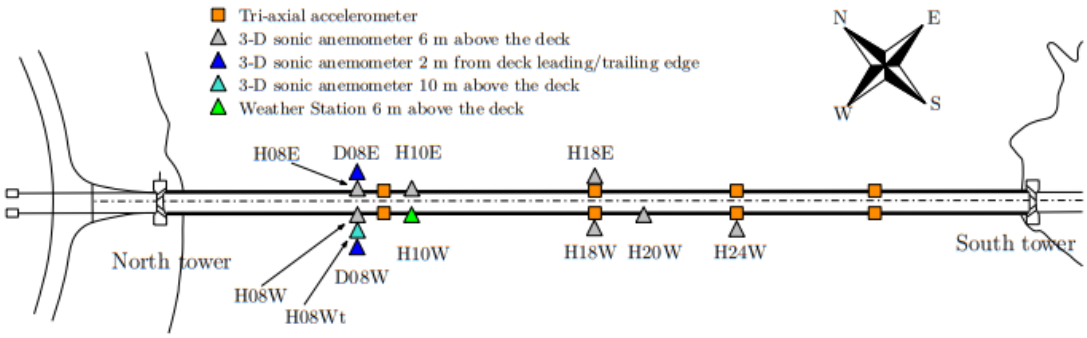

Figure 2: Instrumentation installed on the bridge [26]

The main measurement principle for the anemometers is giving ultrasonic wind measurements in three different axes which translates to the U, V and W vectors. The accelerometers are triaxial microelectromechanical systems (MEMs), which monitors the bridge twisting response along with the translational response.

The bridge deck is also monitored by a Real-Time Kinematic-Global Positioning System (RTK-GPS). This rover is placed on top of the main cable in the middle of the main span and consequently, it is the displacement of the main cable approximately 3 meters above the bridge girder that is being observed.

2.3 Method of data analysis

To collect all the data from the different instruments, a master data logging unit synchronizes it into a single data file. This file is then continuously transmitted to a central server at the University of Stavanger via mobile net. Four different time-series of ten minutes was extracted from this data file and used in the thesis. The dates of these time-series were 09/08/21 – 14:30:00, 23/09/21 – 10:00:00, 18/10/21 – 13:00:00 and 21/10/21 – 15:10:00.

The data gathered was processed, analysed and visualized by using primarily MATLAB. MATLAB is a programming and numeric computing platform used by millions of engineers and scientists to analyse data, develop algorithms and create models [4]. Different types of MATLAB functions were used to implement first and second order statistical analysis of the measurement data. Microsoft Excel was also used to a small degree, to help organize some of the data obtained through MATLAB.

2.4 Limitations

There were several limitations in this thesis, which study the flow conditions along the bridge deck and the related bridge response. The main limitation is that only four time-series, each with a duration of 10 min, are analysed. For a systematic study of the flow conditions and bridge vibrations a much larger data set needs to be analysed.

The four time-series selected turned out to have a relatively low mean horizontal wind velocity. It is uncertain exactly what effects a higher mean wind velocity would have had on the bridge compared to a low mean wind velocity, for example with regards to the acceleration of the bridge deck. D.Anfossi et. al. [5] found that the effect known as meandering starts to occur at low wind speeds (1-2 m/s). Although the mean wind velocities in the datasets used in this thesis is not as low, it might still affect the wind flow to some degree.

Since the Lysefjord bridge is the main point of crossing of Lysefjorden, and the mean wind speeds were limited, the traffic on the bridge during the selected ten-minute periods was making a more important contribution to the response. It would have been more desirable with higher wind speeds and absence of traffic to more directly see the impact of the wind load on the bridge dynamic response.

The present work discusses only the vertical acceleration response of the bridge. Further information could have been obtained if also horizontal and twisting bridge response were studied.

3.0 Structural dynamics and wind effects on suspension bridges

Suspension bridges are some of the largest manmade structures on earth. They are designed to carry people across waters and vast canyons. It is not easy to convey the same sense of stability and security as bridges made with steel and concrete arches. Since suspension bridges are flexible and have low damping, they are at risk of being excited into big motions by environmental forces such as wind.

Suspension bridges carries both the pay load and dead load of the structure as axial tension forces in the suspension cables. The cables transfer the forces into anchorage structures, which in turn transfers the forces into the ground. This way of transferring forces means that suspension bridges can be built with very long spans, up to 5000 meters. In theory the length is only limited by the carrying capacity of the main cables [6]. The bridge with the longest span in the world is the 1915 Çanakkale bridge in Turkey with a main span of 2023 meters [7].

3.1 Structural dynamics of suspension bridges

A suspension bridge consists of different main components where the bridge girder and the main cables are the most significant contributors to the overall structural dynamics. Other notable components are the hangers, towers, and the anchorages. One well known suspension bridge is the Osman Gazi bridge in Turkey. The typical mode shapes for this suspension bridge are restricted to either lateral, vertical, or torsional motion and are shown in figure 3. Although the main span of the Osman Gazi is 1550 metres [8] and hence about three times the length of the main span of Lysefjord bridge, the mode shapes should be somewhat comparable.

Although the decks of both bridges are designed as a trapezoidal closed girder box, the Osman Gazi is a bit more streamlined. The deck width to height ratio is 30.1m/4.75m = 6.3, while the Lysefjord bridge has a deck width to height ratio of 12.3m/2.76m = 4.5. The trapezoidal design helps greatly with providing torsional stiffness, which is now common practice in long span cable supported bridges. If the girder did not provide a lot of torsion stiffness, the modes related to torsion would be substantially affected in two ways. Firstly, the symmetric torsion frequency would have decreased significantly and secondly, the symmetric and the asymmetric torsion mode would have switched ranking with the asymmetric mode having lower eigenfrequency. The latter is because the asymmetric torsion does not involve elastic stretching of the main cables [6].

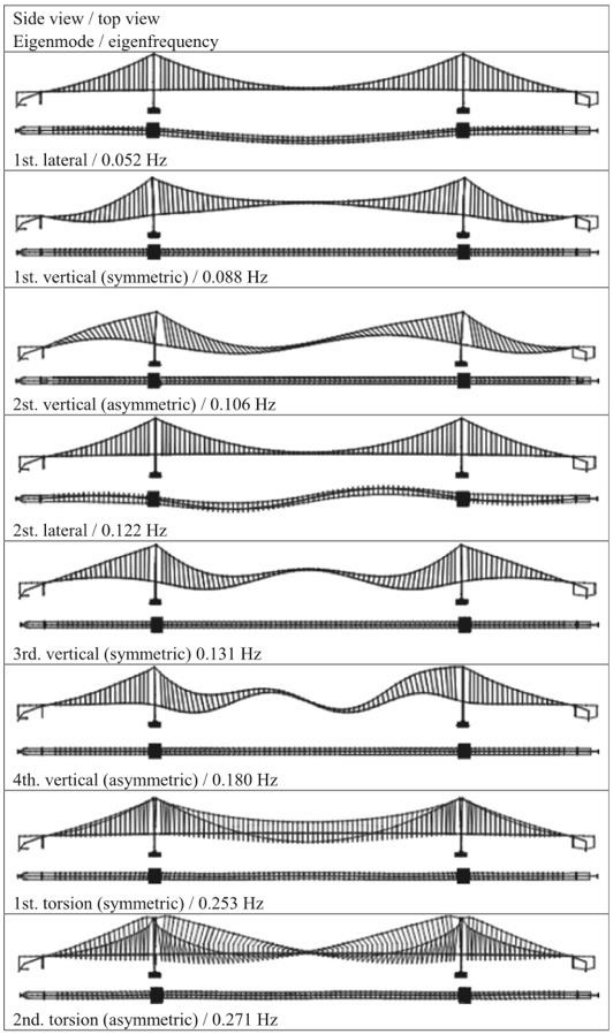

Figure 3: Typical mode shapes for a suspension bridge, from [6]

In the design of modern suspension bridge design, finite element models are important. For their validation, it is of importance to investigate how the calculated eigenfrequencies compare with measurements on the completed structures. Such comparisons for two other suspension bridges, the 1624 metres main span Storebælt in Denmark and the 1210 metres main span Höga Kusten Bridge in Sweden is shown in table 1.

Table 1: Eigen-frequencies of Storebælt Bridge and Höga Kusten Bridge [6]

Eigenmode	Storebælt Bridge		Höga Kusten Bridge	
	FEM (Hz)	Observed (Hz)	FEM (Hz)	Observed (Hz)
1st torsion (sym)	0.281		0.386	0.397
3rd torsion (sym)	–	–	0.648	0.671
1st vertical (sym)	0.096	0.100	0.137	0.139
3rd vertical (sym)	0.128	0.130	0.177	0.177
4th vertical (asym)	0.177	0.174	–	–
5th vertical (sym)	0.205	0.209	0.267	0.281
6th vertical (sym)	0.235	0.242	0.308	0.317

Table 1 shows that a representative FEM is quite accurate when it comes to predicting the eigenfrequencies, which is important when using the computational models to assess wind effects on

bridges. More detailed comparisons between FEM-calculations and measurements in the field on actual suspension bridges can be found in [9] and [10]. Most of the eigen-frequencies in the table above are below 0.5 Hz, which is the frequency range where wind has most of its energy.

3.1.1 Spectral analysis

Spectral analysis is the act of determining the distribution of power over frequency (spectral content) of a time-series from a finite set of measurements [11]. It has applications in many different fields of study. In medicine, it can help give patients the correct diagnosis by measuring for example electroencephalogram signals [12]. In seismology it can give useful information about ground movement prior to or after a seismic event [13]. In economics it can help reveal cyclic behaviour or recurring processes [11] and in vibration monitoring the spectral content can provide information about that will help identifying eigenfrequencies associated with different modes [11].

A lot of the signals from the real-world can be characterized as random. This means that outside the observed signal, the variation can only be specified in statistical terms of averages and not determined exactly [11]. Wind is an example of a random real-world signal which in this case will be considered as a discrete-time signal. This discrete-time signal is a sequence of values that coincide with time-instants [14], which in turn translates to the four ten-minute time-series that is analysed in chapter three and four in this thesis.

3.2 Description of the instruments installed on Lysefjord bridge

3.2.1 Anemometers

Eight of the eleven anemometers used are 3-D WindMaster Pro from Gill Instruments [15]. These sonic anemometers measure the ultrasonic wind in three different axes.

A 2-D weather transmitter is mounted on H10W and gives information on relative humidity, pressure, absolute temperature, horizontal wind components and rainfall with a sampling frequency up to 4 Hz. This anemometer is a WXT520, provided by Vaisala [16] The two last anemometers are 3-D WindMaster HS [17] and are installed at deck level on either side of the bridge deck.

3.2.2 Accelerometers and GNSS

The accelerometers are installed as pairs at hangar 09, 18 and 24, on each side on the deck. The distance between two accelerometers constituting a pair is 7,5 meters. Each accelerometer has a maximum sampling frequency of 200 Hz.

With regards to the RTK-GPS, the accuracy of the measurements is improved by recording the relative displacements between the moving rover and a fixed base station on the northwest side of the bridge. The instruments used are a set of Trimble BD930 GNSS receivers coupled to Trimble AV33 GNSS antennas. The data samples have an accuracy of ±8 mm +1 ppm for the horizontal displacements and ±15mm +1 ppm for the vertical displacements. Due to the large amplitude displacements and the low natural frequency of long span suspension bridges, this GPS technique is ideal for tracking the behaviour of long-span suspension bridges.

3.3 Wind effects on suspension bridges

The wind actions on suspension bridges becomes more and more critical as the spans increase. Extensive wind studies are undertaken for long bridges due to this. The dynamic wind forces can excite resonant response in up to several modes and the motion of the structure itself will also generates forces.

There are mainly three different mechanisms, in various wind speed ranges, that can excite resonant dynamic responses in the decks of suspension bridges [18]:

- Vortex-shedding excitation
- Flutter instabilities
- Buffeting

3.3.1 Vortex-shedding excitation

When certain conditions are met, vortex-shedding excitation can induce significant, but limited, amplitudes of vibration [18]. For this to occur several, or all, of the following conditions must be met:

- A wind direction normal to the longitudinal axis of the bridge
- Low turbulence conditions (typically I_u less than 0.05)
- A wind speed in a narrow critical range (5-12 m/s)
- Low damping (1% of critical or less)

With natural frequencies within the range of 0.1-0.6 Hz and Strouhal numbers in the range of 0.1-0.2 (which is based on the depth of the deck cross section), significant amplitudes can be produced by velocities of 6-15 m/s. Vortex-shedding will not cause sudden collapse of a bridge but over time, long-term fatigue damage can occur. It can however cause large visual displacement and discomfort for users of a bridge [19]. As a measure to suppress these vibrations, the installation of guide vanes has been proven very efficient on the Storebælt suspension bridge [20].

As low turbulence is one of the conditions and vortex-shedding is mostly a problem for longer span suspension bridges, the vibrations from this phenomenon does not apply to the Lysefjord bridge. The main span is 450 meters and the placement at the inlet of a fjord with relatively steep mountains on either side will create downwinds which in turn can create turbulence.

3.3.2 Flutter

Also called aerodynamic instability, flutter can be divided into two types: (1) One-degree-of-freedom flutter or “torsion flutter” and (2) two-degree-of-freedom flutter or “classical flutter”.

Larsen and Larose [6] described “classical flutter” as a coupling between torsional and vertical eigenmodes of a bridge deck. To reach the flutter condition, a certain critical wind speed must be transcended, which can be different from bridge to bridge, depending on the shape and design of the bridge girder. Structural failure due to classical flutter happens as the critical wind speed is exceeded and the coupled bending and torsion modes increases exponentially in magnitude until the bridge collapses.

A prerequisite for classical flutter is that the girder needs to have a smooth shape with a pointy windward edge which prohibits larger edge vortices to form. An example of these types of decks are closed trapezoidal box girders which has a large width to depth ratio. The Lysefjord bridge is designed with this kind of deck. Using Selberg`s formula [21], the critical wind speed for the Lysefjord bridge was found to be approximately 166 m/s [22] and consequently, is very unlikely to feature.

One-degree-of-freedom flutter or torsion flutter is expected to involve the first symmetric torsion mode for contemporary suspension bridges. This is usually the lowest torsion mode of the bridge deck. As opposed to “classical flutter”, torsion flutter is dependent on the formation of large edge vortices due to the design of the bridge girder.

A typical example of a bridge girder that will allow the formation of large edge vortices is the design of the girder on the infamous Tacoma Narrows Bridge. It was designed with a 2.4 metres high vertical solid edge with a triple structural purpose. Even though the design was praised during and after construction, it proved fatal with respect to aerodynamic stability.

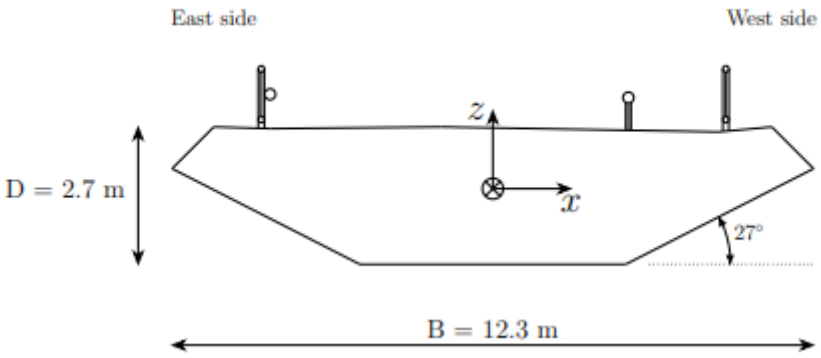

Figure 4: Schematic of the closed trapezoidal deck girder of Lysefjord Bridge [26

3.3.3 Buffeting

Buffeting is defined as the forced response of a structure to random wind and can only take place in turbulent flows [23]. Turbulence resulting from topographical or structural obstructions is called oncoming turbulence. Turbulence induced by bridge itself is called signature turbulence. Since the frequencies of signature turbulence are generally several times higher than the important natural frequencies of the bridge, its effect on buffeting response is usually small. The buffeting response can emerge from a wide variety of wind speeds and this response will usually determine the size of the structural members [18].

Buffeting is a random vibration problem with limited displacement. The effects are similar to those from vortex-shedding, apart from that the vibration from buffeting is random as opposed to the vibration from vortex-shedding. Buffeting influences the ultimate strength behaviour but also affects the bridge`s serviceability behaviour. Over time, buffeting can lead to bridge collapse due to fatigue damage.

4.0 Results and analysis

As mentioned earlier in this thesis, the Lysefjord Bridge has been equipped with different wind measurement systems since 2013. The bridge has been used as a full-scale wind engineering laboratory and is one of the world's most densely instrumented suspension bridges in the world [1]. To collect all the data from the different instruments, a master data logging unit synchronizes it into a single data file. This file is then continuously transmitted to a central server at the University of Stavanger via mobile net.

This part of the thesis will look at results and analyse the wind data from four different 10-minute periods from late summer/fall in 2021. The wind velocity and wind direction will be presented, turbulence intensities will be calculated and correlation coefficients between the anemometers will be looked at. This will provide the insight into the flow conditions on site, with focus on their possible variation along the bridge span. To illustrate the associated bridge dynamic response, vertical acceleration will also be presented and the acceleration spectra for each accelerometer will be introduced lastly.

The acceleration spectra are estimated using Welch`s method in MATLAB [24]. This method is widely used to estimate the power of a signal at different frequencies. It is done by dividing the time signal into consecutive blocks, forming the periodogram for each block and then averaging these blocks [25]. The sampling frequency used was 50 Hz.

The notation used for turbulence intensity is I_u. I_u is calculated for each anemometer by taking the standard deviation divided by the mean horizontal velocity.

All datasets gathered were checked to see whether or not they could be classified as stationary. This was checked by dividing the 10-minute time-series into blocks of five. In these blocks, the maximum moving mean and maximum moving standard deviation had to be less or equal to 1+deviation times the mean and standard deviation of the data respectively. The minimum moving mean and minimum moving standard deviation had to be more than or equal to 1-deviation times the mean and standard deviation respectively. The deviation was set to 30%, or 0.3.

The anemometer H18E was malfunctioning during all the time-series used in the thesis and no data from this was collected. It was later repaired and re-installed on 1st of November, after the time intervals used in this thesis. H10W did not produce any data with regards to the vertical wind velocity since it is a weather station but did provide data for every other measurement.

All results that are not specified in chapter 4 or 5, can be found in the appendix.

4.1 Wind data from 09/08/21 – 14:30:00

With regards to the horizontal velocity, in this time-series none of the anemometers registered data that can be classified as stationary with regards to the specified rules stated above. The same results were found for the vertical wind velocity. Despite of that, the first and the second order statistics has been calculated, providing an overview of the wind conditions.

As for the wind direction, the time-series was stationary with regards to the moving average but not with regards to the moving standard deviation.

The vertical accelerations did not fulfil the criterium for stationarity presented in chapter 4.0

4.1.1 Horizontal velocity and wind direction

For this time interval, the maximum horizontal wind velocity varies between 7.30 m/s recorded at H10W and 9.32 m/s recorded at H10E. This is seen in table 2. The highest maximum velocity appears after 36.9 seconds. As the peak is quite sudden, as seen in figure 5, there is a good chance that this peak is due to statistical noise. The distance between the anemometers presented in figure 5 is 96 meters. The mean of these three anemometers is quite similar and the horizontal velocity follows somewhat the same pattern for the time interval, although with some exceptions.

The mean horizontal wind velocity recorded by the different sensors is mostly in the interval [4.80-5.67] m/s, with one low of 3.28 m/s. This was registered by D08E, while the highest mean wind velocity was recorded from H20W. Since D08E and D08W is located at deck level and measures wind velocity just upstream of the deck and in the wake of the bridge girder, depending on the wind direction. This means that in the wake the wind speed is reduced while the turbulence level is increased as the flow will be highly disturbed by the deck. A schematic of the installed instruments on hangar 08 is seen in figure 7.

Because of this forementioned reduced wind speed the values from D08E and D08W are omitted when calculating the mean horizontal velocity, which is 5.41 m/s. With regards to the standard deviation of the data, anemometer D08W has the lowest value being 0.729 while D08E has the standard deviation with the highest value: 1.057.

The mean wind direction for this time-series is 221.35 degrees. This corresponds to a wind flow from south-west. The wind direction is shown in figure 6.

Table 2: Wind data from 09/08/21

	Wind data 09/08/21 - 14.30.00										
Anemometers	H08Wb	H08Wt	H08E	D08W	D08E	H10W	H10E	H18W	H18E	H20W	H24W
Max velocity [m/s]	7.9200	7.7600	8.9700	7.8500	8.5800	7.3000	9.3200	8.6100	0.0000	8.6000	8.3100
Min velocity [m/s]	2.7800	2.4900	1.5100	2.5900	0.3800	2.2000	0.2000	0.6300	0.0000	1.9000	2.5900
Mean [m/s]	5.2946	5.2203	5.3911	4.8104	3.2830	5.3122	5.4395	5.4916	0.0000	5.6673	5.4294
Standard deviation	0.7721	0.7657	0.8314	0.7287	1.0567	0.8432	0.8943	1.0391	0.0000	0.9168	0.8786

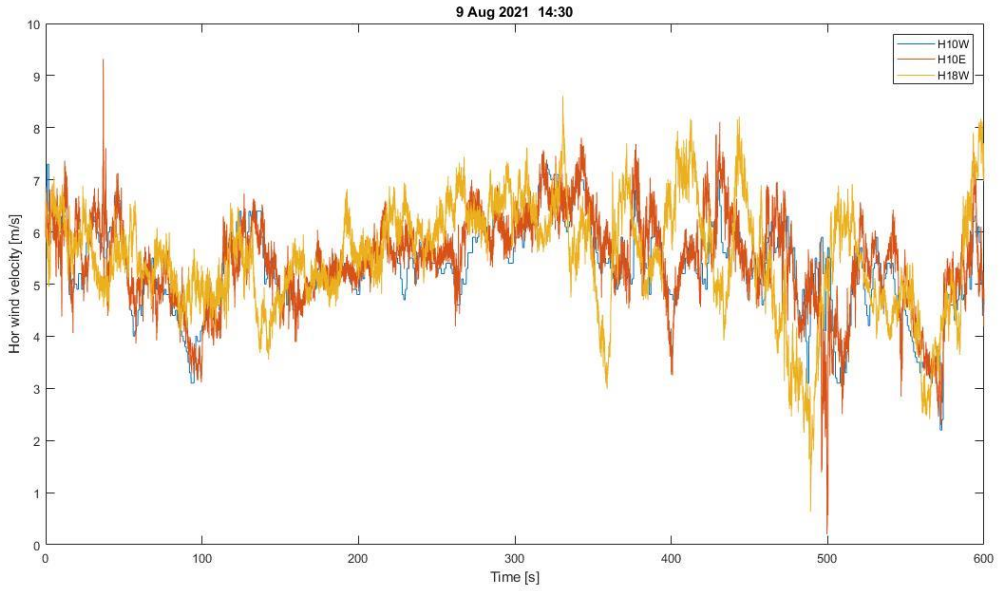

Figure 5: Variation of horizontal wind velocity for selected anemometers

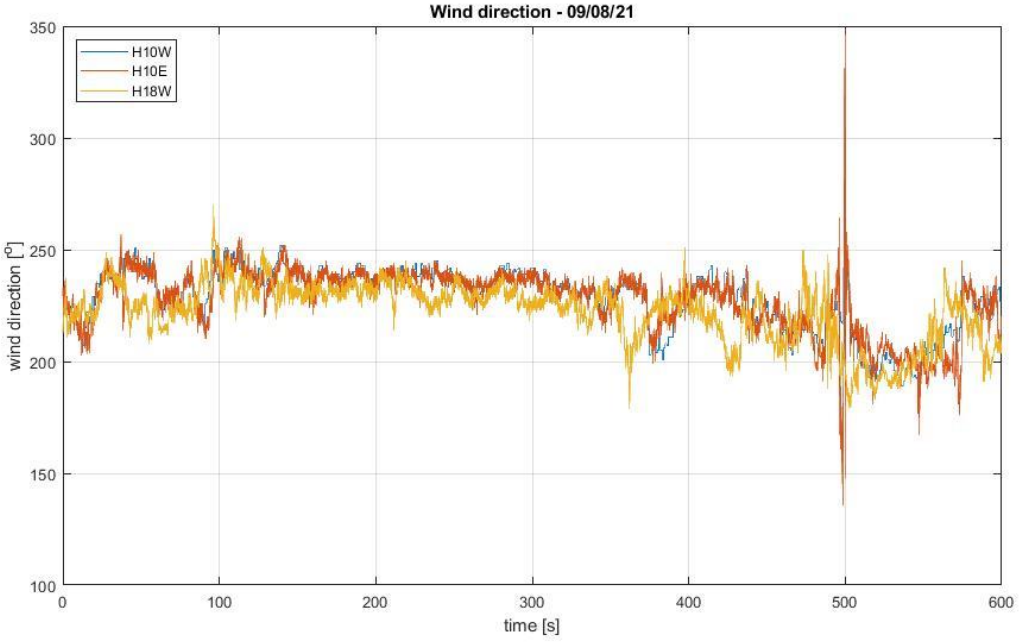

Figure 6: Variation of wind direction for the selected anemometers

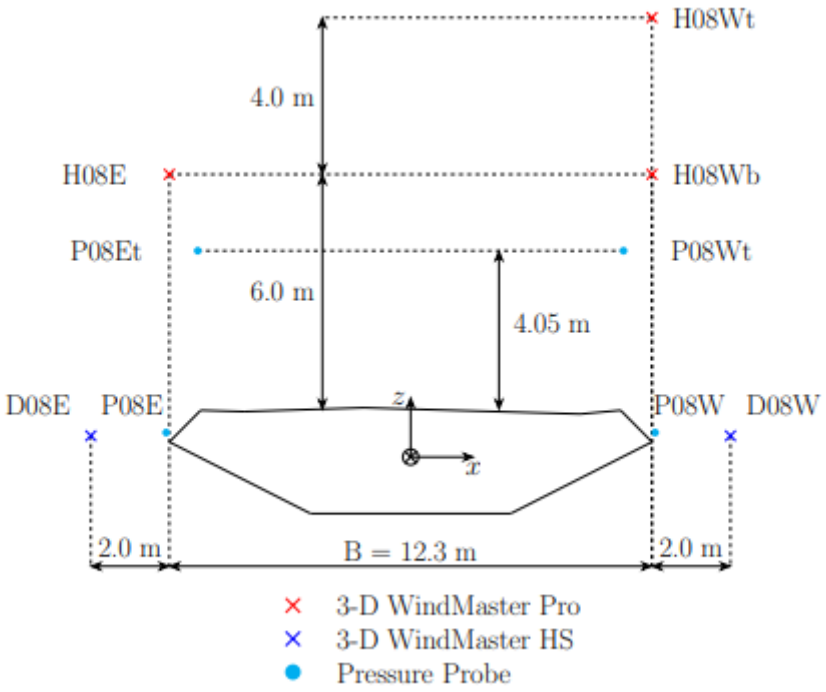

Figure 7: Position of instruments on H08 [26]

4.1.2 Vertical velocity and mean vertical angle

Natural wind is turbulent, i.e., the wind velocity changes continuously in time and space. The vertical velocity component implies that the instantaneous wind velocity acts at a certain angle (so called angle-of attack) with respect to the bridge deck, that influences the wind loading. In the following, vertical velocity along with the variation in the wind angle in the vertical plane will be presented.

The peak vertical velocity was registered by H10E, with a value of 4.3 m/s. The peak is within the same second as the peak of the horizontal velocity, so this value might also be statistical noise. The vertical wind data is presented in table 3.

MATLAB was used to find the mean vertical attack angle. This was done using the inverse tangent of the vertical wind speed measured at each anemometer divided by the horizontal wind speed at the corresponding anemometer. Afterwards the mean of the vertical angles was found. For this time-series, the mean vertical attack angle of the wind was 1.66°.

Table 3: Vertical wind data 09/08/21

	Vertical wind data 09/08/21 - 14.30.00										
Anemometers	H08Wb	H08Wt	H08E	D08W	D08E	H10W	H10E	H18W	H18E	H20W	H24W
Max velocity [m/s]	3.2400	3.0300	3.2200	3.7700	4.2500	0.0000	4.3000	3.5500	0.0000	2.9400	2.6200
Min velocity [m/s]	-2.9800	-2.3500	-2.4300	-3.6500	-3.9400	0.0000	-3.1400	-1.9100	0.0000	-2.0200	-2.7000
Mean [m/s]	0.3851	0.3356	0.1646	0.3392	0.1880	0.0000	-0.0031	0.0996	0.0000	0.0425	-0.1222
Standard deviation	0.6545	0.6217	0.5965	1.0590	1.0272	0.0000	0.6655	0.6665	0.0000	0.6361	0.6300

4.1.3 Turbulence intensity

Turbulence intensity I_u is calculated as the standard deviation divided by the mean velocity. For this time-series the turbulence intensity varies between the different anemometers, $I_u \approx 14.6\%$ at H08Wb to $I_u \approx 18.9\%$ at H18W. There is one outlier value outside this spread, with the value being 32.9% at anemometer D08E. The mean turbulence intensity is $I_u \approx 17.6\%$ when the outlier value is taken into consideration, without it the mean turbulence intensity is $I_u \approx 15.9\%$.

4.1.4 Correlation coefficients

In Figure 8, the cross-correlation coefficient between the horizontal wind velocities recorded by all the anemometers is presented. The exact values are presented in table 4. The most notable correlations between the anemometers when it comes to horizontal wind velocity is that H08Wb, H08Wt and H08E has a relatively high correlation with each other with values above 0.7. The velocities recorded by D08W (anemometer upstream of the bridge girder) have the strongest correlation with the data recorded by H08Wb, i.e., the anemometer at the same location along the bridge, but 6 m above the deck surface. The last four (H10E, H18W, H20W and H24W) does not correlate with each other to the same degree, with values below 0.4. H18W and H20W does however correlate strongly with a value of 0.7.

Another notable observation from the correlation matrix is that D08E shows little to no correlation with the other anemometers. A weak negative correlation is observed with some of the anemometers, with the lowest value being -0.0801 linked to H20W. This has to do with the specific location of the D08E anemometer, which is on the leeward side of the deck, for the wind from SSW, as in the present case. D08E is mounted at the same level as the bridge deck and when the wind is flowing from the opposite side, D08E will record the disturbed flow in the wake of the deck.

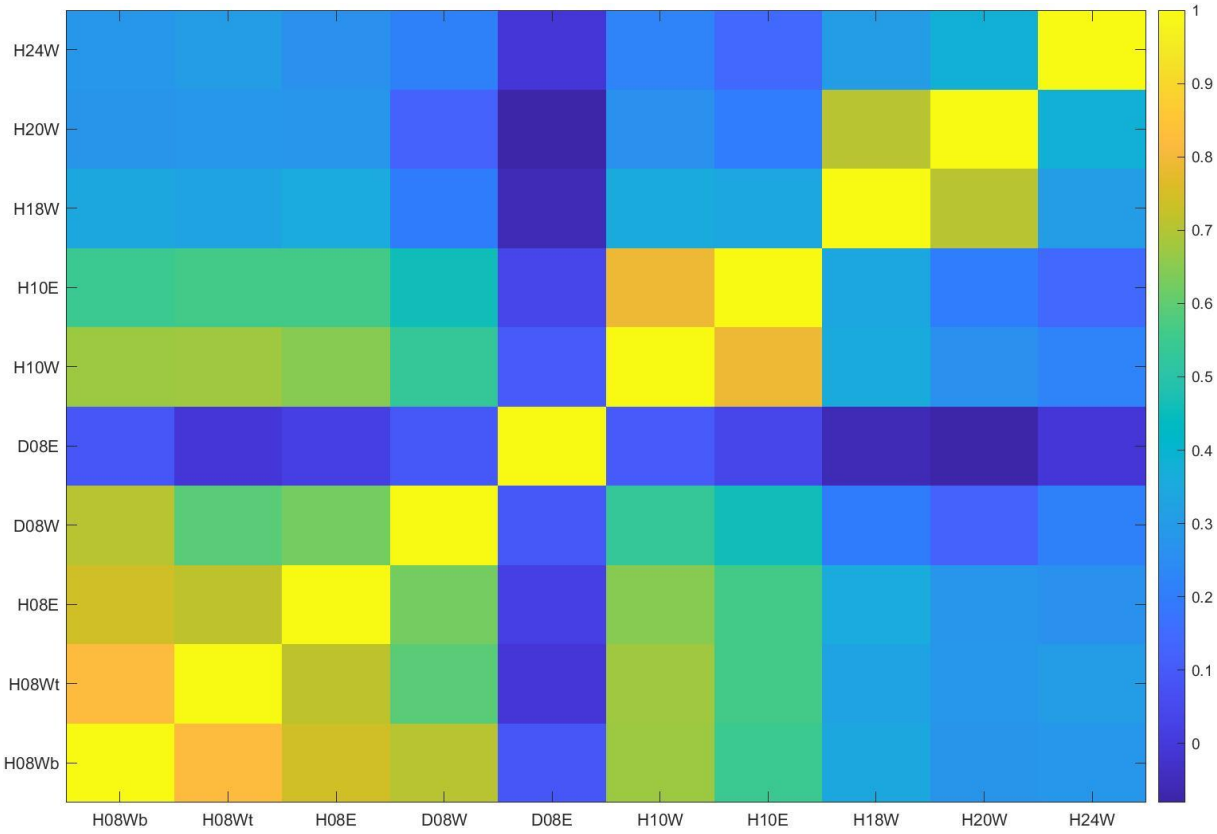

Figure 8: Correlation matrix illustrating the correlation between anemometers in 09/08/21

Table 4: Cross-correlation coefficients for all functioning anemometers

Cross-correlation coefficients - 09/08/21										
H24W	0.2857	0.3029	0.2652	0.2109	-0.0066	0.2192	0.1452	0.3021	0.3801	1.0000
H20W	0.2768	0.2848	0.2788	0.2148	-0.0805	0.2642	0.2039	0.7053	1.0000	0.3801
H18W	0.3487	0.3284	0.3609	0.1989	-0.0580	0.3580	0.3428	1.0000	0.7053	0.3021
H10E	0.5462	0.5642	0.5641	0.4586	0.0380	0.7904	1.0000	0.3428	0.2039	0.1452
H10W	0.6745	0.6790	0.6465	0.5339	0.1051	1.0000	0.7904	0.3580	0.2642	0.2192
D08E	0.0892	-0.0052	0.0184	0.1000	1.0000	0.1051	0.0380	-0.0580	-0.0805	-0.0066
D08W	0.7076	0.5916	0.6244	1.0000	0.1000	0.5339	0.4586	0.1989	0.1248	0.2109
H08E	0.7412	0.7165	1.0000	0.6244	0.0184	0.6465	0.5641	0.3609	0.2788	0.2652
H08Wt	0.8253	1.0000	0.7165	0.5916	-0.0052	0.6790	0.5642	0.3284	0.2848	0.3029
H08Wb	1.0000	0.8253	0.7412	0.7076	0.0892	0.6745	0.5462	0.3487	0.2768	0.2857
	H08Wb	H08Wt	H08E	D08W	D08E	H10W	H10E	H18W	H20W	H24W

4.1.5 Vertical accelerations

In the following, the acceleration data recorded simultaneously with the above discussed wind velocity data are discussed. The three pairs of 3D accelerometers are located inside the bridge girder box, at the positions of hangar 9, 18 and 24 and are denoted H09, H18 and H24 respectively.

The peak positive acceleration recorded by the anemometer at H09E is 15.99 m/s^2 after 51.84 seconds, while H09W peaks at 24.16 m/s^2 at 53.96 seconds into the time-series. The peak negative accelerations for both accelerometers happen within four thousandths of a second of each other, after 53.88 and 53.84 seconds respectively. The values are -17.09 m/s^2 for H09E and -19.80 m/s^2 for H09W, i.e., of the similar magnitude as the maximum accelerations. This is shown in figure 9.

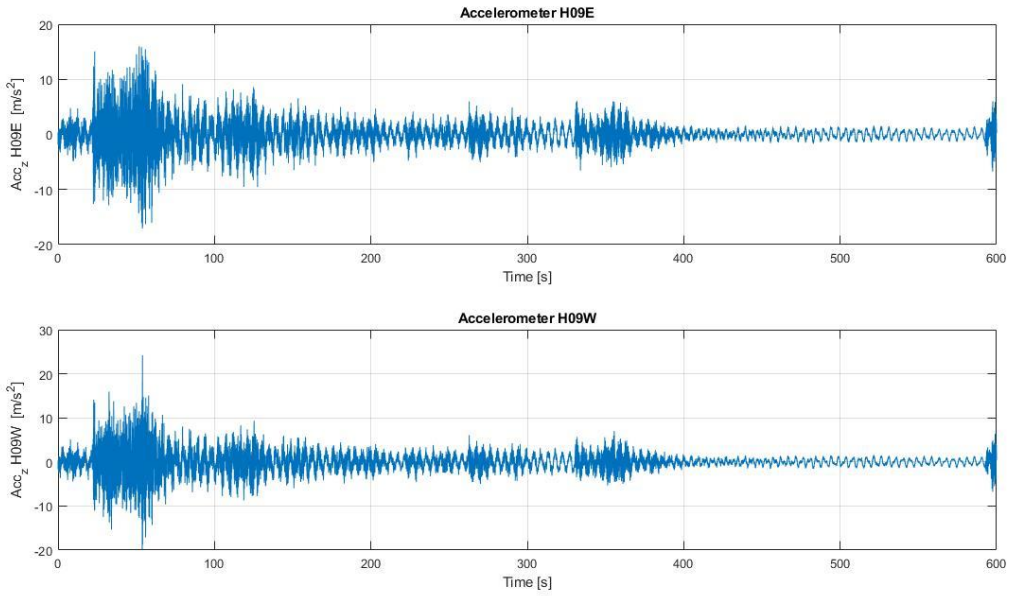

Figure 9: Vertical acceleration of accelerometers installed on H09

For H18E and H18W the displayed vertical accelerations are highly similar to each other. This is reasonable since both accelerometers record the vertical bridge vibrations at the same location along the bridge deck. The highest positive accelerations are 18.59 m/s^2 at 54.08 seconds for H09E and 16.37 m/s^2 at 54.36 seconds for H09W. Both accelerometers have its peak negative acceleration recorded after 54.22 seconds, with values of -21.43 m/s^2 for H18E and -19.29 m/s^2. These accelerations are presented in figure 10.

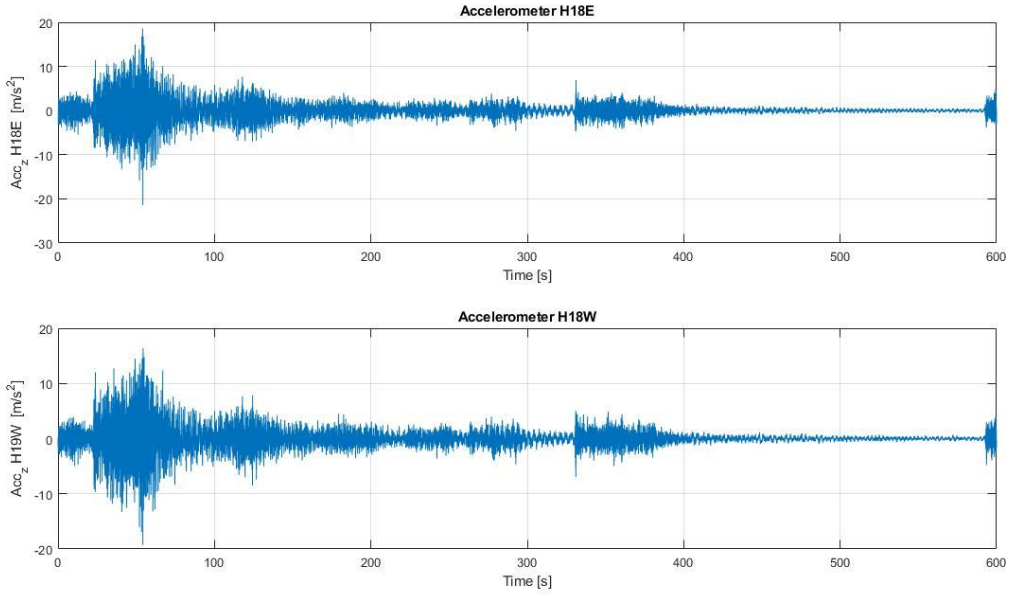

Figure 10: Vertical acceleration of accelerometers installed on H18

Both H24E and H24W has its highest positive acceleration after 45.04 seconds, where the values go up to 22.74 m/s^2 and 22.24 m/s^2. The lowest value for H24E is -21.10 m/s^2 after 54.38 seconds and for H24W the lowest value is -18.76 m/s^2 after 53.34 seconds. The accelerations are shown in figure 11.

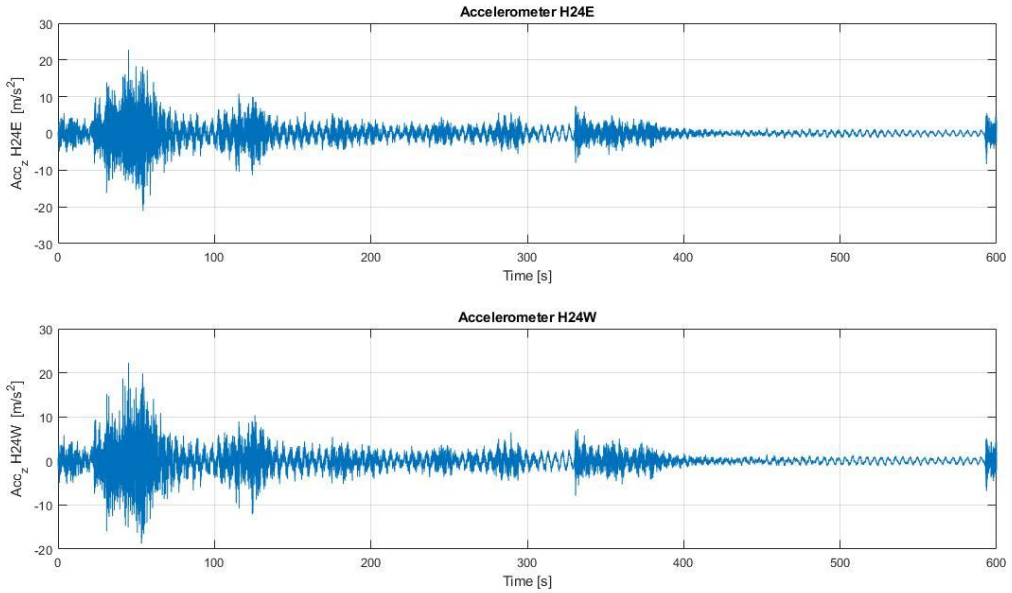

Figure 11: Vertical acceleration of the accelerometers installed at H24

4.1.6 Vertical acceleration spectra

In the following the vertical acceleration spectra will be presented.

The vertical acceleration spectra for the accelerometers installed on H09 is seen in figure 12. The spectra shows that the biggest concentration of vibrations occurs at a frequency of 0.220 Hz. There are some concentrations at higher frequencies as well, but none at the same level as that of the 0.220 Hz.

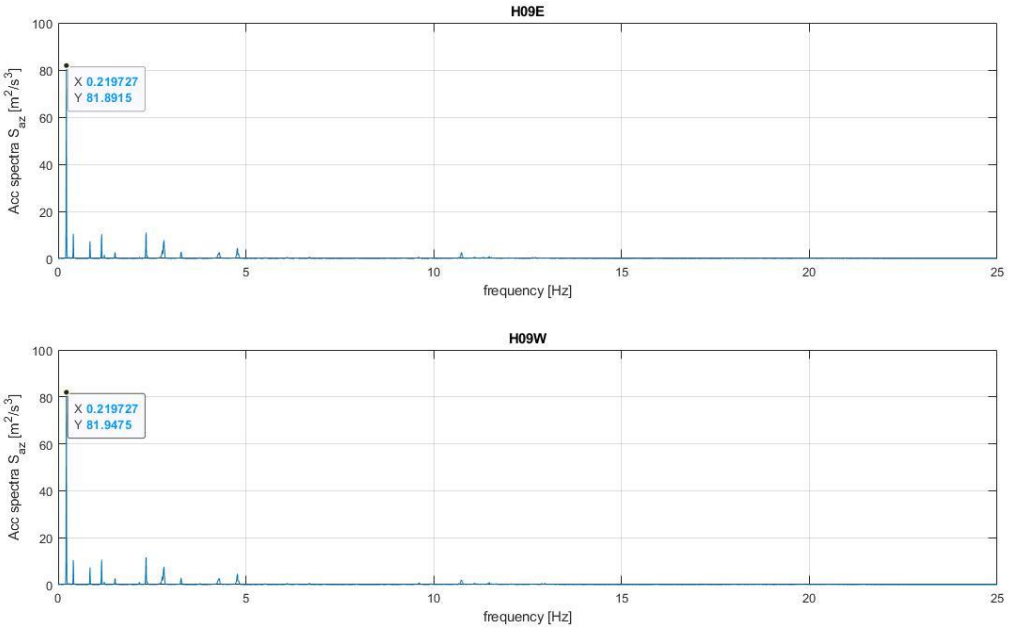

Figure 12: Vertical acceleration spectra from accelerometers installed at H09

For the accelerometers installed on H18, the highest concentration occurs at a frequency of 2.34 Hz. This is presented in figure 13. These accelerometers had more concentrations at different frequencies below 5 Hz, some which relates more to the peaks of both the accelerometers at H09 and H24. The higher concentrations at other frequencies than those found by the other accelerometers will be discussed further in chapter 5.1.6.

For H24E and H24W, the peak concentration is found at the same frequency of 0.220 Hz, the same as that of H09E and H09W. This is seen in figure 14.

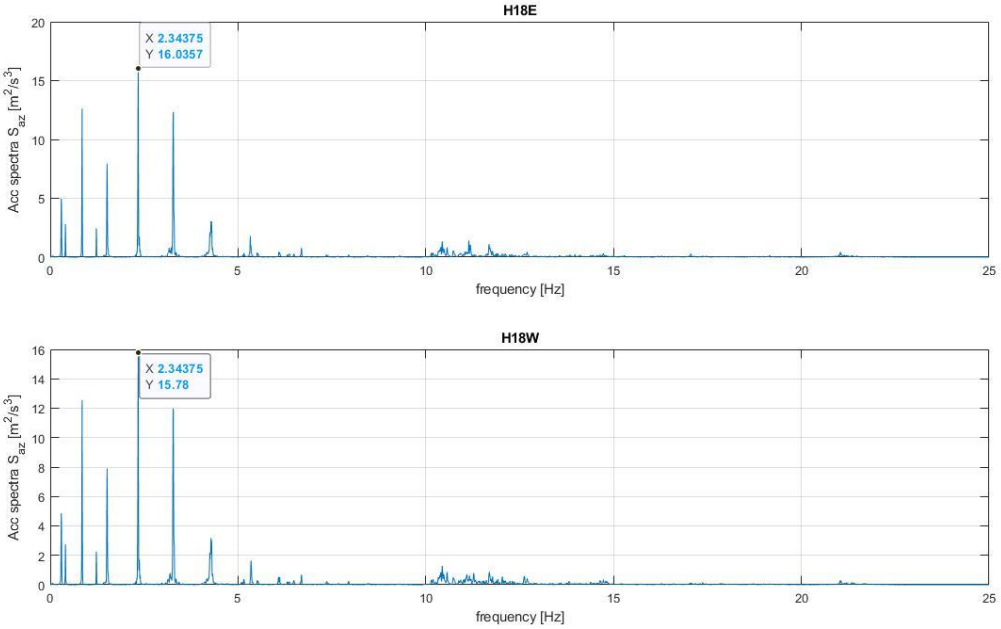

Figure 13: Vertical acceleration spectra from accelerometers installed at H18

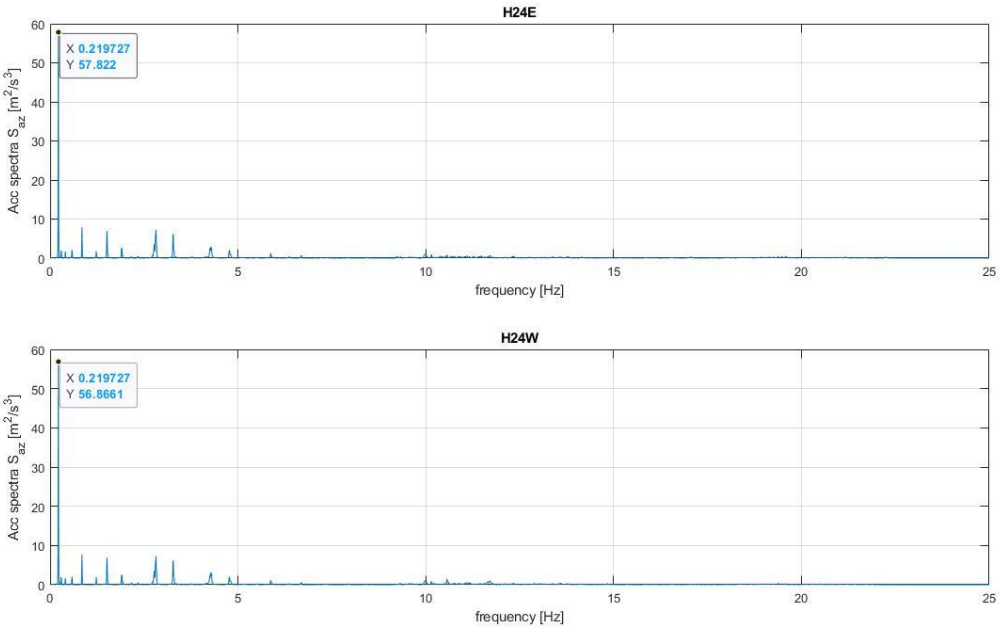

Figure 14: Vertical acceleration spectra from accelerometers installed at H24

4.2 Wind data from 23/09/21 – 10:00:00

In this series, neither the horizontal nor the vertical wind velocity shows signs of stationary according to the criteria that was defined in chapter 4.0.

With regards to the wind direction, the data from anemometers H08Wb, H18W, H20W and H24W can be classified as stationary according to the moving mean criterium. The moving standard deviation criterium is, however, not fulfilled for any of the anemometers.

4.2.1 Horizontal velocity and wind direction

In this time-series the maximum horizontal wind velocity was recorded from anemometer H08Wb and has a value of 17.37 m/s, illustrated in figure 15. This corresponds to a speed of 62.53 km/h and happens at 556 seconds. The lowest maximum was registered as 14.30 m/s from D08E at 559.8 seconds. Minimum velocity during the measured 10 minutes was also registered from D08E with a value of 0.03 m/s, while the highest minimum velocity was found at anemometer H24W. The value was 0.83 m/s. These wind data are seen in table 5.

With regards to the mean horizontal velocity, anemometer H18W showed the highest mean value being 7.52 m/s for the 10-minute period. The lowest mean was recorded at D08E; 4.21 m/s. For the same reason as in 4.1.1, the horizontal velocity values of the deck anemometers are omitted when calculating the mean of the entire time-series. With this in mind, the mean horizontal velocity was 6.70 m/s.

The standard deviation is in the interval [2.125-2.798] with the lowest value from anemometer H24W and the highest from H10E.

The mean wind direction in this time-series is 239.8 degrees. This constitutes to a wind flow from south-west. The variation of wind direction from H08Wb, H08Wt and H08E is presented in figure 16.

Table 5: Wind data from 23/09/21

	Wind data 23/09/21 - 10.00.00										
Anemometers	H08Wb	H08Wt	H08E	D08W	D08E	H10W	H10E	H18W	H18E	H20W	H24W
Max velocity [m/s]	17.3700	16.6200	16.6100	14.7100	14.3000	14.6000	16.4900	16.6200	0.0000	16.0900	15.1300
Min velocity [m/s]	0.0600	0.1100	0.0700	0.0600	0.0300	0.3000	0.0200	0.0800	0.0000	0.0800	0.8300
Mean [m/s]	6.2004	6.0481	6.1768	5.5207	4.2068	5.9813	6.6873	7.5204	0.0000	7.4675	7.4949
Standard deviation	2.4768	2.3783	2.7002	2.2718	2.2888	2.7570	2.7982	2.7884	0.0000	2.6184	2.1252

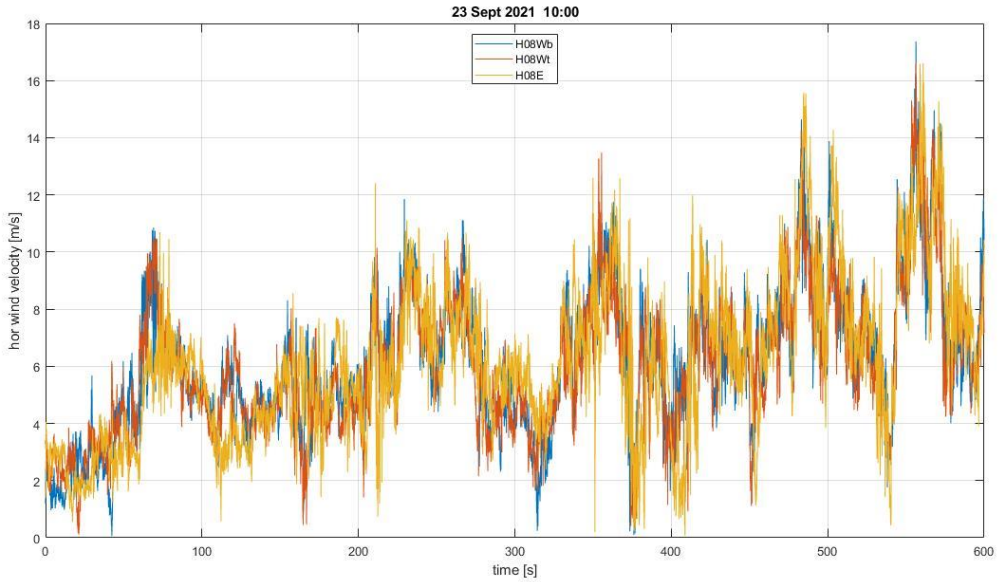

Figure 15: Variation of horizontal wind velocity for selected anemometers

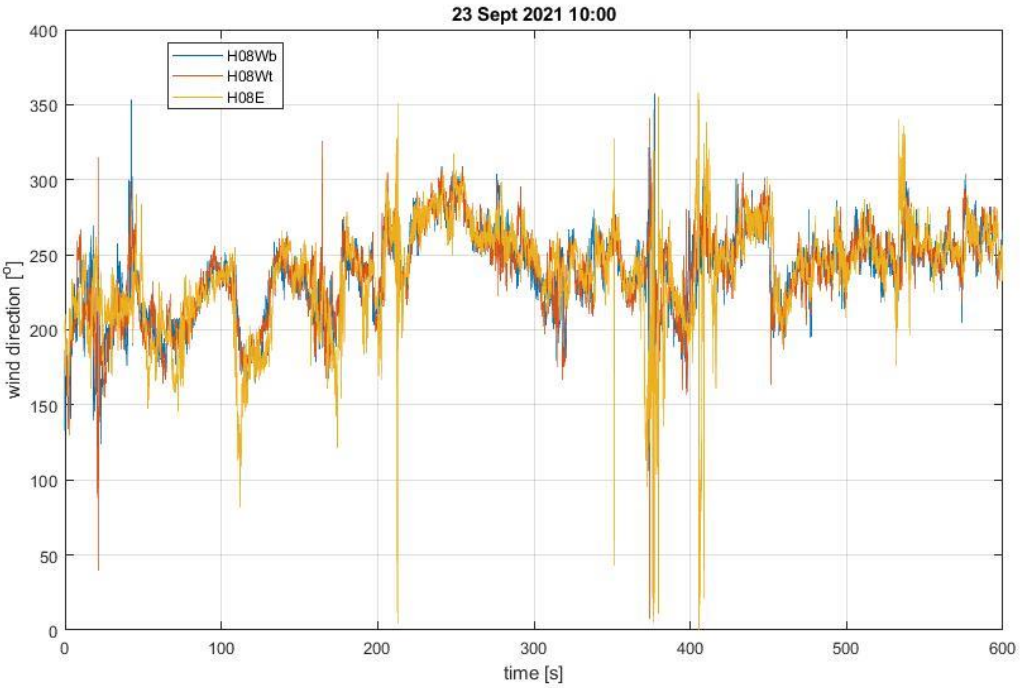

Figure 16: Variation of wind direction for selected anemometers

4.2.2 Vertical velocity and vertical angle

The general vertical wind data is seen in table 6., while the variation in wind velocity is seen in figure 17. In this time-series, the peak vertical velocity was recorded by D08W with a value of 9.70 m/s after 501.1 seconds. The lowest negative velocity was recorded by D08E, at -11.15 m/s after 579.0 seconds. Both the peak and the lowest negative was recorded by the deck anemometers, with the peak upstream of the wind flow and the lowest negative in the wake of the bridge girder.

The same procedure as in chapter 4.1.2 was used to find the mean vertical angle. From this, the mean vertical angle of attack was calculated to 1.49°.

Table 6: Vertical wind data from 23/09/21

	Vertical wind data 23/09/21 - 10.00.00										
Anemometers	H08Wb	H08Wt	H08E	D08W	D08E	H10W	H10E	H18W	H18E	H20W	H24W
Max velocity [m/s]	7.1400	5.4500	7.0400	9.7000	8.8000	0.0000	6.1500	8.1900	0.0000	8.0200	8.8900
Min velocity [m/s]	-5.7200	-5.5700	-6.9100	-10.8300	-11.1400	0.0000	-7.8000	-6.5000	0.0000	-5.5400	-8.7500
Mean [m/s]	0.7041	0.5866	0.0520	0.3510	0.5793	0.0000	-0.0171	0.2983	0.0000	0.1881	0.3275
Standard deviation	1.7041	1.6491	1.4381	2.8947	2.0969	0.0000	1.5397	1.6845	0.0000	1.7692	1.7039

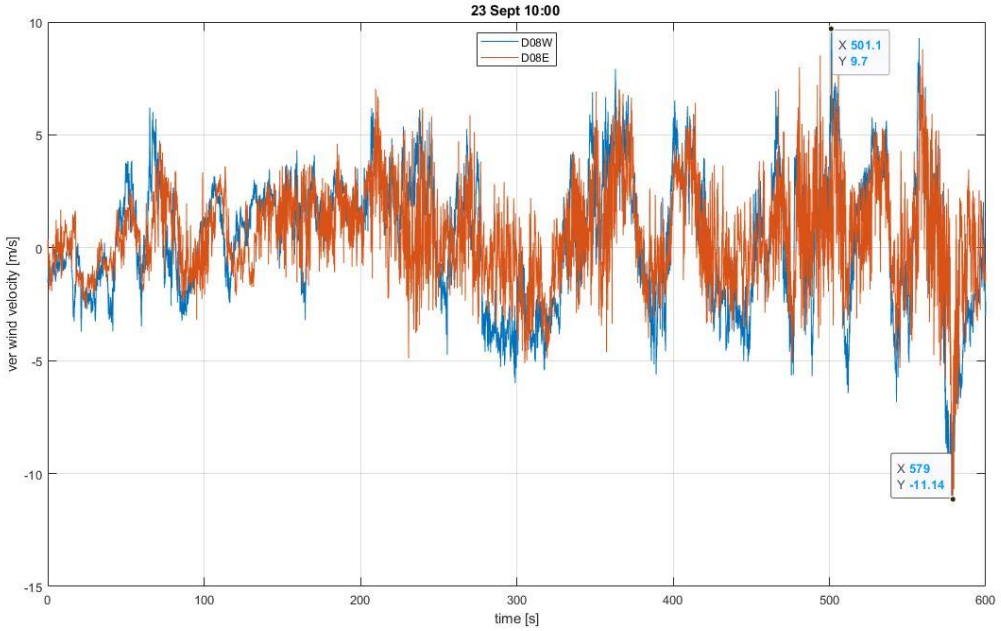

Figure 17: Variation of vertical wind velocity for the anemometers installed at deck level

4.2.3 Turbulence intensity

The turbulence intensity has huge values in this time-series, varying in the interval [28.3%-46.1%]. The lowest value comes from anemometer H24W and the highest from H10W. Again, an outlier value is registered at D08E. This outlier is calculated as $I_u \approx 54.4\%$. With the outlier value, the mean turbulence intensity is $I_u \approx 40.7\%$. Without it, the intensity goes slightly down to $I_u \approx 39.2\%$.

4.2.4 Correlation matrix

H08Wb, H08Wt, H08E and D08W show a high correlation with each other with values at or above 0.7, except for H08E and D08W, where the correlation is 0.65. Other notable correlating pairs are H10W and H10E (0.73) and H18W and H20W (0.7). H08E also has a high correlation with H10W and H10E where the values are 0.708 and 0.697 respectively.

H08Wb shows very high correlation with H08Wt, with a value of 0.877. It also has high correlation with H08E (0.754) and H08W (0.785).

D08E shows little correlation with the other anemometers, with the least correlation with the anemometers that are placed the closest. The same phenomenon as in the data from 09/08/21 is highly likely to be the reason for this observation. Figure 18 illustrates these correlations, while table 7 shows the exact correlation coefficients.

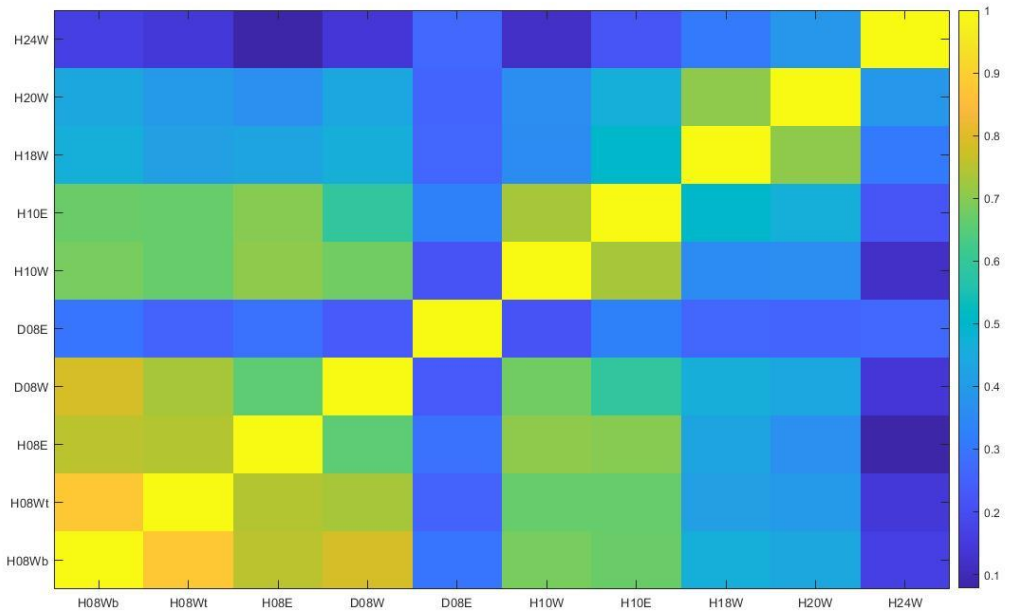

Figure 18: Correlation matrix illustrating the correlation between anemometers in 23/09/21

Table 7: Cross-correlation coefficients for all functioning anemometers

Cross-correlation coefficients - 23/09/21										
H24W	0.1640	0.1435	0.0782	0.1429	0.2708	0.1189	0.2198	0.3097	0.3907	1,0000
H20W	0.4433	0.3961	0.3671	0.4390	0.2618	0.3661	0.4664	0.7062	1,0000	0.3907
H18W	0.4668	0.4160	0.4285	0.4627	0.2633	0.3576	0.5027	1,0000	0.7062	0.3097
H10E	0.6710	0.6680	0.6988	0.5962	0.3299	0.7316	1,0000	0.5027	0.4664	0.2198
H10W	0.6864	0.6673	0.7082	0.6767	0.2130	1,0000	0.7316	0.3576	0.3661	0.1189
D08E	0.2989	0.2548	0.2936	0.2352	1,0000	0.2130	0.3299	0.2633	0.2618	0.2708
D08W	0.7851	0.7333	0.6575	1,0000	0.2352	0.6767	0.5962	0.4627	0.4390	0.1429
H08E	0.7543	0.7474	1,0000	0.6575	0.2936	0.7082	0.6977	0.4285	0.3671	0.0782
H08Wt	0.8777	1,0000	0.7474	0.7333	0.2548	0.6673	0.6680	0.4160	0.3961	0.1435
H08Wb	1,0000	0.8777	0.7543	0.7851	0.2989	0.6864	0.6710	0.4668	0.4433	0.1640
	H08Wb	H08Wt	H08E	D08W	D08E	H10W	H10E	H18W	H20W	H24W

4.2.5 Vertical accelerations

This time-series showed bigger bursts of accelerations over a longer period than the previous data. For H09E and H09W the accelerations start of as somewhat consistent for approximately 200 seconds, ranging between -7.8 m/s^2 and 8.0 m/s^2 before slowly decreasing until the 200 second mark. After this the accelerations increases for both accelerometers with peaks at 24.72 m/s^2 after 255.68 seconds for H09E and 23.40 m/s^2 after 255.7 seconds for H09W. The lowest negative is -22.54 m/s^2 after 253.94 seconds for H09E and 23.75 m/s^2 after 253.92 seconds for H09W. It is notable that both the highest positive and the lowest negative for these accelerometers happens in the same second during this series. Figure 19 illustrates these accelerations.

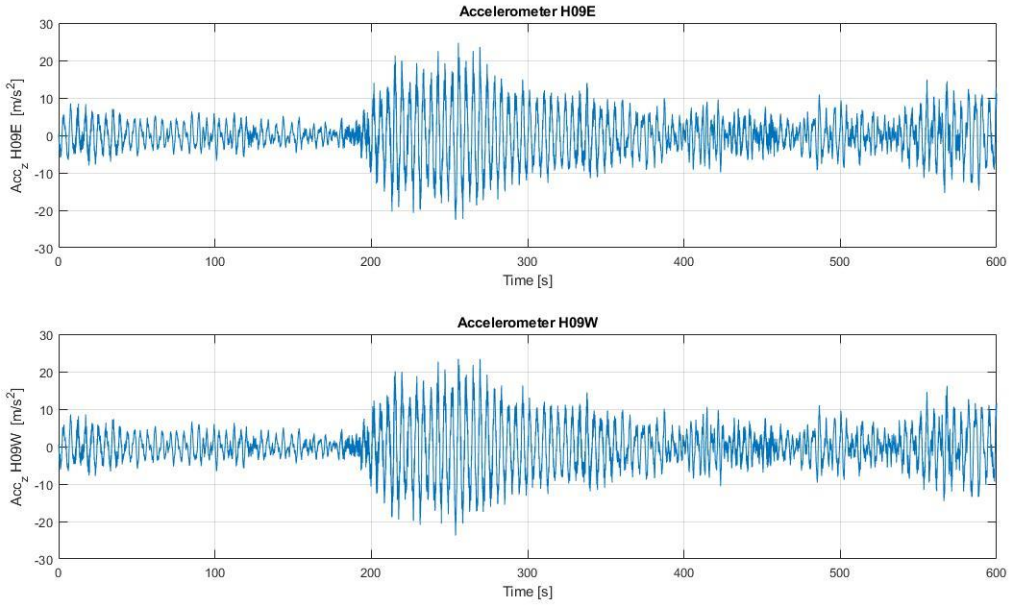

Figure 19: Vertical acceleration of accelerometers installed on H09

The accelerometers H18E and H18W have generally lower acceleration than H09E and H09W but shows three different bursts of accelerations during this 10-minute period. The first one happens at around 200 seconds, which is the same period where H09E and H09W had their extremes. However, the extremes for H18E and H18W is registered during the second burst. H18E has a peak acceleration of 17.19 m/s^2 after 418.44 seconds and a low of -17.91 m/s^2 after 409.88 seconds. H18W has its peak acceleration registered as 18.26 m/s^2 after 408.34 seconds and the lowest negative as -16.55 m/s^2 after 409.90 seconds. This is seen in figure 20.

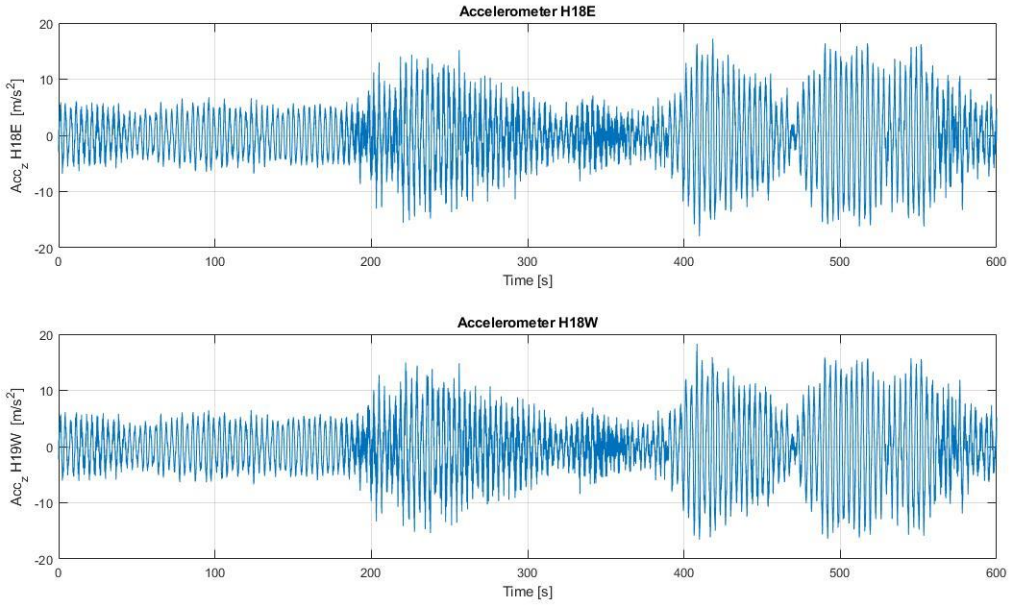

Figure 20: Vertical acceleration of accelerometers installed on H18

H24E and H24W peaks after 233.68 seconds and 220.08 seconds with values of 23.09 m/s^2 and 24.24 m/s^2 respectively. Although the peaks have about 13 seconds between them, the lowest negatives are recorded within one hundredth of a second of one another at 236.04 seconds and 235.94 seconds. Figure 21 illustrates this.

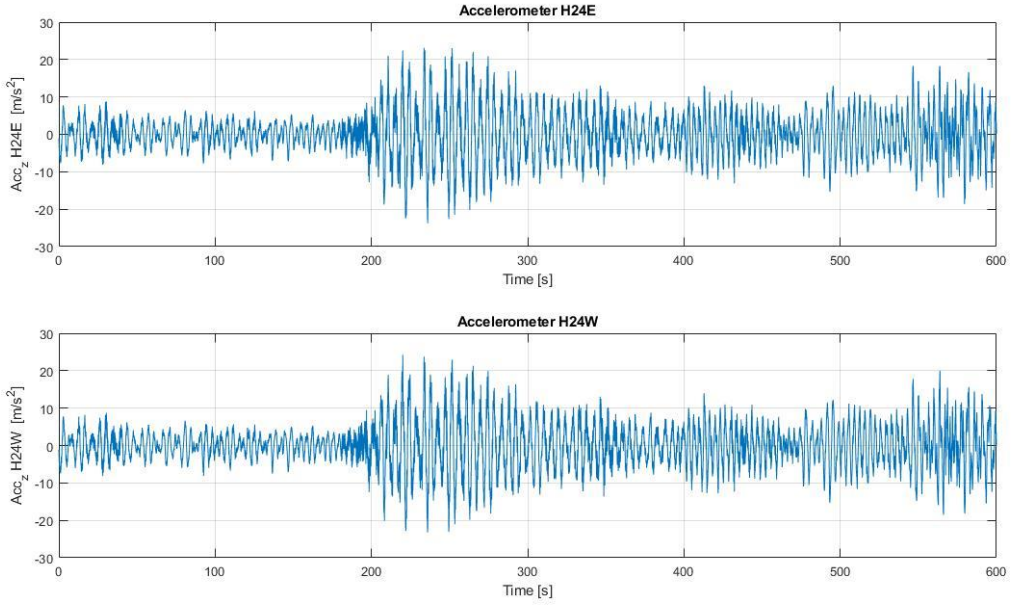

Figure 21: Vertical acceleration of accelerometers installed on H24

4.2.6 Vertical acceleration spectra

As seen in chapter 4.2.5, the accelerations in this time-series are much larger than those of the pervious time-series. This is clearly visible in figures 15-17. As for the spectra, the concentration of vibrations is also much higher than those in chapter 4.1.6. The highest concentration is about 20 times as high, but for the same frequency as that of 4.1.6; 0.220 Hz. This applies to both accelerometers installed on H09 and is seen in figure 18. There are some other concentrations at higher frequencies, but they are miniscule compared to concentration at 0.220 Hz. This acceleration spectra are seen in figure 22.

Figure 23 shows that the acceleration spectra from H18E and H18W shows greater resemblance to the spectra of the other accelerometers in this time-series, as opposed to those from 09/08/21. The vibrations are concentrated at a frequency of 0.293 Hz, higher than the most concentrated frequency for H09E and H09W. Some other concentrations can be seen at higher frequencies, although they are limited compared to the main concentration at 0.293 Hz.

H24E and H24W showed the highest concentration at the same frequency as H09E and H09W, at 0.220 Hz. The accelerations spectra also showed a concentration at about half the magnitude at 0.293 Hz, the same frequency as H18E and H18W. Very small concentrations can be found at higher frequencies, but these are almost negligible compared to the larger concentrations. This is seen in figure 24.

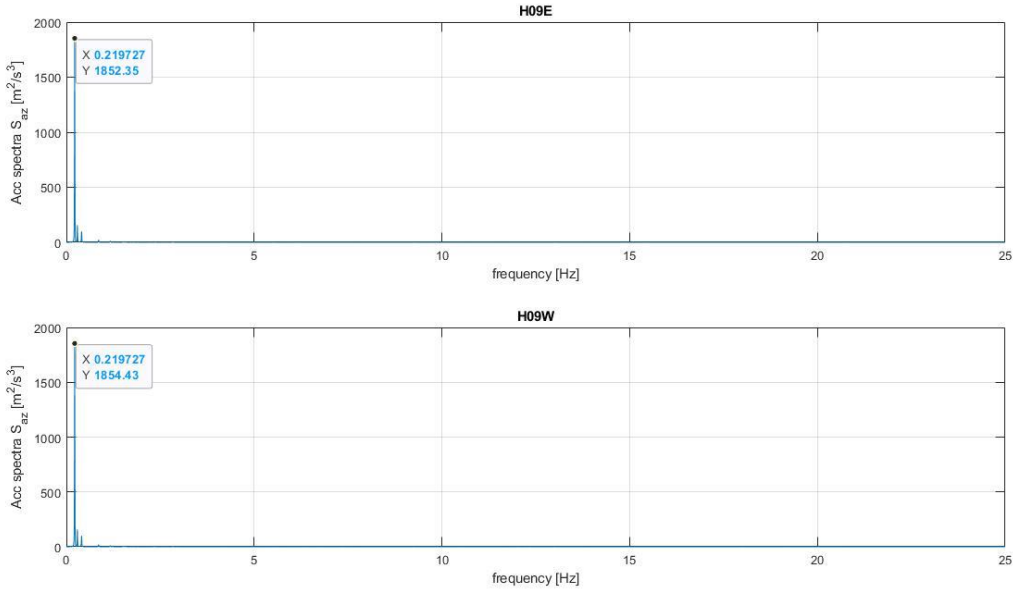

Figure 22: Vertical acceleration spectra from accelerometers installed at H09

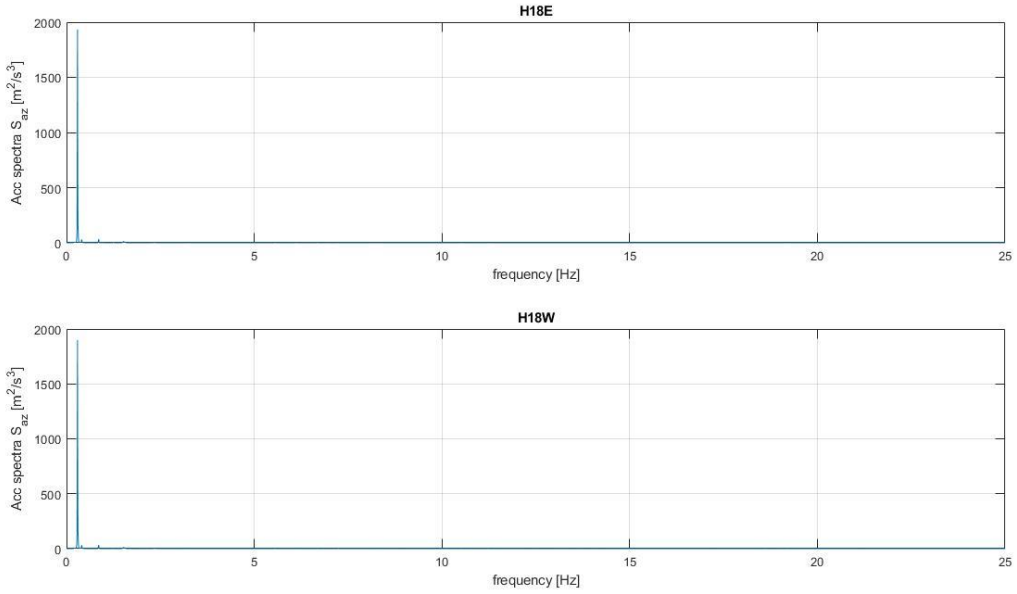

Figure 23: Vertical acceleration spectra for accelerometers installed at H18

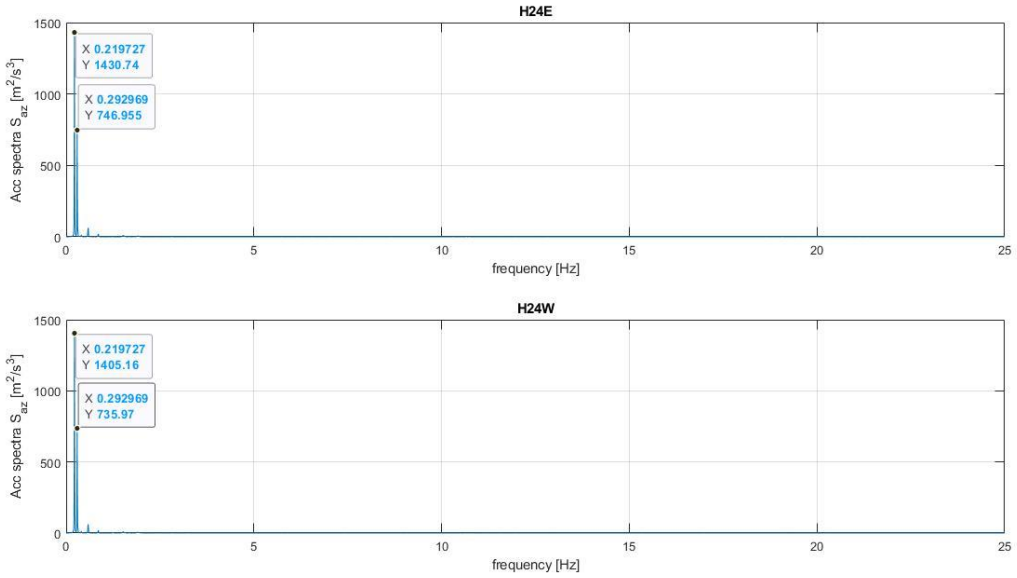

Figure 24: Vertical acceleration spectra for accelerometers installed at H24

4.3 Wind data from 18/10/21 – 13:00:00

Neither of the different datasets from this time-series showed stationarity with regards to the criterium presented in chapter 3.0.

4.3.1 Horizontal velocity and wind direction

This time-series has a registered maximum horizontal velocity at 14.59 m/s from anemometer H18W, recorded at 490 seconds. Figure 25 illustrates this. The lowest maximum velocity was 10.30 m/s, recorded at 506 seconds from H10W. Lowest minimum velocity was registered at D08W with a value of 0.01 m/s, while the highest minimum velocity had a value of 0.50 m/s from anemometer H10W. The background for such a miniscule minimum velocity at D08W was explained in chapter 4.1.1 and is likely due to the change in wind direction during this time-series.

Mean velocity varied from 4.59 m/s at H08Wt and 3.35 m/s at H24W, but the whole time-series the mean was 4.09 m/s. The mean velocities of the deck anemometers are omitted from this calculation. For this series of data, H18W had the highest standard deviation with a value of 2.266. The lowest standard deviation was 1.571 from anemometer D08W. Table 8 illustrates these data.

The mean direction of the wind flow is 154.8 degrees in this series of data. This equals a wind flow from south-east.

Table 8: Horizontal wind data from 18/10/21

	Wind data 18/10/21 - 13.00.00										
Anemometers	H08Wb	H08Wt	H08E	D08W	D08E	H10W	H10E	H18W	H18E	H20W	H24W
Max velocity [m/s]	13.6300	11.0500	11.5300	12.5600	11.0600	10.3000	13.5000	14.5900	0.0000	12.3000	11.1400
Min velocity [m/s]	0.0600	0.0200	0.1400	0.0100	0.0300	0.5000	0.0600	0.0200	0.0000	0.0200	0.0300
Mean [m/s]	4.3557	4.5946	4.5536	3.6386	3.9136	4.1588	4.3793	3.7362	0.0000	3.5633	3.3537
Standard deviation	2.0839	1.8074	1.7967	1.8606	1.5715	1.9739	1.9576	2.2666	0.0000	2.2601	1.8008

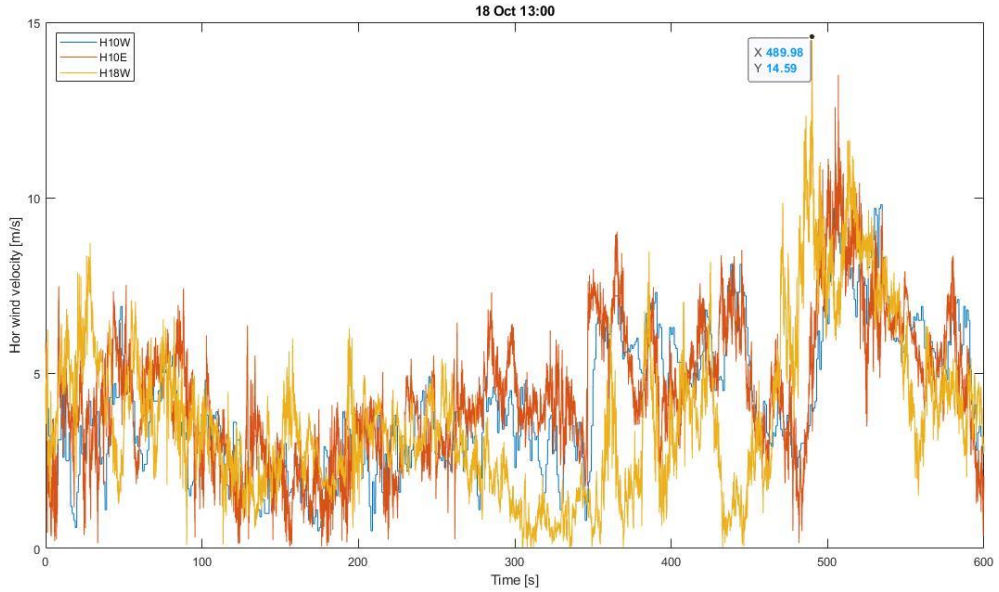

Figure 25: Variation of horizontal wind velocity for H10W, H10E and H18W

4.3.2 Vertical velocity and vertical angle

The peak vertical wind velocity during this time-series was 9.22 m/s, recorded by H08E. It can be seen from figure 26 that this peak is not in line with the trend during the rest of the time-series. It happens abruptly, before the value goes down to a magnitude that is more in line with the other values. This might make one believe that this value can be statistical noise. Different wind data for the time period is presented in table 9.

The variation of the vertical angle-of attack for H08E, D08E, D08W and H10E is very large compared to the angles of previous time periods. Especially for the deck anemometers D08E and D08W the angle deviates a lot. This is seen in figure 27. The reason for this variation might be statistical noise.

Since the mean angle for the four forementioned anemometers are 12.82°, 15.86°, 14.59° and 11.73° respectively, the mean for the whole time period will be larger than in previous chapters. With these large values included, the mean is calculated as 6.55°. If these large values are omitted, the mean vertical angle-of attack is 0.99°, a value that is more in line with the mean vertical angles of the other time-series.

Table 9: Vertical wind data from 18/10/21

	Vertical wind data 18/10/21 - 13.00.00										
Anemometers	H08Wb	H08Wt	H08E	D08W	D08E	H10W	H10E	H18W	H18E	H20W	H24W
Max velocity [m/s]	4.1900	5.0800	9.2200	5.7900	7.8300	0.0000	6.7800	4.8500	0.0000	4.7700	4.3500
Min velocity [m/s]	-4.5000	-3.6500	-4.9200	-5.6400	-6.4800	0.0000	-5.9600	-5.0700	0.0000	-4.4900	-4.2700
Mean [m/s]	-0.0428	0.1322	0.8521	1.0754	0.8388	0.0000	0.6594	-0.0809	0.0000	-0.1199	-0.1694
Standard deviation	1.0188	1.0839	1.8208	1.6320	2.2148	0.0000	1.6923	1.1084	0.0000	1.1441	1.0847

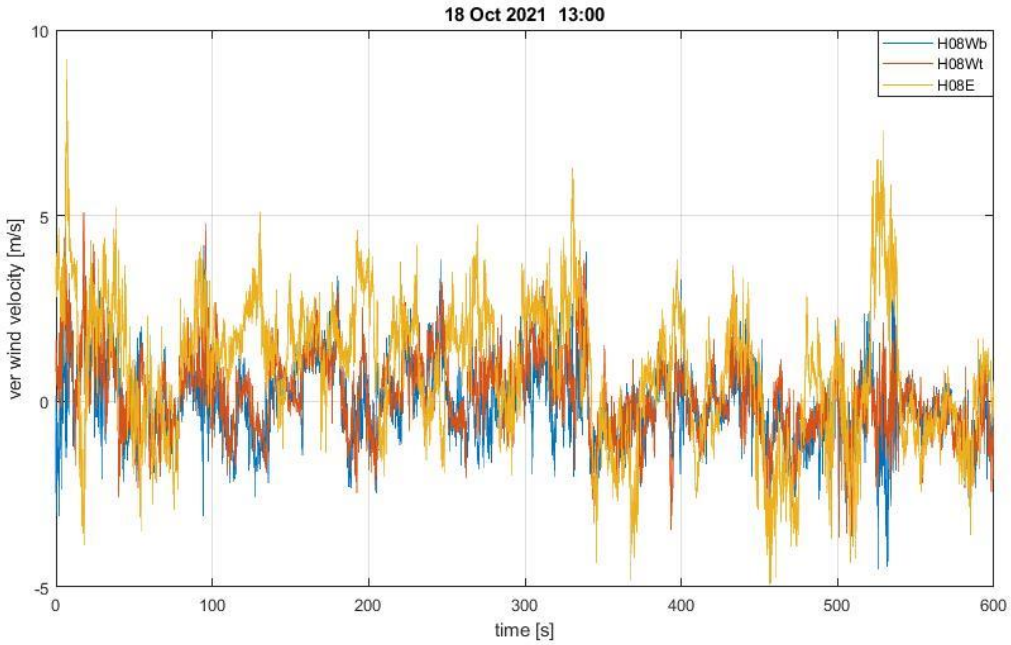

Figure 26: Variation of vertical wind velocity for specified anemometers

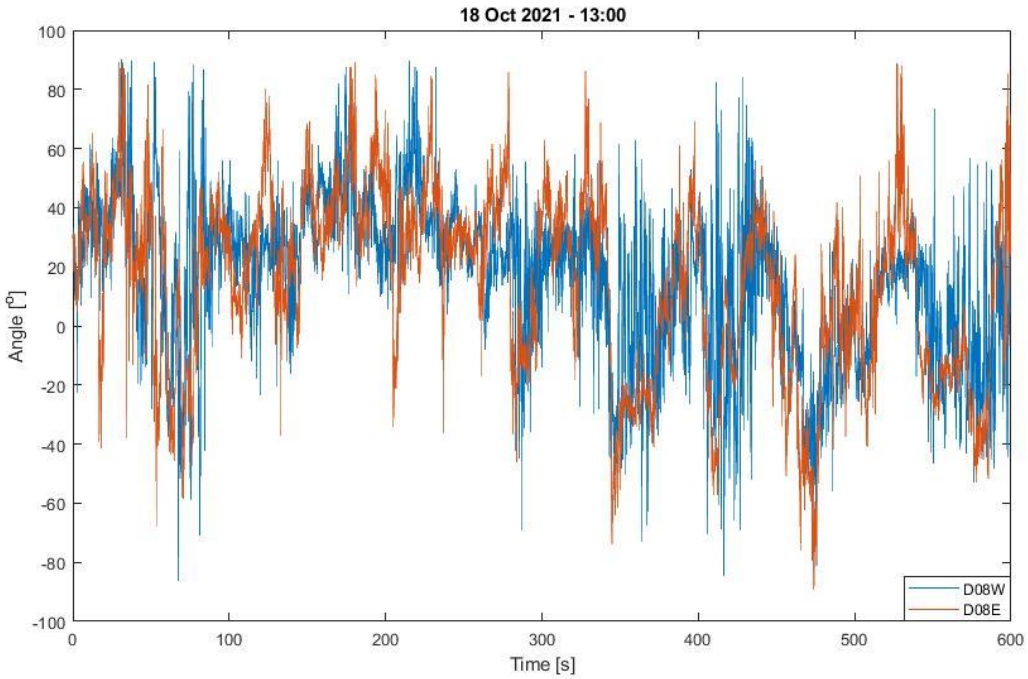

Figure 27: Variation of vertical angle for the deck anemometers

4.3.3 Turbulence intensity

In this time-series the turbulence intensity also has extremely high values, ranging from 39.3% at H08Wt to 63.4% at H20W. The mean turbulence intensity is 48.8%. For this south-east wind direction, the turbulence intensity of the deck anemometers was more in line with the rest of the anemometers.

4.3.4 Correlation coefficients

The correlation matrix is presented in figure 28, while the exact coefficients is presented in table 10. H08E shows less of a correlation with its neighbouring anemometers during this 10-minute time-series than the previous series, with values slightly below 0.7. H10W have a high correlation with H08Wb and H08Wt, where the correlation value is 0.738 and 0.730.

H18W, H20W and H24W shows generally lower correlation with the other anemometers than in the previous time-series, but higher correlation with each other.

As opposed to the earlier data where D08E showed the least correlation with the other anemometers, in this time-series it is D08W that shows very low correlation with any of the others. The highest correlation D08W has is 0.391 with H08Wt. This illustrates that the flow of the wind has changed direction as opposed to previous time-series. Here it comes from the south-east and since D08W is mounted at deck level it will not experience the same wind flow as the rest of the anemometers. The wind will curve around the bridge deck before it is registered at D08W and will behave in a more random way as opposed to the wind registered by the other anemometers.

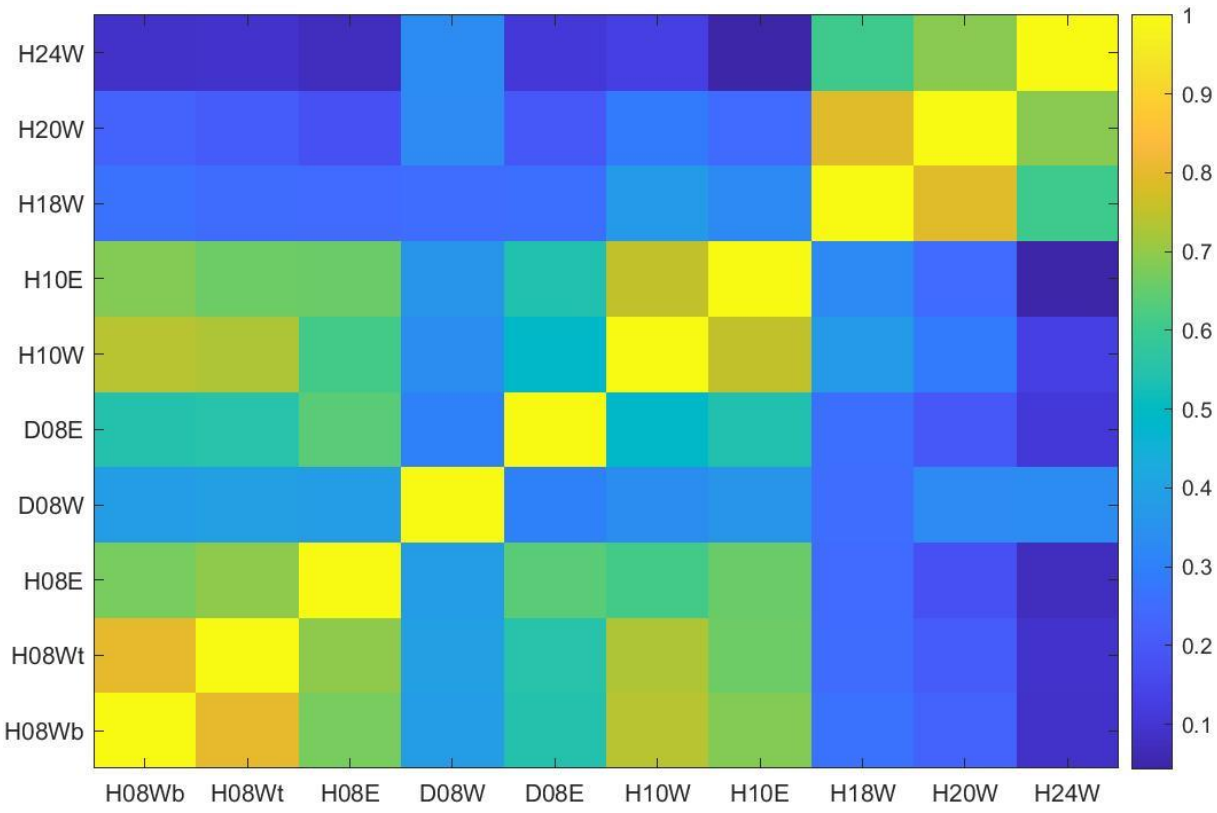

Figure 28: Correlation matrix illustrating the correlation between anemometers in 18/10/21

Table 10: Cross-correlation coefficients for all functioning anemometers

Cross-correlation coefficients - 18/10/21										
H24W	0.0912	0.0939	0.0762	0.3330	0.1128	0.1352	0.0429	0.6052	0.6902	1.0000
H20W	0.2271	0.2081	0.1769	0.3270	0.2019	0.2880	0.2455	0.7938	1.0000	0.6920
H18W	0.2654	0.2522	0.2459	0.2542	0.2583	0.3727	0.3265	1.0000	0.7938	0.6052
H10E	0.6857	0.6631	0.6592	0.3593	0.5432	0.7509	1.0000	0.3265	0.2455	0.0429
H10W	0.7385	0.7308	0.6127	0.3375	0.4879	1.0000	0.7509	0.3727	0.2880	0.1352
D08E	0.5456	0.5540	0.6386	0.3009	1.0000	0.4879	0.5432	0.2583	0.2019	0.1128
D08W	0.3839	0.3917	0.3838	1.0000	0.3009	0.3375	0.3593	0.2542	0.3270	0.3330
H08E	0.6734	0.6959	1.0000	0.3838	0.6386	0.6127	0.6592	0.2459	0.1769	0.0762
H08Wt	0.8033	1.0000	0.6959	0.3917	0.5540	0.7308	0.6631	0.2522	0.2081	0.0939
H08Wb	1.0000	0.9033	0.6734	0.3839	0.5456	0.7385	0.6857	0.2654	0.2271	0.0912
	H08Wb	H08Wt	H08E	D08W	D08E	H10W	H10E	H18W	H20W	H24W

4.3.5 Vertical accelerations

In this time-series both H09E and H09W have the extremes recorded at the same time, illustrated in figure 29. The peaks of 40.12 m/s^2 and 41.89 m/s^2 are both registered after 514.44 seconds, while the lows of -43.06 m/s^2 and -44.92 m/s^2 are recorded after 119.64 seconds.

H18E and H18W also has the extremes at the same time. Here, the peak acceleration is registered after 119.40 seconds with values of 44.48 m/s^2 and 43.47 m/s^2 respectively. Both accelerometers recorded the lowest negative within two hundredths of a second of the peak accelerations, with values of -40.10 m/s^2 and -39.26 m/s^2 after 119.26 seconds. This is presented in figure 30.

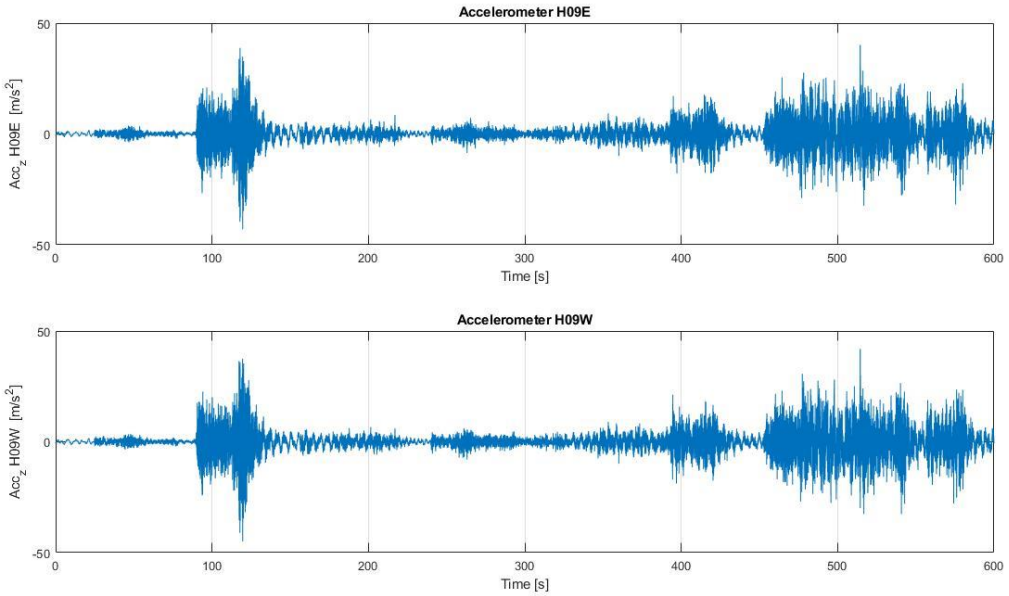

Figure 29: Vertical accelerations of accelerometers installed on H09

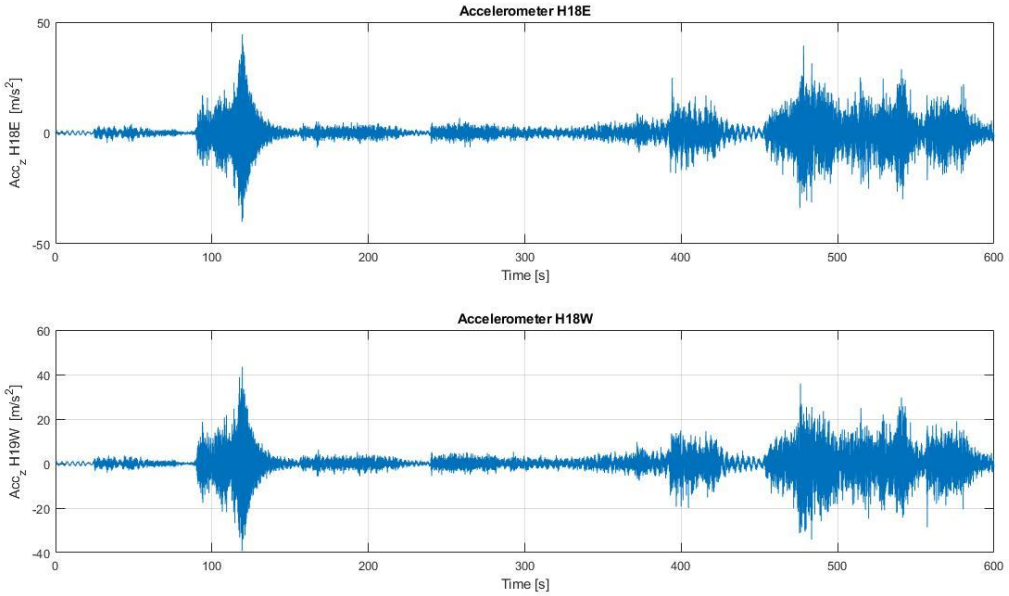

Figure 30: Vertical accelerations of accelerometers installed on H18

For H24E the peak acceleration is recorded at 44.29 m/s^2 after 479.96 seconds, while the lowest negative acceleration happens after 121.24 seconds. The value here is -44.07 m/s^2. H24W has its extremes much closer in time, with the peak acceleration at 43.96 m/s^2 after 117.47 seconds and the lowest negative at -39.48 seconds after 120.54 seconds. These accelerations are presented in figure 31.

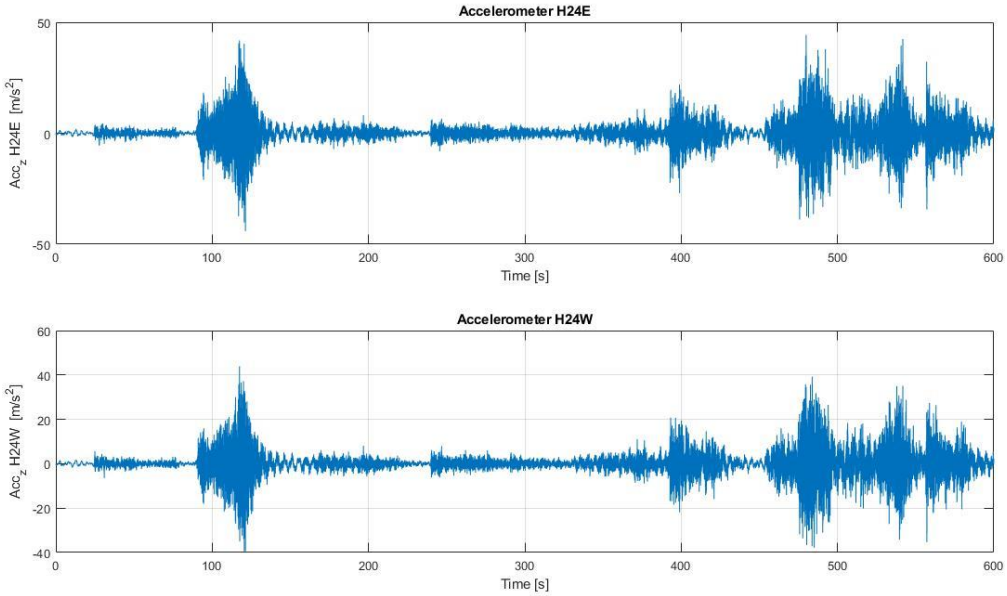

Figure 31: Vertical acceleration of accelerometers installed at H24

4.3.6 Vertical acceleration spectra

In this series the spectra from the accelerometers installed at H09 is presented in figure 32. Multiple noticeable concentrations of vibrations are seen. The first concentration is at 0.214 Hz. The second is a slightly lower concentration at 0.403 Hz. The third and largest concentration is connected to the frequency 4.334 Hz. This high frequency will be further discussed in chapter 5.3.6.

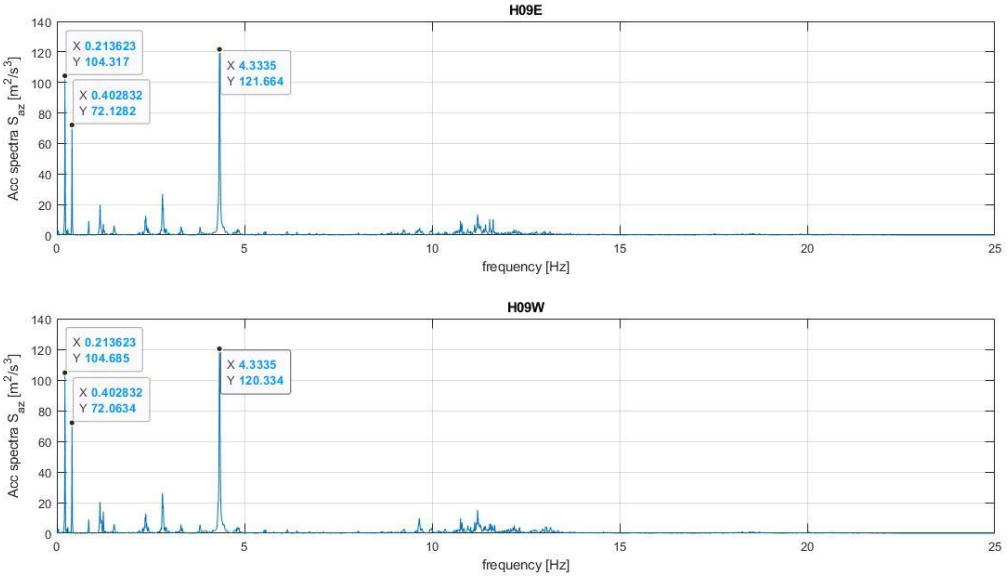

Figure 32: Vertical acceleration spectra from accelerometers installed at H09

The spectra from H18E and H18W has two significant concentrations of vibrations: at 0.293Hz and 4.334 Hz. This is seen in figure 33. The second concentration corresponds to the same frequency as the third from H09E/H09W but has a higher value.

The two largest concentrations from the spectra of H24E and H24W has the same frequency as the two largest concentrations from H09E and H09W. Other concentrations can be seen at frequencies between the two main ones in figure 34, but with substantial lower values.

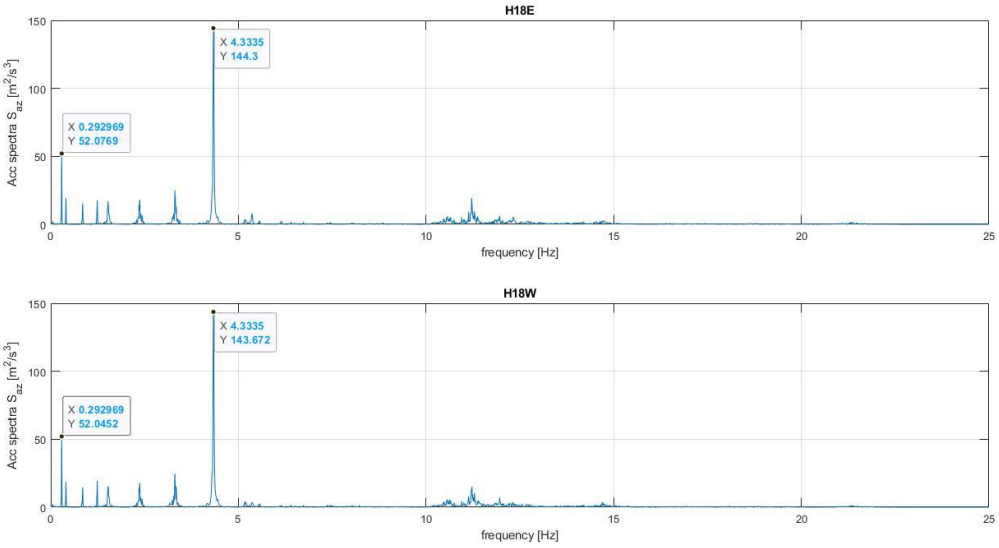

Figure 33: Vertical acceleration spectra from accelerometers installed at H18

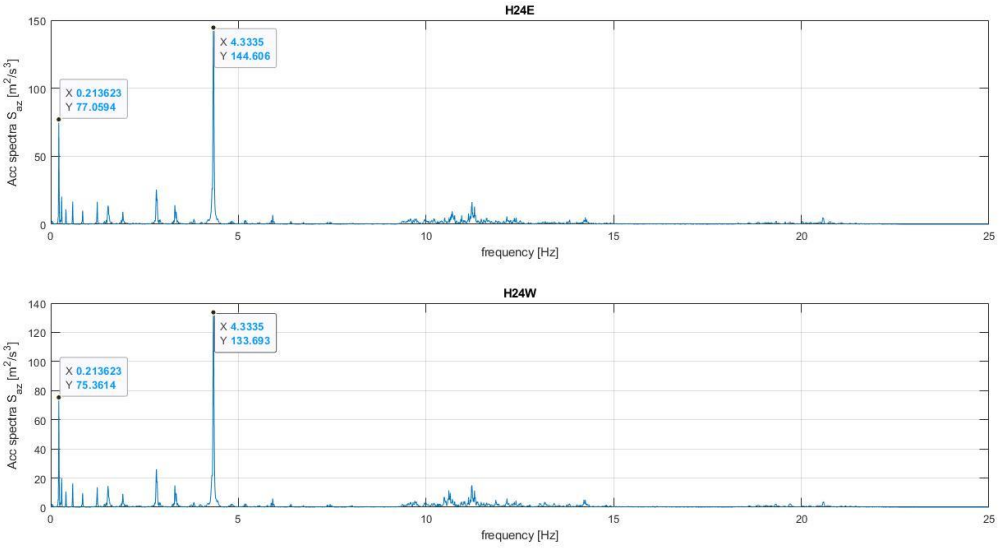

Figure 34: Vertical acceleration spectra from accelerometers installed at H24

4.4 Wind data from 21/10/21 – 15:10:00

The horizontal and vertical velocity, along with the wind direction, did not pass the criterium for stationarity listed in chapter 3.0 during this 10-minute time period.

4.4.1 Horizontal velocity and wind direction

The records from this series of data have the highest recorded maximum wind velocity at 23.24 m/s from anemometer H18W, seen in figure 35. As this value does not follow the general pattern for this time-series, it might be statistical noise. Nevertheless, it is used in further calculations and discussions as it is hard to verify if it is noise or not. D08E recorded the lowest maximum velocity, at 16.73 m/s. The lowest minimum was registered at H20W with a value of 0 m/s. The second lowest value of velocity was 0.01 m/s which was registered from H08Wb, H08Wt and H08E, while the highest minimum was 1.10 m/s recorded at H10W. The general wind data of the time-series is presented in table 11.

For this time-series the highest mean was recorded by H24W, with a value of 6.71 m/s. D08W measured the lowest mean in this series to be 4.04 m/s. Since the deck anemometers does not have the same exposure to the wind flow as the other anemometers, their mean will be omitted when calculating the mean for the entire time-series. This mean is calculated to 6.17 m/s.

This series also had the highest standard deviations, with a peak at 3.715 from anemometer H24W. D08W had the lowest standard deviation with a value of 2.269.

The wind flow has a mean direction of 99.8 degrees. This equals a wind coming almost straight from the east.

Table 11: Horizontal wind data from 21/10/21

	Wind data 21/10/21 - 15.10.00										
Anemometers	H08Wb	H08Wt	H08E	D08W	D08E	H10W	H10E	H18W	H18E	H20W	H24W
Max velocity [m/s]	22.1000	22.6100	22.9100	18.7800	16.7300	17.0000	20.5500	23.2400	0.0000	20.2700	20.0800
Min velocity [m/s]	0.0100	0.0100	0.0100	0.0200	0.0500	1.1000	0.1000	0.0500	0.0000	0.0000	0.0200
Mean [m/s]	6.1150	6.2850	6.1037	4.0440	5.0130	5.6542	5.6584	6.3189	0.0000	6.5465	6.7131
Standard deviation	2.8724	2.7781	2.8012	2.2695	2.3774	2.8602	2.6882	3.4722	0.0000	3.6995	3.7157

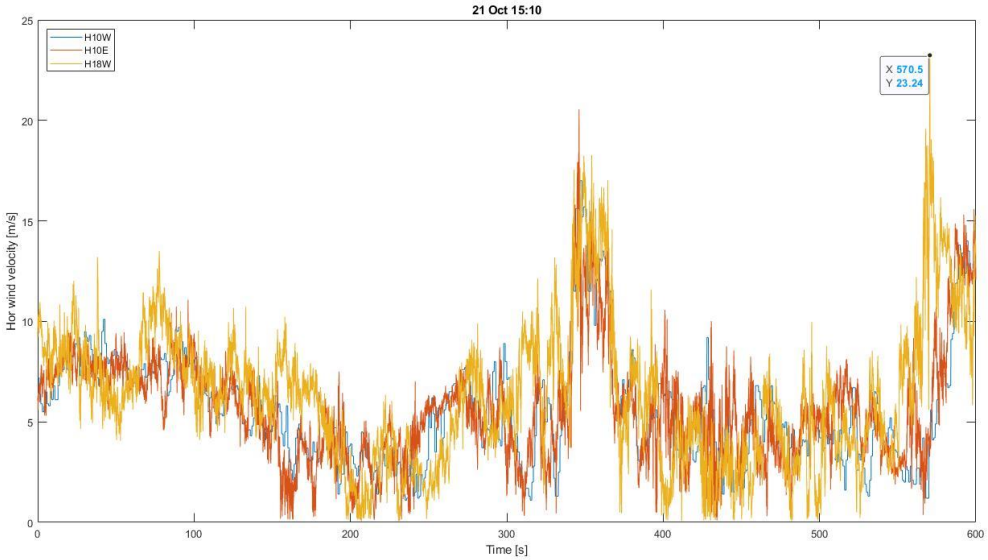

Figure 35: Variation of horizontal wind velocity for H10W, H10E and H18W

4.4.2 Vertical velocity and vertical angle

The general vertical wind data of this time-series is presented in table 12.

The highest vertical velocity is 15.03 m/s, recorded by H08E after 345.9 seconds. The lowest negative velocity is within a second of the peak velocity, recorded by the same anemometer. When looking at figure 36, both the peak and the lowest negative value looks likely to be statistical noise, as it deviates a lot from the general pattern of the time-series. This is, however, quite hard to verify.

The mean vertical attack angle for this ten-minute period was -1.12°, the only mean negative vertical angle-of attack seen from either one of the time-series in this thesis.

Table 12: Vertical wind data for 21/10/21

	Vertical wind data 21/10/21 - 15:10:00										
Anemometers	H08Wb	H08Wt	H08E	D08W	D08E	H10W	H10E	H18W	H18E	H20W	H24W
Max velocity [m/s]	7.5600	6.8600	15.0300	10.6600	10.5300	0.0000	12.2200	7.0000	0.0000	4.8100	7.1100
Min velocity [m/s]	-8.5900	-9.8300	-15.5500	-12.0200	-15.0000	0.0000	-10.6200	-7.6900	0.0000	-6.4300	-7.7600
Mean [m/s]	-0.2358	-0.1250	0.2750	0.3416	-0.1389	0.0000	0.2817	-0.2819	0.0000	-0.1682	-0.0898
Standard deviation	1.4307	1.7139	2.3109	2.3772	2.9103	0.0000	2.4052	1.5598	0.0000	1.4895	1.3348

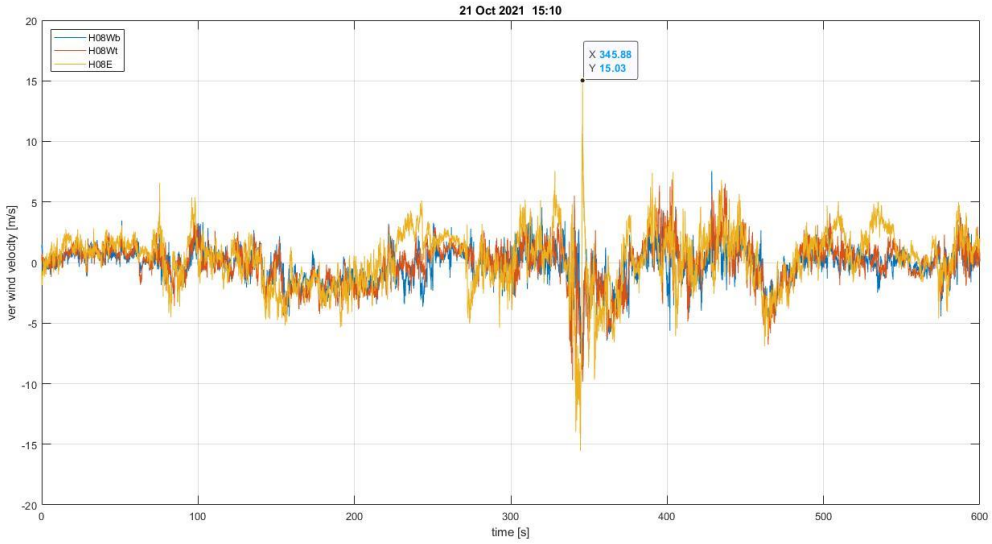

Figure 36: Variation of vertical wind velocity for H08Wb, H08Wt and H08E

4.4.3 Turbulence intensity

The lowest turbulence intensity in this time-series is 44.2%, recorded at H08Wt. The highest comes from H20W and is 56.5%. There is no notable outlier outside of this interval and the mean turbulence intensity is 50.6%.

4.4.4 Correlation coefficients

In general, this correlation matrix shows higher correlation between all anemometers than the previous data. This is seen from figure 37. The three first shows very high correlation with each other, with values in the interval [0.747-0.849]. D08E, H10W and H10E correlates moderately with the three first and each other. H10W and H10E does however correlate strongly with a value of 0.777. The last three, H18W, H20W and H24W, does also correlate more than in the previous data. The exact correlation coefficients are presented in table 13.

As seen in the data from 18/10/21, D08W does only faintly correlate with the other anemometers. The highest correlation is with the closest one, D08E, where the correlation value is 0.245. This is due to the same fact as in 18/10/21, that the flow of wind comes from north north-east and curves around the bridge deck before being registered at D08W.

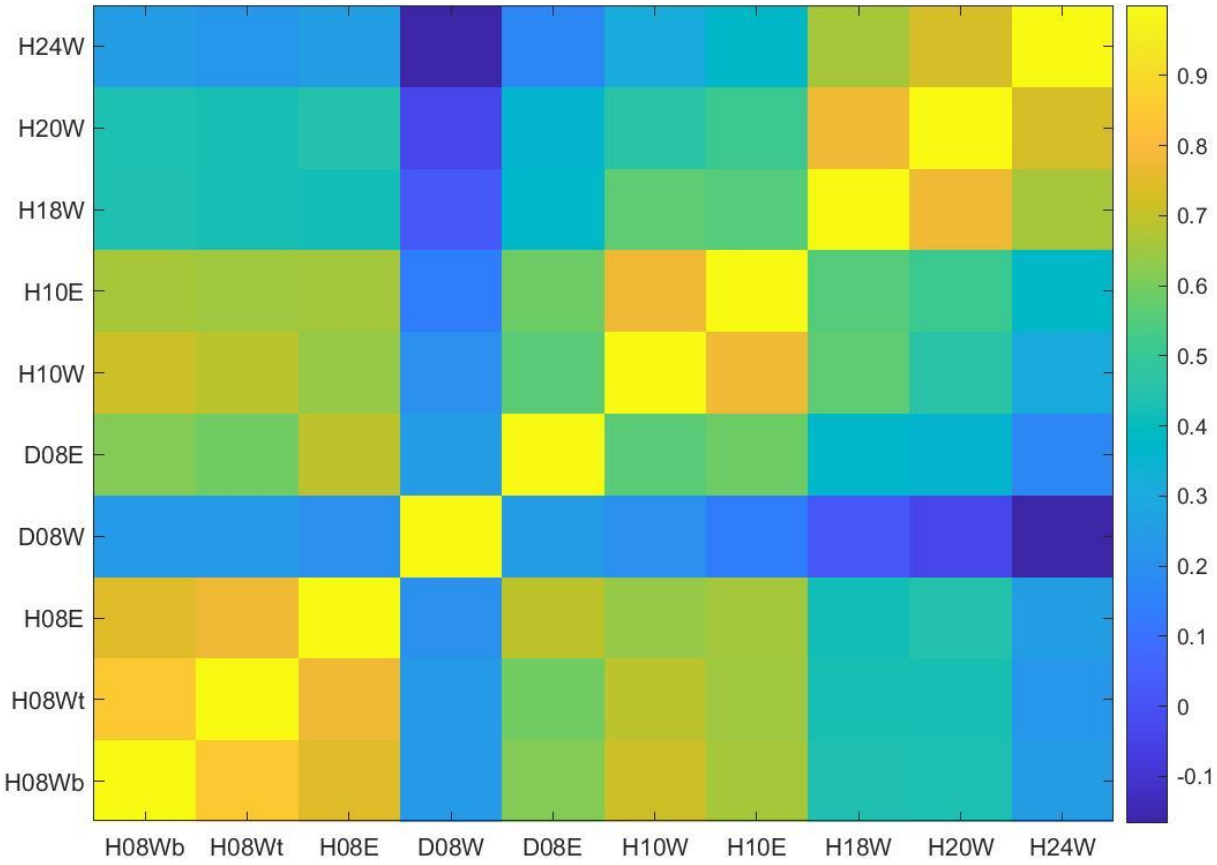

Figure 37: Correlation matrix illustrating the correlation between the anemometers

Table 13: Cross-correlation coefficients for all functioning anemometers

Cross-correlation coefficients - 21/10/21										
H24W	0.2457	0.2265	0.2569	-0.1669	0.1722	0.3037	0.3792	0.6591	0.7296	1,0000
H20W	0.4338	0.4299	0.4463	-0.0376	0.3533	0.4606	0.5081	0.7805	1,0000	0.7296
H18W	0.4355	0.4302	0.4204	0.0234	0.3672	0.5640	0.5499	1,0000	0.7805	0.6591
H10E	0.6625	0.6508	0.6553	0.1349	0.5894	0.7776	1,0000	0.5499	0.5081	0.3792
H10W	0.7148	0.6880	0.6394	0.1981	0.5611	1,0000	0.7776	0.5640	0.4606	0.3037
D08E	0.6145	0.5928	0.6914	0.2458	1,0000	0.5611	0.5894	0.3672	0.3533	0.1722
D08W	0.2371	0.2391	0.2030	1,0000	0.2458	0.1981	0.1449	0.0234	-0.0376	-0.1669
H08E	0.7476	0.7793	1,0000	0.2030	0.6914	0.6394	0.6553	0.4204	0.4463	0.2565
H08Wt	0.8496	1,0000	0.7783	0.2391	0.5928	0.6880	0.6508	0.4302	0.4299	0.2265
H08Wb	1,0000	0.8496	0.7476	0.2371	0.6145	0.7148	0.6625	0.4355	0.4338	0.2457
	H08Wb	H08Wt	H08E	D08W	D08E	H10W	H10E	H18W	H20W	H24W

4.4.5 Vertical acceleration

The last time-series considered in this thesis showed two main bursts of accelerations of the bridge. At H08E the peak acceleration was 33.47 m/s^2 after 150.24 seconds. The lowest negative happened during the same second, after 150.50 seconds and the value was -23.90 m/s^2. H08W also had its peak recorded during the same second as H08E, after 150.56 seconds, with a value of 31.16 m/s^2. The lowest negative, however, was recorded after 139.24 seconds with a magnitude of -25.66 m/s^2. This is seen from figure 38.

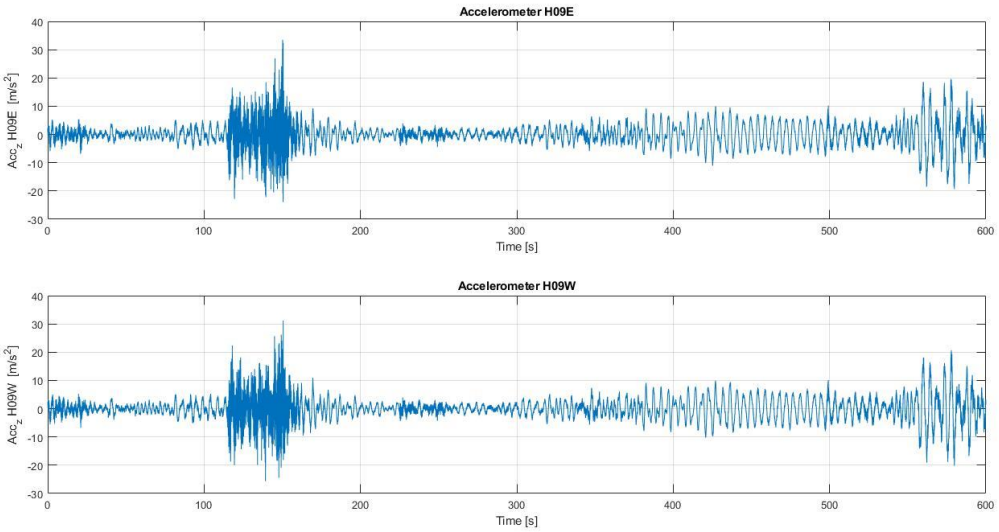

Figure 38: Vertical acceleration of accelerometers installed at H09

H18E and H18W had its peaks registered inside the same second, after 577.56 seconds and 577.70 seconds respectively. The values of the peaks are 28.16 m/s^2 and 26.73 m/s^2. The lowest negatives are also recorded inside the same second, after 572.30 seconds for H18E and 572.32 seconds for H18W. The values were -27.04 m/s^2 and -24.50 m/s^2. These accelerations is seen in figure 39.

H24E showed the largest discrepancy with regards to the vertical accelerations in this time-series. The peak acceleration was registered as 28.25 m/s^2 after 121.82 seconds, while the lowest negative was -30.64 m/s^2 after 570.98 seconds. H24W had its peak after 149.18 seconds where the acceleration was 26.77 m/s^2. The lowest negative acceleration was recorded as -31.55 m/s^2 after 125.12 seconds. Figure 40 illustrates this.

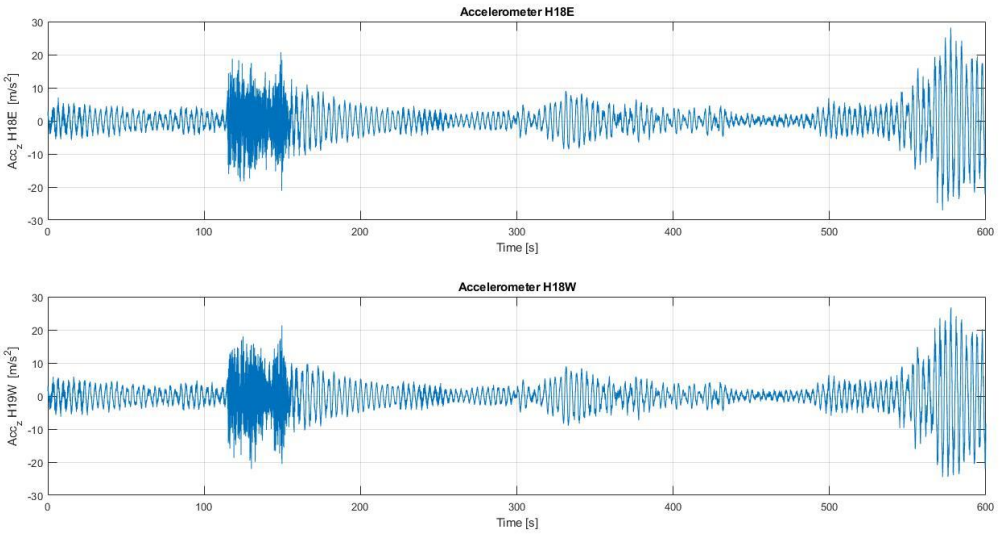

Figure 39: Vertical accelerations of accelerometers installed at H18

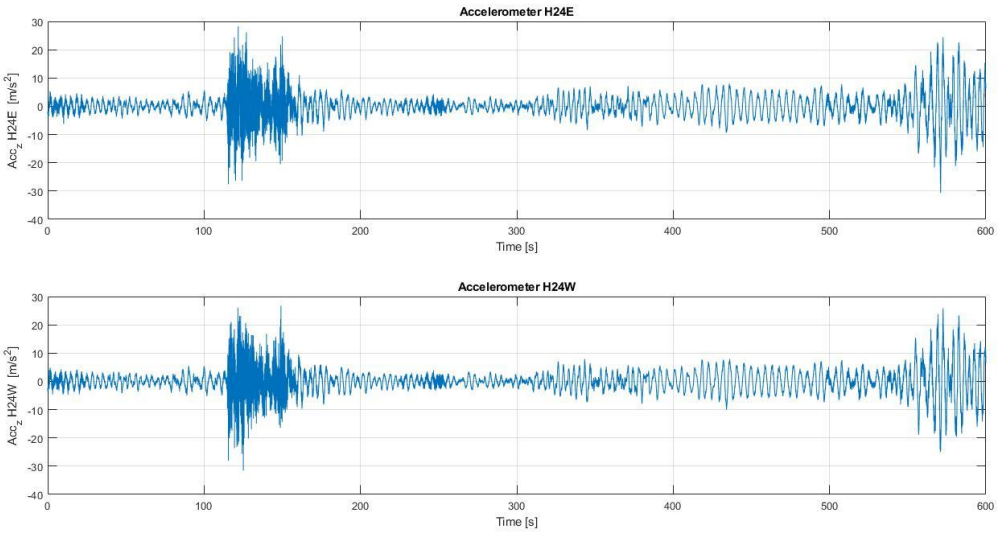

Figure 40: Vertical accelerations of accelerometers installed at H24

4.4.6 Vertical acceleration spectra

There are two significant concentrations of vibrations seen from the acceleration spectra from H08E and H08W, seen in figure 41. They correspond to a frequency of 0.226 Hz and 0.410 Hz. A smaller concentration can be seen between these frequencies, but the magnitude is small compared to those of the forementioned frequencies.

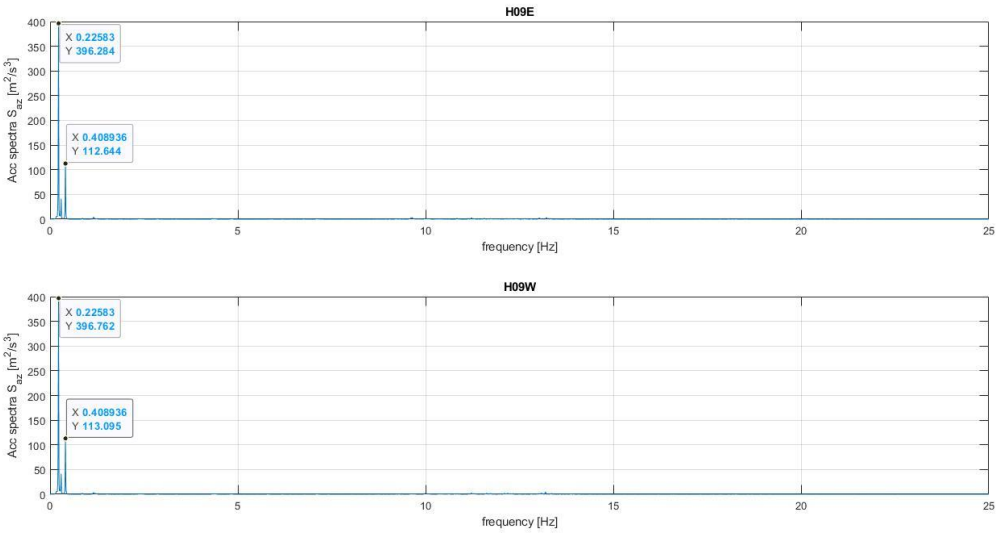

Figure 41:Vertical accelerations spectra from accelerometers installed at H09

For the acceleration spectra for H18E and H18W, the largest concentration corresponds to a frequency of 0.293 Hz. This is seen in figure 42. Another, but very small concentration can be seen at 0.410 Hz. This smaller concentration is at the same frequency as the second concentration seen from the spectra of H09E/H09W, but at a much smaller magnitude.

From figure 43, it is seen that the two main concentrations of H24E and H24W correspond to 0.226 Hz and 0.293 Hz. Both frequencies are the same as the first main concentration of the two other pairs of accelerometers respectively. Other concentrations are so small that they are negligible.

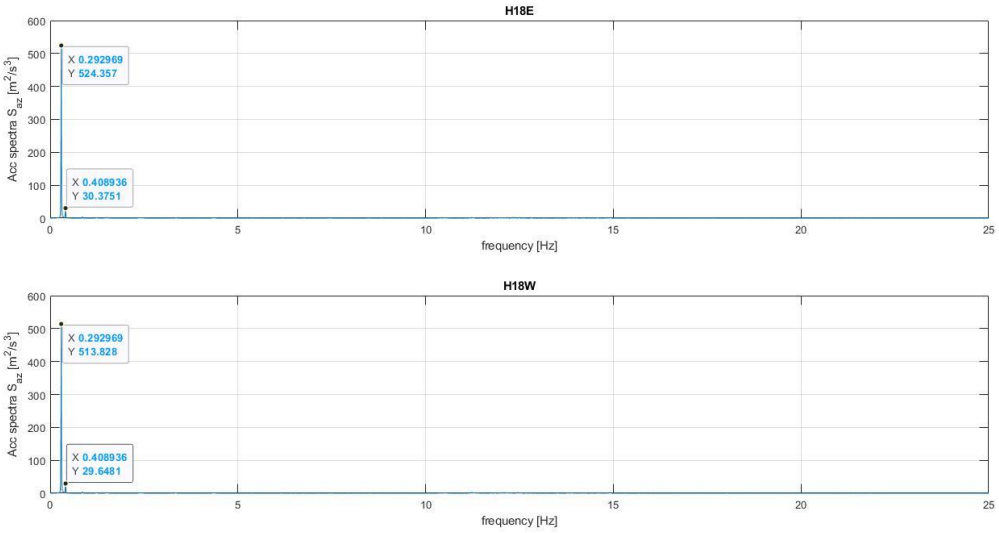

Figure 42: Vertical accelerations spectra from accelerometers installed at H18

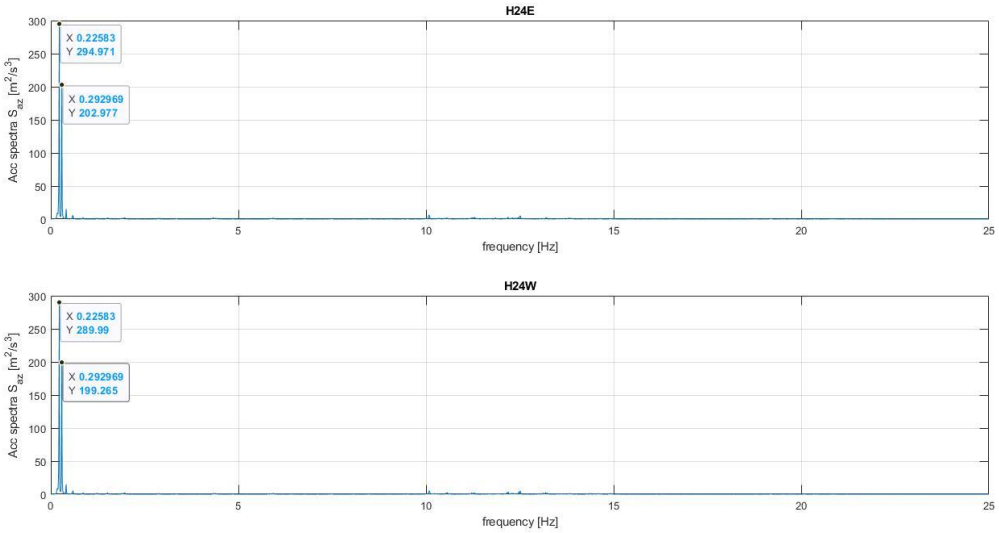

Figure 43: Vertical acceleration spectra from accelerometers installed at H24

5.0 Discussion

In this part of the thesis, the results and findings from chapter 4 will be further discussed. The different data from both the anemometers and the accelerometers will be compared and put into context to see what most likely causes the different reactions of the instruments on the Lysefjord bridge.

5.1 Wind data from 09/08/21 – 14:30:00

5.1.1 Horizontal wind velocity

As mentioned in chapter 3.1.1 the maximum horizontal velocity was 9.32 m/s, registered at H10E. This corresponds to a wind flow of 33.55 km/h. The mean velocity was somewhat consistent, except for the one anemometer installed at the east side at deck level of the bridge. D08E showed a mean horizontal velocity of 3.28 m/s, which is a dip of almost 2 m/s from the mean of 5.41 m/s. This is highly likely since the wind direction in this time-series mainly came from the south-west, with a mean wind direction of 221.35° relative to the bridge. The bridge deck will act as a kind of buffer from the wind and D08E will not be exposed to the same flow as the other anemometers that are installed freely exposed to the wind. D08E also had the highest standard deviation at 1.05, barely higher than H18W with a value of 1.039. The mean standard deviation was 0.79. The values for the mean horizontal wind velocity and the standard deviations can be seen in figure 44.

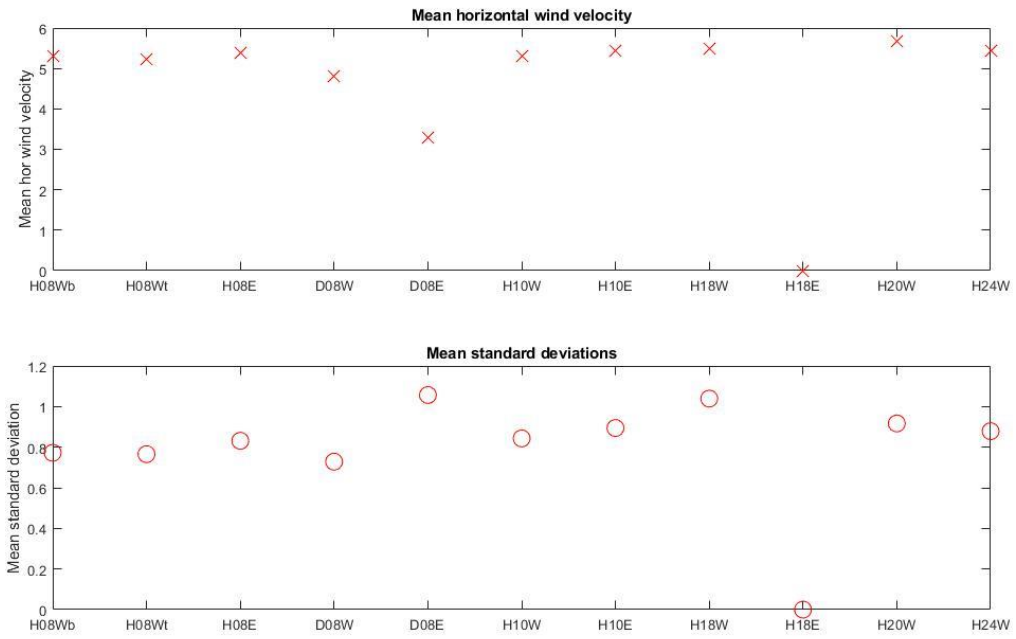

Figure 44: Mean horizontal velocity and mean standard deviation for each anemometer

5.1.2 Vertical wind velocity and vertical angle

The vertical wind velocity fluctuates between positive and negative values depending on whether the wind flows upwards or downwards onto the bridge. Therefore, the mean vertical wind velocity is not that good of a pointer as it will most likely show values around zero. This is the case for this time-series, as the mean velocity is 0.15 m/s. The standard deviation is mostly lower than that of the horizontal wind velocity, except for D08W and D08E which has notably higher values than the rest of the anemometers. The values can be seen in table 3 in chapter 4.1.2, where the mean is 0.72.

The vertical angle of the wind varied a lot through the 10-minute time period and for the different anemometers. It did however show some correlation with the wind direction, with the angle changing relatively abruptly as the direction of the wind changed. This is a quite natural and logical behaviour though. Figures 45 and 46 shows the variation in vertical angles and the wind direction. It is seen that when the wind direction ≈ >225°, the vertical angle is positive while a wind direction ≈ <225° gives a vertical angle that is negative for this anemometer. H10E is more stable with regards to wind direction, which in turn makes the vertical angle more stable as well.

The mean vertical angle varies in the interval [-1.32-4.33] between the different anemometers, with a grand mean vertical angle of 1.65°.

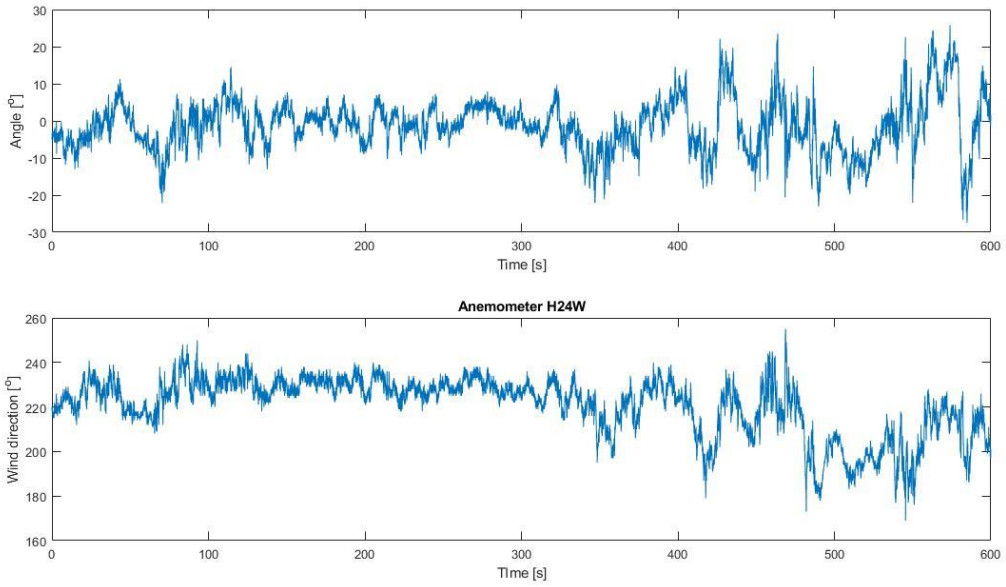

Figure 45: Vertical angle and wind direction at H24W

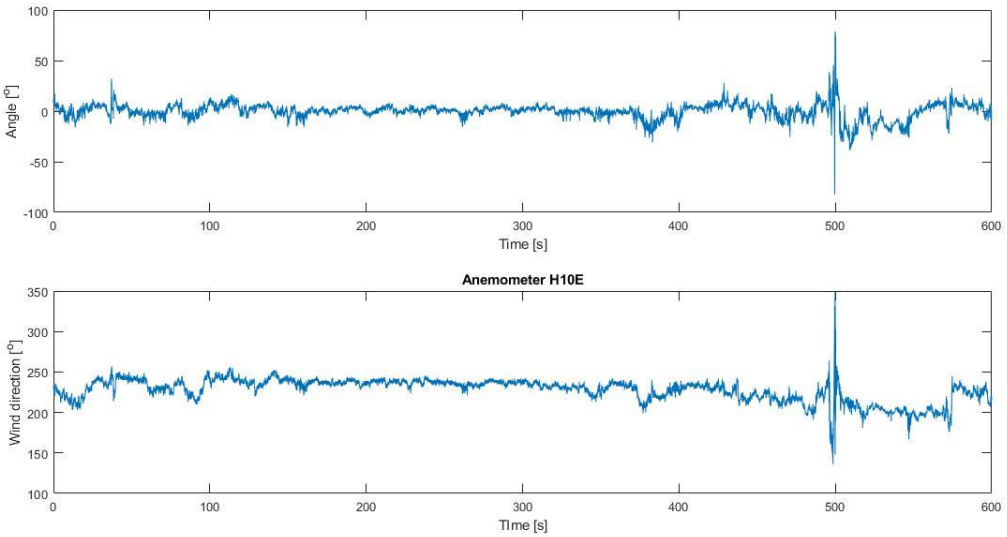

Figure 46: Vertical angle and wind direction at H10E

5.1.3 Turbulence intensity

As reported by Cheynet et al. [27], for a wind blowing from south-west, i.e., towards the inside of the fjord, with a mean wind speed less than 14 m/s and a wind direction between 175° and 195°, the wind is highly turbulent with $I_u \approx 19\%$. When the direction is between 210° and 230° and the mean wind speed is higher than 14 m/s associated a turbulence intensity $I_u \approx 15\%$.

From the data analysed during the 10-minute time period in question, a mean turbulence intensity was found $I_u = 17.6\%$ with the wind direction 221.35° and a mean horizontal wind velocity of 5.13 m/s. This mean turbulence intensity is included with the abnormal value from D08E where $I_u = 32.9\%$. This abnormally high value compared to the others is likely because D08E is installed at deck level and on the opposite side of the bridge related to the wind flow. Since the mean wind velocity is relatively low the wind will curve around the bridge deck and when it reaches the east side, it will behave much more random than on the western side where the flow hits the anemometers directly. If the value from D08E is disregarded, the mean turbulence intensity is calculated to $I_u = 15.9\%$. This corresponds more with the data found by Cheynet et al. [27], although the mean wind speed is much lower in the data analysed in this thesis than that of [27].

5.1.4 Correlation coefficients

With regards to the horizontal wind velocity, it is seen from figure 8 in chapter 4.1.4 that the first three anemometers (H08Wb, H08Wt and H08E) correlate greatly with each other. The values here are all above 0.7. H10E, H18W, H20W and H24W does not correlate to the same degree. The values here are mostly below 0.4. H18W and H20W does however correlate strongly, which is natural as they are close to each other in distance and installed on the same side of the bridge.

The most notable correlations between the anemometers when it comes to horizontal wind velocity is that the first four mostly shows relatively high correlation with each other with values above 0.7.

D08W correlates mostly with H08Wb. The last four does not correlate with each other to the same degree, with values below 0.4. H18W and H20W does however correlate strongly with a value of 0.7.

The most notable from the correlation matrix is that D08E shows little to no correlation with the rest of the anemometers. It is the only instrument that shows a negative correlation, in particular with H20W where the value is -0.801.

This is due to the wind direction in this time-series coming from the south-west. D08E is mounted at the same level as the bridge deck and when the wind is flowing from the opposite side, D08E will have a somewhat unique wind encounter with regards to the other anemometers that are mounted six metres up into the air.

Figure 47 shows that the correlation coefficients for H08Wb, H08Wt and H08E follow very similar patterns relative to the distance from the other anemometers. H10W and H10E has comparable patterns, as seen in figure 48. Figure 49 shows that H20W and H24W generally correlate less with the closest anemometers than those in figures 47 and 48. This is quite natural, as the distance between H20W and H24W is larger than those installed on H08 and H10. It is quite curious that H24W correlates more with the anemometers installed at H08 than those installed at H10. This seems illogical and the reason for this is uncertain, although this could be influenced by a certain wind velocity or direction. It could also be due to lack of precision in the instruments or noise/wrong measurements.

Since the deck anemometers D08E and D08W are exposed to wind conditions that are relatively different from the other anemometers, they are omitted from figures 46, 47 and 48.

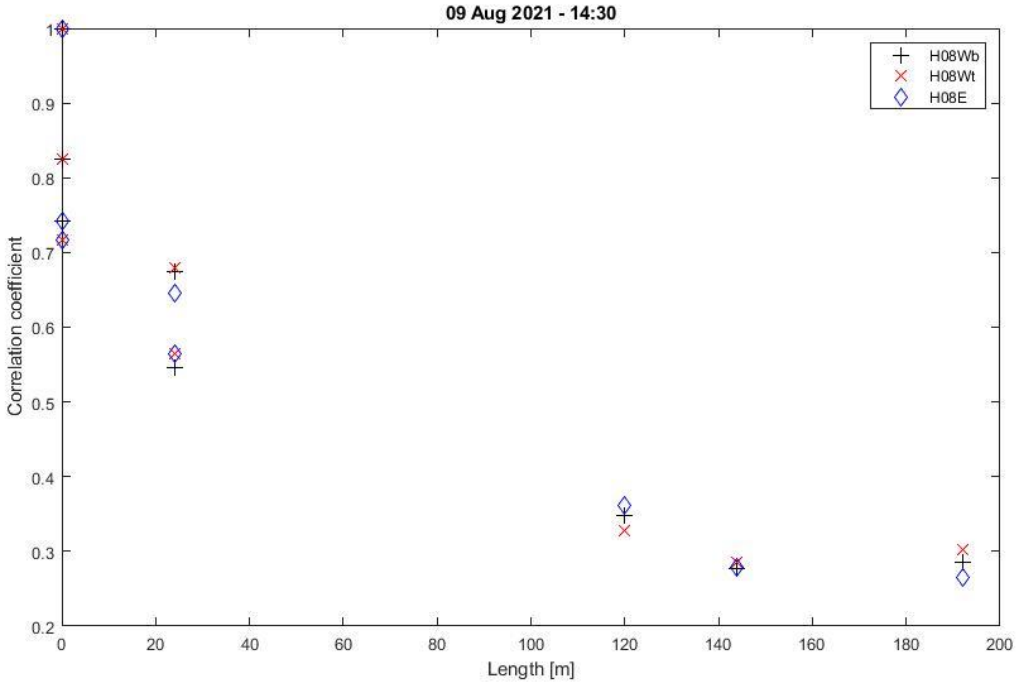

Figure 47: Correlation of specified anemometers as a function of distance along the bridge to the other anemometers. D08E and D08W are omitted

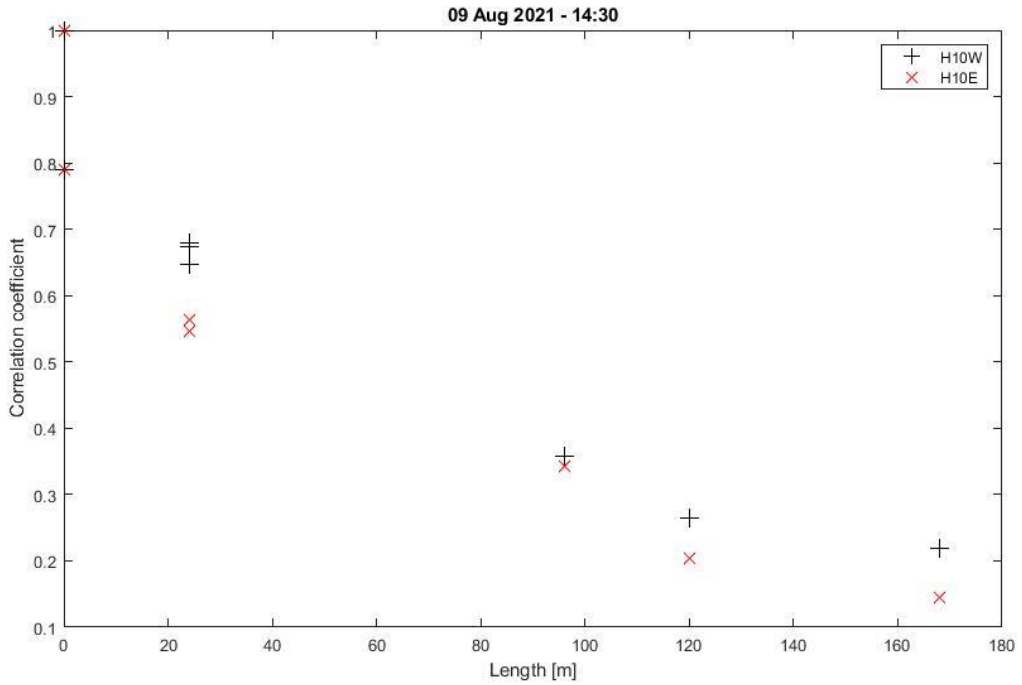

Figure 48: Correlation of specified anemometers as a function of distance along the bridge to the other anemometers. D08E and D08W are omitted

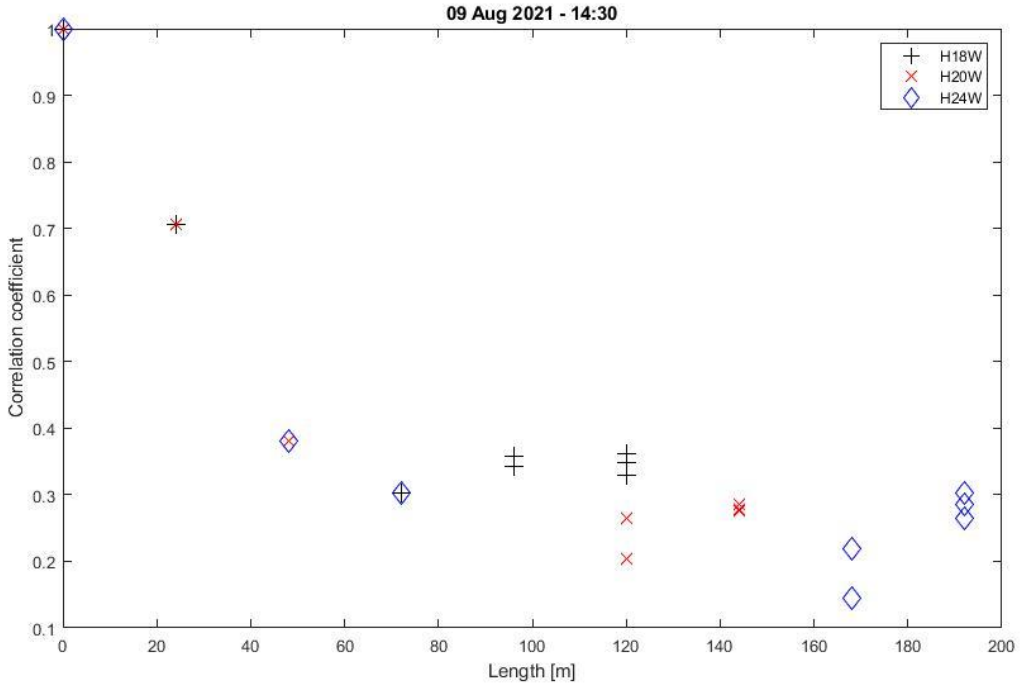

Figure 49: Correlation of specified anemometers as a function of distance along the bridge to the other anemometers. D08E and D08W are omitted

5.1.5 Vertical acceleration

As stated in chapter 4.1.5 the peak positive acceleration registered at H09E was 15.99 m/s^2 after 51.84 seconds, while the lowest negative acceleration was -17.09 m/s^2 after 53.88 seconds. H09W peaked at 24.16 m/s^2 after 53.96 seconds and had the lowest negative registered as -19.80 m/s^2 after 53.84 seconds. Figures 50 and 51 show no clear correlation between the horizontal wind velocity and the accelerations at the forementioned time. Therefore, it can be assumed that the accelerations registered by H09E and H09W is largely caused by traffic.

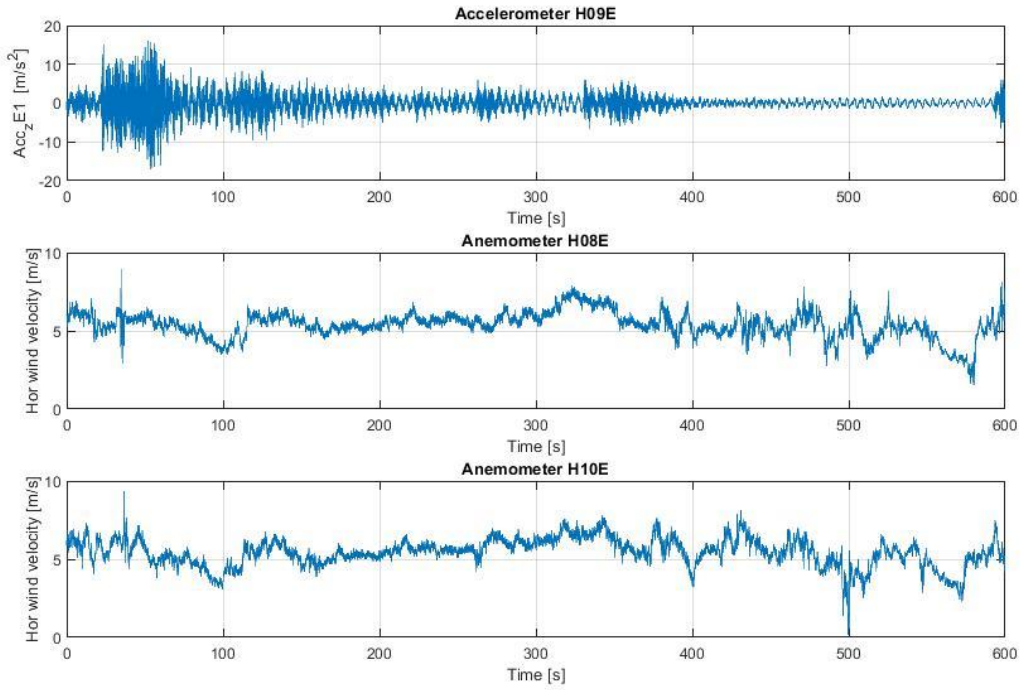

Figure 50:Vertical acceleration at H09E and horizontal wind velocity at H08E and H10E

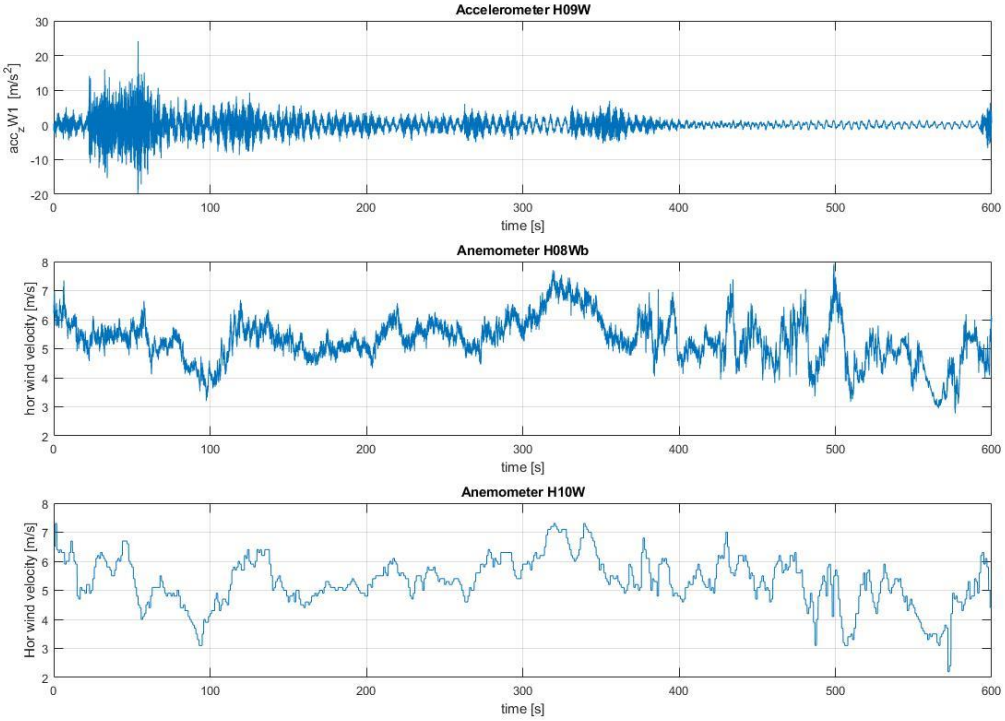

Figure 51: Acceleration at H09W and horizontal wind velocity at H08Wb and H10W

The accelerations recorded from H18E and H18W are seen in figures 52 and 53 below. The accelerations from H18E are compared to the horizontal wind velocity of anemometer H18W and H20W since anemometer H18E was malfunctioning at the time of recording and there are no other anemometers installed close to the accelerometer H18E at the east side of the bridge.

Both the positive and negative acceleration of H18E and H18W happens almost simultaneous. The peak positive was recorded after 54.08 seconds and 54.36 seconds, with values reaching 18.59 m/s^2 and 16.37 m/s^2 respectively. The lowest negative was registered at the same time for both accelerometers, with values of -21.43 m/s^2 and -19.29 m/s^2. Neither of these accelerations seem to be particularly linked to the horizontal wind velocity, which leads to the assumption that traffic is to blame for the forementioned accelerations.

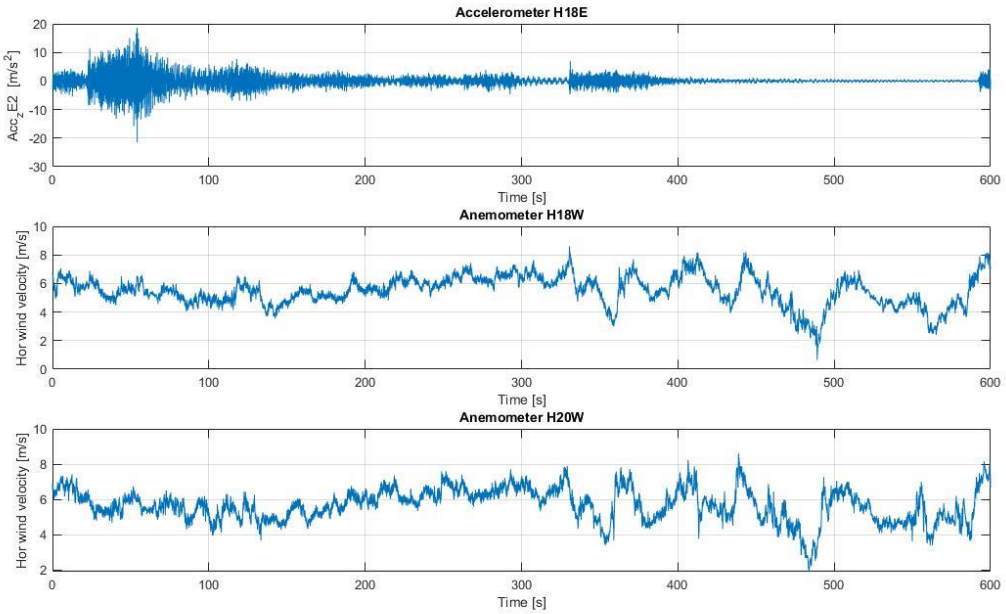

Figure 52: Acceleration at H18E and horizontal wind velocity at H18W and H20W

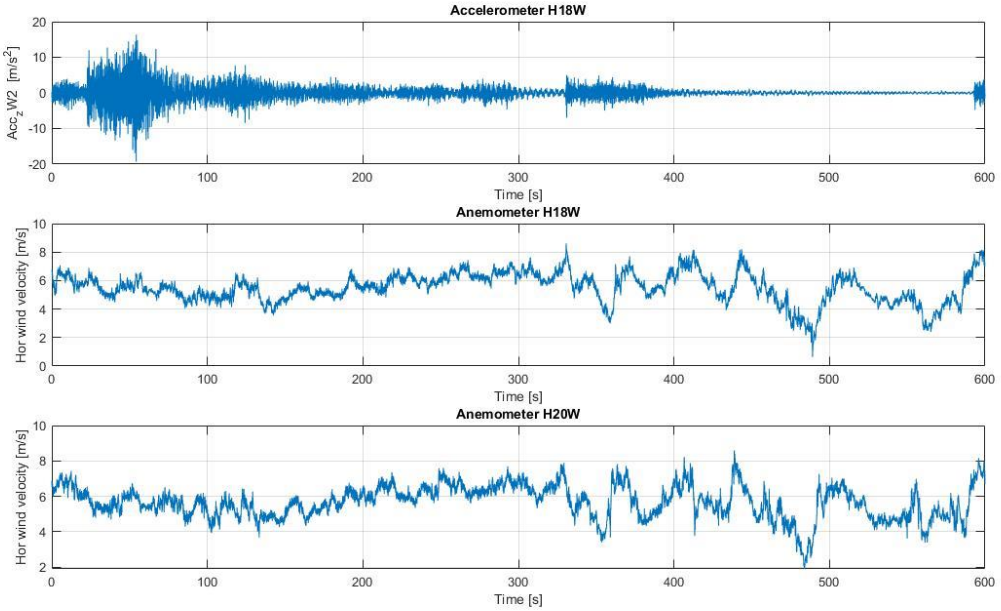

Figure 53: Acceleration at H18W and horizontal wind velocity at H18W and H20W

The two remaining accelerometers H24E and H24W, has their peak acceleration registered at the same time. Both happen after 45.04 seconds with values of 22.74 m/s^2 and 22.24 m/s^2 respectively. The lowest negative values were recorded within a second of each other, after 54.38 seconds and 53.34 seconds. These values are -21.10 m/s^2 and -18.76 m/s^2. The peaks and the lows can be seen in figures 54 and 55.

There is hard to see an immediate correlation between the horizontal wind velocity and the accelerations measured by H24E and H24W. There is no significant gust of wind at the times for these accelerations, which further can lead one to assume that traffic is the main reason for the accelerations recorded on this part of the bridge as well.

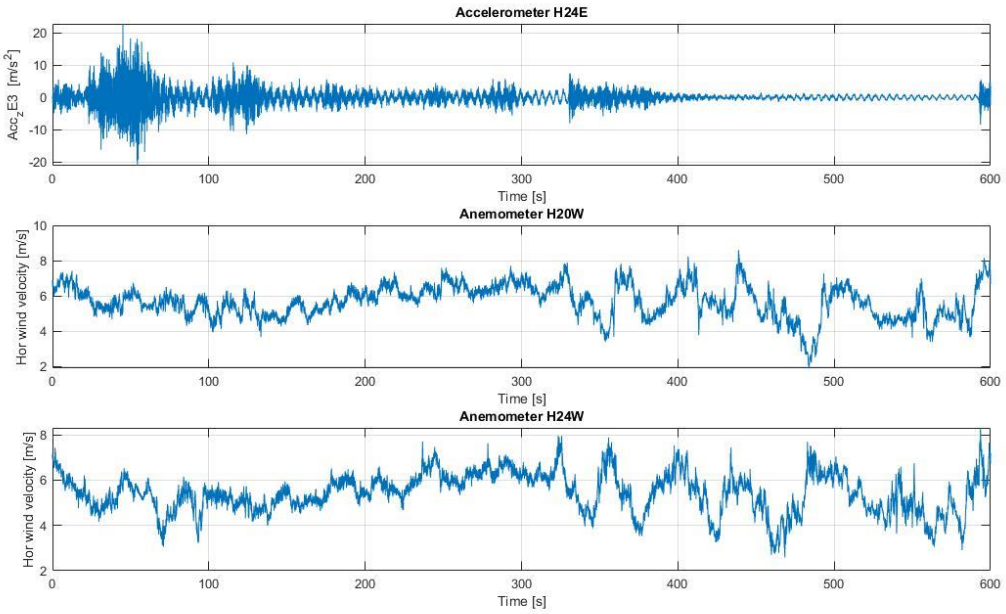

Figure 54: Acceleration at H24E and horizontal wind velocity at H20W and H24W

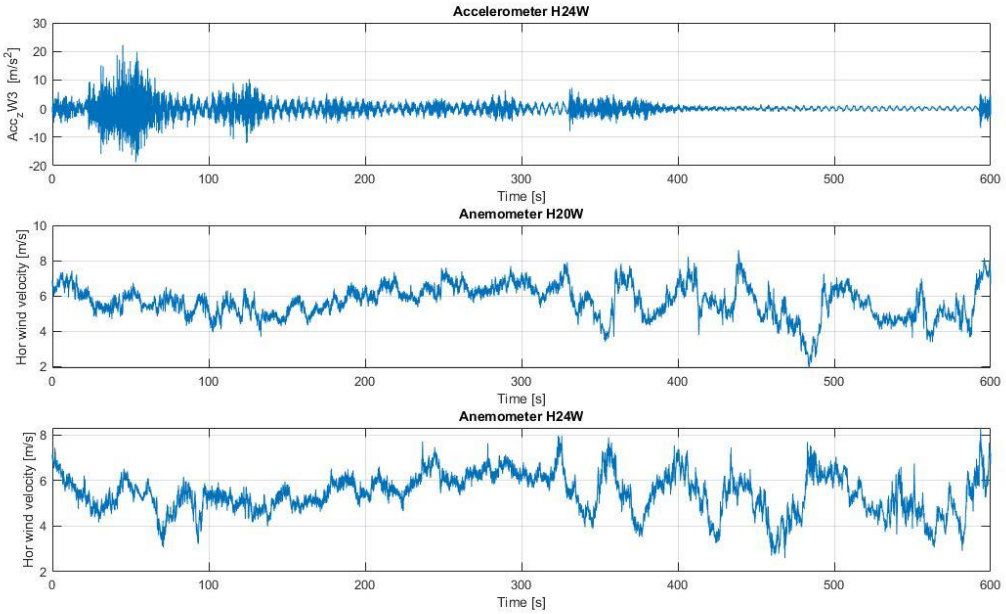

Figure 55: Acceleration at H24W and horizontal wind velocity at H20W and H24W

From the figures and paragraphs above it is clear that the accelerations in this time-series culminating in a short period around t=53 seconds, with the maximum values concentrated in just few seconds. None of the accelerations seems to be mainly caused by the wind, as there is no significant difference in the wind speed during this short window of time. From this, it is assumed that traffic is the main reason for the accelerations during this ten-minute period. The main burst of acceleration recorded in each accelerometer lasts for approximately 30 seconds before it starts

decaying, from which one might deduct that heavy traffic was only present once or twice during the time-series.

5.1.6 Vertical Acceleration spectra

In this section, the vertical acceleration spectra are used to estimate the bridge`s eigen-frequencies and compare them with those reported in a in a previous study by Cheynet [22] and Wang [28]

Figure 56 shows the vertical acceleration spectra for the accelerometers installed at H09. The spectra have a peak value at a frequency of 0.220 Hz, for both H09E and H09W. This corresponds well with the eigen-frequency of the first vertical asymmetric mode found by Cheynet at 0.223 Hz [22]. The discrepancy between the values is -1.35%. Wang [28] found the value for this mode to be 0.222Hz. The same concentration of vibration energy at 0.220 Hz is found at H24E and H24W for the same frequency, as seen in figure 57. This seems logical as both sets of accelerometers are placed at the respective quarter spans on each side of the bridge and will naturally have larger vibrations concentrated at the frequencies corresponding with the asymmetrical vertical modes. H09 is the quarter span closest to the northern tower of the bridge, while H24 is closer to the southern tower.

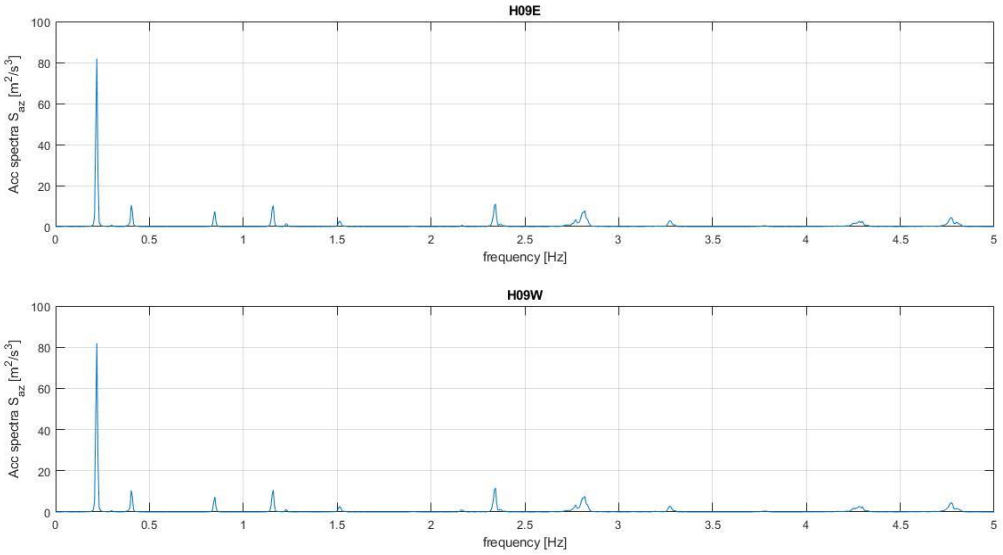

Figure 56: Vertical acceleration spectra for accelerometers mounted on H09

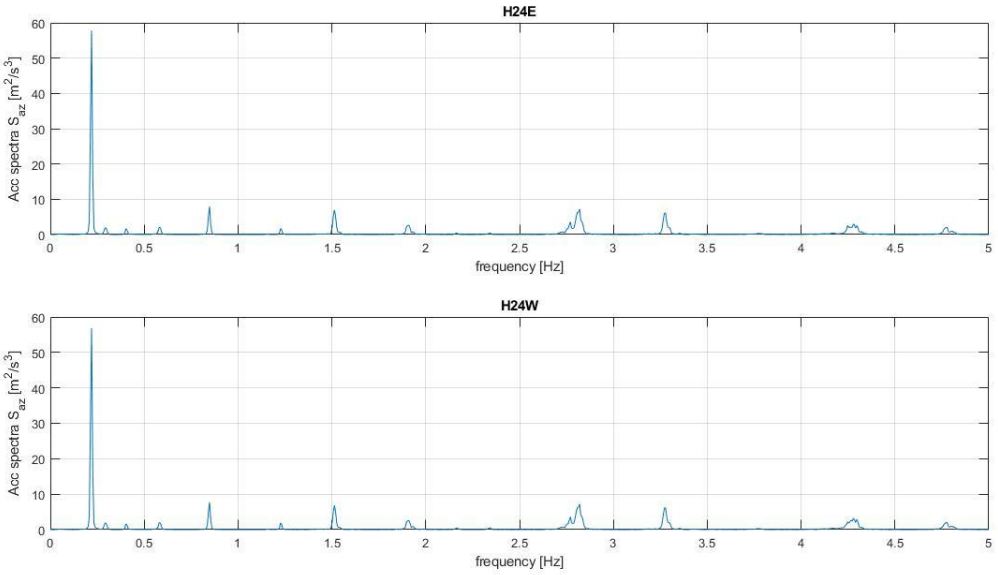

Figure 57: Vertical acceleration spectra for accelerometers mounted on H24

The spectra from both sets of accelerometers also have minor peaks at 0.403 Hz, corresponding to the second vertical symmetrical mode (0.408 Hz [22]), but the spectral values are only 1/6 and 1/8 of the values for the first vertical asymmetric mode. Minor peaks are also found at 0.850 Hz (corresponding to the third vertical symmetrical mode [22]) in both sets of accelerometers and 1.23 Hz [22] (1.234 Hz by Wang [27]) for H09E and H09W - the eigen-frequency of the first symmetric torsional mode, associated with vertical accelerations outside of the shear center. There are also other spectral peaks at higher frequencies. The eigen-values for these higher modes, likely excited by traffic, are not further discussed in the following.

The acceleration data are stored with the sampling frequency of 50 Hz, so the spectral values are calculated up to fs/2. As the magnitudes of the vibration amplitudes at higher frequencies are negligible, the above figures show the spectral values up to 5 Hz only, for an easier discussion of the spectral content at lower frequencies.

The vertical acceleration spectra at bridge mid span, at hangers H18E and H18W, (Figure 58) are concentrated at different frequencies than those at the bridge quarter spans. The first spectral peak is at a frequency of 0.293 Hz, which largely corresponds with the first symmetrical vertical mode with a frequency of 0.294 Hz, estimated by Cheynet [22] and by Wang [27] of 0.293 Hz. The next spectral peak, albeit with a lower value than the previous one, is found at 0.403 Hz. This appears to correspond with the second symmetrical vertical mode, which has a frequency of 0.408 Hz [22]. The third noticeable concentration of the vibration energy is at a frequency of 0.848 Hz. The third symmetrical vertical mode had a frequency of 0.853 Hz [22], a difference of mere 0.6%. Since these accelerometers are installed at half span, it is quite natural that the frequencies corresponding with the symmetrical vertical modes are the ones with the largest acceleration amplitudes.

There are other spectral peaks at higher frequencies, which are expected to correspond with other modes. One of the spectral peaks at these higher frequencies is seen at 3.228 Hz from figure 58. This corresponds to the second symmetrical torsion mode found by Tveiten [33], with a frequency of

3.241 Hz. The other high frequencies likely correspond with more traffic on the bridge, but it is difficult to be completely certain about the cause of these vibrations.

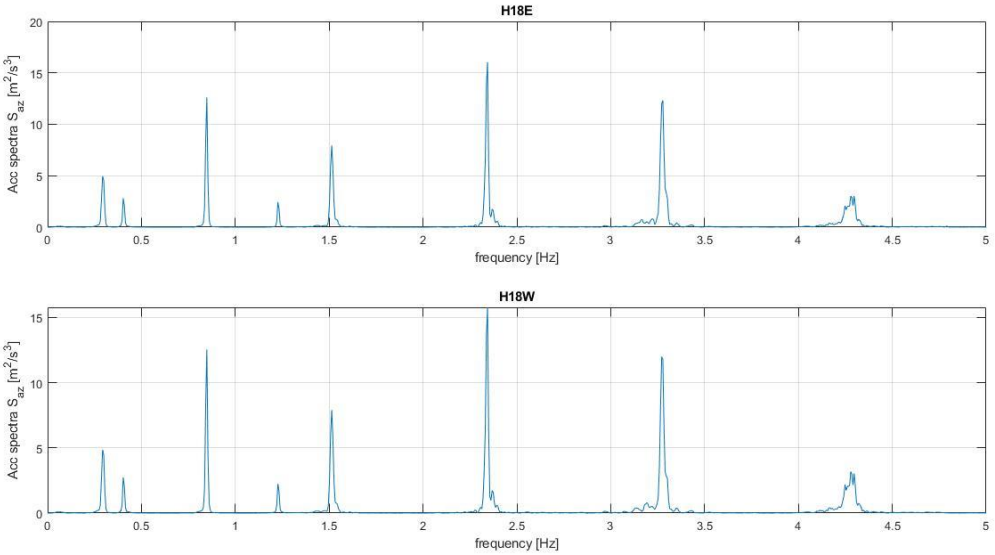

Figure 58: Vertical acceleration spectra for accelerometers mounted on H18

5.2 Wind data from 23/09/21 – 14:30:00

5.2.1 Horizontal wind velocity

The maximum horizontal wind velocity was registered after 556 seconds by anemometer H08Wb and had a value of 17.37 m/s, seen in figure 59. This velocity equals a speed of 62.53 km/h. The peaks recorded by each anemometer varied from 14.30 m/s to the forementioned maximum. Similar to chapter 4.1.1, it was the deck anemometer installed at the opposite side of the wind flow that registered both 14.30 m/s and the lowest velocity of 0.03 m/s during this time-series. D08E also registered the lowest mean wind velocity of 4.21 m/s, while the mean velocity when the deck anemometers are omitted is 6.70 m/s.

Again, it is seen that D08E has a mean velocity of approximately 2 m/s less than the general mean. The time-series from 09/08/21 showed a comparable drop in mean velocity at D08E, although with a somewhat different mean wind direction than that of the time-series under study in this chapter. In 4.1.1, the mean wind direction was 221.35°, while in the data from 23/09/21 the mean wind direction was 239.8°. This angle also equals a wind flow from south-west. From this, and looking at Figure 57 below, it seems that the wind direction from the two different time-series has little impact on the maximum horizontal velocity. The angle of the wind direction at the time of the maximum velocity is very different from the mean direction, but it is relatively stable at approximately 150^0 at 556 seconds. This is illustrated in figure 59.

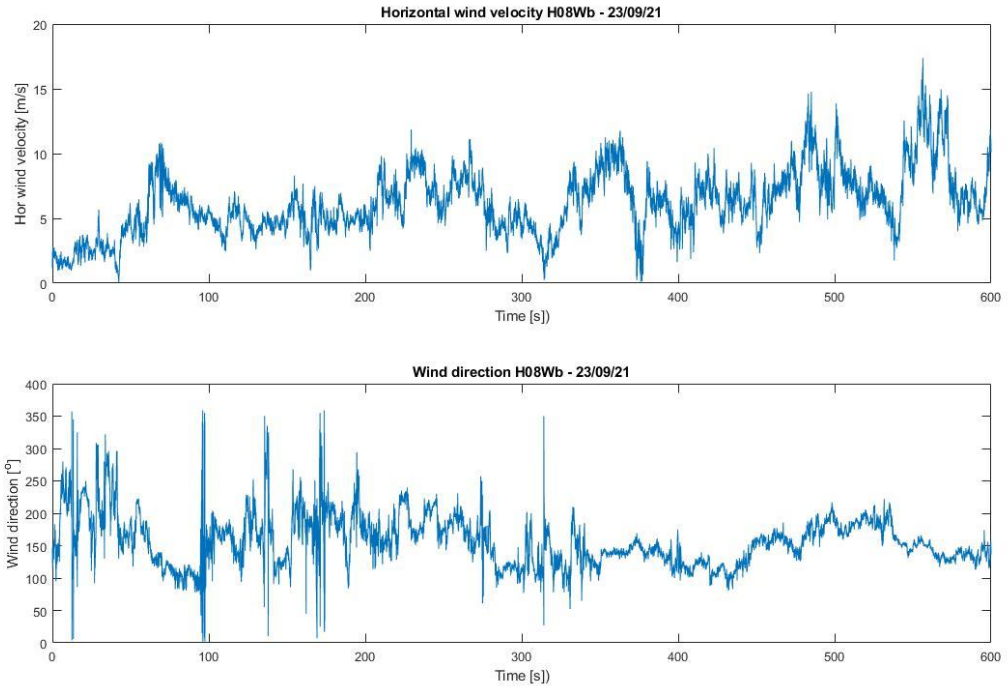

Figure 59: Variation of horizontal wind velocity and wind direction for H08Wb

5.2.2 Vertical wind velocity and vertical angle

During this time-series the vertical wind velocity has bigger peaks and lower negatives than that of the previous one. The deck anemometer D08W recorded the peak value of 9.7 m/s, while the other deck anemometer D08E had the lowest negative with -11.14 m/s. The mean velocity of the time-series was 0.34 m/s, more than double that of the 09/08/21 time-series. This seems reasonable, as the vertical velocity also was higher than that of the previous time-series. The standard deviation of this series was also higher because of the higher peaks and lower negative velocities. It can be noted that it was the deck anemometers that recorded the peaks and lows, which was the same in the previous time-series.

Since the main wind direction of both series corresponded to a wind flow from south-west, it might seem that the wind direction has an influence over the vertical velocity. The fact that the fjord inlet that the Lysefjord bridge crosses is relatively narrow with steep vertical hills on both sides of the bridge will also likely play a large role when it comes to the vertical velocity.

The mean vertical angle was found to be 1.49°. Compared to the mean angle of 09/08/21 it is a bit lower. From figure 60 it is seen that when the direction of the wind changes abruptly from larger angles (350°-360^0) to small ones (0°-10°) the vertical angle also changes abruptly from large positives angles to big negative angles. This suggests that the wind direction plays as big part when it comes to the vertical angles. This is most notable at D08E, shown in figure 61.

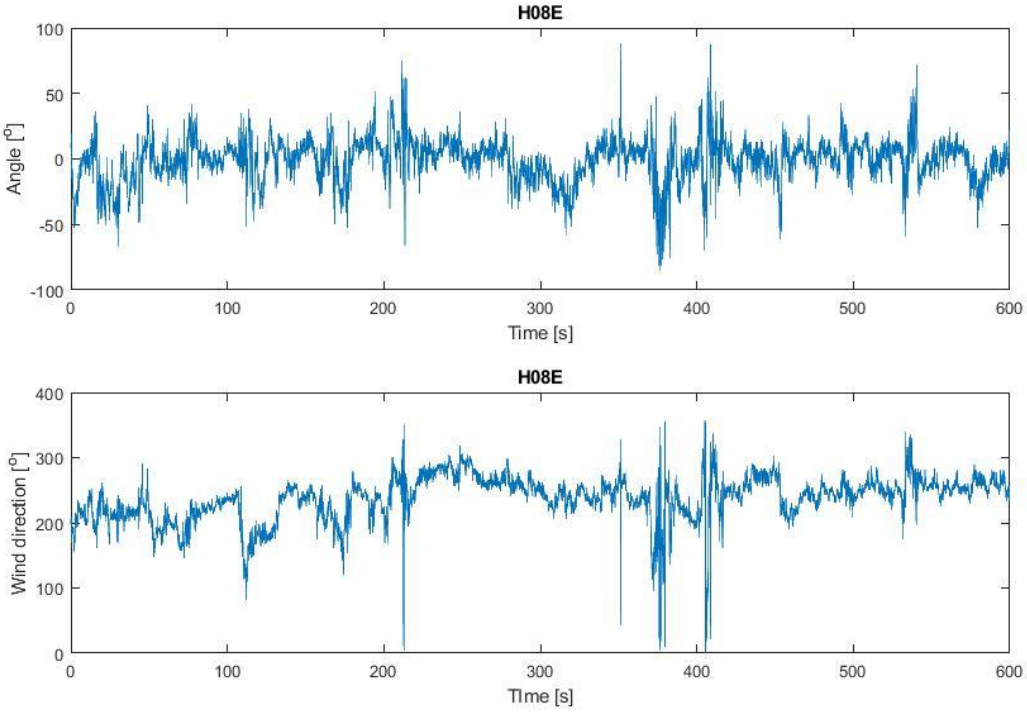

Figure 60: Vertical angle and wind direction for H08E

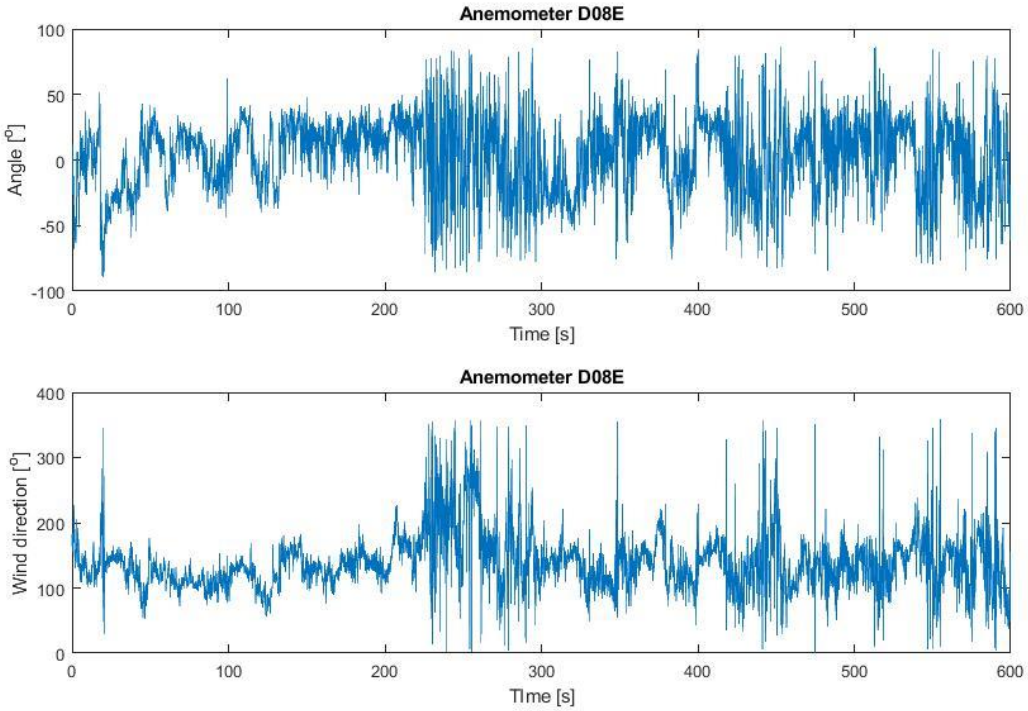

Figure 61: Vertical angle and wind direction for D08E

5.2.3 Turbulence intensity

As mentioned in chapter 4.1.3, Cheynet et. Al [27]. reported that for a wind flow from southwest, two different main turbulence intensities were found. These were associated with a direction between 175° and 195° that had a mean wind speed of less than 14 m/s and a direction between 210° and 230° that had a wind speed of more than 14 m/s respectively. In this case, extremely high turbulence intensities were found from all the anemometers. The values ranged from 0.28 at H24W to 0.54 at D08E. The intensity at D08E is an outlier in this time-series, although not as influential on the mean as the turbulence intensity at D08E in chapter 4.1.3. The outlying value is likely due to the same fact as in 4.1.3, that D08E is mounted at the east side of the bridge when the mean direction is from southwest. It is noted that the second highest turbulence intensity was found at H10W, an anemometer mounted at the west side of the bridge, with a value $I_u \approx 46\%$. With these values included, the mean turbulence intensity is $I_u \approx 41\%$.

These intensities are not easily explained, as they are almost double those of Cheynet [27]. One reason can be that since the mean wind velocities are not particularly high, the wind acts more random compared to a wind flow with a high velocity. The bridge deck itself may also play a part in this, as the wind may be distorted due to the bridge blocking and disturbing the flow. This is further documented and explained by Cheynet et al. [29] and Cheynet et al. [30]

5.2.4 Correlation coefficients

The correlation matrix of the different anemometers is shown in figure 62. There are large similarities between this matrix and figure 8 from chapter 4.1.4. This was expected, as the wind has somewhat the same character in both time-series. The first four anemometers show largely the same correlation as in chapter 4.1.4, although D08W has a slight reduction in correlation with H08Wt compared to that of 09/08/21.

The deck anemometer D08E, which is mounted on the opposite side of the bridge with regards to the wind direction, does show more of a correlation with the other anemometers in this time-series with no negative correlation values. It correlates mostly with H10E, which is natural considering that these anemometers are both mounted relatively close on the east side. Other notable differences from chapter 4.1.4 is that H10W and H10E correlates more than in the previous time-series while H24W correlates generally less with all other anemometers.

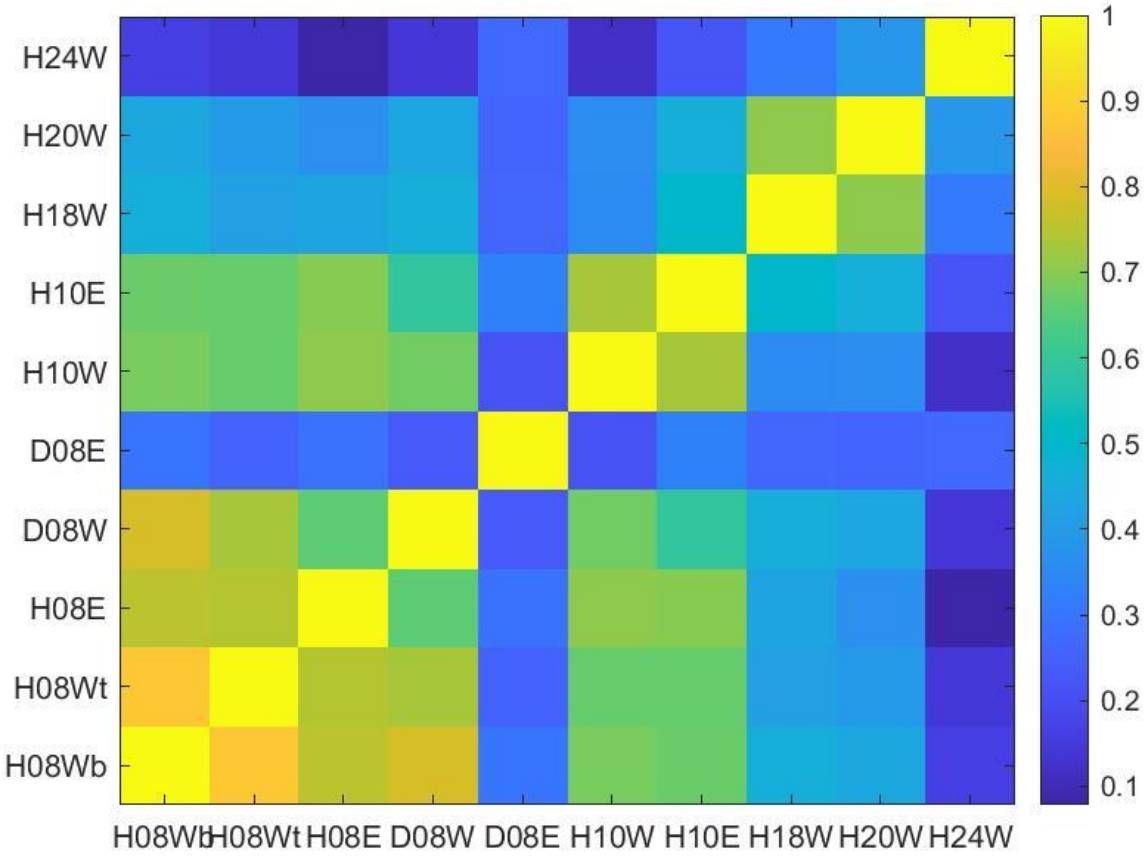

Figure 62: Correlation matrix illustrating the correlation between the anemometers

It is seen from figure 63 that the first three anemometers follow somewhat the same pattern as in figure 47 in chapter 5.1.4, although with generally higher correlation. H08E correlates the least with the anemometers that are further away, which can be explained by the wind direction coming from south-west.

From figure 64 it is seen that H10E correlates more with the anemometers further away than H10W, while figure 65 shows that H24W less with the anemometers furthest away than it did in the time-series from 09/08/21. The changes are limited, however.

The deck anemometers D08E and D08W are omitted from figures 61, 62 and 63, as the wind conditions are different for those anemometers than it is for the others. This has been thoroughly discussed earlier in the thesis. It is worth noting however, that both deck anemometers correlate somewhat more with the others for the wind direction discuss3ed in the present chapter.

From this it can be determined that the slight change in mean wind direction, along with the change in velocity has small effects overall with regards to the correlation between the anemometers. The change in these parameters from 09/08/21 to 18/10/21 had the most notable effect on the deck anemometers D08W, D08E and on H24W. The slight change in direction looks like it affected the deck anemometer the most, as the wind had more of a perpendicular angle of attack in the data discussed in this chapter than that of chapter 5.1.4.

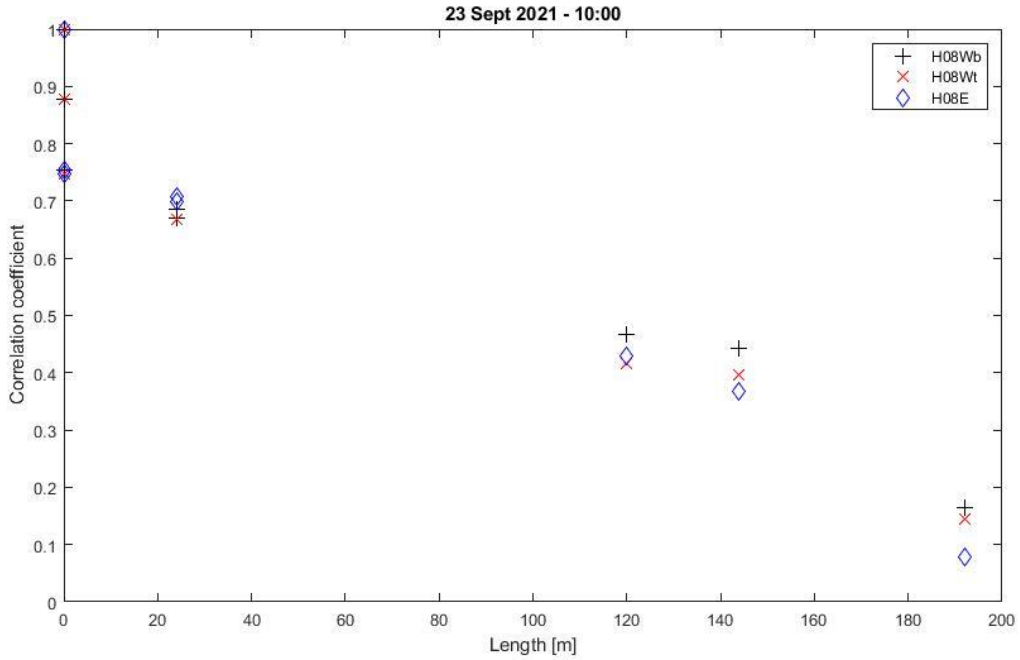

Figure 63: Correlation of specified anemometers as a function of distance along the bridge to the other anemometers. D08E and D08W are omitted

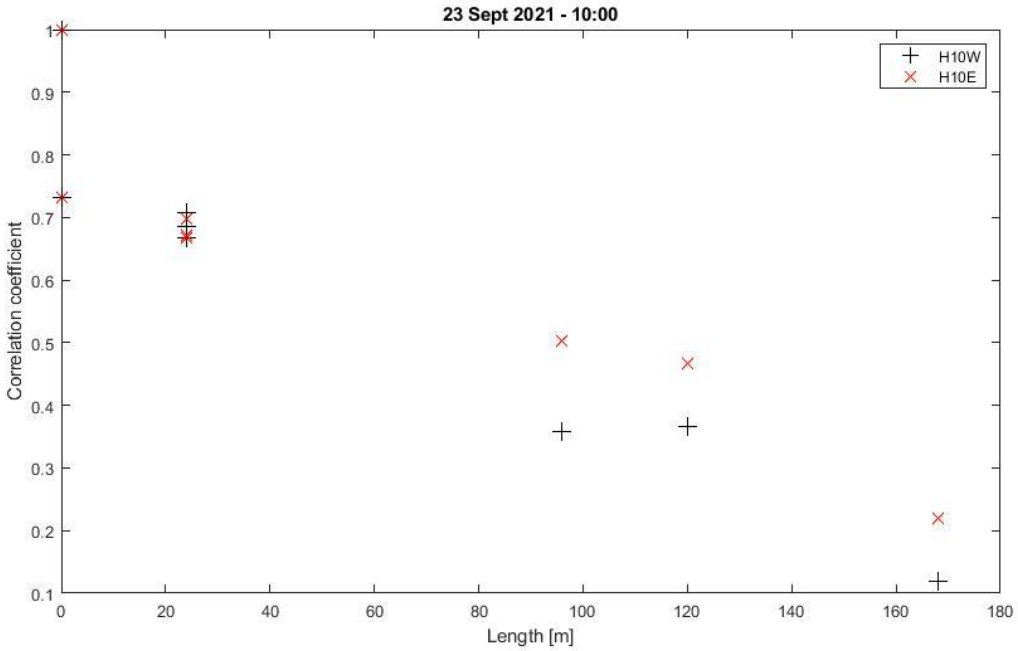

Figure 64: Correlation of specified anemometers as a function of distance along the bridge to the other anemometers. D08E and D08W are omitted

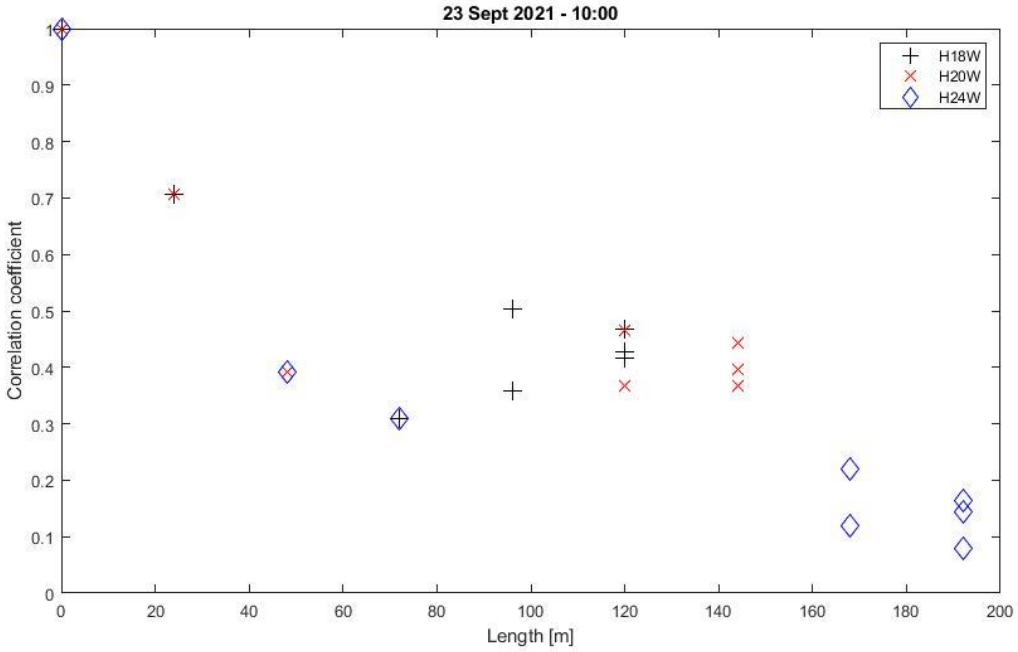

Figure 65: Correlation of specified anemometers as a function of distance along the bridge to the other anemometers. D08E and D08W are omitted

5.2.5 Vertical acceleration

For the accelerometers H09E and H09W, the vertical acceleration is relatively constant before the 200 second mark. At this time a burst of accelerations happens, which lasts for approximately a minute before it decreases until about 550 seconds where another, smaller burst happens. From figures 66 and 67 it is hard to notice a clear impact on the accelerations at H08E and H08W from the horizontal wind velocity. There is a sudden drop followed by a quick increase in horizontal velocity at the 200 second mark, but there is no particular pattern, and the accelerations seem somewhat random when compared to both the horizontal velocity and the wind direction measured at the nearby anemometers.

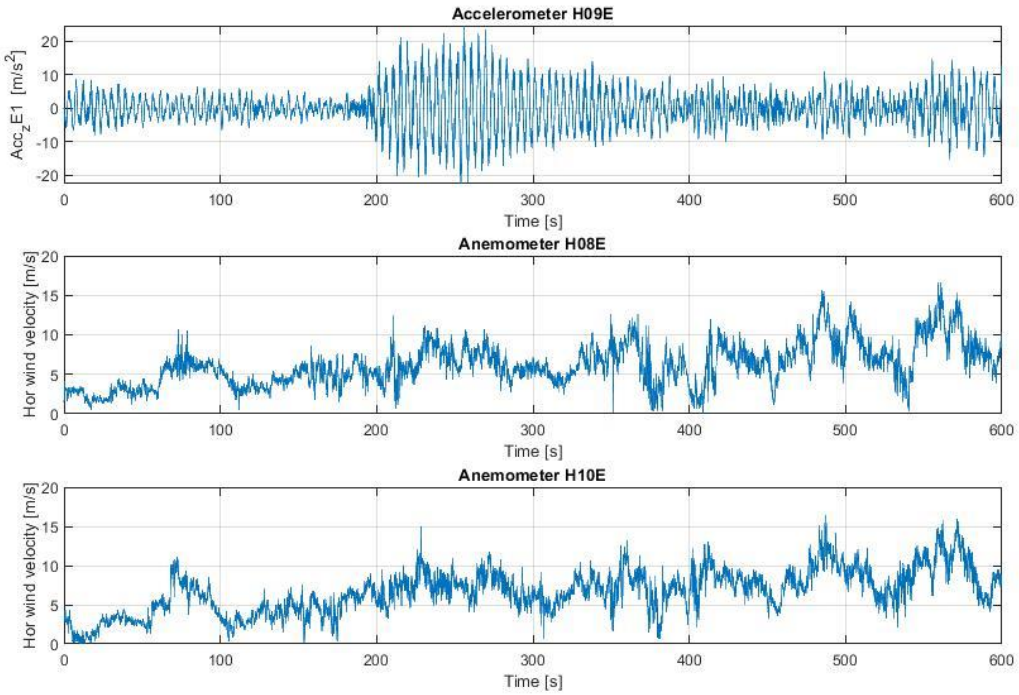

Figure 66: Vertical acceleration at H09E and horizontal wind velocity at H08E and H10E

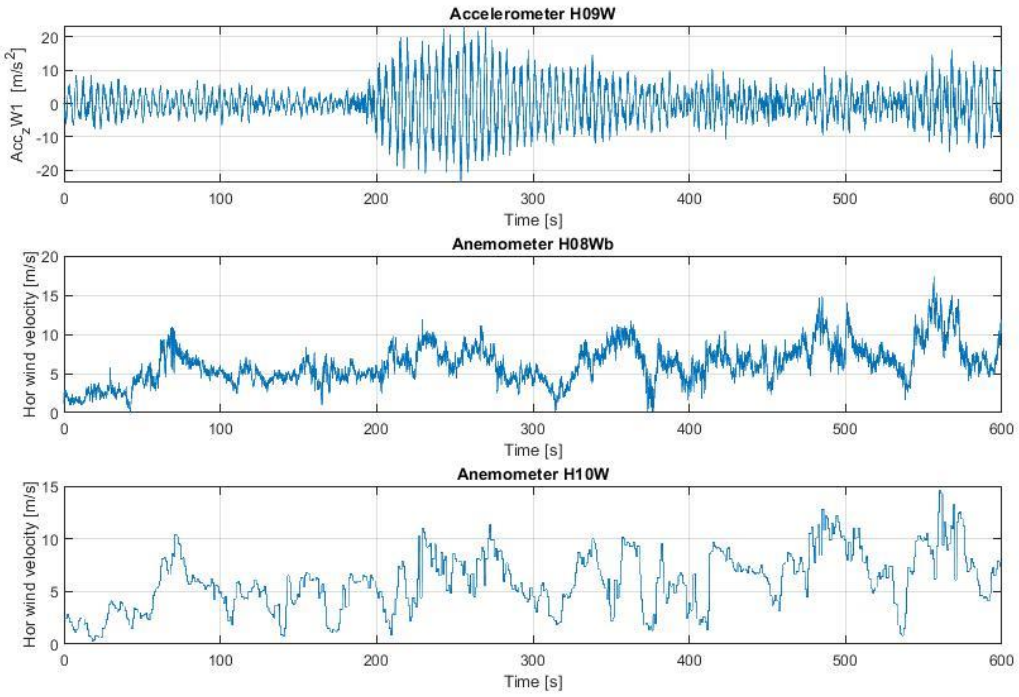

Figure 67: Vertical acceleration at H09W and horizontal wind velocity at H08E and H10E

The accelerations recorded at H18E and H18W is shown in figures 68 and 69, follow the same pattern as the ones mentioned above. At about 200 seconds the same burst of accelerations as seen at H08E and H08W is registered, although with smaller oscillations. This lasts for the same amount of time as before but after approximately 400 seconds a second burst of accelerations is registered. This was not registered by H08E and H08W. This second burst lasts until about 465 seconds where the oscillations go almost to zero, before another burst of accelerations was registered approximately five seconds later. The two last bursts were not notable from the data registered by H08E and H08W, which is quite curious. There is no indication of these bursts happening due to the horizontal wind velocity or the wind direction at the time or at the anemometers closest to the accelerometers in question.

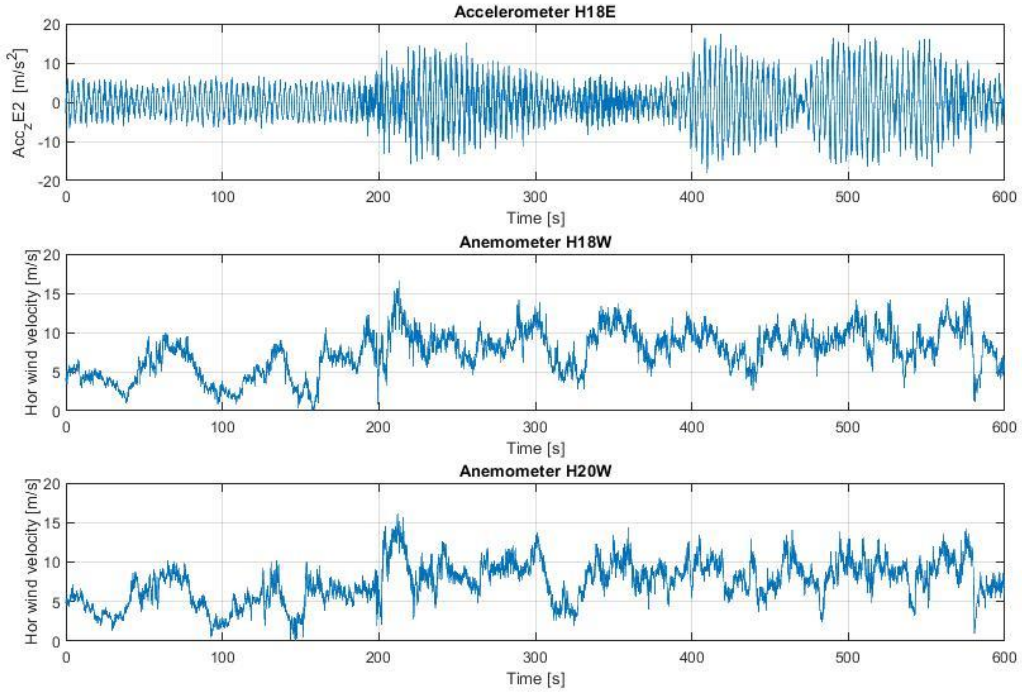

Figure 68: Vertical acceleration at H18E and horizontal wind velocity at H18W and H20W

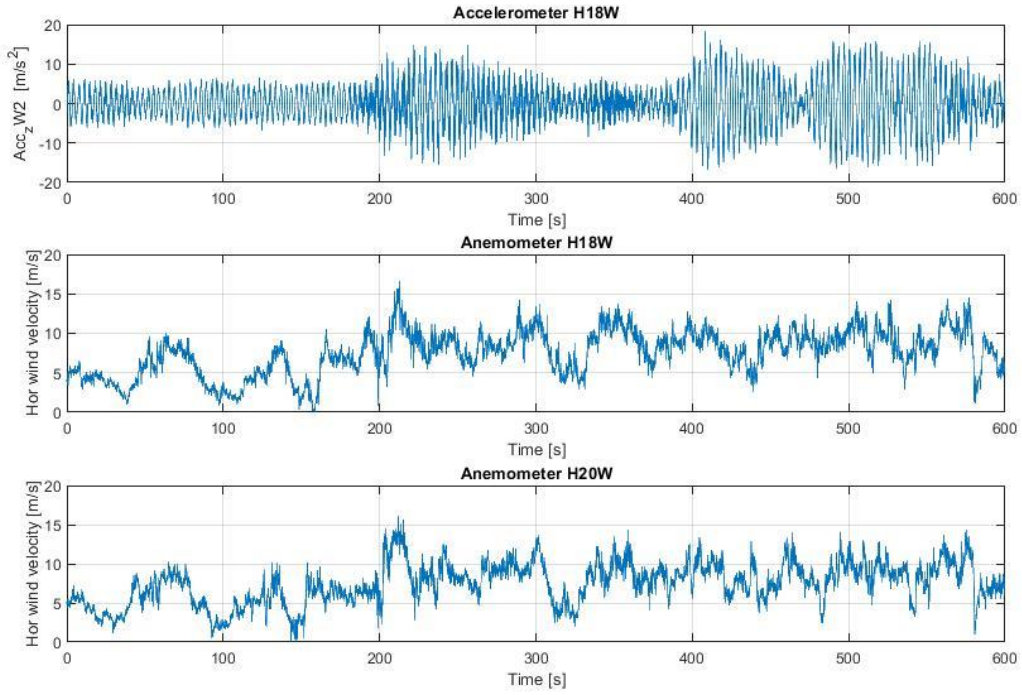

Figure 69: Vertical acceleration at H18W and horizontal wind velocity at H18W and H20W

From the last two accelerometers that are mounted on H24, the same burst of acceleration after 200 seconds was registered with values close to those from H08E and H08W. This is seen in figures 70 and 71. Another small burst can be distinguished after 412 seconds, but this dies down much faster than the one registered by accelerometers H18E and H18W. Yet again, the oscillations go almost to

zero after approximately 465 seconds, before a third burst can be seen. This is, however, much smaller in both magnitude and time, as the values ranges from 10 m/s to -10 m/s until another burst is registered. These oscillations have the same values up until 546 seconds where a fourth burst is registered. This burst is bigger than the second and the third and is the same as registered by H08E and H08W.

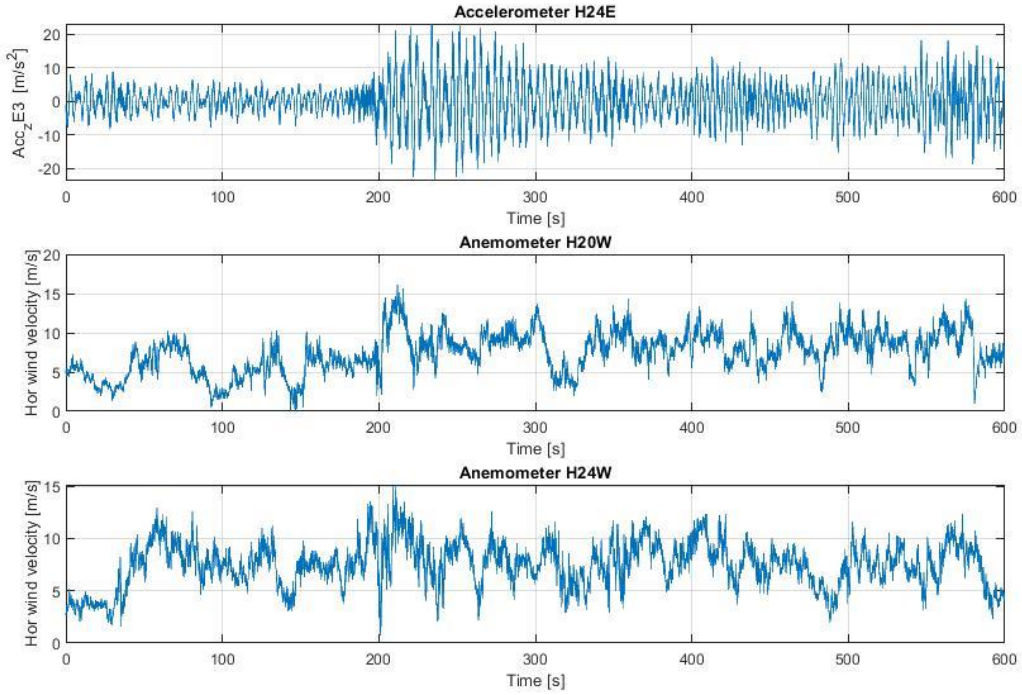

Figure 70: Vertical acceleration at H24E and horizontal wind velocity at H20W and H24W

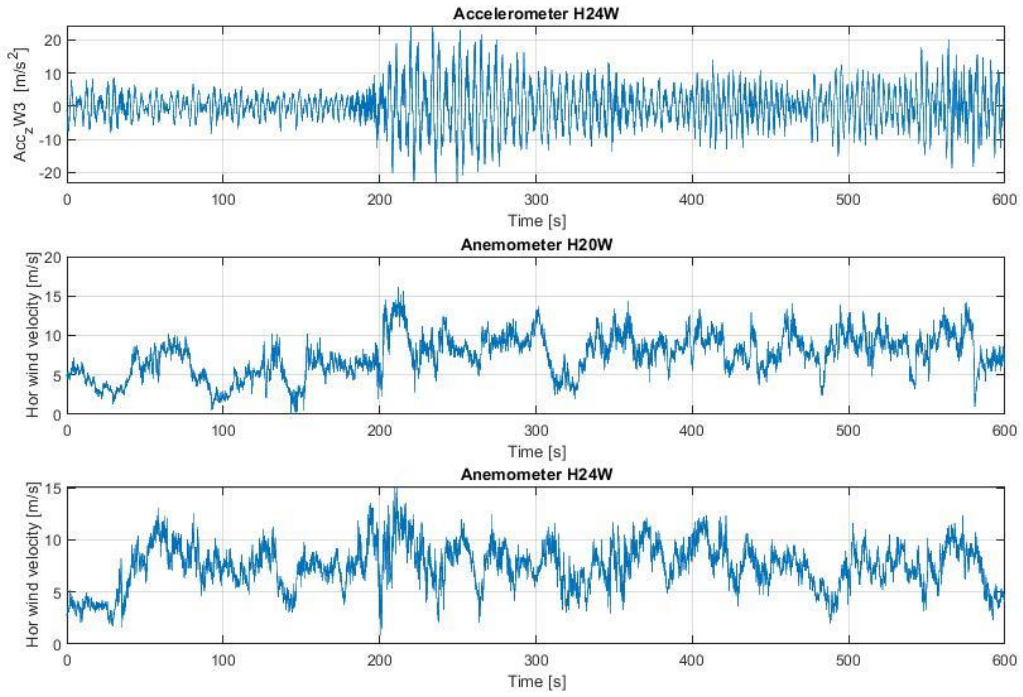

Figure 71: Vertical acceleration at H24W and horizontal wind velocity at H20W and H24W

It is curious that H18E and H18W registers a large burst after 400 seconds which is nowhere near the magnitude of that registered at the other two pairs of accelerometers. What is clear however, is that it seems the horizontal wind velocity and wind direction has a small impact on the vertical acceleration of the bridge. This leads one to believe that traffic is the main accelerator during this time-series. The five second timeslot between the second and third burst recorded by H18E and H18W is particularly interesting. It is difficult to confirm what caused this. It might be caused by a somewhat rare traffic incident, perhaps by two heavily loaded semitrucks passing each other at a particular point at the bridge.

5.2.6 Acceleration spectra

As mentioned in chapter 5.1.6, the acceleration data are stored with the sampling frequency of 50 Hz, so the spectral values are calculated up to fs/2. As the magnitudes of the vibration amplitudes at higher frequencies are negligible, the figures below show the spectral values up to 5 Hz only, for an easier discussion of the spectral content at lower frequencies.

Figure 72 shows the vertical acceleration spectra for both accelerometers installed at H09. Both spectra have a peak value of 0.220 Hz. This corresponds with well with 0.223 Hz, which was the eigen-frequency for the first vertical asymmetric mode estimated by Cheynet [22]. Wang [28] found the eigen-frequency for this mode to be 0.222 Hz, so the peak values from figure 70 corresponds well with these findings as well. The spectra from this set of accelerometers does also have minor peaks at 0.293 Hz and 0.403 Hz. This corresponds to the first vertical symmetrical mode (0.294 Hz) and the second symmetrical mode (0.408 Hz) found by Cheynet [22]. Wang [28] found the eigen-frequency of the first symmetrical mode to be 0.293 Hz. Since the accelerometers H09E and H09W are installed at

the quarter span of the bridge, it is natural that the largest vibrations are concentrated at a frequency corresponding with the asymmetrical vertical mode.

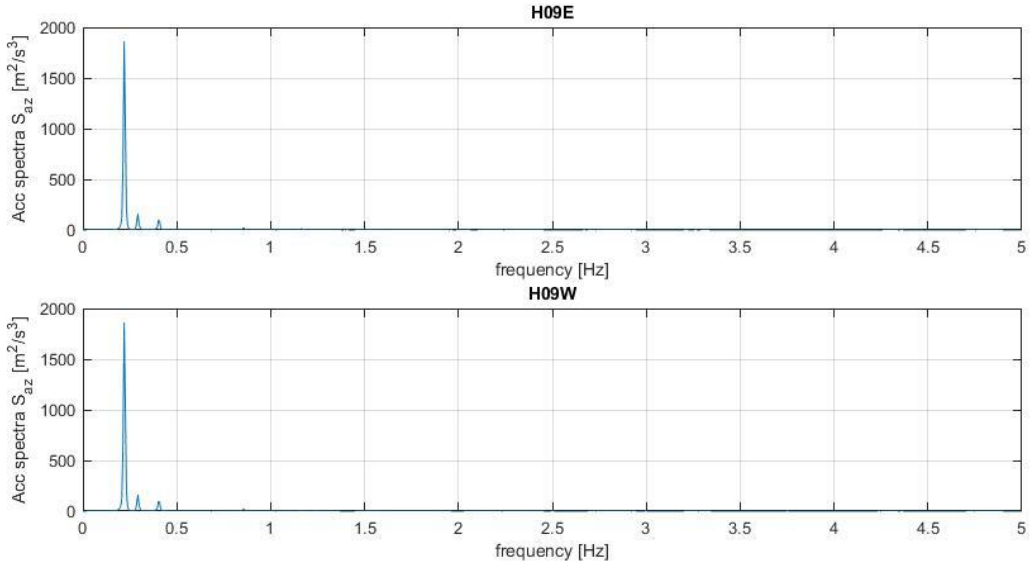

Figure 72: Vertical acceleration spectra for accelerometers mounted on H09

For the accelerometers installed at mid span (H18E and H18W), the vertical acceleration spectra is concentrated at a frequency of 0.293 Hz, seen in figure 73. This corresponds largely to the first symmetrical vertical mode estimated by both Cheynet [22] (0.294 Hz) and Wang [28] (0.293 Hz). It is natural that the frequency corresponding with the first symmetrical vertical mode is the one with the largest acceleration amplitude, since the accelerometers are installed at mid span of the bridge.

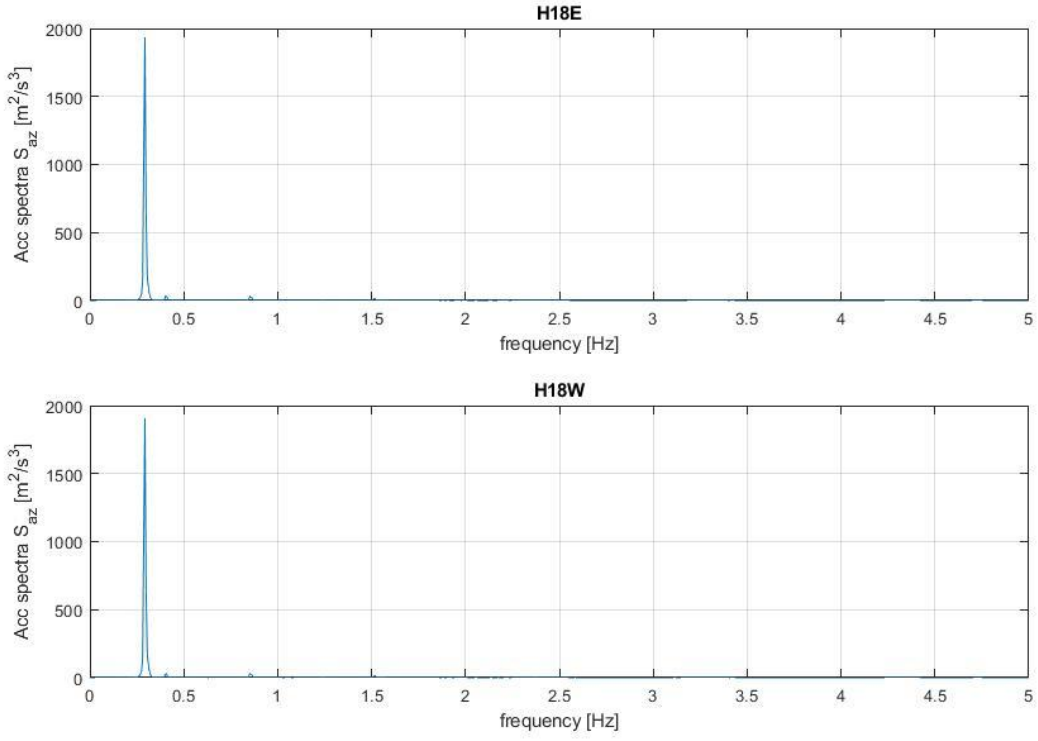

Figure 73: Vertical acceleration spectra for accelerometers mounted on H18

The vertical acceleration spectra from H24E and H24W is presented in figure 74 below. The spectra have a peak value at a frequency of 0.220 Hz, for both H24E and H24W. As stated previous in this chapter, this frequency corresponds well with the findings of both Cheynet [22] (0.223 Hz) and Wang [28] (0.222 Hz) for the first vertical asymmetric mode of the bridge. The second spectral peak, albeit with about half the concentration of vibration energy, is seen at a frequency of 0.293 Hz. It was stated above that this frequency corresponds with the first symmetrical vertical mode estimated by both Cheynet [22] and Wang [28]. Another minor concentration of vibration energy is at a frequency of 0.586 Hz. From the findings of Cheynet [22], it is seen that this frequency corresponds to the second asymmetrical vertical mode at 0.587 Hz. Again, since H24E and H24W is installed at a quarter span, it is quite natural that two of the recognisable spectral peaks corresponds to the vertical asymmetrical modes.

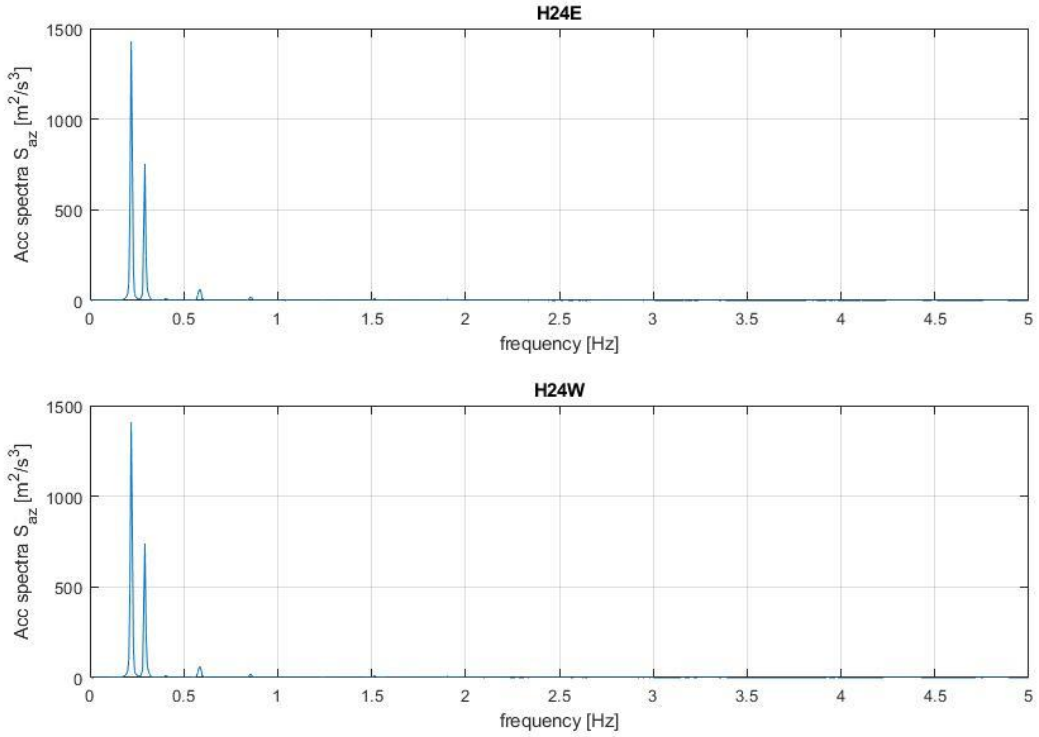

Figure 74: Vertical acceleration spectra for accelerometers mounted on H24

5.3 Wind data from 18/10/21 – 13:00:00

5.3.1 Horizontal wind velocity and wind direction

The maximum horizontal wind velocity in this time-series was registered at H18W, with velocities reaching 14.59 m/s after 490 seconds. This equals a wind speed of 52.52 km/h. Contrary to the data discussed in chapter 4.1 and 4.2, the lowest peak was recorded by H10W and not by a deck anemometer. The lowest velocity was however registered by the deck anemometer D08W, with a value of 0.01 m/s. The lowest mean wind velocity was 3.35 m/s, recorded by H24W, while the mean horizontal wind velocity for the whole time-series was 4.09 m/s. This means that for this time-series, the drop from the mean velocity of the time-series to the lowest mean velocity was smaller than in chapter 4.1.1 and 4.2.1.

The reason for this might be a combination of a lower mean wind speed overall than that of the previous chapters and the change in wind direction during this time-series compared to 09/08/21 and 23/09/21. The mean wind direction here was 154.80°. This equals a wind flow from southeast.

It does not look like the wind direction has a large impact on the horizontal wind velocity, as the peak velocity of H18W is registered at a time where the wind direction is relatively stable compared to the rest of the time-series recorded at this anemometer. This is illustrated in figure 75.

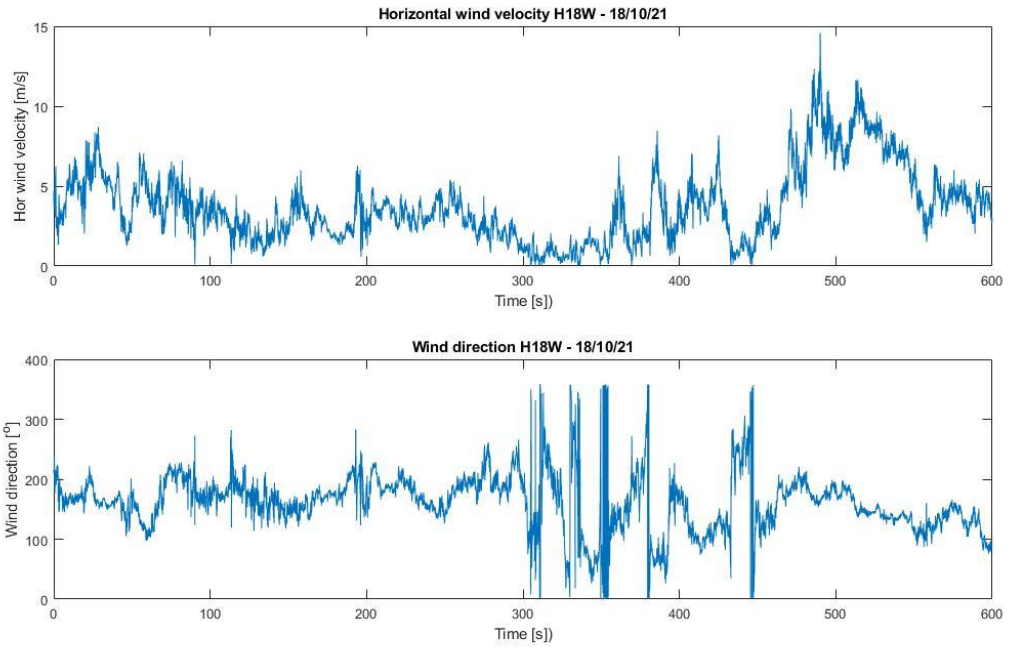

Figure 75: Variation of horizontal wind velocity and wind direction for H18W

5.3.2 Vertical wind velocity and vertical angle

The vertical wind velocity also fluctuates between positive and negative values during this time-series. Because of this fluctuation, the mean velocity will give a skewed image of the horizontal conditions on the bridge. It is however included here, where the value is 0.35 m/s. The highest peak velocity was 9.22 m/s registered at H08E, while the lowest negative was -6.48 m/s registered at

D08E. The difference from the previous time-series, is that in this time-series the deck anemometers on the same side as the wind direction did not record the peak, while the same side deck anemometer recorded the lowest negative.

The mean vertical angle is 6.55°, which is very large compared to the mean vertical angles of the previous time-series. The largest contributors to this are the mean angles of H08E, D08W, D08E and H10E with values of 12.81°, 15.86°, 14.59° and 11.73° respectively. From this, it looks like the wind flow from southeast does have a larger contribution to the vertical angle than that of the flow from southwest. From figure 76 and 77 it is seen the same as in chapter 5.2.2 however, that an abrupt change in the angle of the wind direction will force an equally abrupt change in the vertical angle.

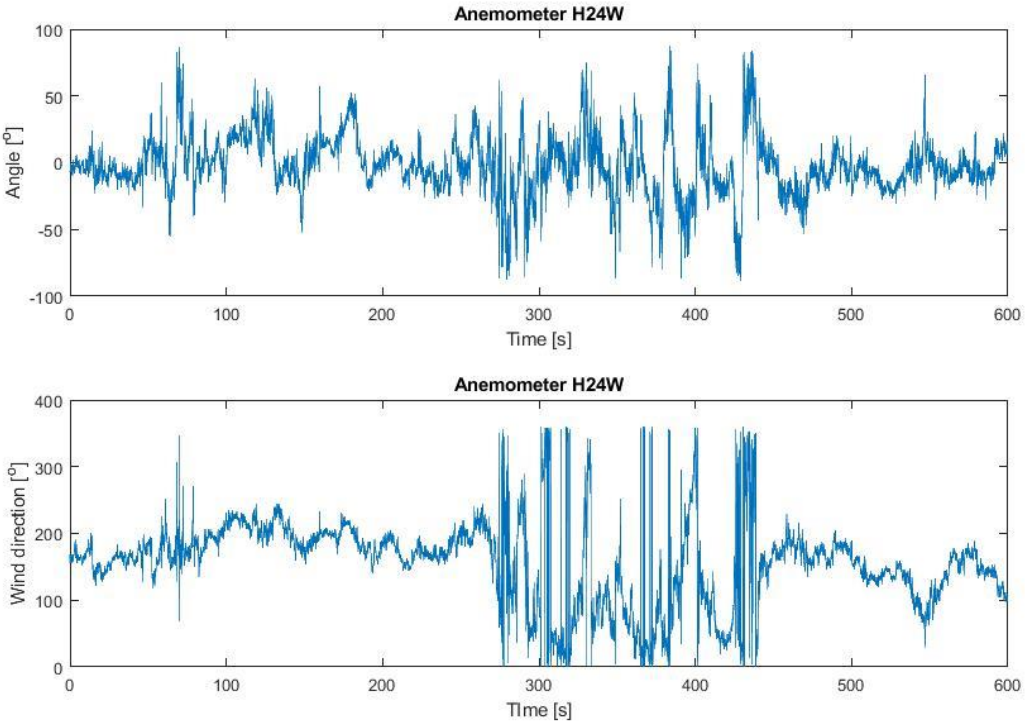

Figure 76: Variation of vertical angle and wind direction for H24W

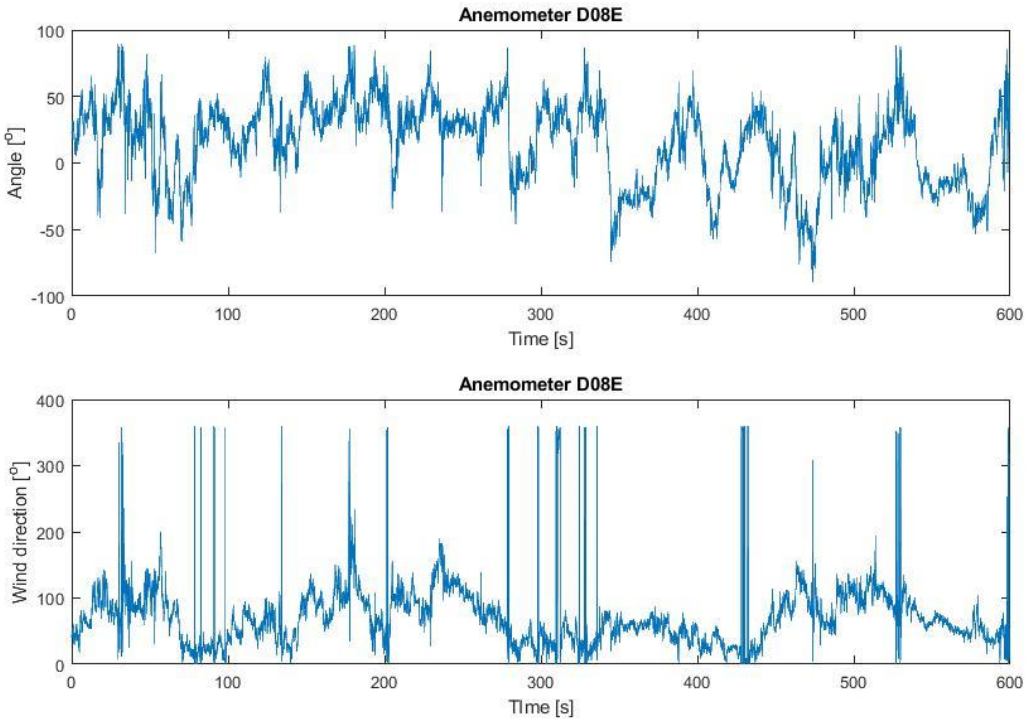

Figure 77: Variation of vertical angle and wind direction for D08E

5.3.3 Turbulence intensity

The turbulence intensities were even larger in this time-series than those of 23/09/21. Cheynet et. al [27] reported that a wind blowing from inside the fjord, i.e., a wind direction from south-east often was characterized by unusual large turbulence intensities with $I_u \approx 24\%$. From the data provided in this time-series, the mean turbulence intensity was $I_u \approx 49\%$, with the highest intensities registered from H20W and H18W at $I_u \approx 63\%$ and $I_u \approx 61\%$ respectively.

These extremely high values of the calculated turbulence intensities come from the non-stationary wind conditions which are frequently accounted at low wind speeds, as in this case. At higher wind speeds, the wind directions follow the fjord orientation with less variability than in case of a less, developed and unstable flow at low mean wind speeds. A comparison of the distribution of the mean wind speed and turbulence intensity, in terms of so-called wind roses, for all the records and those above the mean wind speed of 8 m/s is presented by Cheynet [22].

5.3.4 Correlation coefficients

Figure 78 show the correlation matrix of this time-series. As opposed to the correlation matrix in chapter 4.1.4 and 4.2.4, in this matrix it is D08W that show limited correlation with the rest of the anemometers. The correlation values are higher from D08W as opposed to the values from D08E from previous chapters, especially with the other anemometers mounted on hangar 08. Other notable differences from the other time-series are that H18W, H20W and H24W correlates less with the other anemometers and more with each other. The reason for this is perhaps that the wind direction has shifted from south-west to south-east, as there is no other notable change in this time-series compared to the previous ones.

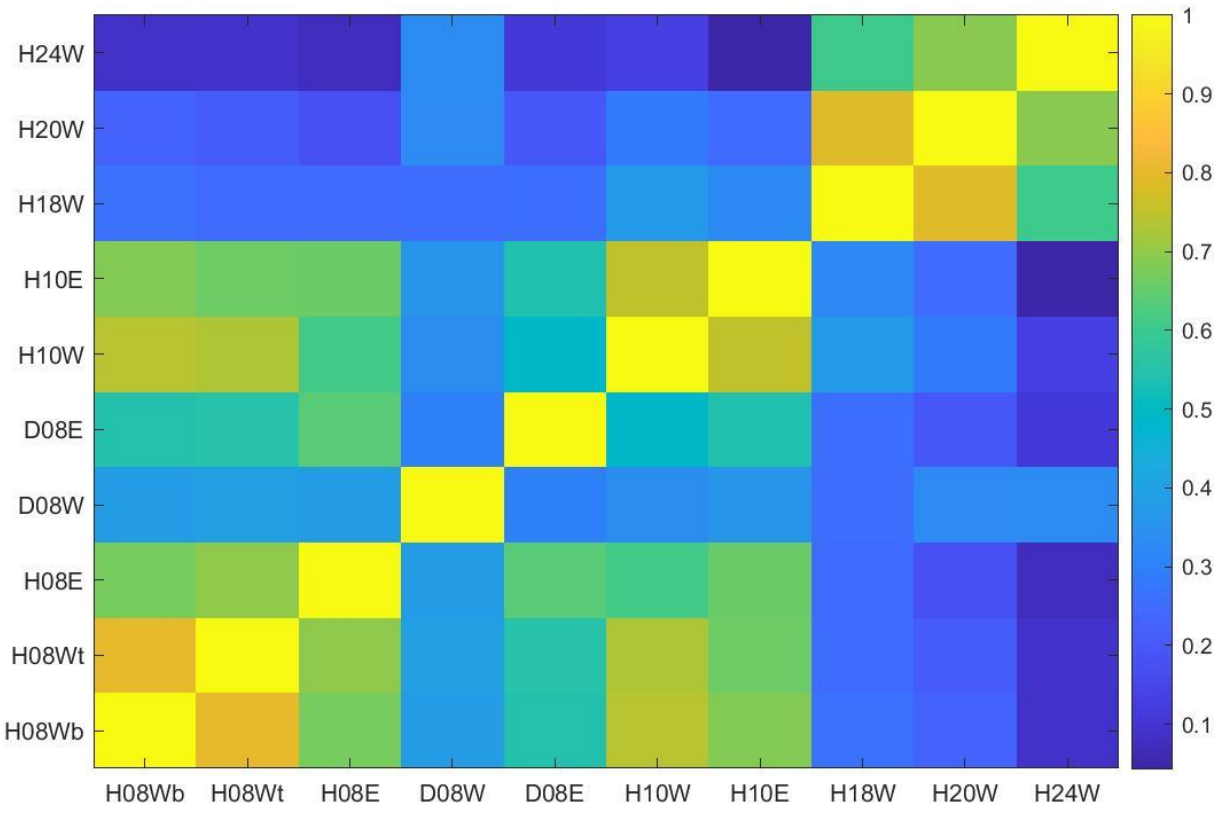

Figure 78: Correlation matrix illustrating the correlation between the anemometers

Figure 78 also illustrates the shift in wind direction and D08W is now the anemometer which the bridge deck disrupts the wind flow in front of and consequently, it correlates less with the other anemometers.

Figure 79 shows that H08Wb, H08Wt and H08E follows relatively the same pattern with regards to correlation as a function of distance to the other anemometers. H08Wb has a slightly larger correlation coefficient in general than H08Wt and H08E. Figure 79 also shows that the correlation for H08Wb, H08wt and H08E decreases faster as the distance to the other anemometers increases with this wind direction, as opposed to figure 63 in chapter 5.2.4.

For H10E and H10W, figure 80 shows that H10W generally correlates more with the other anemometers. The decrease in correlation as the distance increases does look somewhat consistent for both anemometers.

The patterns of H18W, H20W and H24W does look very similar, as seen in figure 81. H24W shows the lowest correlation with the anemometers furthest away, with is natural. It does however, correlate much more with H20W and H18W in this time-series as opposed to the two previous ones.

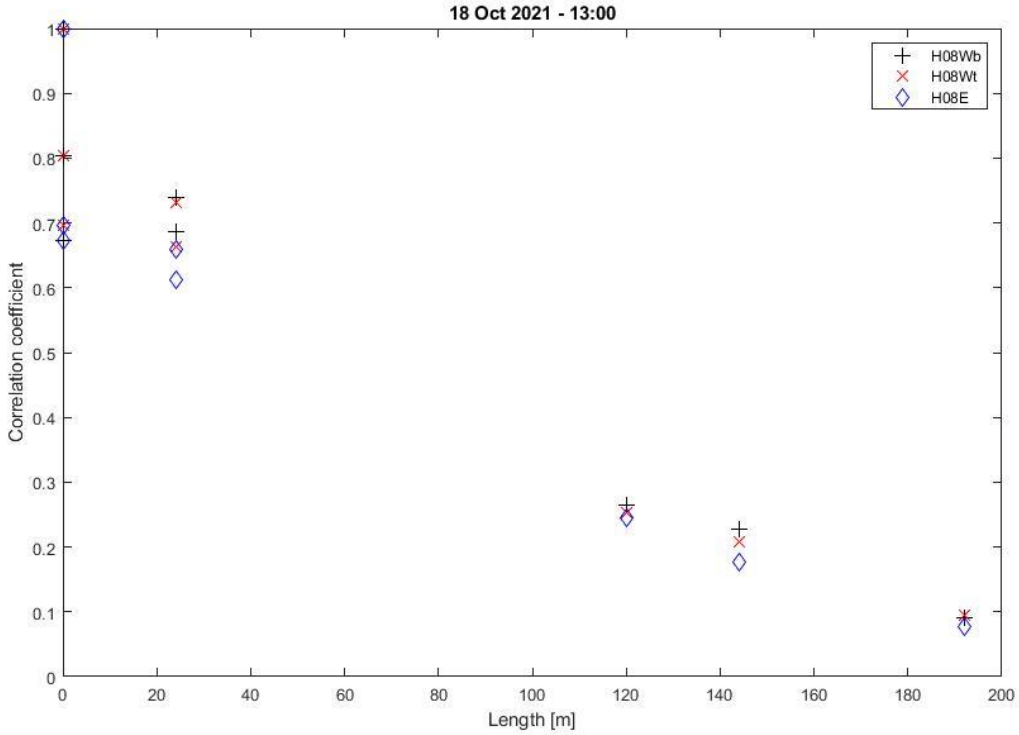

Figure 79: Correlation of specified anemometers as a function of distance along the bridge to the other anemometers. D08E and D08W are omitted

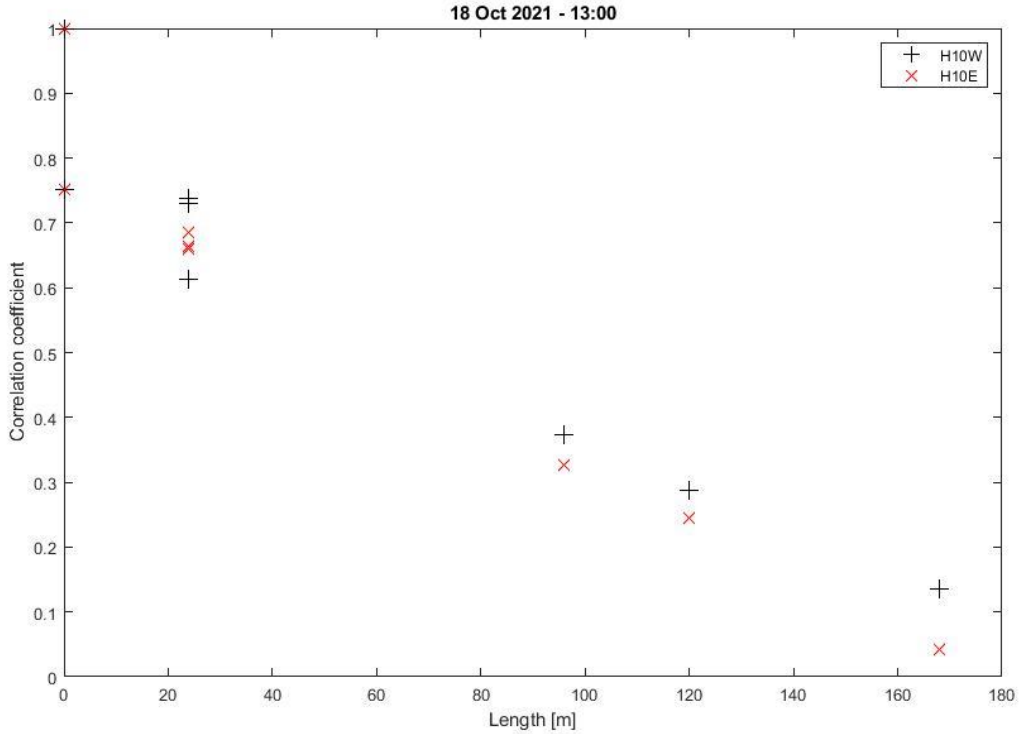

Figure 80: Correlation of specified anemometers as a function of distance along the bridge to the other anemometers. D08E and D08W are omitted

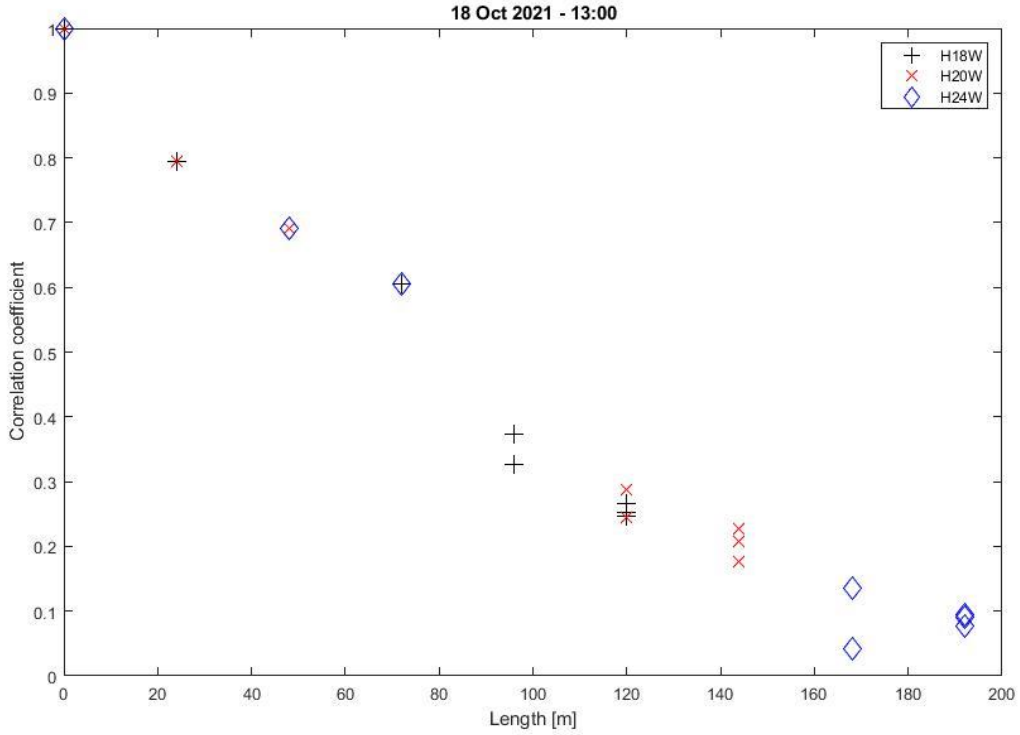

Figure 81: Correlation of specified anemometers as a function of distance along the bridge to the other anemometers. D08E and D08W are omitted

5.3.5 Vertical acceleration

Accelerometers H09E and H09W has their peaks and lowest negatives registered at the exact same time, with peaks after 514 seconds and lowest negatives after 119 seconds. The peaks were 40.12 m/s^2 and 41.89 m/s^2, which is almost twice the value recorded in 09/08/21 and 23/09/21. For the lowest negatives, the result is the same with negative values approximately twice those from the previous time-series.

After approximately 90 seconds the first burst of accelerations are registered. This burst last for around 20 seconds before another, stronger burst is registered. It is in this second burst the lowest negative values of -43.06 m/s^2 and -44.92 m/s^2 are recorded. As seen in figures 82 and 83, there looks to be no apparent connection between the horizontal wind velocity and the accelerations at those times.

A third, but smaller burst of accelerations is registered after approximately 390 seconds. This burst dies down after 420 minutes, before a fourth burst of accelerations is registered. This burst is both considerably stronger and longer than the third burst. The horizontal wind velocity does peak during this fourth burst, which might have a slight impact on the accelerations. It is seen however, that the peak acceleration is recorded at a time where the horizontal velocity is below 10 m/s. This might lead one to believe that the horizontal velocity has a small impact on the larger oscillations.

From figures 84 and 85 it is seen that H18E and H18W has the same number of bursts of accelerations are shown as in figures 82 and 83. The accelerations are approximately of the same magnitude, although H18E and H18W has both their peaks and lowest negatives registered during

the first burst. The peak of the fourth burst is considerably earlier during this burst than that recorded by H08E and H08W. Yet again, the horizontal wind velocity looks to play an almost indistinguishable role in affecting the accelerations. When the peak accelerations are registered at H18E and H18W, the anemometers around them recorded horizontal wind velocity with values in the interval [1 m/s – 3 m/s]. It is then natural to assume that is has little effect on the accelerations.

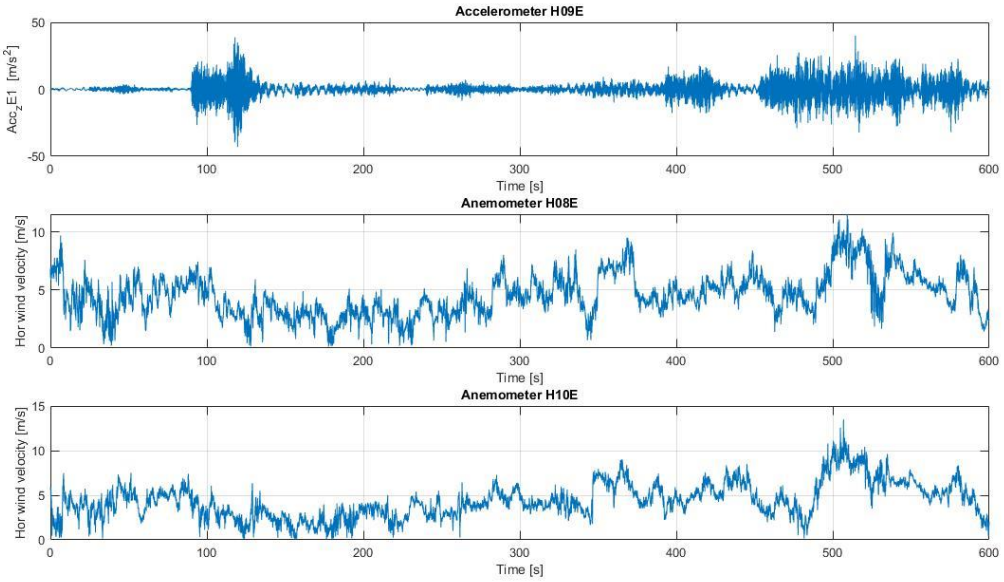

Figure 82: Vertical acceleration at H09E and horizontal wind velocity at H08E and H10E

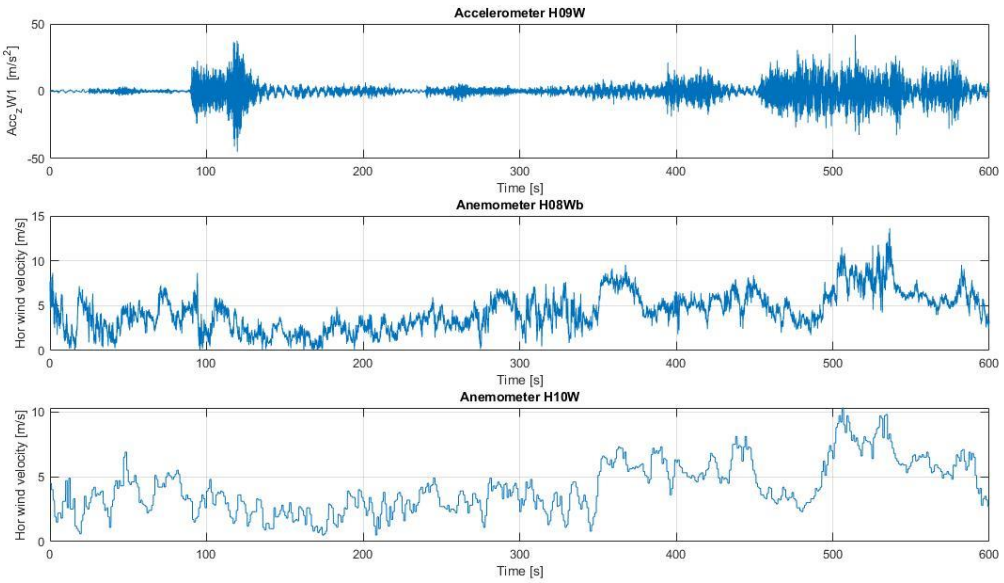

Figure 83: Vertical acceleration at H09W and horizontal wind velocity at H08Wb and H10W

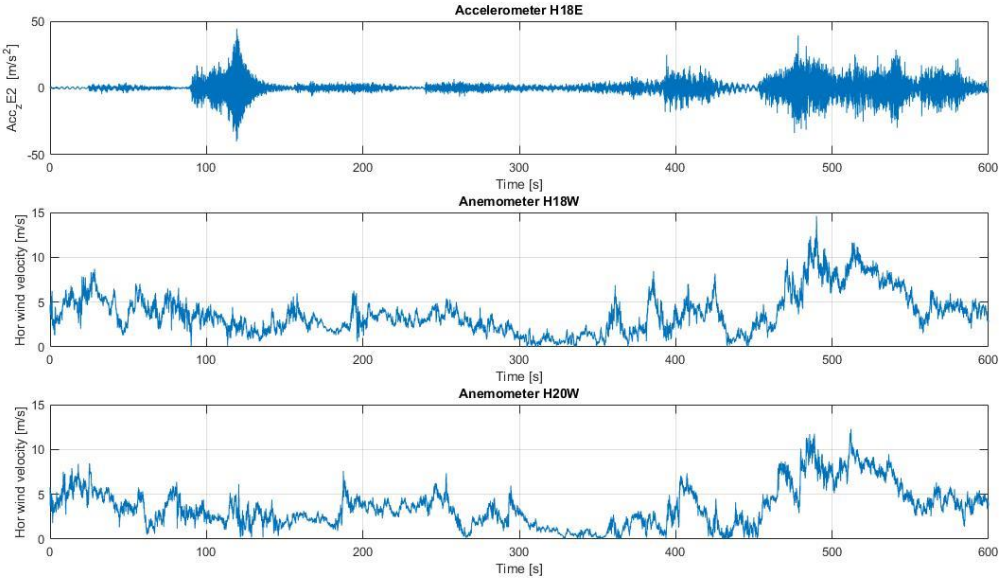

Figure 84: Vertical acceleration at H18E and horizontal wind velocity at H18W and H20W

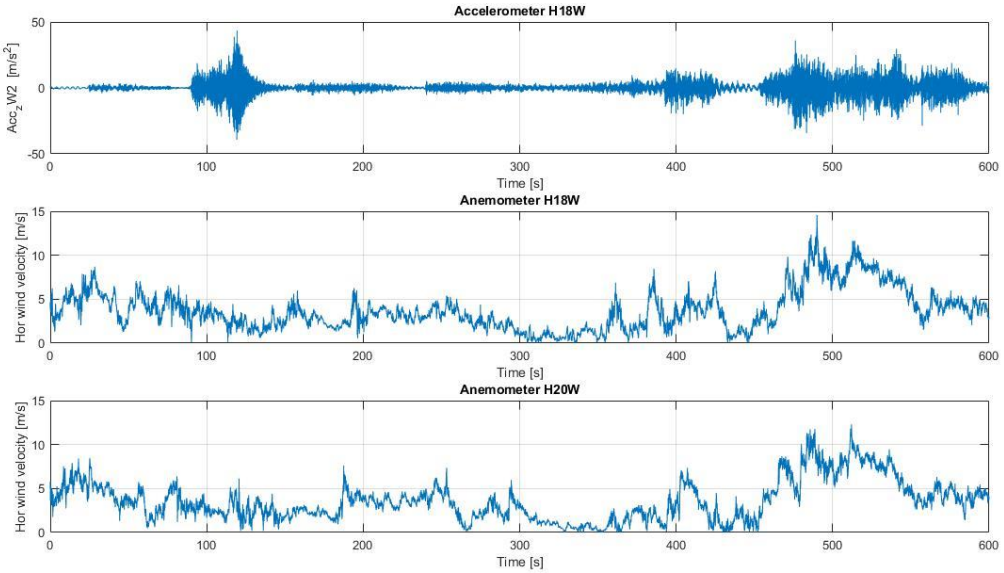

Figure 85: Vertical acceleration at H18W and horizontal wind velocity at H18W and H20W

H24E and H24W has the same number of bursts at the same timestamps as the other accelerometers. The peaks and lows are registered at approximately the same time as the peaks of the other accelerometers. Again, the horizontal wind velocity does not look like it has the main impact on the accelerations. Some increase in velocity up to and higher than 10 m/s is seen towards t=500 s, and vibrations towards the end of the recorded period are likely due to increased wind loads at this period. Figures 86 and 87 confirms this.

If the horizontal accelerations were to be examined, one might also see that an increase in wind velocity would in fact increase the vibration. This is, however, not investigated in this thesis.

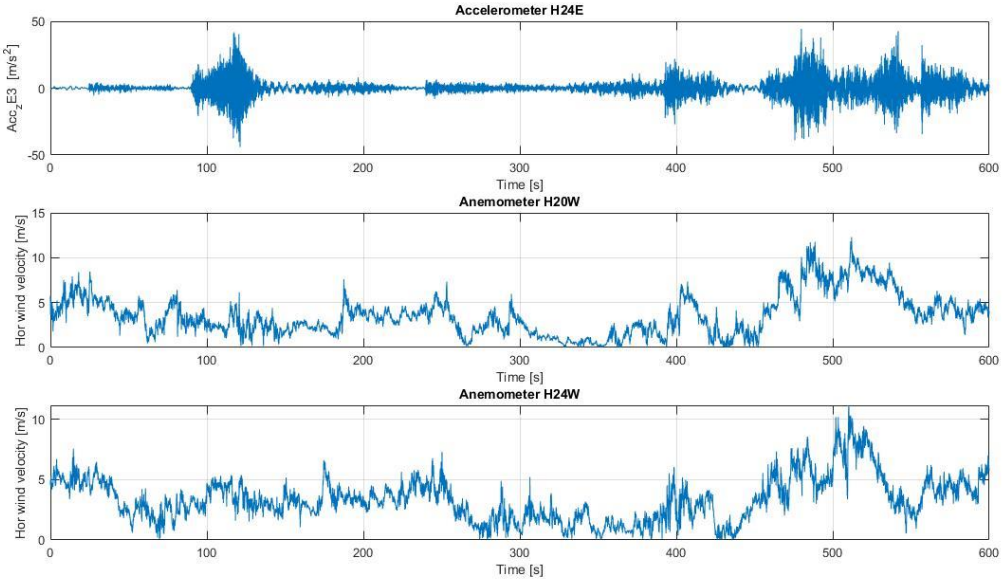

Figure 86: Vertical acceleration at H24E and horizontal wind velocity at H20W and H24W

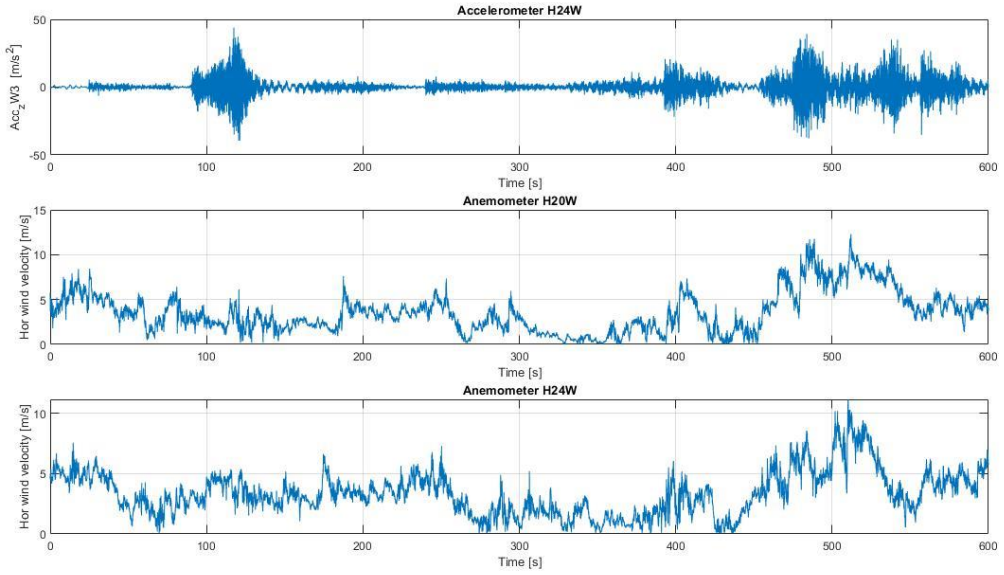

Figure 87: Vertical acceleration at H24W and horizontal wind velocity at H20W and H24W

5.3.6 Vertical acceleration spectra

The vertical acceleration spectra for H09E and H09W can be seen in figure 88 below. The first peak for both spectra is at a frequency of 0.217 Hz. From the findings of both Cheynet [22] and Wang [28] it is seen that this frequency corresponds to the first asymmetrical vertical mode, which Cheynet [22] estimated as 0.223 Hz while Wang [28] estimated it to 0.222 Hz. The second spectral peak is found at 0.403 Hz. This corresponds to the second symmetrical vertical mode, which Cheynet [22] estimated to have an eigen-frequency of 0.408 Hz. The third concentration of vibration energy is found at 0.848 Hz, although this concentration is much lower than the two first peaks. This third spectral peak corresponds well to the frequency of the third symmetrical vertical mode found by Cheynet [22]

(0.853 Hz). The fourth peak has a frequency of 1.154 Hz. It looks like this frequency corresponds to the first symmetrical torsion mode, which were found by Cheynet [22] and Wang [28] to be 1.237 Hz and 1.234 Hz respectively. Figure 88 also shows spectral peaks at higher frequencies, among others the largest concentration of vibration energy at a frequency of 4.334 Hz. The eigen-values for these higher modes are not further discussed and is likely to be excited by traffic on the bridge.

Figure 89 presents the vertical acceleration spectra for the accelerometers installed at H18. The first two spectral peak are found at 0.214 Hz and 0.403 Hz. 0.214 Hz corresponds to the frequency of the first asymmetrical mode found by both Cheynet and Wang and 0.403 Hz corresponds to the second symmetrical vertical mode estimated by Cheynet. The estimated values by Cheynet [22] and Wang [28] for both modes is mentioned in the section above. Other minor peaks are found at 0.848 Hz (third symmetrical vertical mode with 0.853), 1.240 Hz (first symmetrical torsion mode) and 2.368 Hz (first asymmetrical torsion mode). The first symmetrical torsion mode was estimated to have an eigen-frequency of 1.234 Hz by Wang [28] and 1.237 Hz by Cheynet [22]. The estimated frequency for the first asymmetrical mode was 2.125 Hz and 2.184 Hz by Wang [28] and Cheynet [22] respectively. The found frequency of 2.368 Hz corresponds to this first asymmetrical mode. Another concentration of vibration energy is seen at 3.308 Hz, which according to the findings of Tveiten [33], corresponds to the second symmetrical torsion mode with a frequency of 3.241 Hz. The spectral peak, however, is found at 4.335 Hz, a frequency that is likely mostly excited by traffic.

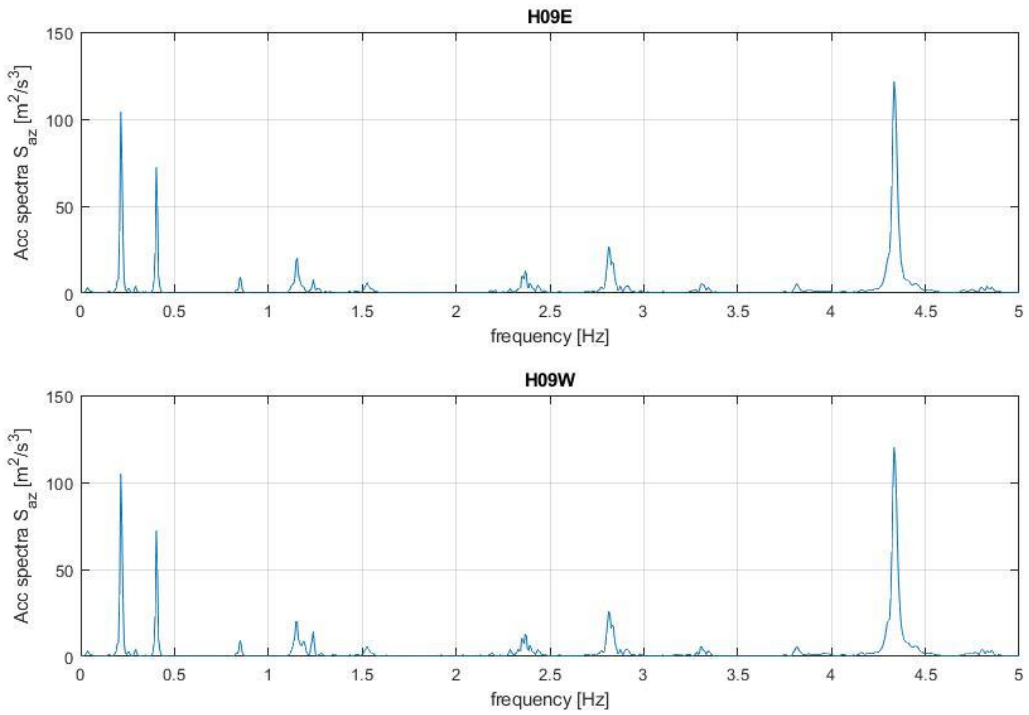

Figure 88: Vertical acceleration spectra for accelerometers mounted on H09

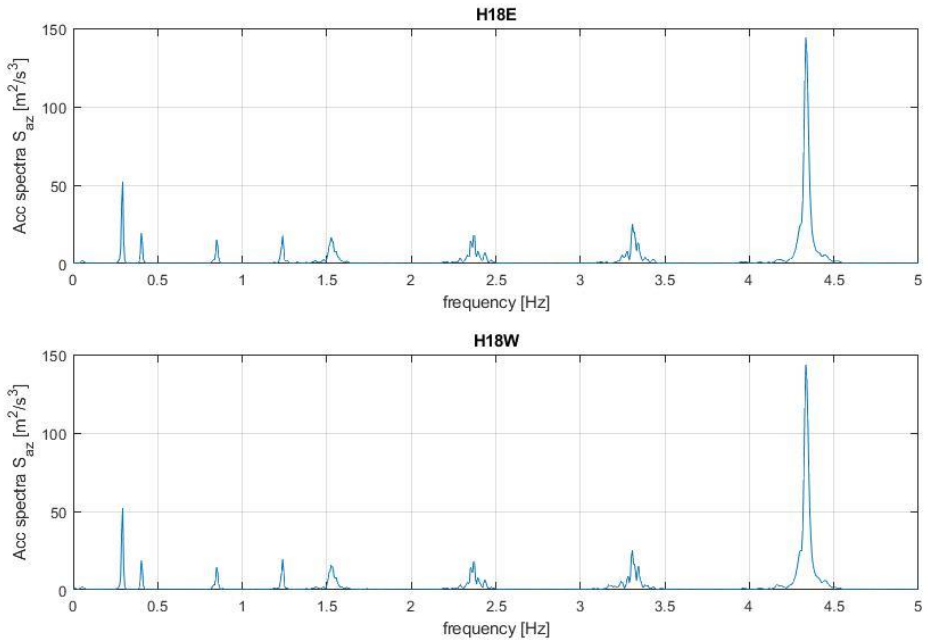

Figure 89: Vertical acceleration spectra for accelerometers mounted on H18

The spectra for H24E and H24W has the peak at a frequency of 0.214 Hz. This frequency has been thoroughly discussed earlier in this chapter as it corresponds well with the first asymmetrical mode found by both Cheynet and Wang. The spectra have minor peaks at 0.293 Hz (first symmetrical vertical mode), 0.403 Hz (second symmetrical vertical mode), 0.586 Hz (second asymmetrical vertical mode) and 0.848 Hz (third symmetrical vertical mode). There were concentrations of vibration energy at higher frequencies as well, with the largest spectral peak found at a frequency of 4.334 Hz. This frequency is likely to correspond with more traffic on the bridge and is presented in figure 90.

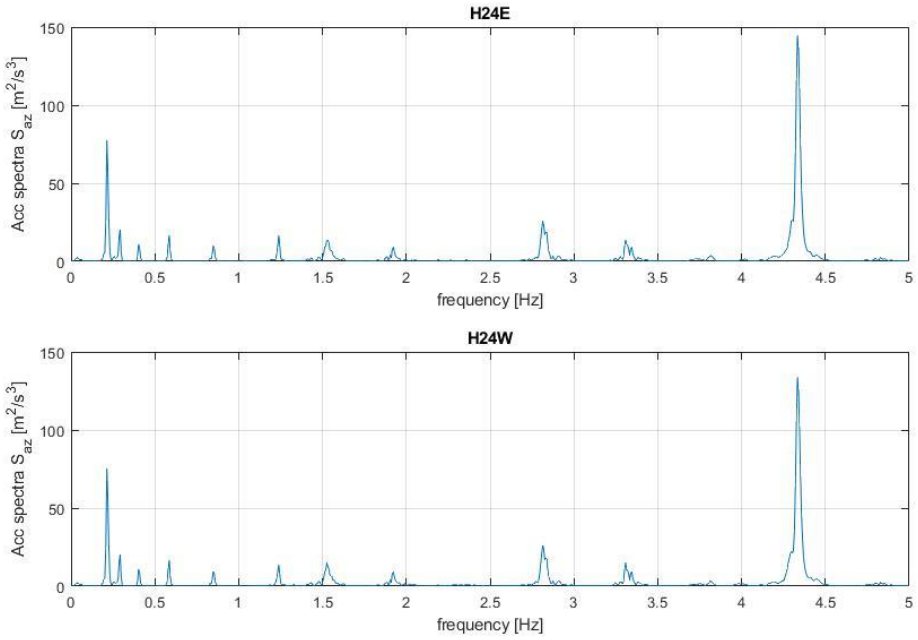

Figure 90: Vertical acceleration spectra for accelerometers mounted on H24

5.4 Wind data from 21/10/21 – 15:10:00

5.4.1 Horizontal wind velocity and wind direction

This time-series had the highest maximum wind velocity of all the time-series analysed in this thesis, with H18W registering a maximum of 23.24 m/s after 570.5 seconds. This equals a wind speed of 83.66 km/h. From figure 91, it does look like the peak might be statistical noise as it looks very different from the rest of the series. From figure 92 it is seen that the wind direction is relatively consistent at 570 seconds and there is nothing out of the ordinary that would explain the sudden peak of horizontal velocity.

It is also the only time-series where a functioning anemometer recorded a minimum velocity of 0 m/s, from H20W.

Even though this series had the highest maximum horizontal velocity, the mean velocity was not the highest at 6.17 m/s with the means of D08E and D08W omitted. The mean was relatively stable throughout the time-series, with only the anemometers installed at deck level with values of 5 m/s or lower. The reason for this has been discussed thoroughly previously and the reader is referred to chapter 5.1.1 and 5.2.1. The standard deviation is the highest of the time-series analysed, with a mean value of 2.95. As the horizontal velocity has larger peaks and somewhat the same lows as the previous time-series, it is natural that the standard deviation gets larger.

When the wind direction shifts angles quickly from 360° to 1°, the plots of the directions look arbitrary and irrational. This is seen in figure 93. Nevertheless, the mean direction was found with the help of MATLAB to have an angle of 99.9°. This equals a wind flow almost perpendicular to the bridge.

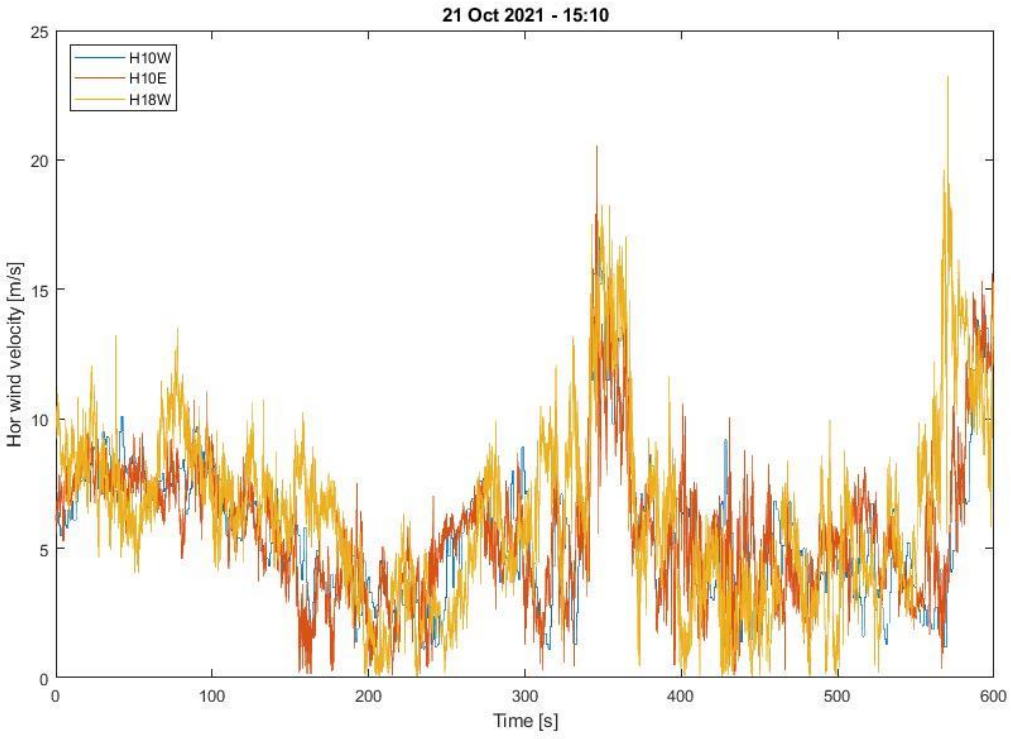

Figure 91: Variation of horizontal velocity for H10W, H10E and H18W

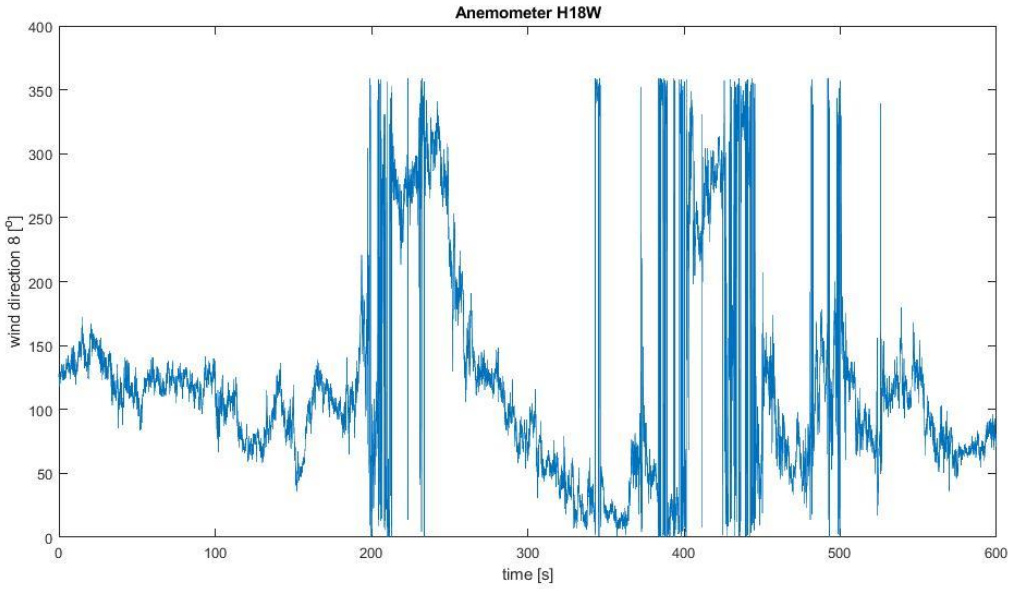

Figure 92: Variation of wind direction for H18W

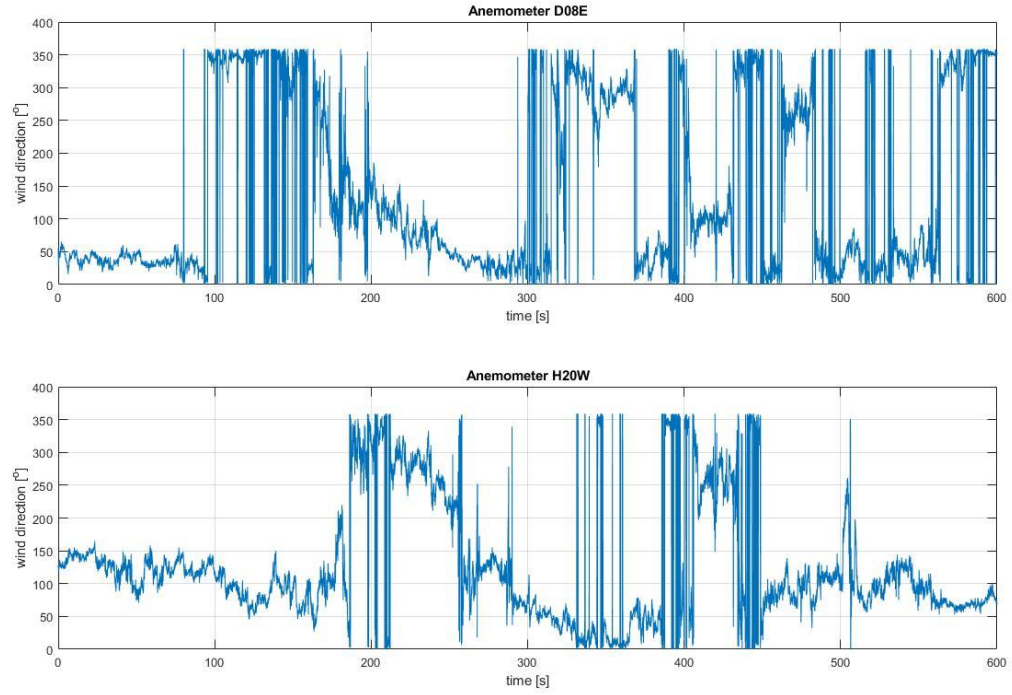

Figure 93: Variation of wind direction for D08E and H20W

5.4.2 Vertical wind velocity and vertical angle

The vertical wind velocity had the largest peaks and lowest negatives in this time-series compared to the others. These extremums are seen in table 14. It is the only time-series with a negative mean vertical velocity, with a value of -0.02 m/s. As stated in chapter 4.1.2, the mean value is not a good value to use as the velocity fluctuates between positive and negative values. It does look however like a negative mean vertical velocity correlates with a negative mean vertical angle, as the angle is found to be -1.12°.

Table 14: Vertical wind data from 21/10/21

	Vertical wind data 21/10/21 - 15:00:00										
Anemometers	H08Wb	H08Wt	H08E	D08W	D08E	H10W	H10E	H18W	H18E	H20W	H24W
Max velocity [m/s]	7,5600	6,8600	15,0300	10,6600	10,5300	0,0000	12,2200	7,0000	0,0000	4,8100	7,1100
Min velocity [m/s]	-8,5900	-9,8300	-15,5500	-12,0200	-15,0000	0,0000	-10,6200	-7,6900	0,0000	-6,4300	-7,7600
Mean [m/s]	-0,2358	-0,1250	0,2750	0,3416	-0,1389	0,0000	0,2817	-0,2819	0,0000	-0,1682	-0,0898
Standard deviation	1,4307	1,7139	2,3109	2,3772	2,9103	0,0000	2,4052	1,5598	0,0000	1,4895	1,3348

The case of vertical angles changing abruptly when the wind direction changes abruptly does seem to correlate during this time-series, but not in the same way as discussed in chapter 4.1.2. Here, the vertical angle seems somewhat consistent when the wind direction stays relatively within a small interval. When the wind changes direction from the 350°-360° to the 1°-10° the vertical angle stops being consistent and becomes more unpredictable. This is illustrated by figures 94 and 95, where the vertical angle and wind direction are plotted beneath each other to see the changes happening at the same timestamps.

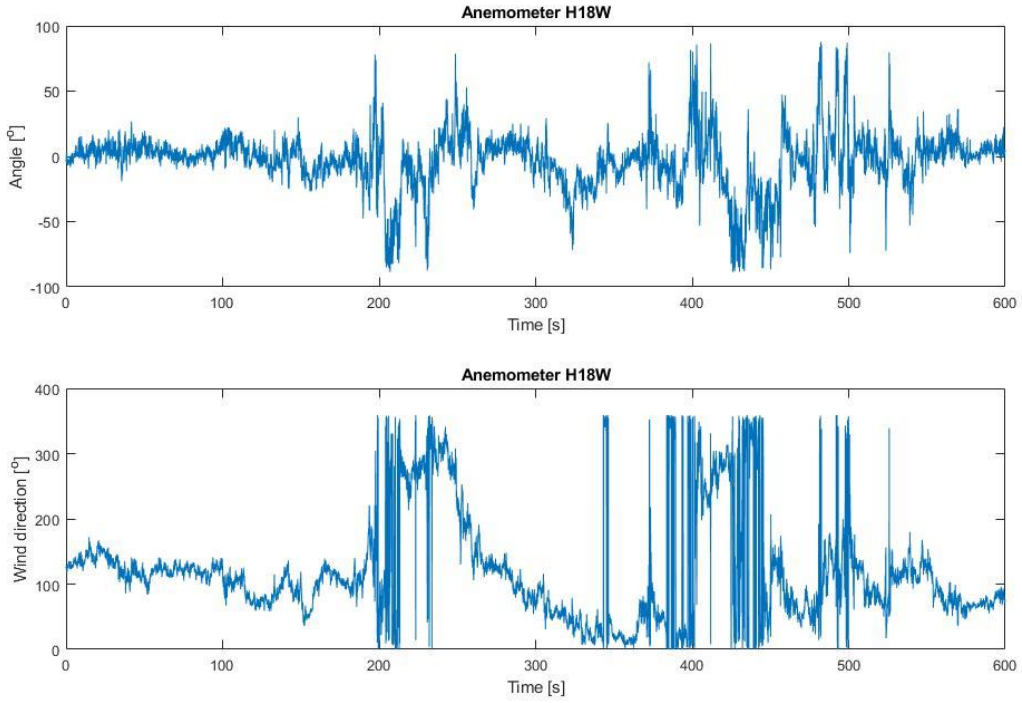

Figure 94: Variation of vertical angle and wind direction for H18W

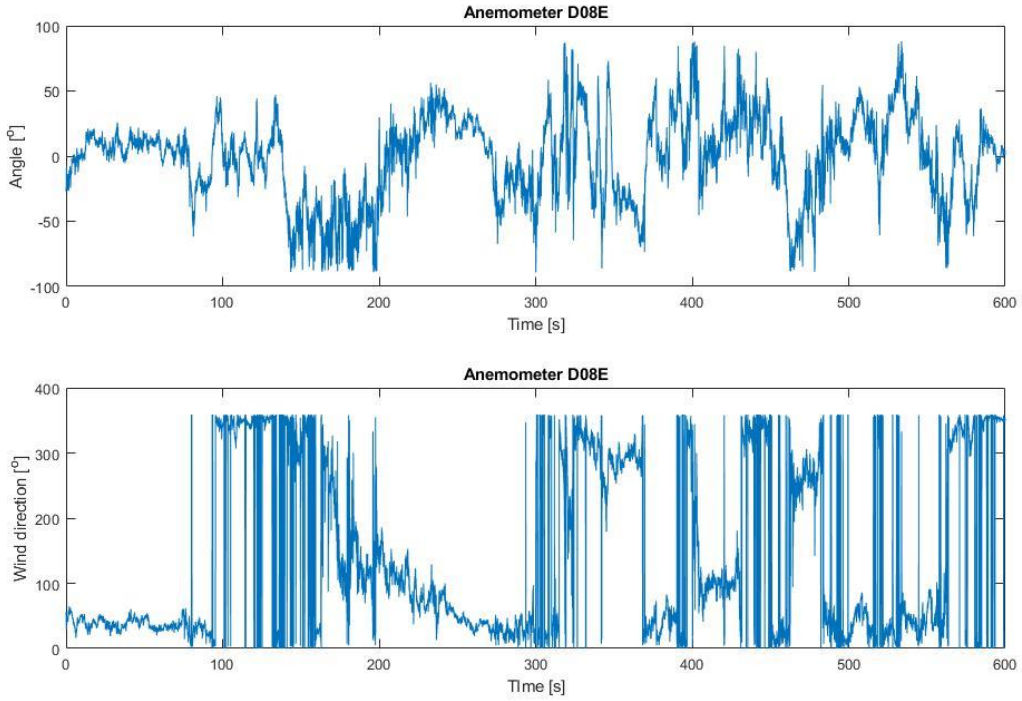

Figure 95: Variation of vertical angle and wind direction for D08E

It can be noted that both the direction and the vertical angle looks less predictable at the deck anemometers compared to the other anemometers. This can be seen by comparing figure 94 to figures 95 and 96. D08W also has much more randomness in its plot. Therefore, it seems like the reaction of the deck anemometers mounted on the opposite side of the wind direction is less predictable than its peers.

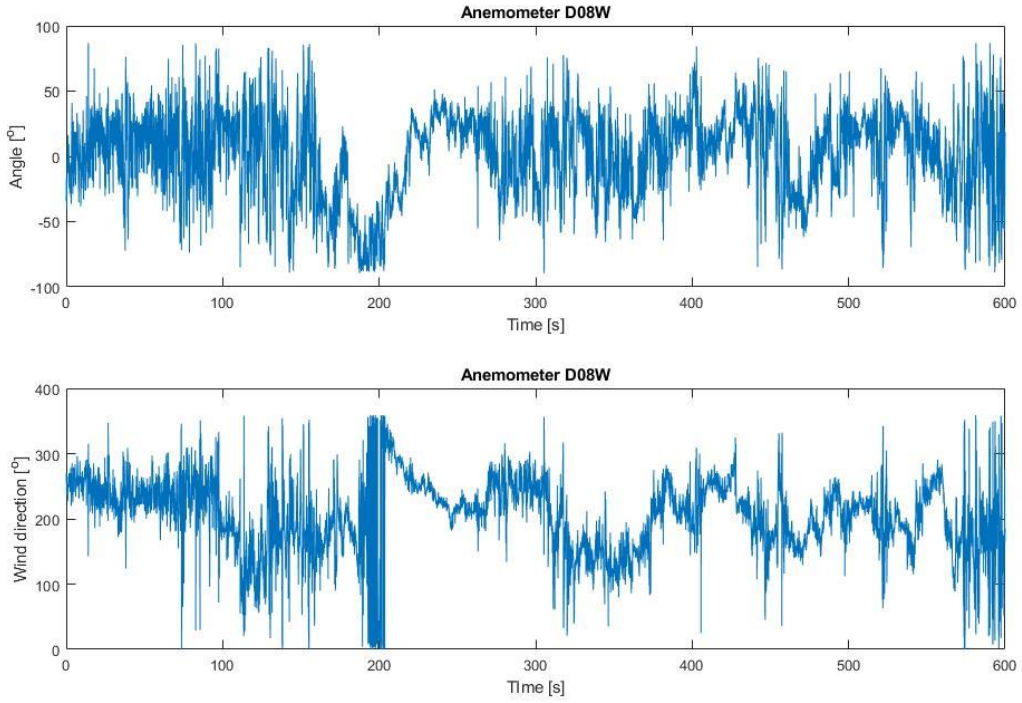

Figure 96: Variation of vertial angle and wind direction for D08W

5.4.3 Turbulence intensity

As seen in chapter 4.3.3, the turbulence intensities in this time-series are also seemingly extremely high compared to that of previous research conducted on the Lysefjord bridge [27]. The highest intensities are registered at H20W and D08W, where the value is $I_u \approx 56\%$ at both anemometers. Although lower than the largest registered intensities during the 18/10/21 time-series, the values are still extremely high and may seem erroneous and faulty. The mean turbulence intensity is $I_u \approx 51\%$, which is more than the intensity found in chapter 4.3.3. As unusual large intensities are recorded seemingly unrelated to the different wind directions or horizontal velocities discussed in this thesis. The answer is perhaps that the mean velocities here are too small to create accurate results that are comparable to the turbulence intensities found by previous research.

5.4.4 Correlation coefficients

The correlation matrix in figure 97 is relatively similar to the one in chapter 5.3.4. The same main pattern seems to be recurring, namely that the deck anemometer installed on the opposite side of the wind direction show low correlation with the other anemometers. However, it seems that most anemometers correlate more with each other than in previous matrixes. For example, H20W and H08Wb correlates more in figure 97 compared to figure 78 in chapter 5.3.4.

Figure 98 shows that H08Wb, H08Wt and H08E follows somewhat the same pattern as in previous chapters but with some small differences. It is curious that H08E has a larger correlation with H20W than H18W. This is likely to be a mistake of some sort and has perhaps something to do with the precision of the instruments.

H10E and H10W follows somewhat the same pattern as previous, with the exception that H10E now correlates more with the anemometers furthest away (H20W and H24W) than H10W. This is illustrated in figure 99.

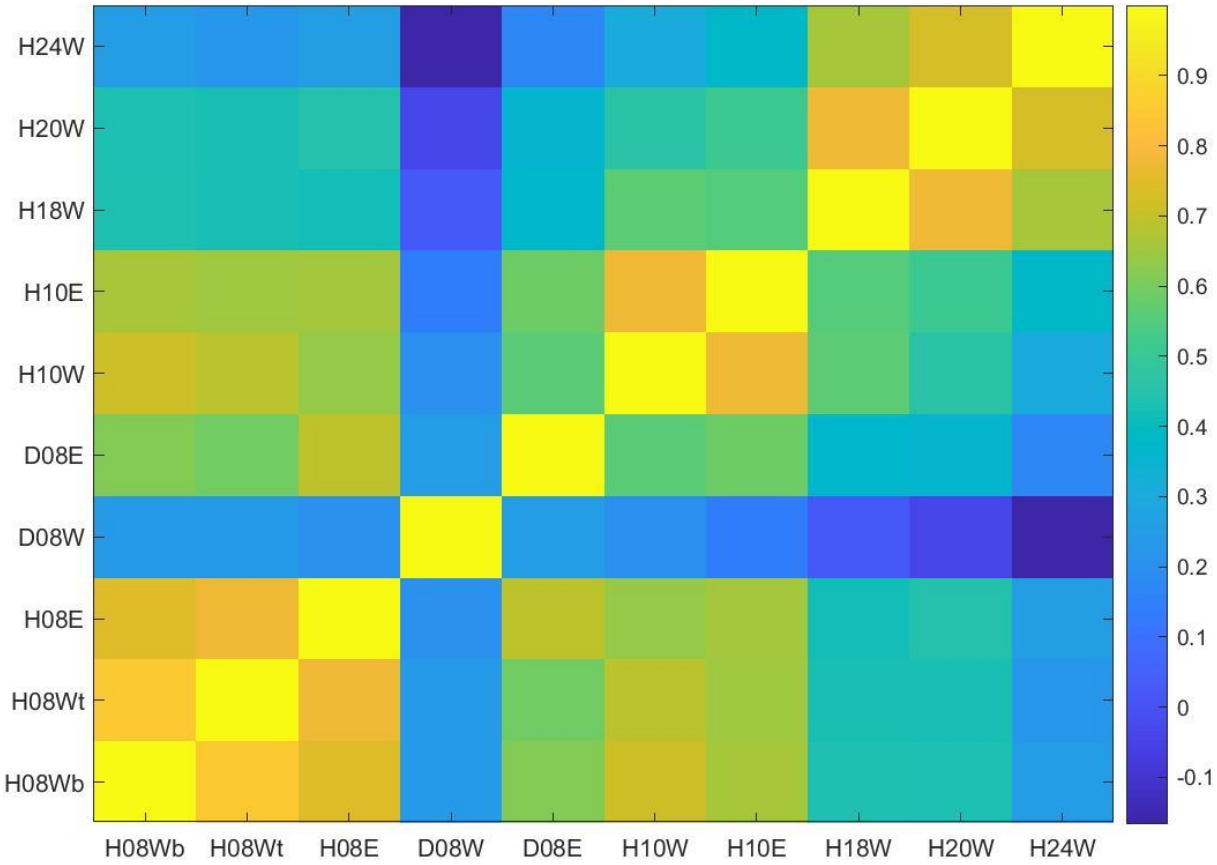

Figure 97: Correlation matrix illustrating the correlation between the anemometers

Figure 100 illustrates that H18W, H20W and H24W correlates more with the anemometers furthest away, and to somewhat the same degree with each other as in chapter 5.3.4. From these forementioned figures, the general assumption is that a higher horizontal velocity coupled with the wind direction during this time-series makes the anemometers correlate stronger. The exception is the deck mounted anemometers, which correlates less.

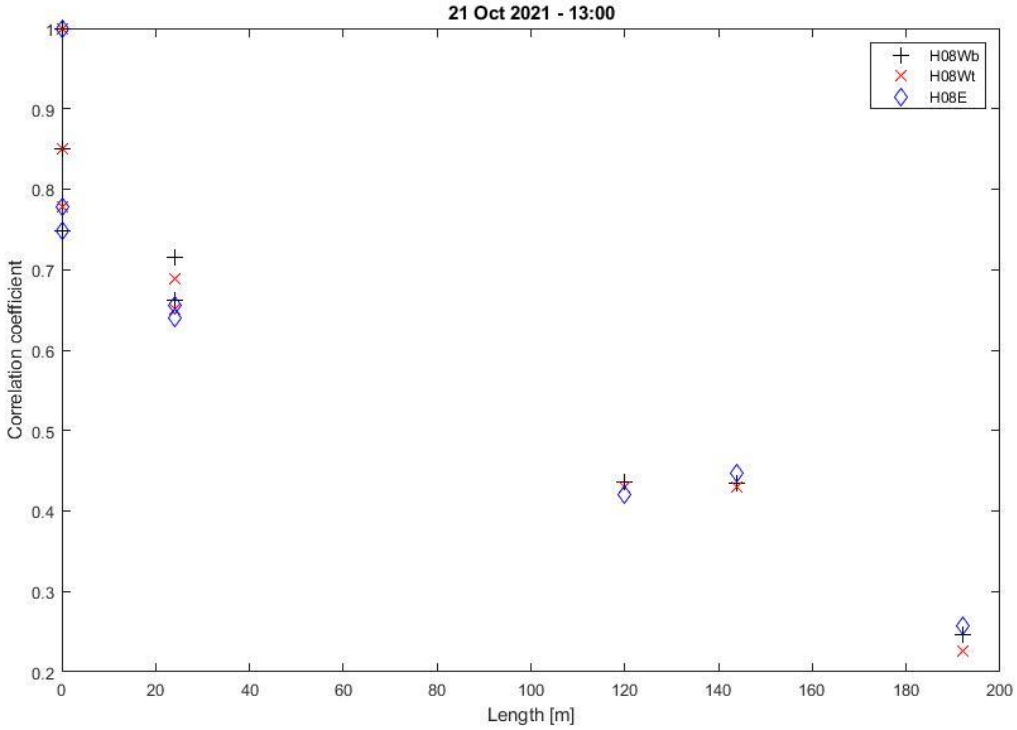

Figure 98: Correlation of specified anemometers as a function of distance along the bridge to the other anemometers. D08E and D08W are omitted

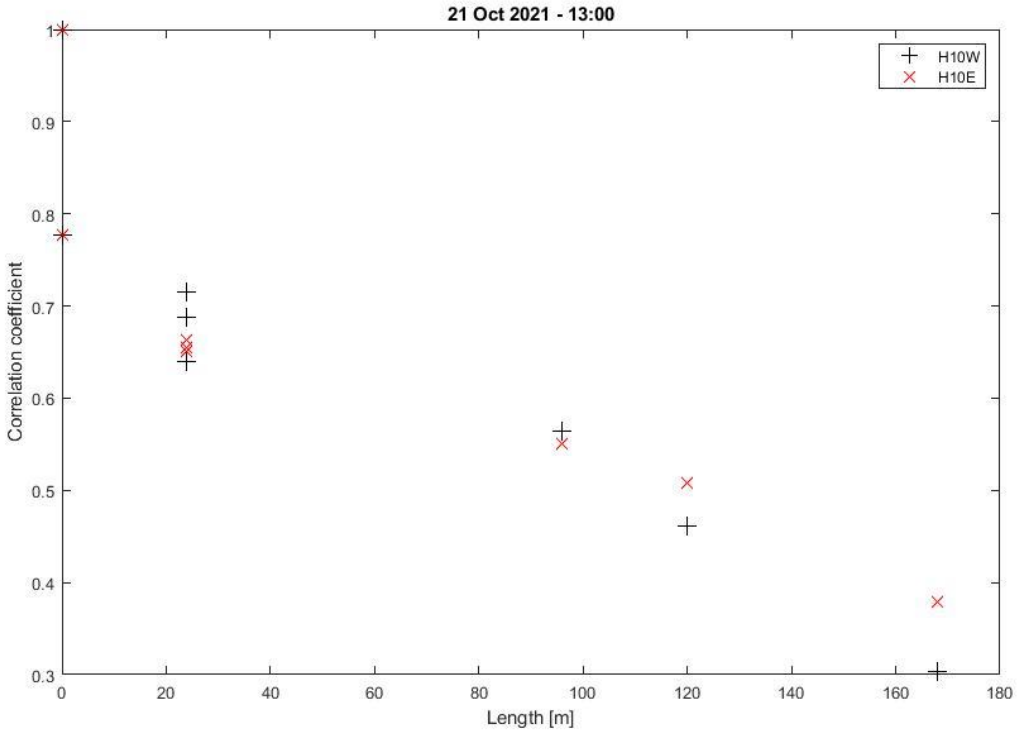

Figure 99: Correlation of specified anemometers as a function of distance along the bridge to the other anemometers. D08E and D08W are omitted

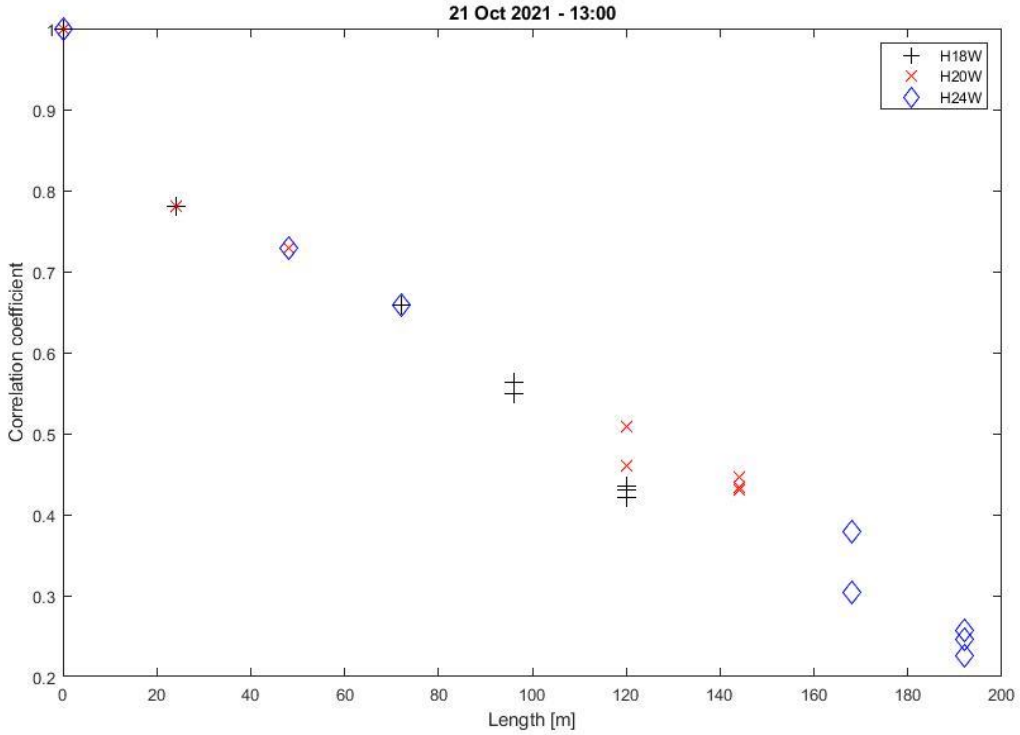

Figure 100: Correlation of specified anemometers as a function of distance along the bridge to the other anemometers. D08E and D08W are omitted

5.4.5 Vertical accelerations

Figures 101 and 102 illustrates that during this time-series, the first burst of accelerations registered by H09E and H09W came after approximately 114 seconds. This first burst also produced the highest values recorded from these accelerometers, as well as the lowest negatives. The peak values are about 3/4 as high as the ones from 18/10/21, while the lowest negatives are approximately half of those from the previous time-series. This, coupled with the fact that there is seemingly no clear connection between the higher horizontal velocities registered in this time-series and the bursts shown by the accelerometers, is another indication that the horizontal wind has little impact on the accelerations of the bridge.

Accelerometers H18E and H18W shows the same first burst as H09E and H09W. This is seen from figures 103 and 104. The extremums are registered at the second noticeable burst however, after approximately 545 seconds. The values of the extremums are a bit lower than those recorded by H09E and H09W. It is worth noticing that the horizontal velocity of the anemometers closest to the accelerometers H18E and H18W have their peak velocity recorded at approximately the same time as the extremums of H18E and H18W. It is hard to say what effect this has on the accelerations though, as the accelerations at H09E and H09W showed no sign of correlation with the horizontal velocity. H18E and H18W are mounted more to the middle of the bridge, which might make them more susceptible to the effects of the wind.

The peaks of both accelerometers H24E and H24W came during the first burst, but the lowest negative was registered at the second burst for H24E. H24W had its lowest negative during the first burst, i.e., the negatives were registered at different bursts. During the first burst, the velocity varies

between 5-10 m/s. The horizontal velocity does spike after 350 seconds, but this looks to have a negligible impact on the acceleration of both accelerometers. These accelerations are seen in figures 105 and 106.

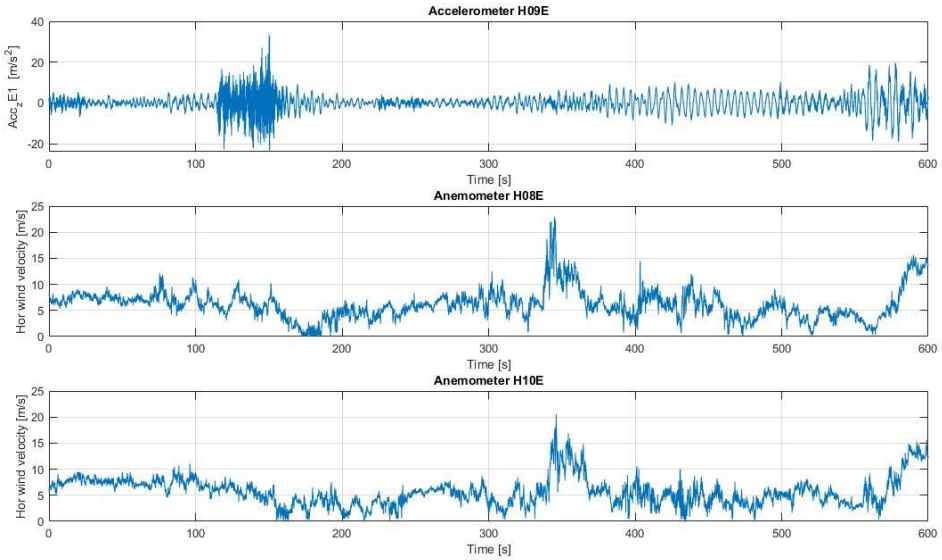

Figure 101: Vertical acceleration at H09E and horizontal wind velocity at H08E and H10E

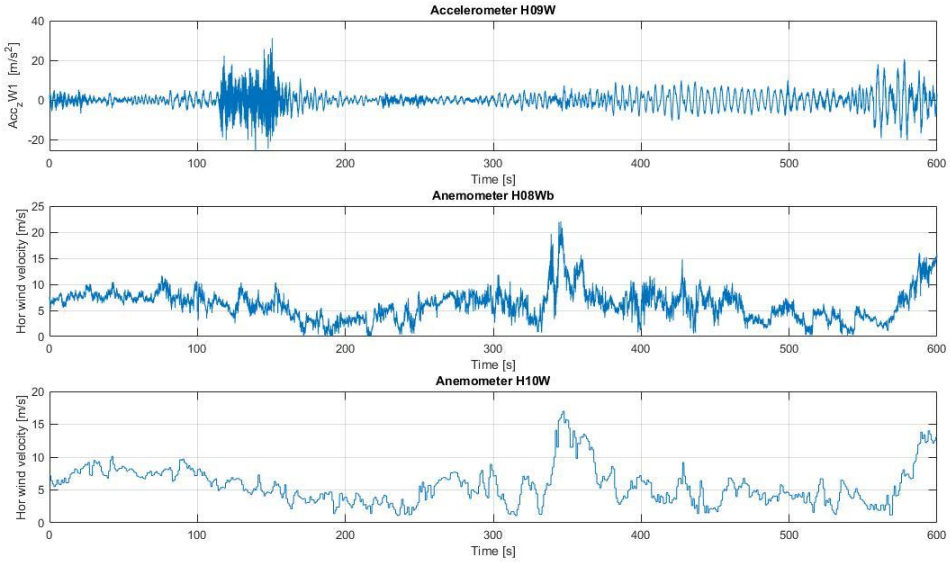

Figure 102: Vertical acceleration at H09W and horizontal wind velocity at H08Wb and H10W

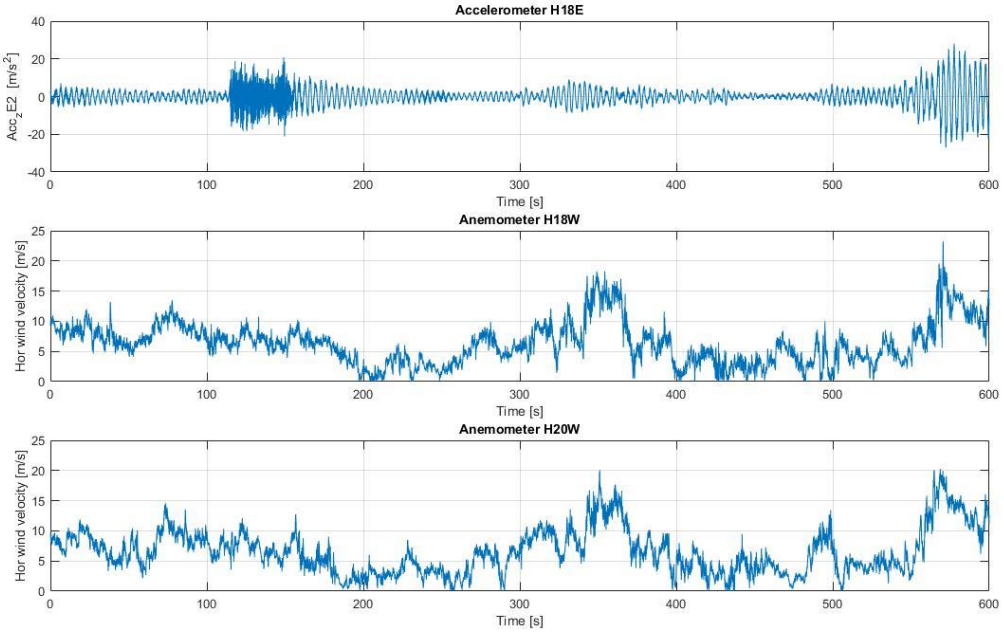

Figure 103: Vertical acceleration at H18E and horizontal wind velocity at H18W and H20W

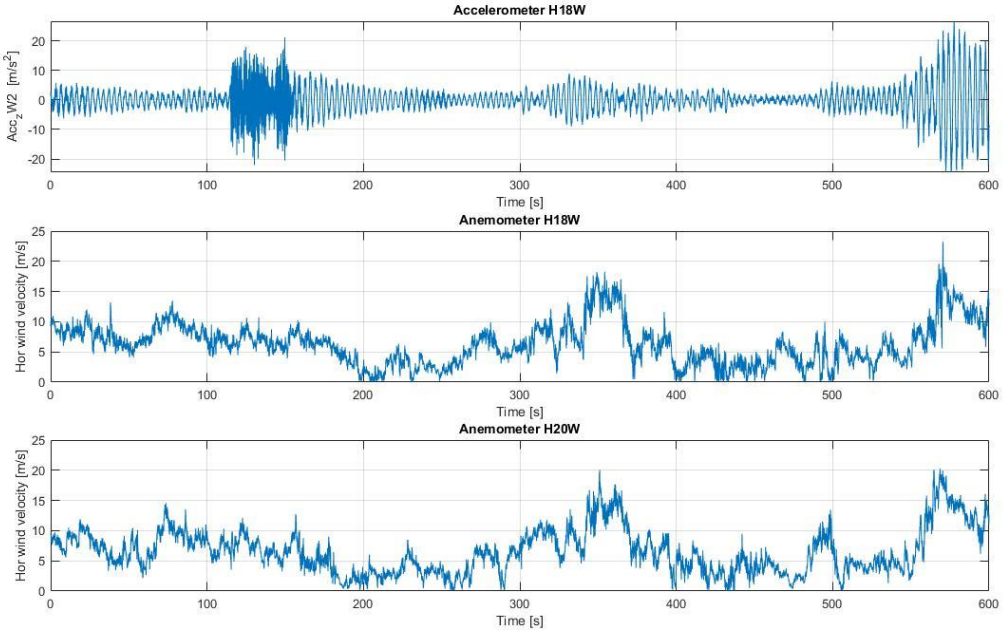

Figure 104: Vertical acceleration at H18W and horizontal wind velocity at H18W and H20W

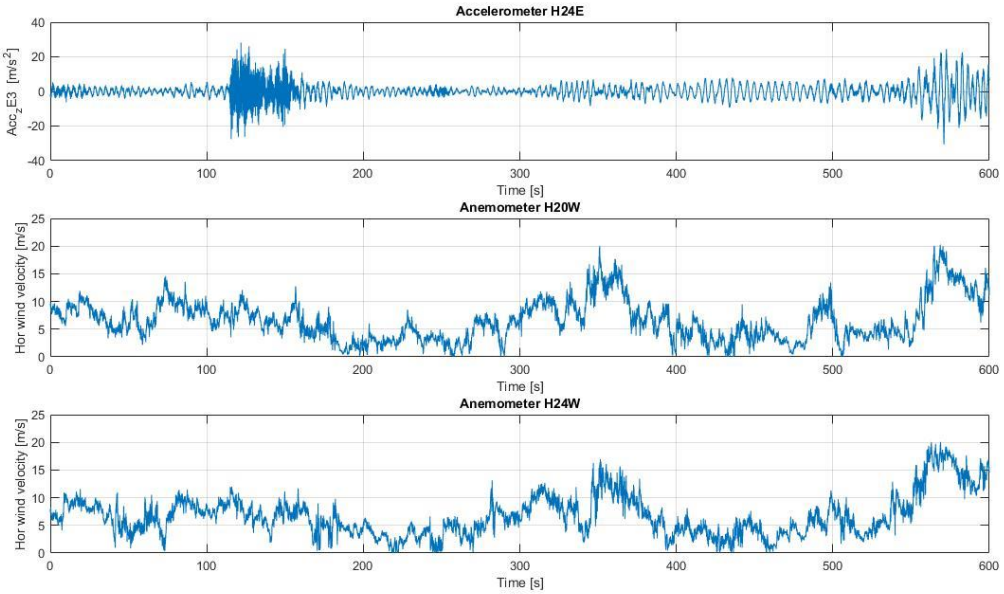

Figure 105: Vertical acceleration at H24E and horizontal wind velocity at H20W and H24W

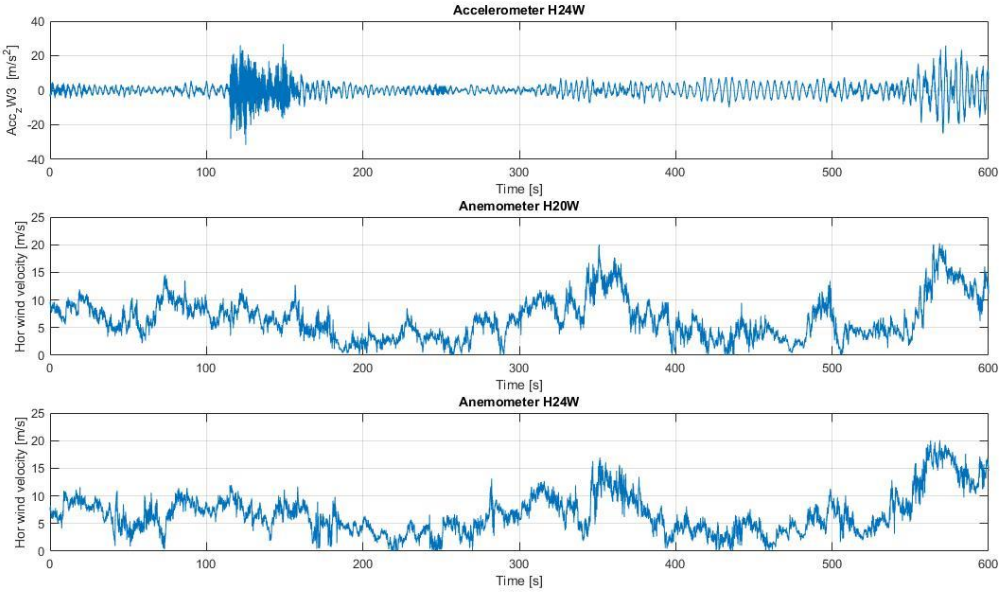

Figure 106: Vertical acceleration at H24W and horizontal wind velocity at H20W and H24W

5.4.6 Vertical acceleration spectra

In figure 107, the vertical acceleration spectra for the accelerometers installed at H09 is presented. The spectra have a peak value at a frequency of 0.226 Hz, for both H09E and H09W. This corresponds well with the first asymmetrical vertical mode found by Cheynet [22] at 0.223 Hz and by Wang [28] at 0.222 Hz. A minor peak is found at 0.293 Hz (first symmetrical vertical mode) and a third concentration of vibration energy is at 0.401 Hz, albeit with a concentration that is about 1/4 of the first peak. This 0.401 Hz frequency corresponds to the second symmetrical vertical mode. Since the accelerometers H09E and H09W are installed at one of the quarter spans of the bridge, it seems

logical that the largest vibrations are concentrated at a frequency corresponding with the first asymmetrical mode.

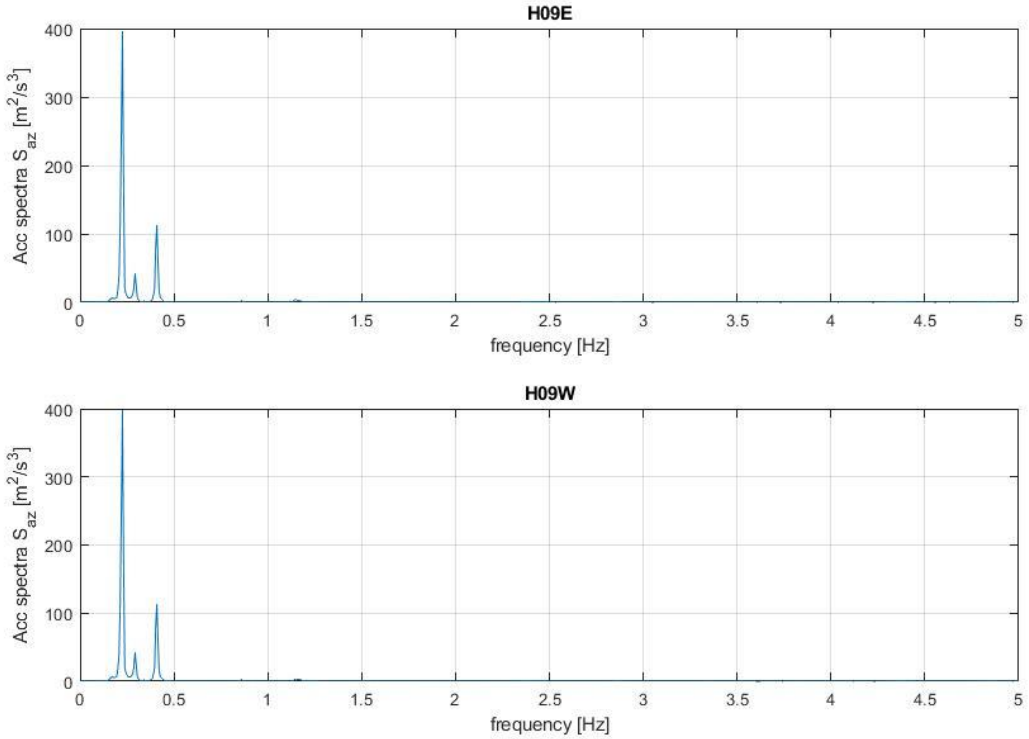

Figure 107: Vertical acceleration spectra for accelerometers mounted on H09

The acceleration spectra for the accelerometers installed at hangars H18E and H18W, are concentrated mostly at a frequency of 0.293 Hz, this largely corresponds with the first symmetrical vertical mode. The second, and only other, spectral peak is found at 0.409 Hz. This concentration of vibration energy is about 1/15 of the first spectral peak and corresponds to the second symmetrical vertical mode (0.408 Hz). Since these accelerometers are installed at half span, it follows naturally that the frequencies with the largest spectral peaks corresponds with the symmetrical vertical modes. The spectra can be seen in figure 108.

Figure 109 presents the vertical acceleration spectra for the accelerometers installed at H24. The peak value of the spectra is at a frequency of 0.226 Hz, for both H24E and H24W. Again, as expected since H24 is at the quarter span, this frequency corresponds well with the first asymmetrical vertical mode estimated by both Cheynet [22] and Wang [28]. A second peak is found at 0.293 Hz, which corresponds to the same mode as one of the minor peaks from the spectra of H09E and H09W, the first symmetrical vertical mode. Another, albeit very small concentration of vibration energy, is seen at 0.409 Hz. This corresponds well with the second symmetrical vertical mode.

There are no other noticeable spectral peaks at higher frequencies in any of the spectra presented in this section.

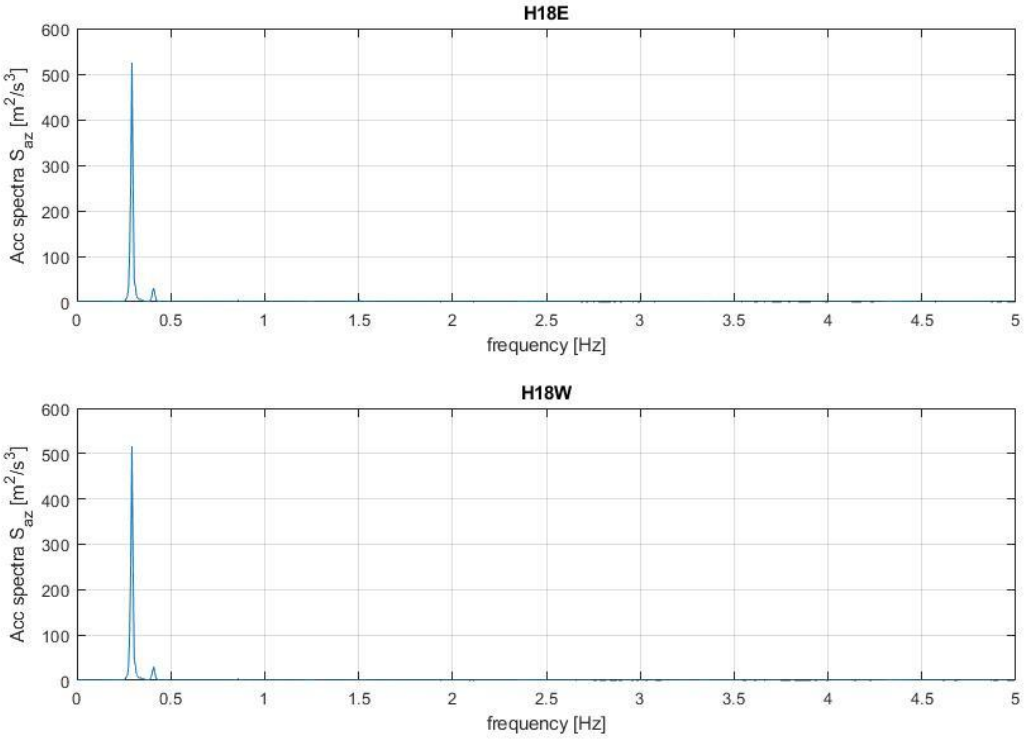

Figure 108: Vertical acceleration spectra for accelerometers mounted on H18

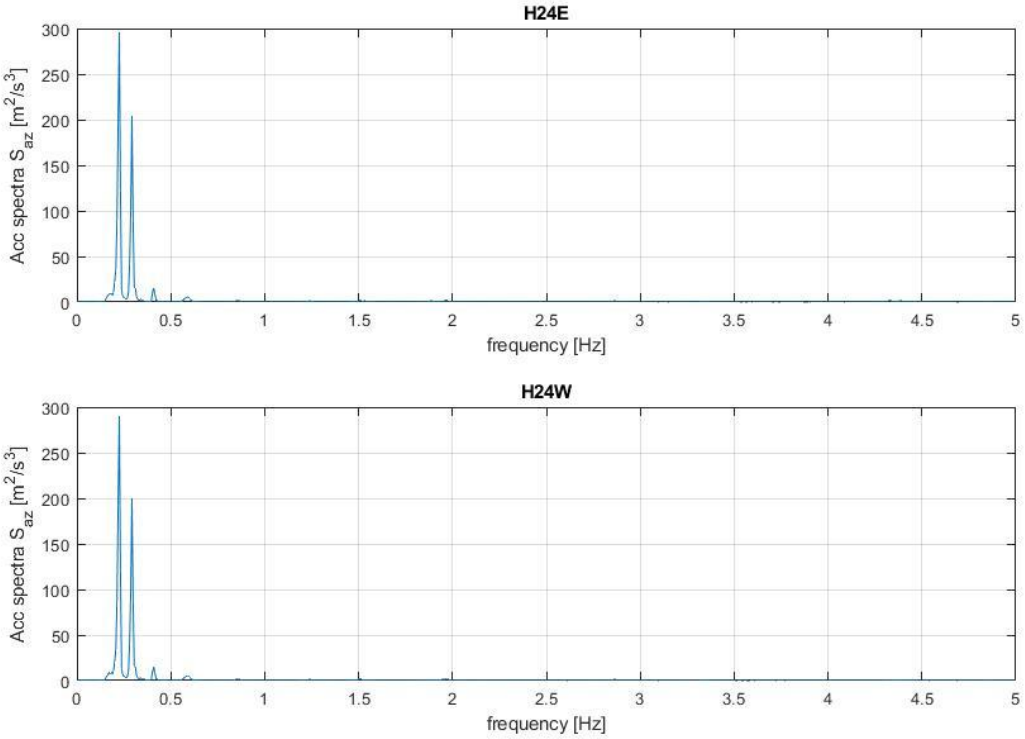

Figure 109: Vertical acceleration spectra for accelerometers mounted on H24

6.0 Conclusion and further work

In this chapter the conclusion and suggestions for further work will be presented.

6.1 Conclusion

The problem description states "*This thesis will look at the horizontal and vertical wind velocity, the correlation of anemometers, the turbulence intensity and the wind direction at the Lysefjord Bridge, and link some of these factors with the vertical accelerations of the bridge deck measured by the three pairs of accelerometers installed at different hangars. The goal is to gain knowledge about the wind effects on a suspension bridge and to see whether the different wind data can be linked to each other and to the vertical accelerations or not".*

Different wind data from measurements at the Lysefjord bridge has been analysed in this thesis and the results have been presented, discussed and compared to the findings of previous research performed on the bridge.

The results suggest that neither the mean horizontal nor the mean vertical wind velocity of the four different time-series has a large effect on the vertical accelerations of the bridge deck. When large bursts of vertical accelerations were registered, none of the corresponding anemometers showed any significant increase in wind speed. This leads to the conclusion that traffic is the main accelerator during the four time-series under investigation. The results could have been different however, if time-series with higher mean wind velocities were selected. It is possible that the wind-induced vibrations of the time-series in question are masked by the response due to the traffic, but this is difficult to verify.

The wind direction seems to have little impact on the horizontal wind velocity but looked to affect the vertical velocity and the mean vertical angle-of attack to a larger degree. Rapid changes in the wind direction were linked to rapid changes in the vertical angle-of attack, and a wind flow from south-east looked to have the greatest impact with regards to the vertical angle-of attack.

With regards to the turbulence intensity, only the time-series of 09/08/21 showed some resemblance with that of previous research. For the other three time-series, the turbulence intensity was much larger than other findings, which was concluded to be due to the general mean wind velocity of the time-series being relatively small.

The correlation of the anemometers varied between the time-series. The general conclusion was that a higher horizontal velocity coupled with a wind direction from east or south-east made the anemometers correlate more as opposed to a low velocity and a wind direction from the south-west. The exception was for the anemometers installed at deck level, which changed their correlation based on the wind direction. The leeward deck anemometer in each time-series showed very little correlation with the others.

As for the vertical acceleration spectra, the spectral peaks corresponded well to the eigen-frequencies of both symmetrical and asymmetrical vertical modes from previous research, depending on the location of the accelerometers.

6.2 Further work

As the horizontal and torsional accelerations were not discussed in this thesis, it would be suggested that these accelerations were investigated as well. They could give more insight into the wind-induced vibrations of the bridge.

Another aspect of further work would be to find time-series with larger mean wind velocities and to see to what degree the dynamic response of the bridge changes as the velocities are increased. It would be of great interest to find a time-series with more extreme wind speeds, such as during a storm, to see the similarities and differences from results presented in this thesis.

The calculated mean velocities, turbulence intensities and vertical angle-of attack could be used for further work when calculating the wind loading on the bride. As shown by Jacobsen [31], calculation of fluctuating wind-loading on a line-like structure (such as a bridge) can be done by taking the instantaneous relative wind velocity acting at an instantaneous angle-of attack. The reader is referenced to figures 2.2 and 2.4 in [31] for further information on this subject.

A suggestion for further work could also be to calculate the corresponding displacements of the vertical accelerations presented in this thesis, and the displacements corresponding to both the horizontal and torsional accelerations.

References

[1] E. Cheynet. “Wind Engineering.” Windengineeringuis.github.io. Downloaded from: https://windengineeringuis.github.io/. (Downloaded: 24.03.22).

[2] H. Johnson Nenty, “Writing a Quantitative Research Thesis”, *International Journal of Educational Sciences*, 1:1, p. 19-32, 2009. [Online]. Downloaded from: https://doi.org/10.1080/09751122.2009.11889972

[3] SINTEF. “Signal processing and machine learning.” Sintef.no. Downloaded from: https://www.sintef.no/en/expertise/digital/sustainable-communication-technologies/signal-processing-and-machine-learning/. (Downloaded: 06.06.22).

[4] MathWorks. “Math. Graphics. Programming.” Se.mathworks.com. Downloaded from: https://se.mathworks.com/products/matlab.html. (Downloaded: 06.06.22).

[5] Anfossi, D., Oettl, D., Degrazia, G. et al., “An Analysis of Sonic Anemometer Observations In Low Wind Speed Conditions,” *Boundary-Layer Meteorol* 114, 179–203, 2005. [Online]. Downloaded from: https://doi.org/10.1007/s10546-004-1984-4

[6] A. Larsen, G.L. Larose, “Dynamic wind effects on suspension and cable-stayed bridges,” *Journal of Sound and Vibration*. Volume 334, 2015,Pages 2-28, 2015. [Online]. Downloaded from: https://doi.org/10.1016/j.jsv.2014.06.009.

[7] 1915 Canakkale. “The longest mid-span suspension bridge in the world.” 1915canakkale.com. Downloaded from: https://www.1915canakkale.com/en-us. (Downloaded: 27.03.22).

[8] COWI. “Extended highway system linking Izmir and Istanbul.” cowi.com. Downloaded from: https://www.cowi.com/solutions/infrastructure/osman-gazi-bridge-turkey. (Downloaded: 03.04.22).

[9] J.M.W. Brownjohn, “Estimation of damping in suspension bridges,” in *Structures and Buildings*, vol. 104, nr. 4, ICE Proceedings, 1994, p. 401-415. [Online]. Available: https://www.icevirtuallibrary.com/doi/10.1680/istbu.1994.27199.

[10] J.M.W. Brownjohn, A.A. Dumanoglu, R.T. Severn, “Ambient vibration survey of the fatih sultan mehmet (second Bosporus) suspension bridge,” *The Journal of the International Association of Earthquake Engineering*, vol. 21, nr. 10, p. 907-924, 1992. [Online]. Downloaded from: https://doi.org/10.1002/eqe.4290211005

[11] P. Stoica, R. Moses, “Basic concepts,” in *Spectral Analysis of Signals*. Upper Saddle River, NJ, USA: Prentice-Hall, 2005, p. 1-21. [Online]. Available: https://www.maths.lu.se/fileadmin/maths/personal_staff/Andreas_Jakobsson/StoicaM05.pdf.

[12] D. J. Buysse, MD et al., “EEG Spectral Analysis in Primary Insomnia: NREM Period Effects and Sex Differences,” *Sleep*, vol. 31, Issue 12, Pages 1673–1682, Dec 2008. [Online]. Downloaded from: https://doi.org/10.1093/sleep/31.12.1673

[13] V. Oropeza, M. Sacchi, “Simultaneous seismic data denoising and reconstruction via multichannel singular spectrum analysis,” *Geophysics*, vol. 76, nr. 3, p. 1MJ-Z74, May 2011. [Online]. Downloaded from: https://library.seg.org/doi/abs/10.1190/1.3552706.

[14] MathWorks. “Discrete-time signals.” Se.mathworks.com. Downloaded from: https://se.mathworks.com/help/dsp/ug/discrete-time-signals.html. (Downloaded: 15.04.22).

[15] Gill Instruments. Wind Master PRO. 3-axis Ultrasonic Anemometer. Technical data sheet: https://gillinstruments.com/wp-content/uploads/2021/12/WindMaster-Pro-iss7.pdf.

[16] Vaisala. "Weather Transmitter WXT530 Series," Vaisala.com. Downloaded from: https://www.vaisala.com/en/products/weather-environmental-sensors/weather-transmitter-wxt530-series. (Downloaded: 17.03.22).

[17] Gill Instruments. Wind Master HS. 3-Axis Horizontal-Head Anemometer. Technical data sheet: https://gillinstruments.com/wp-content/uploads/2021/12/1951-002-Windmaster-HS-Iss-5.pdf.

[18] J. D. Holmes, "Bridges", in *Wind Loading of Structures,* 2nd edition, London, UK: Taylor & Francis, 2007, p. 290-311

[19] R. Brincker, J.B. Frandsen, P. Andersen, "Ambient Response Analysis of the Great Belt Bridge," *IMAC*, Feb 2000. [Online]. Downloaded from: https://www.semanticscholar.org/paper/Ambient-Response-Analysis-of-the-Great-Belt-Bridge-Brincker-Frandsen/78782934a34c4ecb8bbcefd49a43c2fb69aa098d.

[20] A. Larsen, S. Esdahl, J. E. Andersen, T. Vejrum, "Storebælt suspension bridge – vortex shedding excitation and mitigation by guide vanes", *Journal of Wind Engineering and Industrial Aerodynamics,* vol. 88, nr. 2-3, Dec, 2000. [Online]. Downloaded from: https://doi.org/10.1016/S0167-6105(00)00054-4

[21] A. Selberg, *Oscillation and aerodynamic stability of suspension bridges*, vol. 13 Trondheim, Norway: Norges Teknisk-Naturvitenskapelige Forskningsrad, 1961.

[22] E. Cheynet, "Wind-induced vibrations of a suspension bridge: A case study in full-scale," Dr.Philos., Department of Mechanical and Structuring Engineering and Materials Science, University of Stavanger, Stavanger, Phd. No. 326, 2016. [Online]. Downloaded from: https://uis.brage.unit.no/uis-xmlui/handle/11250/2425472?show=full.

[23] C.S. Cai, W. Zhang, S. Montens, "Wind Effects on Long Span Bridges," *Bridge Engineering Handbook*, vol. 2, p. 535-556, 2016. [Online]. Downloaded from: https://www.researchgate.net/publication/313890810_Wind_Effects_on_Long_Span_Bridges.

[24] MathWorks. "pwelch". Se.mathworks.com. Downloaded from: https://se.mathworks.com/help/signal/ref/pwelch.html. (Downloaded 25.06.22).

[25] J.O. Smith. "Welch`s method." Stanford.edu. Downloaded from: https://ccrma.stanford.edu/~jos/sasp/Welch_s_Method.html. (Downloaded 25.06.22).

[26] N. Daniotto, "Bridge deck aerodynamics: A case study in full-scale," Dr.Philos., Department of Mechanical and Structural Engineering and Materials Science, University of Stavanger, Stavanger, Phd. No. 634, 2022. [Online]. Downloaded from: https://uis.brage.unit.no/uis-xmlui/handle/11250/2988684.

[27] E. Cheynet, J. B. Jakobsen, J. Snæbjörnsson, "Buffeting response of a suspension bridge in complex terrain," *Engineering Structures*, vol. 128, p. 474-487, 2016. [Online]. Downloaded from: https://doi.org/10.1016/j.engstruct.2016.09.060

[28] J. Wang, E. Cheynet, J. B. Jakobsen, J. Snæbjörnsson, "Time-domain analysis of wind-induced response of a suspension bridge in comparison with the full-scale measurements," *ASME*, 2017. Downloaded from: https://windengineeringuis.github.io/papers/Wang2017a.pdf.

[29] E. Cheynet, J. B. Jakobsen, J. Snæbjörnsson, “Flow distortion recorded by sonic anemometers on a long-span bridge: Towards a better modelling of the dynamic wind load in full-scale,“ *Journal of Sound and Vibration*, vol. 450, p. 214-230, 2019. [Online]. Downloaded from: https://doi.org/10.1016/j.jsv.2019.03.013

[30] E. Cheynet, S. Liu, M. C. Ong, J. B. Jakobsen, J. Snæbjörnsson, I. Gatin, “The influence of terrain on the mean wind flow characteristics in a fjord”, *Journal of Wind Engineering and Industrial Aerodynamics*, vol. 205, 2020. [Online]. Downloaded from: https://doi.org/10.1016/j.jweia.2020.104331

[31] J. B. Jakobsen, “Fluctuating wind load and response of a line-like engineering structure with emphasis on motion-induced wind forces,” Chapter 2: Quasi-steady theory of fluctuating wind loading on a line-like structure, NTH 1995: 62, Department of Structural Engineering, Norwegian Institute of Technology, University of Trondheim, Norway, 1995. Obtained by email.

[32] Broer.no. “Lysefjordbrua.” broer.no. Downloaded from: https://broer.no/bro/index.php?ID=156. (Downloaded: 28.06.22).

[33] J. Tveiten, “Dynamic analysis of a suspension bridge,” Master thesis, Department of Mechanical and Structural Engineering and Materials Science, University of Stavanger, Stavanger, 2012. [Online]. Downloaded from: https://uis.brage.unit.no/uis-xmlui/handle/11250/182770.

Appendix A: 09/08/21

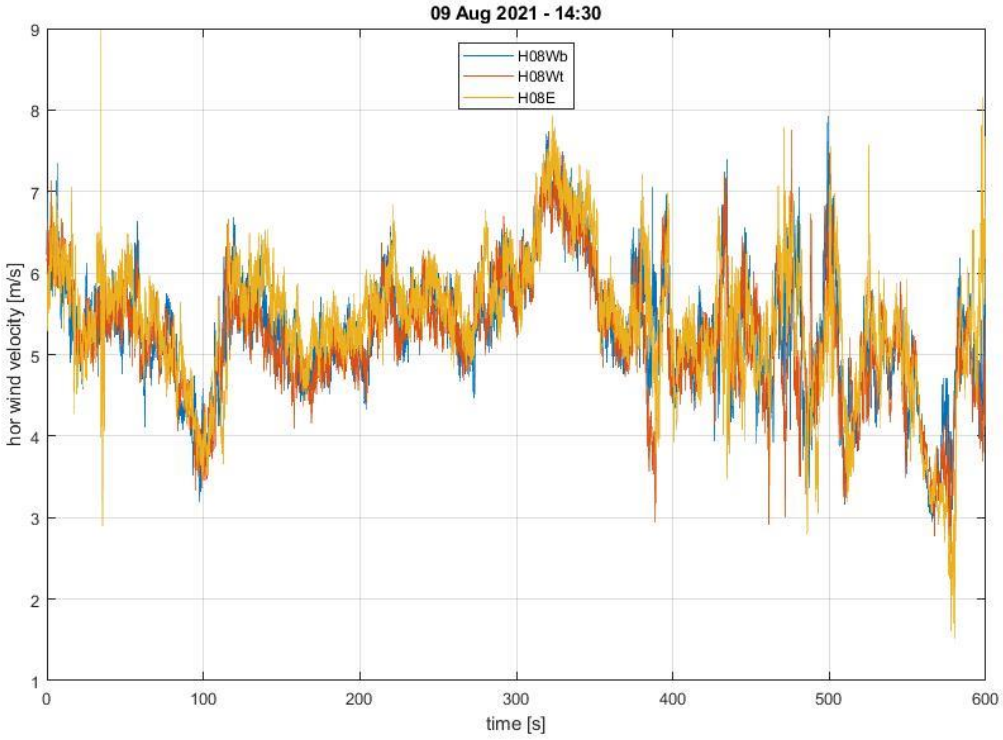

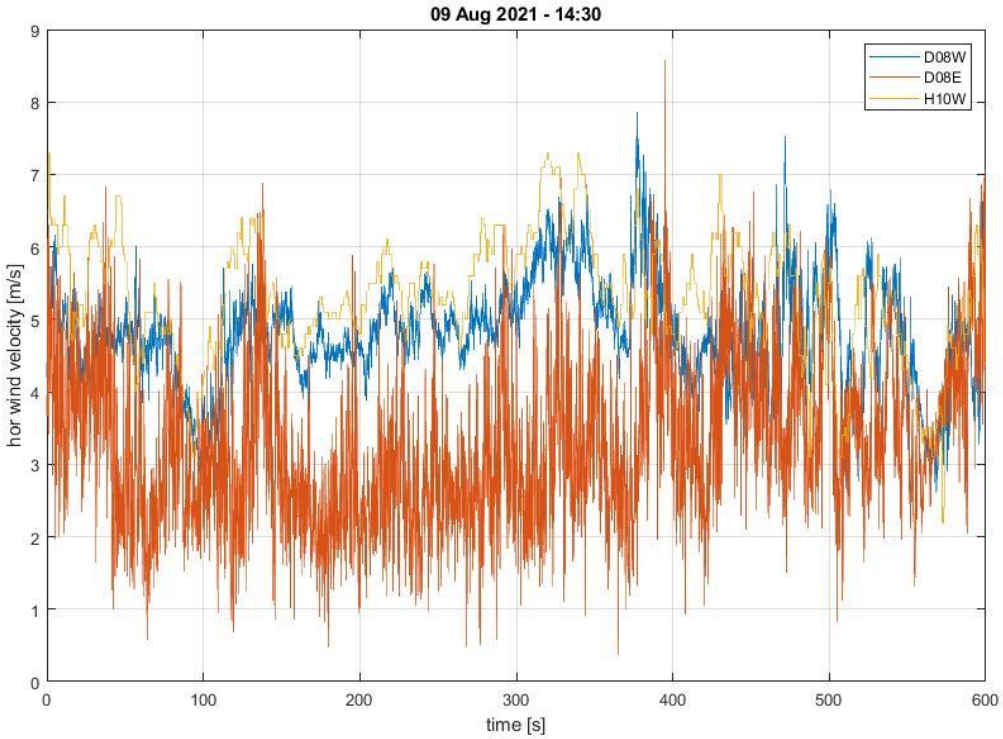

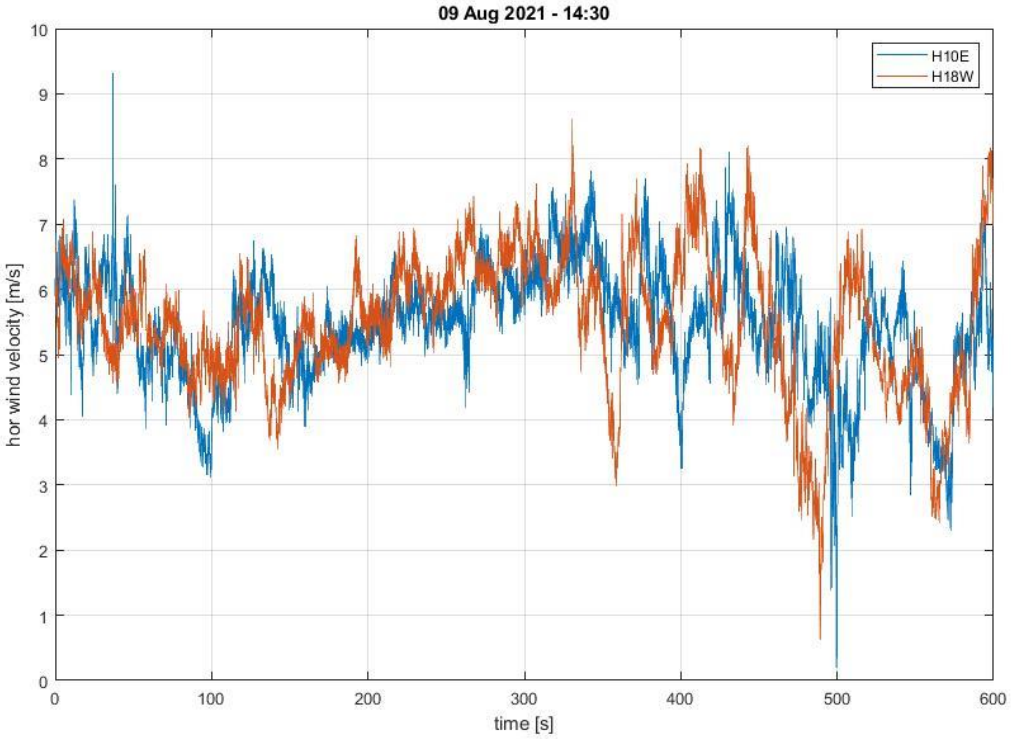
09 Aug 2021 - 14:30
H10E
H18W
hor wind velocity [m/s]
time [s]
0
1
2
3
4
5
6
7
8
9
10
0
100
200
300
400
500
600

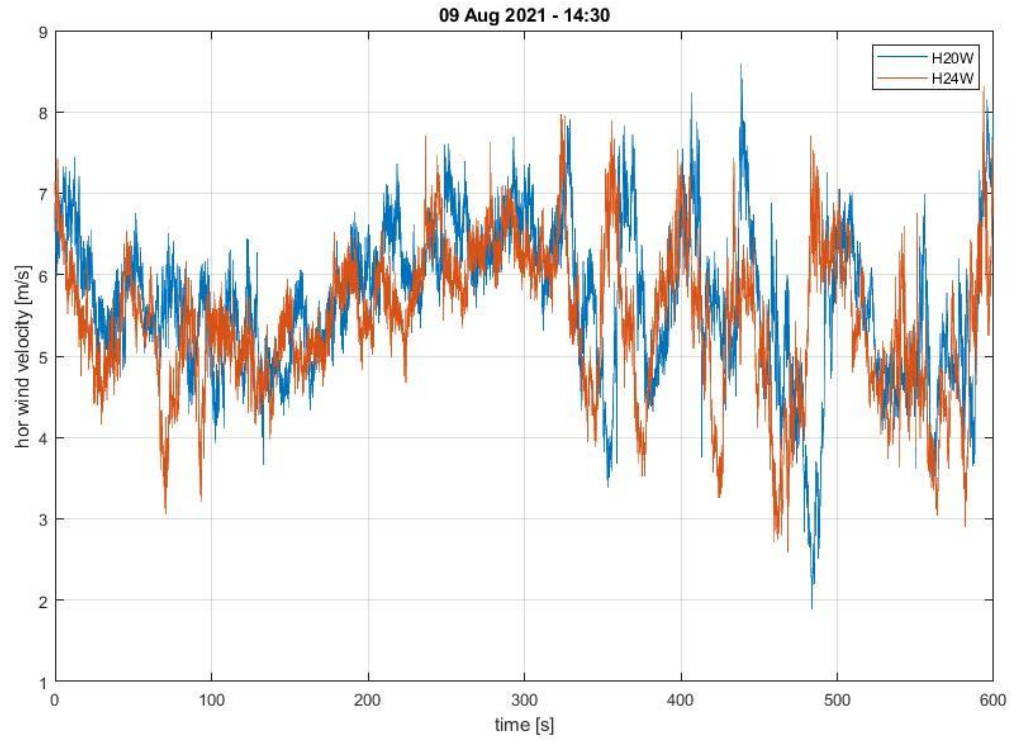
09 Aug 2021 - 14:30
H20W
H24W
hor wind velocity [m/s]
time [s]
1
2
3
4
5
6
7
8
9
0
100
200
300
400
500
600

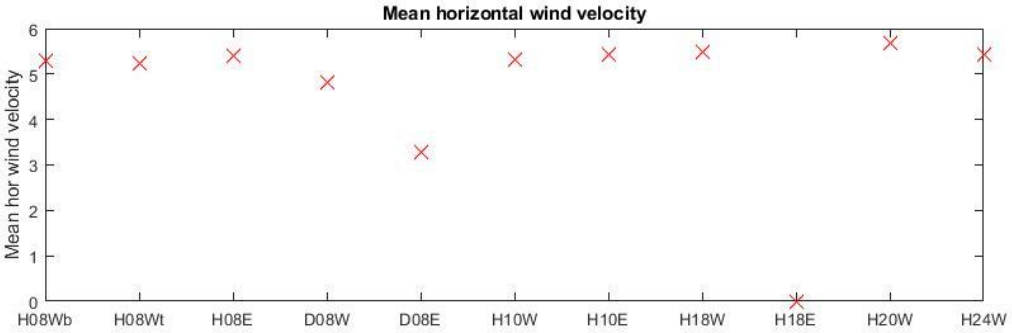
Mean horizontal wind velocity
Mean hor wind velocity
0
1
2
3
4
5
6
H08Wb
H08Wt
H08E
D08W
D08E
H10W
H10E
H18W
H18E
H20W
H24W

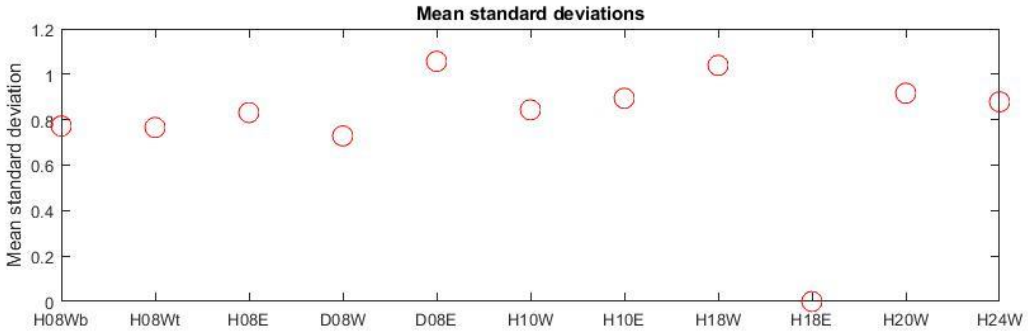
Mean standard deviations
Mean standard deviation
0
0.2
0.4
0.6
0.8
1
1.2
H08Wb
H08Wt
H08E
D08W
D08E
H10W
H10E
H18W
H18E
H20W
H24W

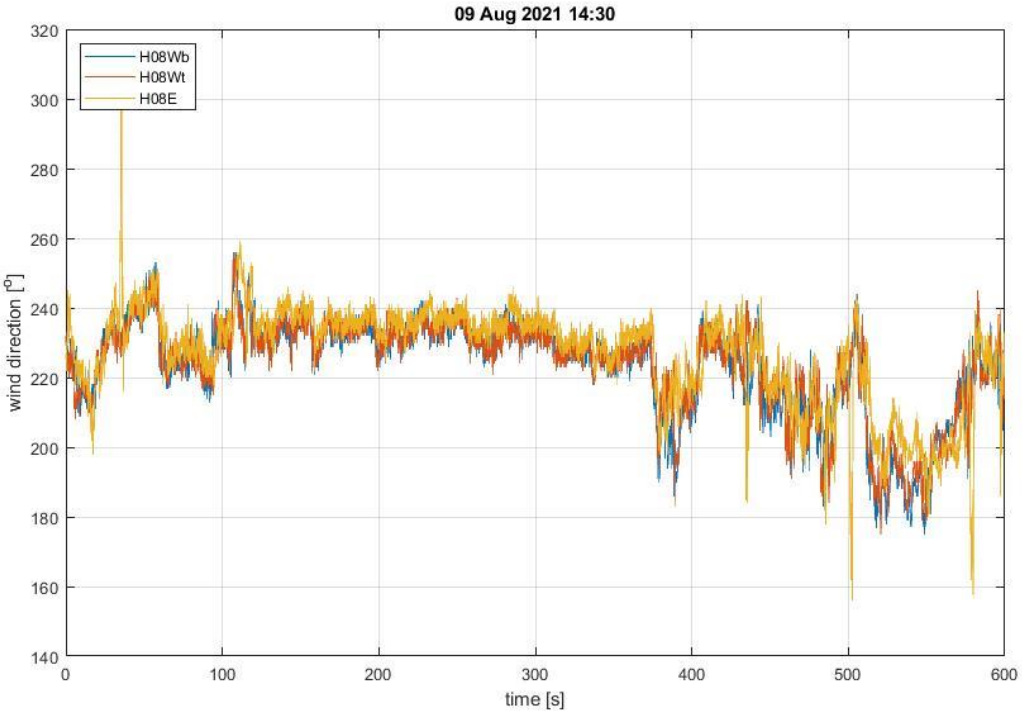
09 Aug 2021 14:30
H08Wb
H08Wt
H08E
wind direction [°]
140
160
180
200
220
240
260
280
300
320
0
100
200
300
400
500
600
time [s]

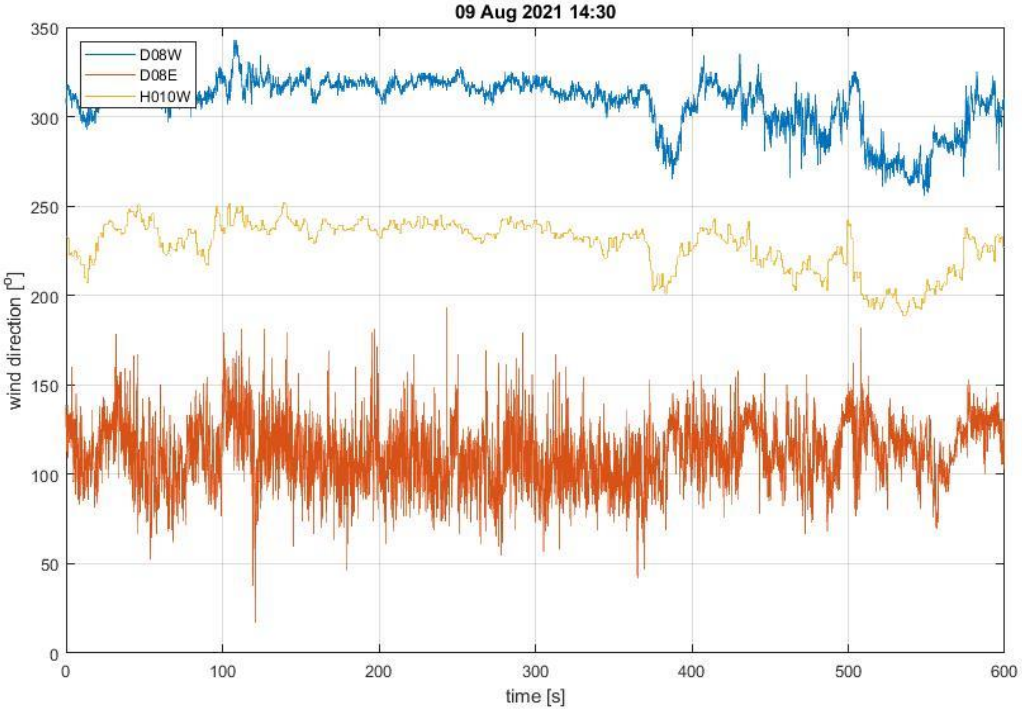
09 Aug 2021 14:30
D08W
D08E
H010W
wind direction [°]
time [s]
0
50
100
150
200
250
300
350
0
100
200
300
400
500
600

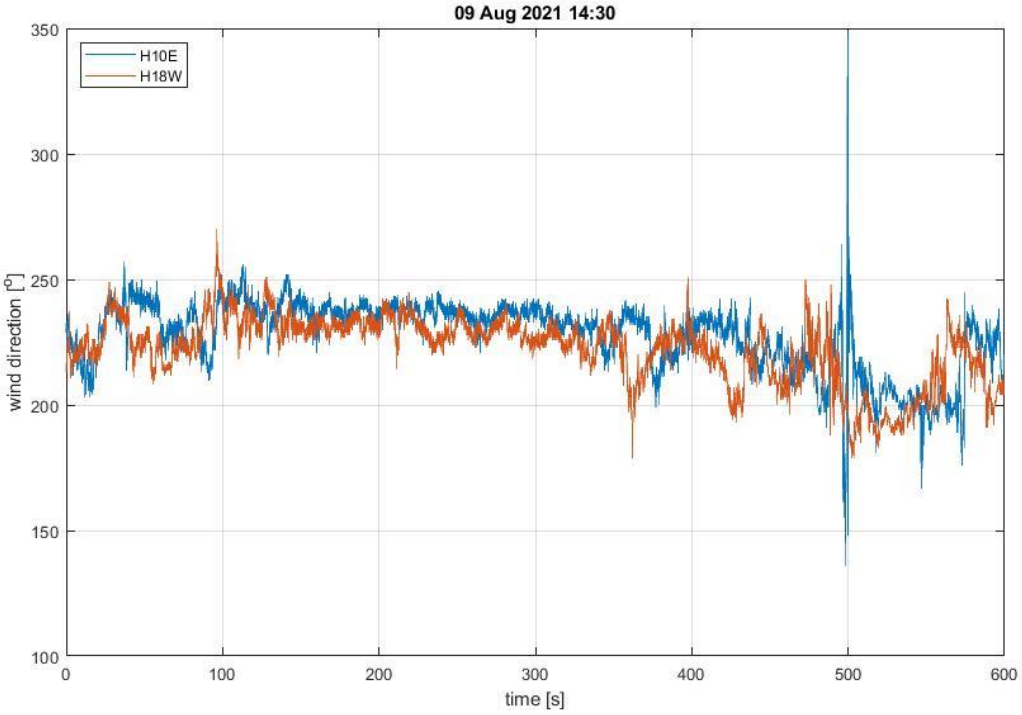
09 Aug 2021 14:30
H10E
H18W
wind direction [°]
time [s]
100
150
200
250
300
350
0
100
200
300
400
500
600

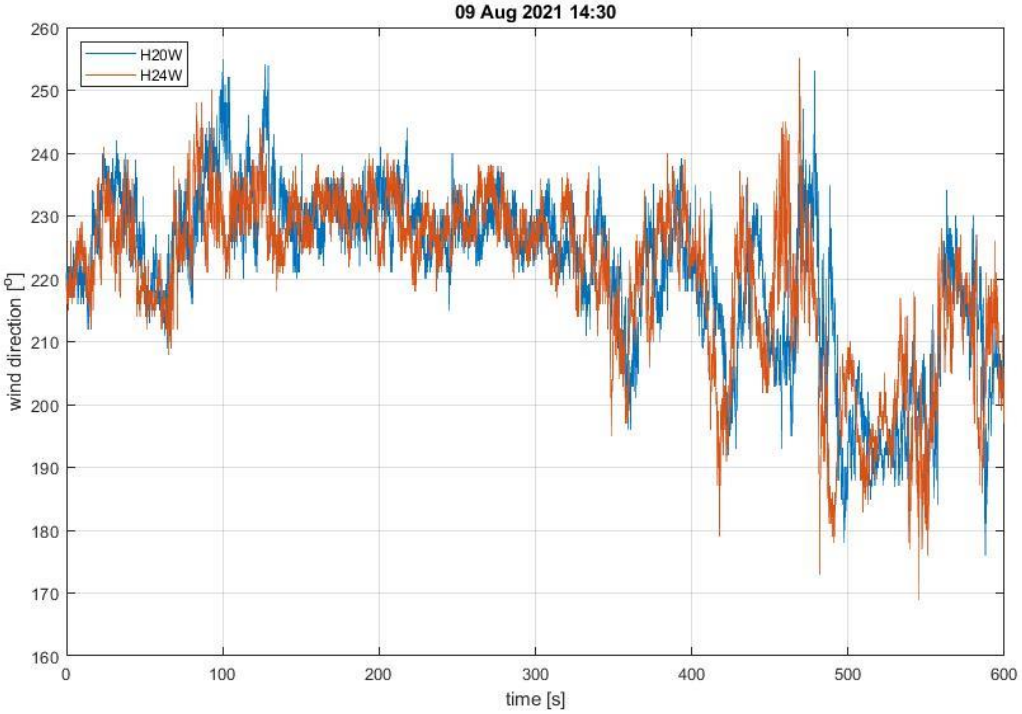
09 Aug 2021 14:30
H20W
H24W
wind direction [°]
time [s]

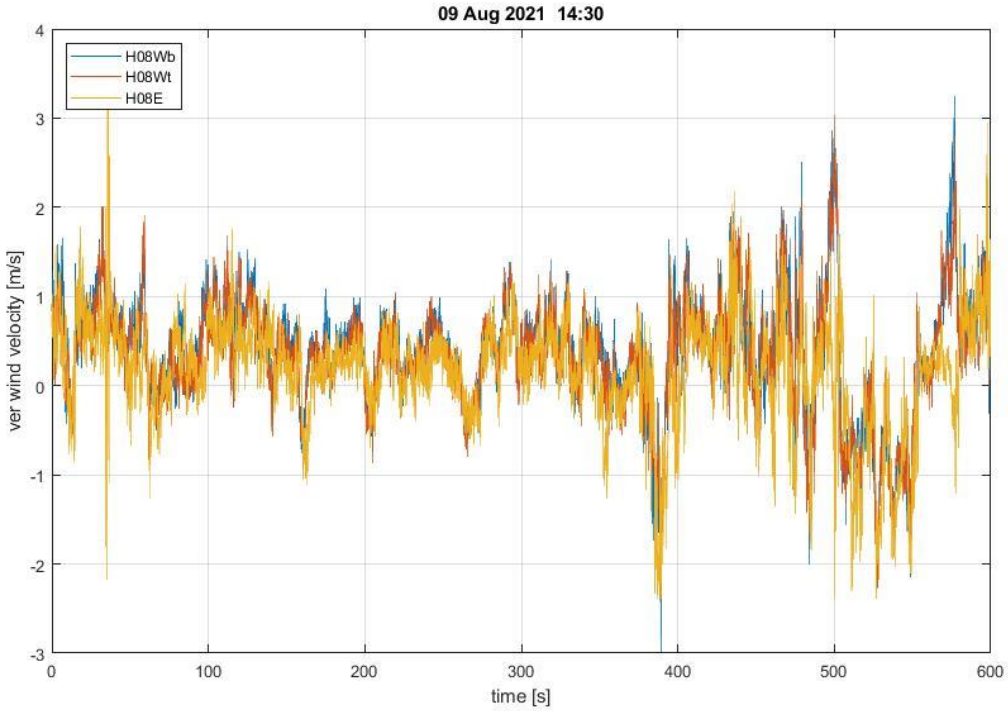
09 Aug 2021 14:30
H08Wb
H08Wt
H08E
ver wind velocity [m/s]
time [s]

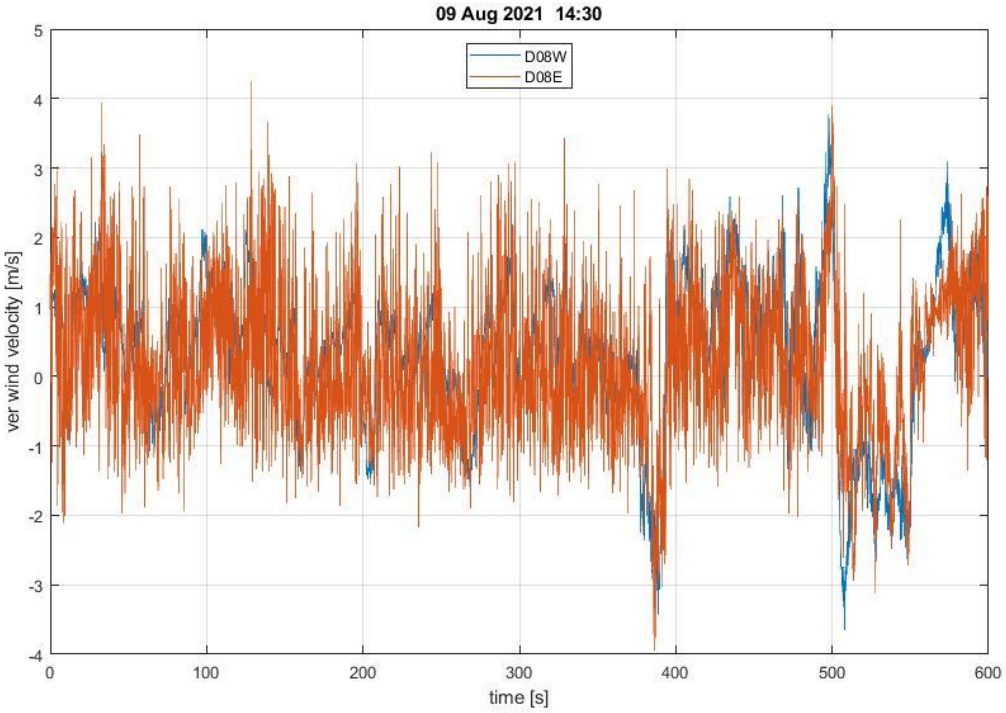
09 Aug 2021 14:30
D08W
D08E
ver wind velocity [m/s]
time [s]

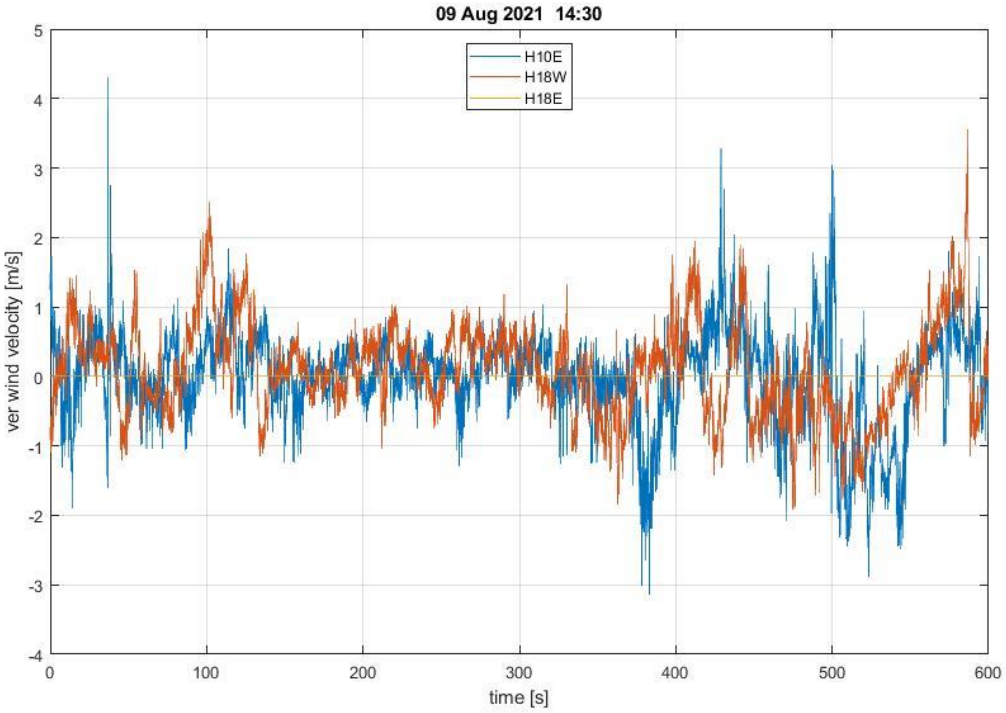
09 Aug 2021 14:30
H10E
H18W
H18E
ver wind velocity [m/s]
time [s]

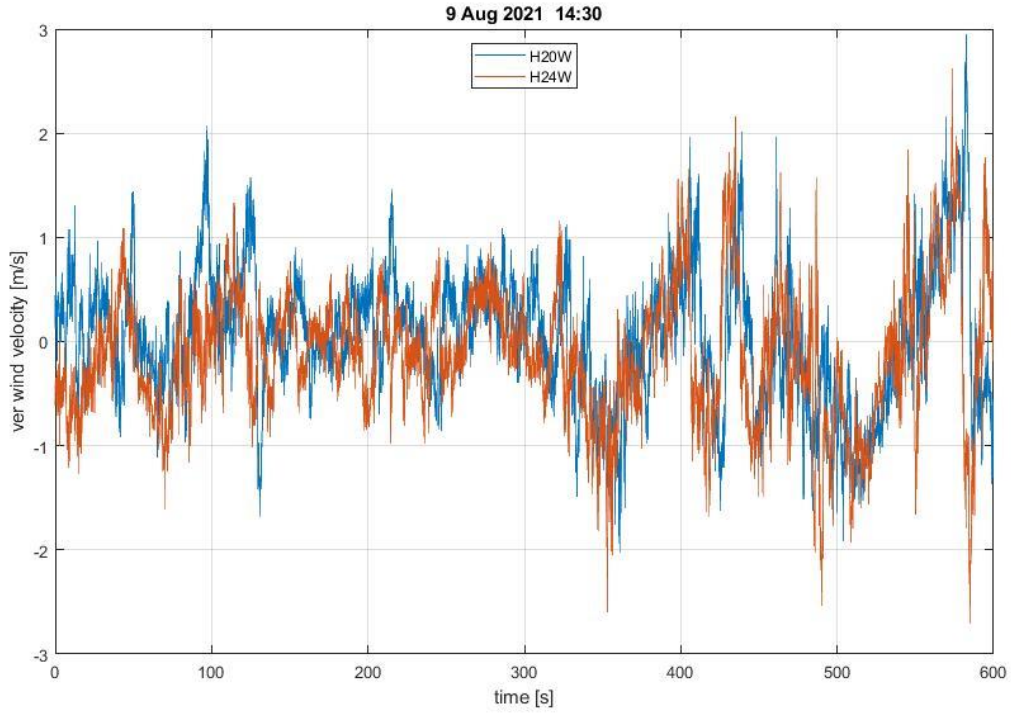
9 Aug 2021 14:30
H20W
H24W
ver wind velocity [m/s]
time [s]

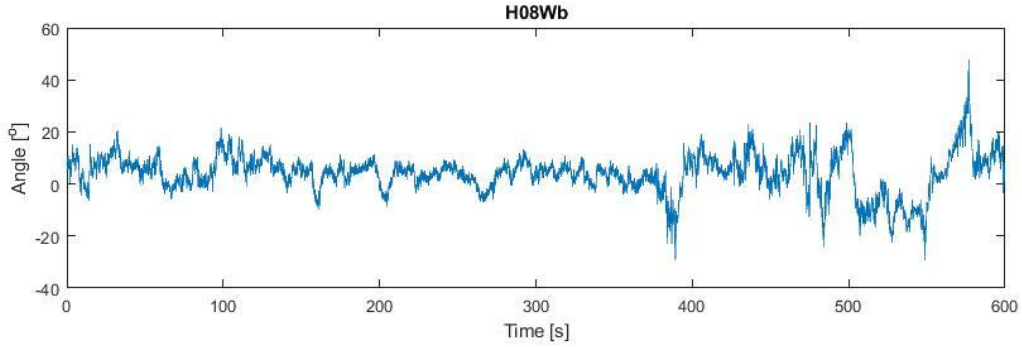
H08Wb
Angle [°]
Time [s]

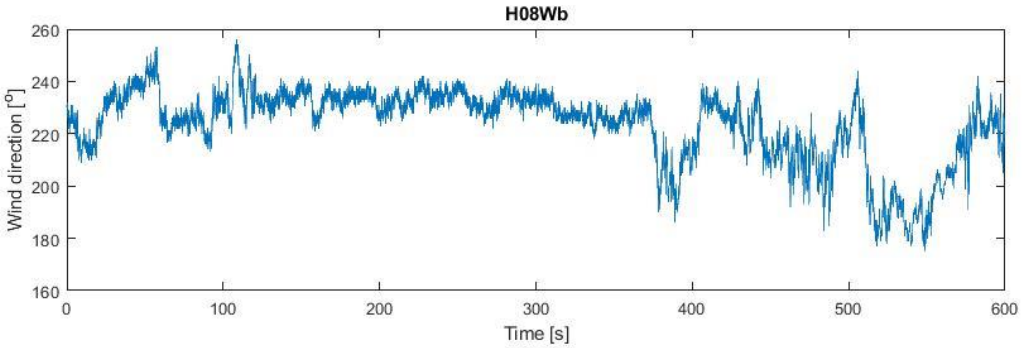
H08Wb
Wind direction [°]
Time [s]

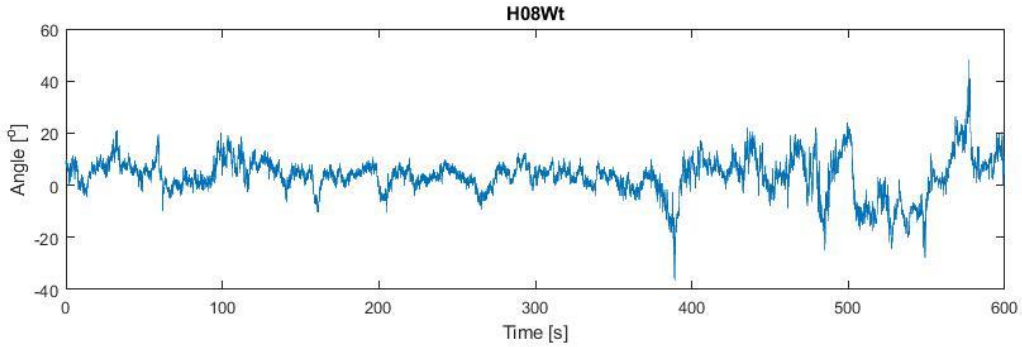
H08Wt
Angle [°]
Time [s]

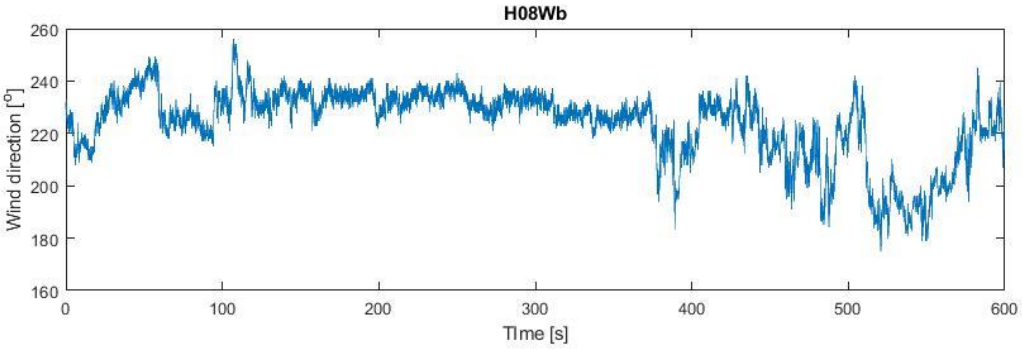
H08Wb
Wind direction [°]
Time [s]

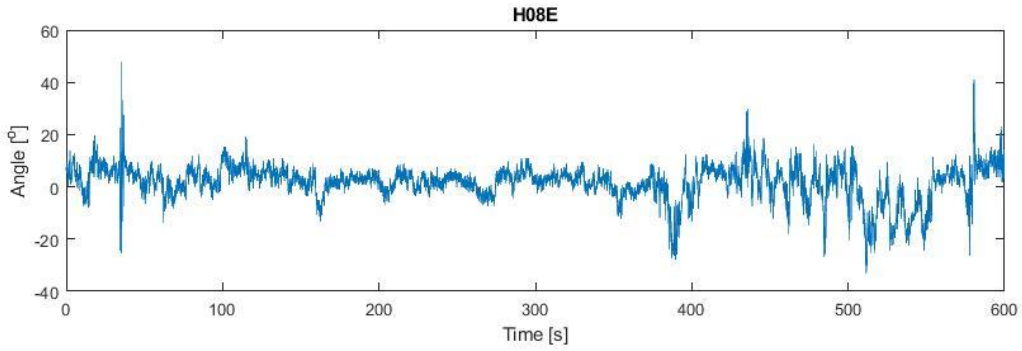
H08E
Angle [°]
Time [s]

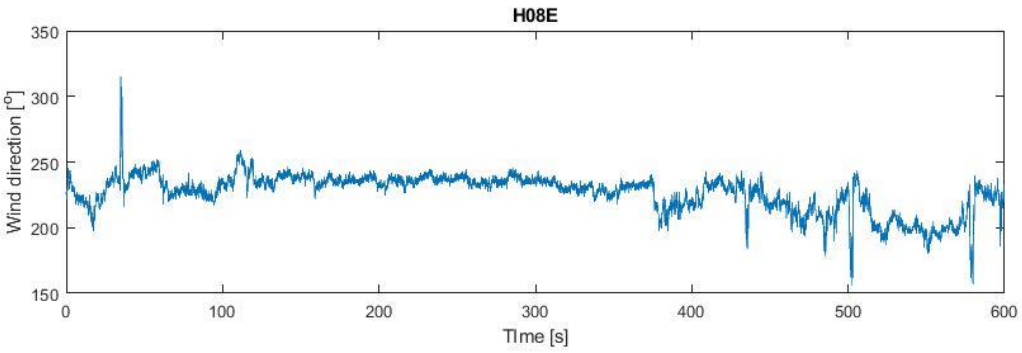
H08E
Wind direction [°]
Time [s]

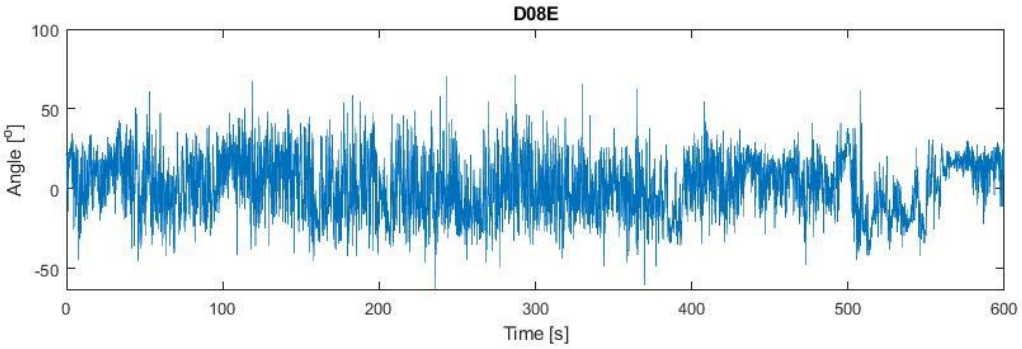
D08E
Angle [°]
Time [s]

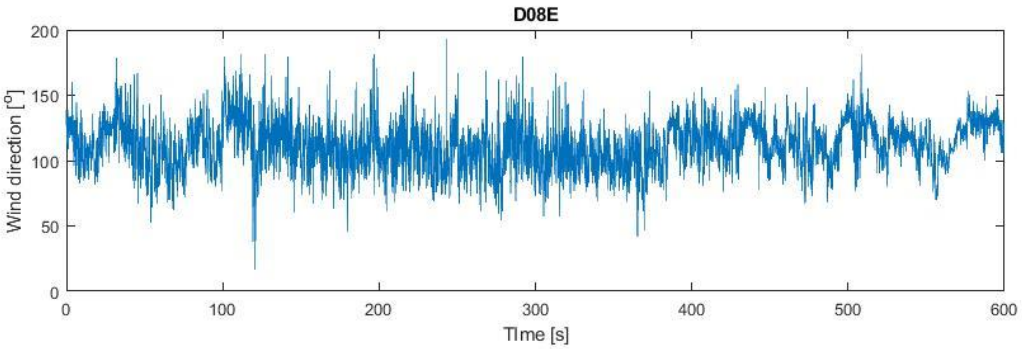
D08E
Wind direction [°]
TIme [s]

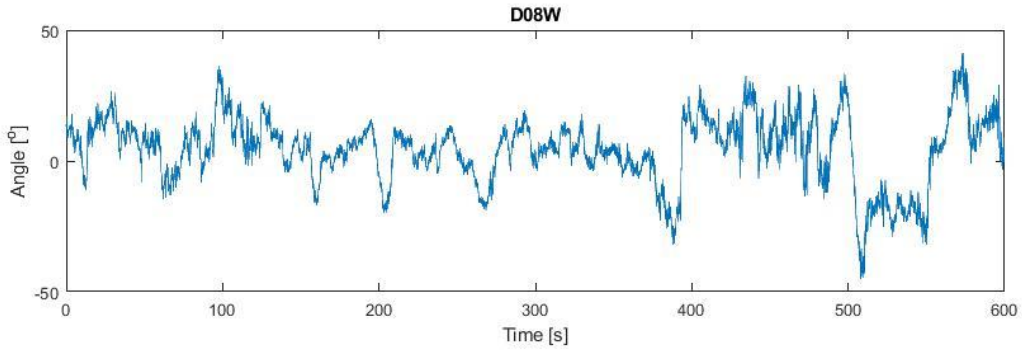
D08W
Angle [°]
Time [s]

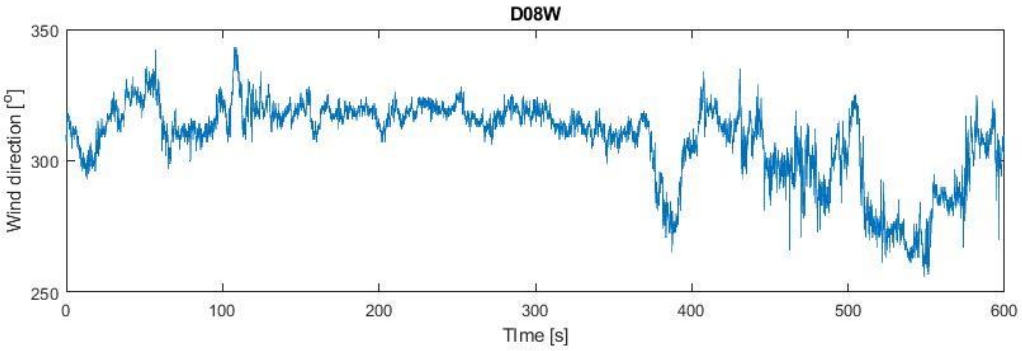
D08W
Wind direction [°]
TIme [s]

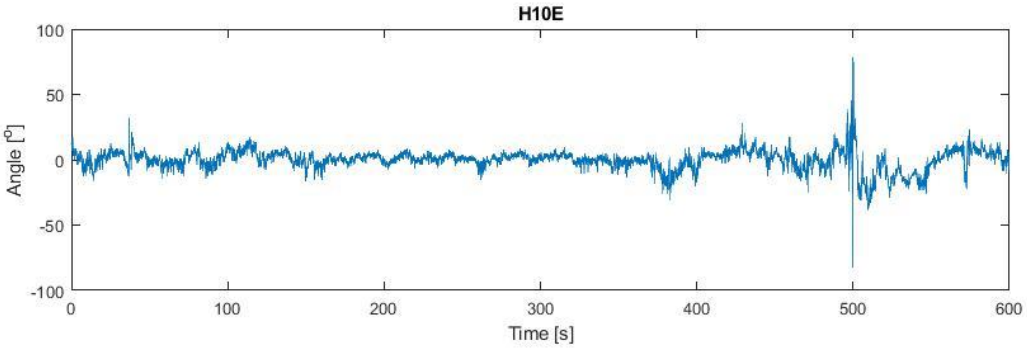
H10E
Angle [°]
Time [s]

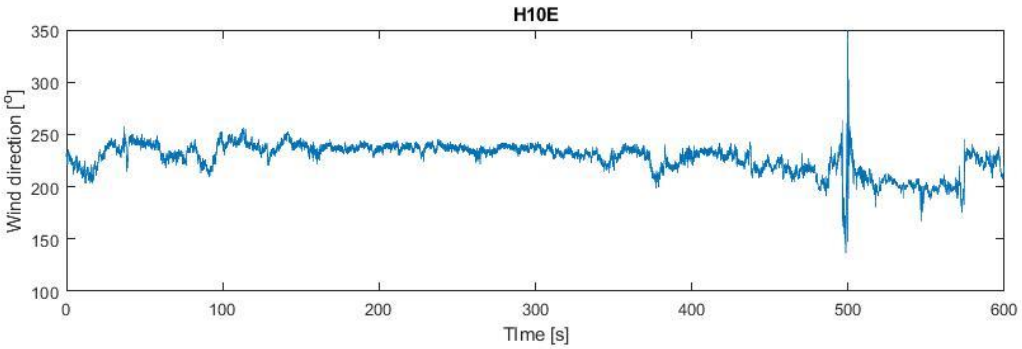
H10E
Wind direction [°]
TIme [s]

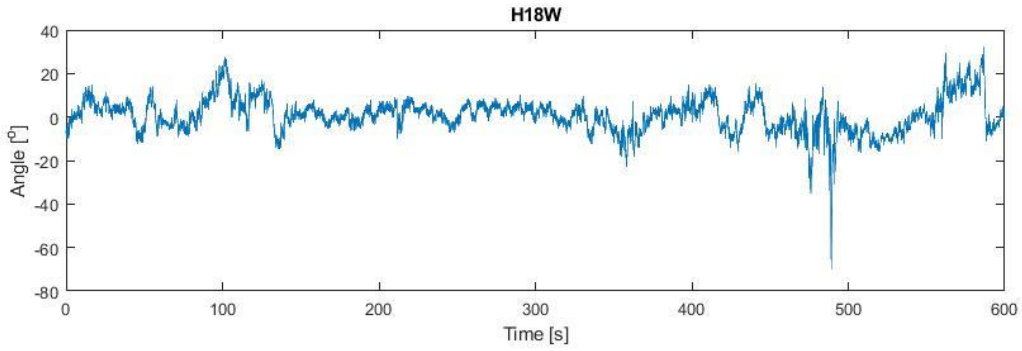
H18W
Angle [°]
Time [s]

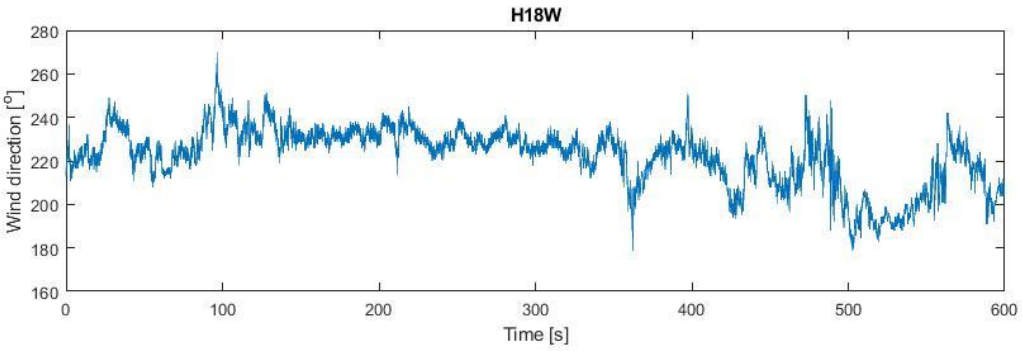
H18W
Wind direction [°]
Time [s]

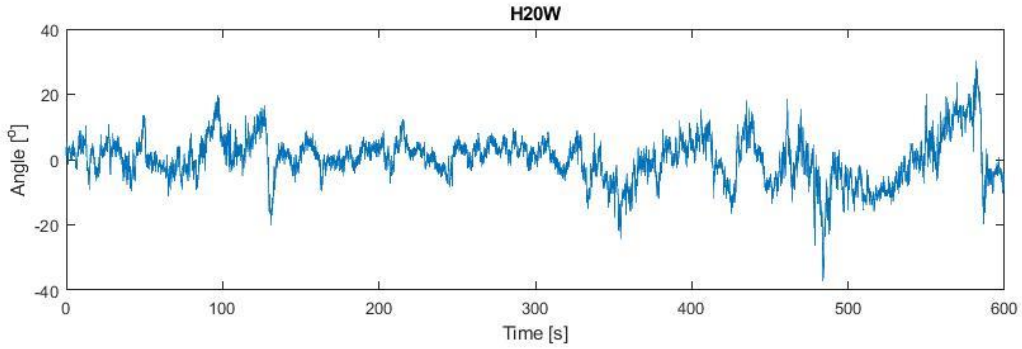
H20W
Angle [°]
Time [s]

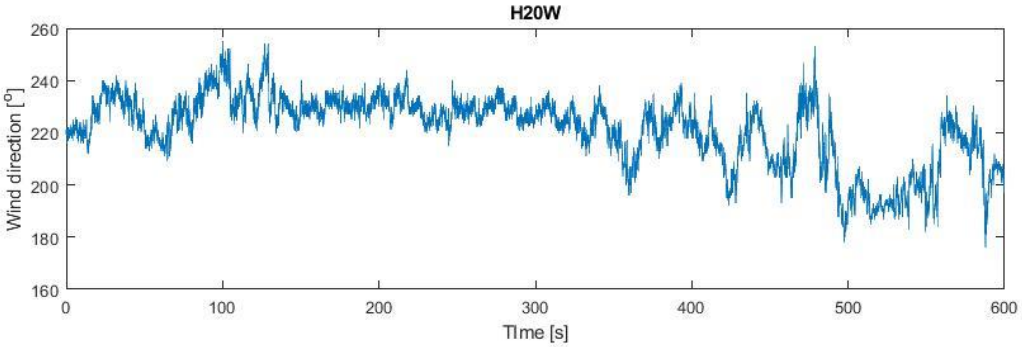
H20W
Wind direction [°]
TIme [s]

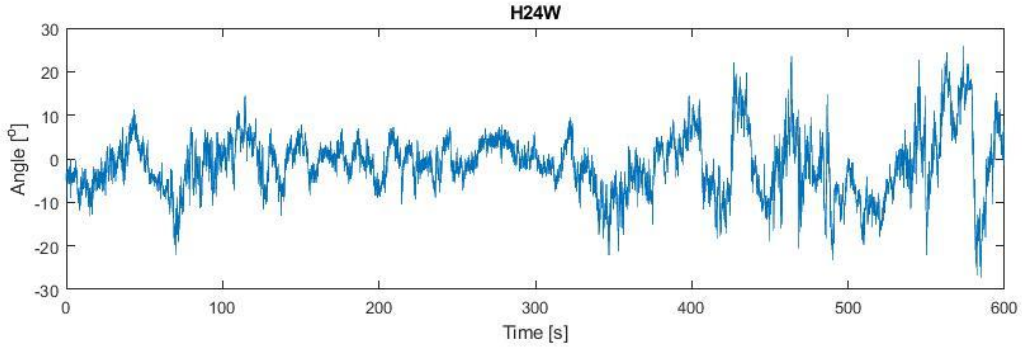
H24W
Angle [°]
Time [s]

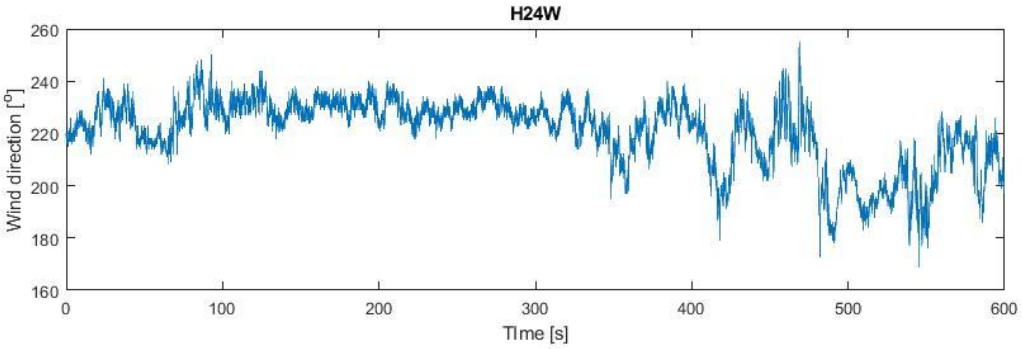
H24W
Wind direction [°]
TIme [s]

Appendix B: 23/09/21

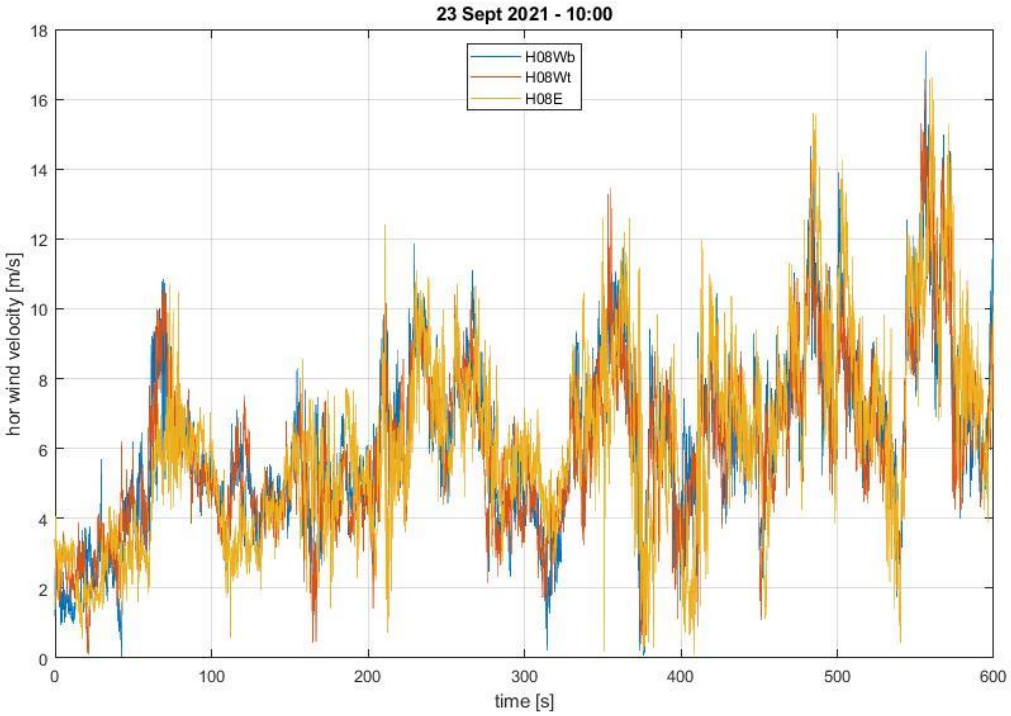

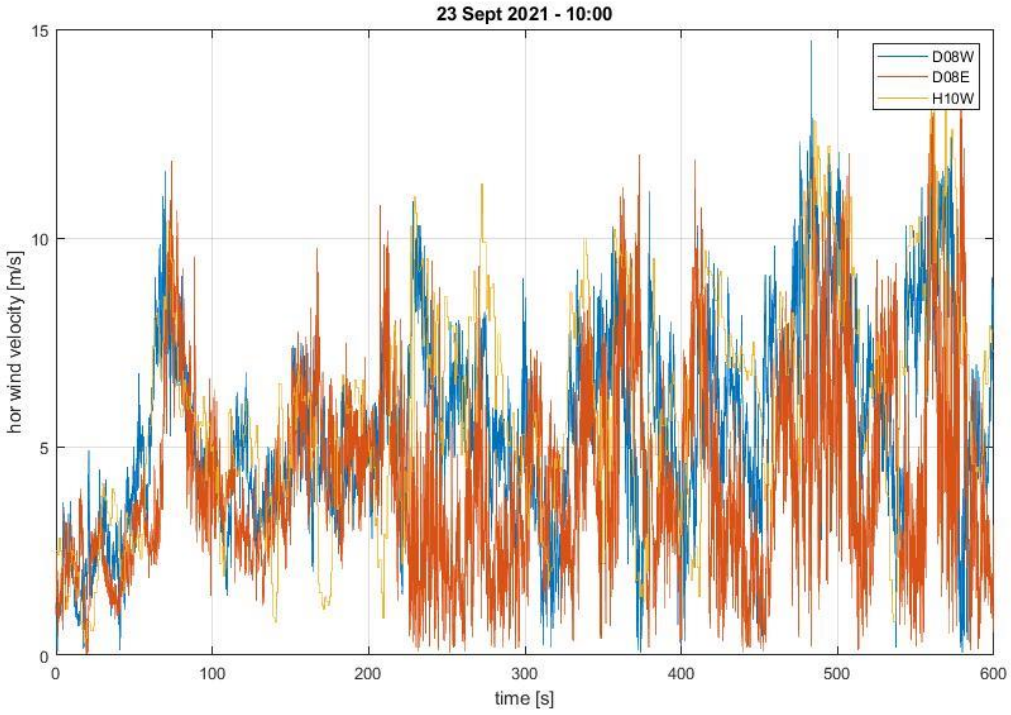

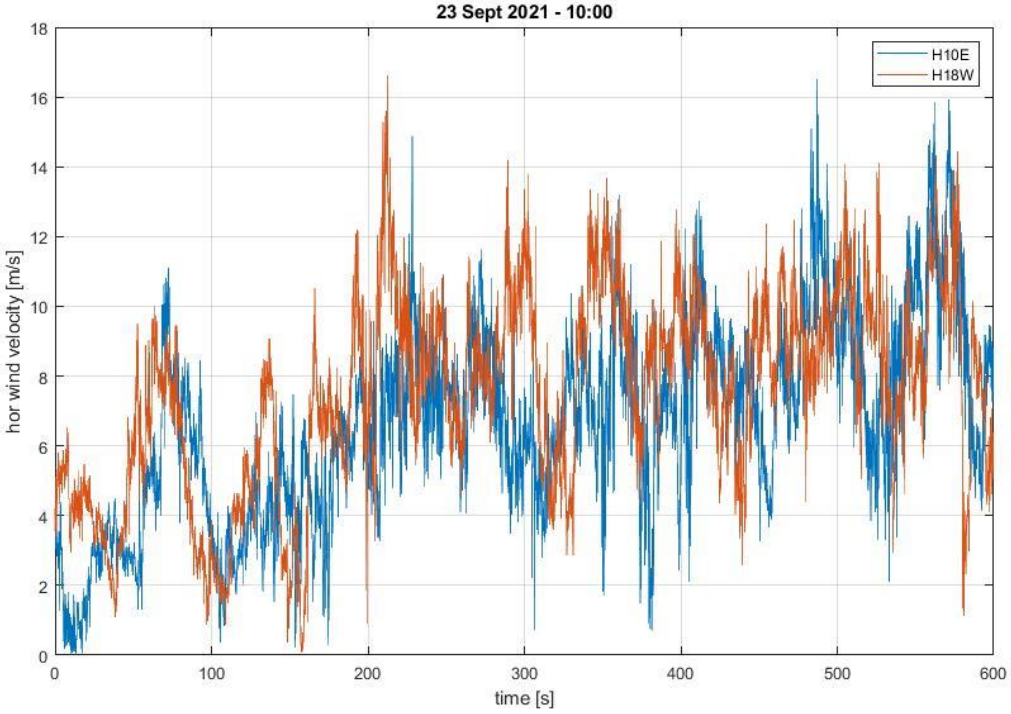
23 Sept 2021 - 10:00
H10E
H18W
hor wind velocity [m/s]
time [s]
0
2
4
6
8
10
12
14
16
18
0
100
200
300
400
500
600

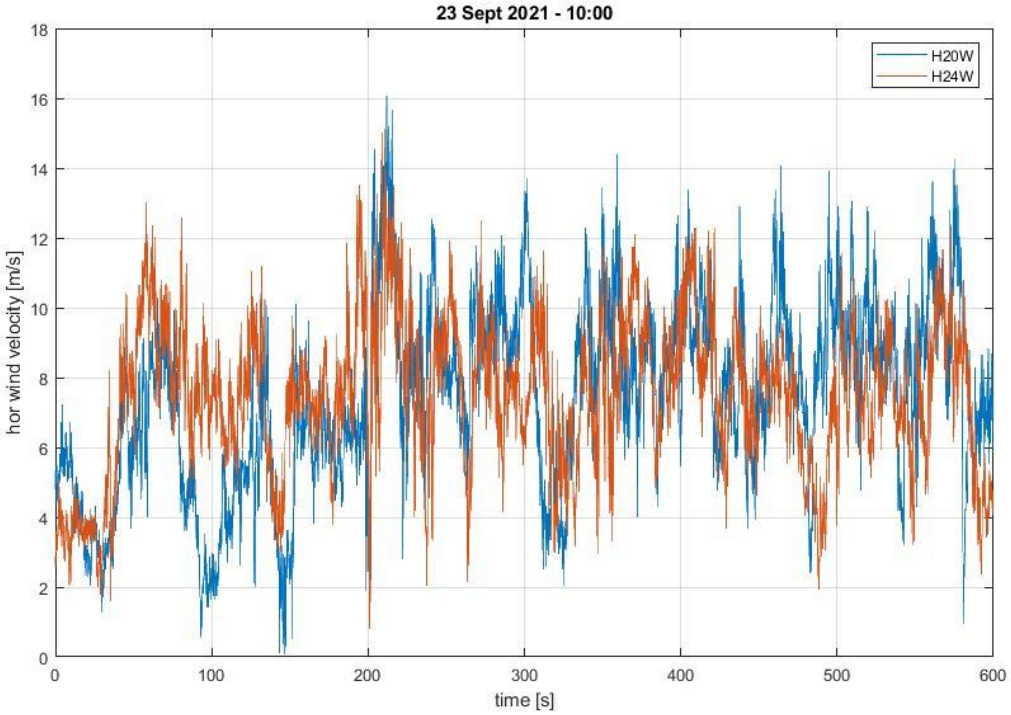
23 Sept 2021 - 10:00
H20W
H24W
hor wind velocity [m/s]
time [s]
0
2
4
6
8
10
12
14
16
18
0
100
200
300
400
500
600

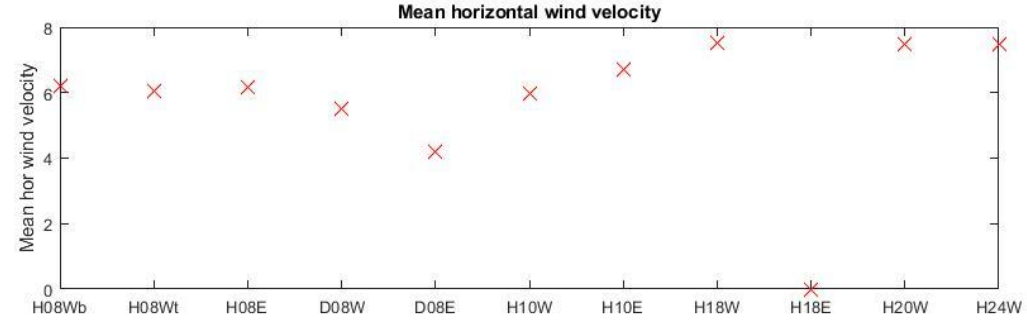
Mean horizontal wind velocity
Mean hor wind velocity
0
2
4
6
8
H08Wb
H08Wt
H08E
D08W
D08E
H10W
H10E
H18W
H18E
H20W
H24W

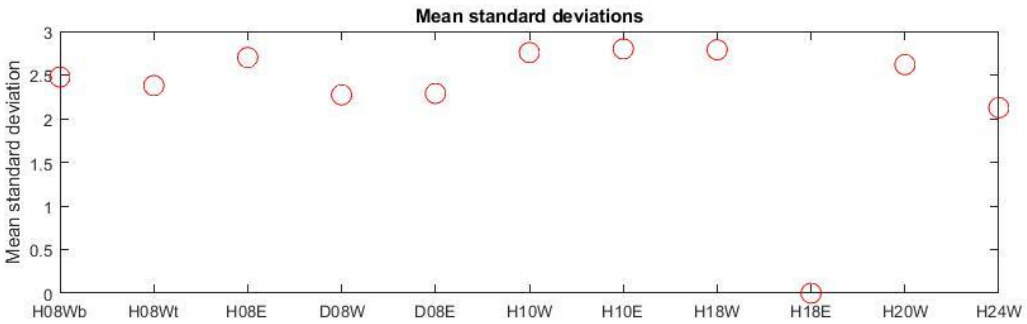
Mean standard deviations
Mean standard deviation
0
0.5
1
1.5
2
2.5
3
H08Wb
H08Wt
H08E
D08W
D08E
H10W
H10E
H18W
H18E
H20W
H24W

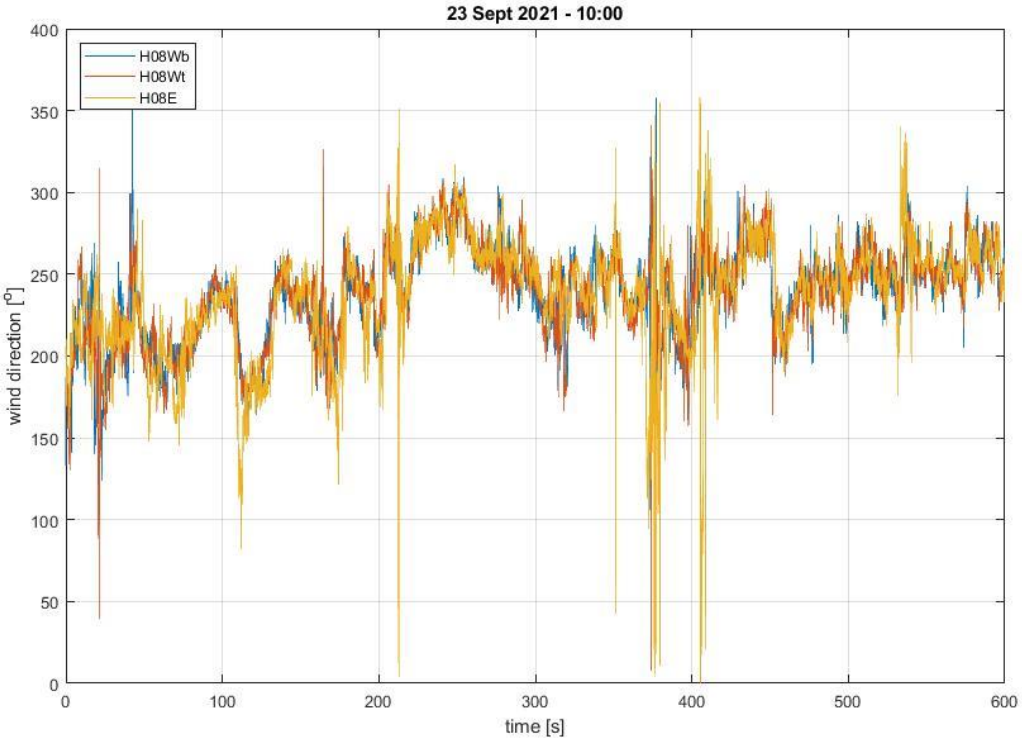
23 Sept 2021 - 10:00
H08Wb
H08Wt
H08E
wind direction [°]
0
50
100
150
200
250
300
350
400
0
100
200
300
400
500
600
time [s]

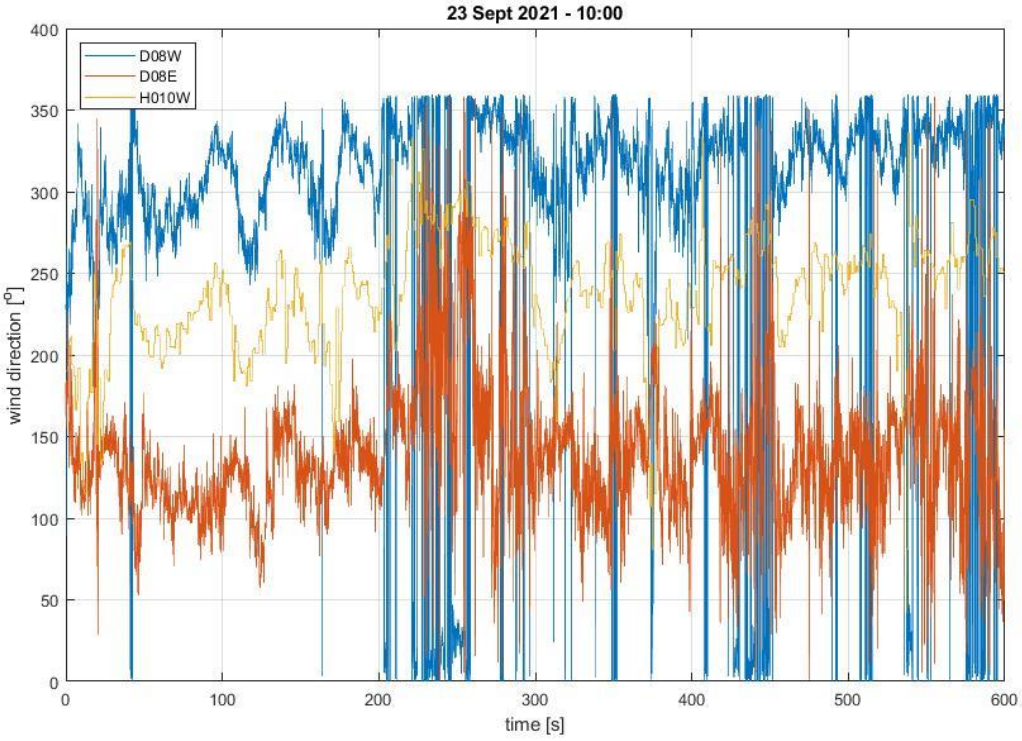
23 Sept 2021 - 10:00
D08W
D08E
H010W
wind direction [°]
time [s]
0
50
100
150
200
250
300
350
400
0
100
200
300
400
500
600

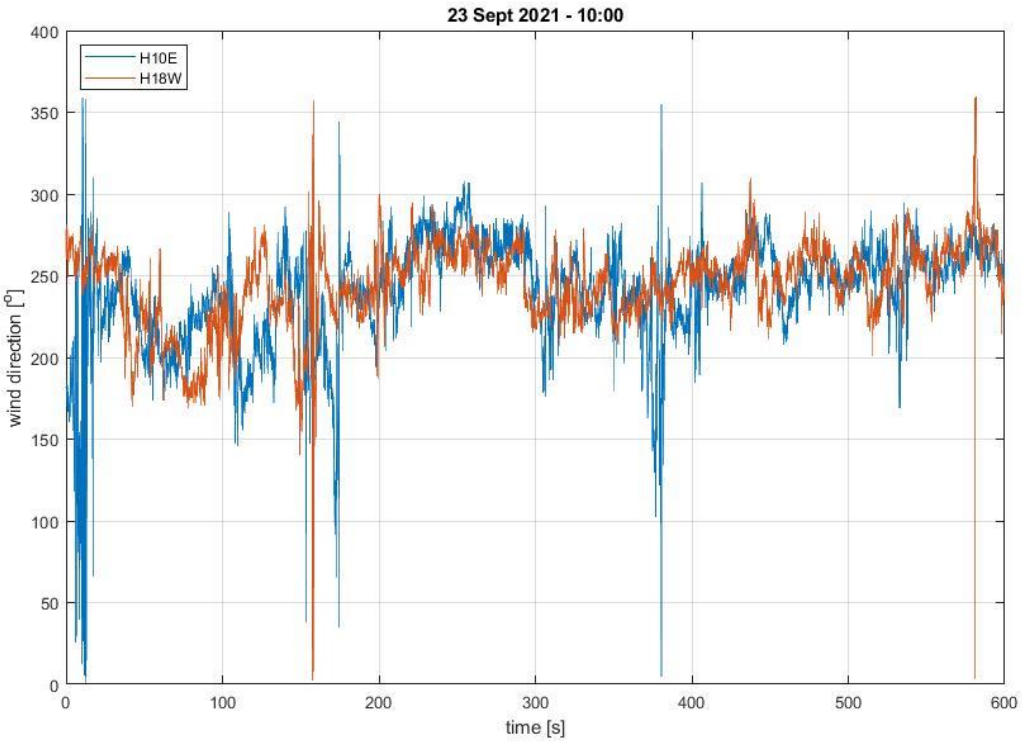
23 Sept 2021 - 10:00
H10E
H18W
wind direction [°]
time [s]
0
50
100
150
200
250
300
350
400
0
100
200
300
400
500
600

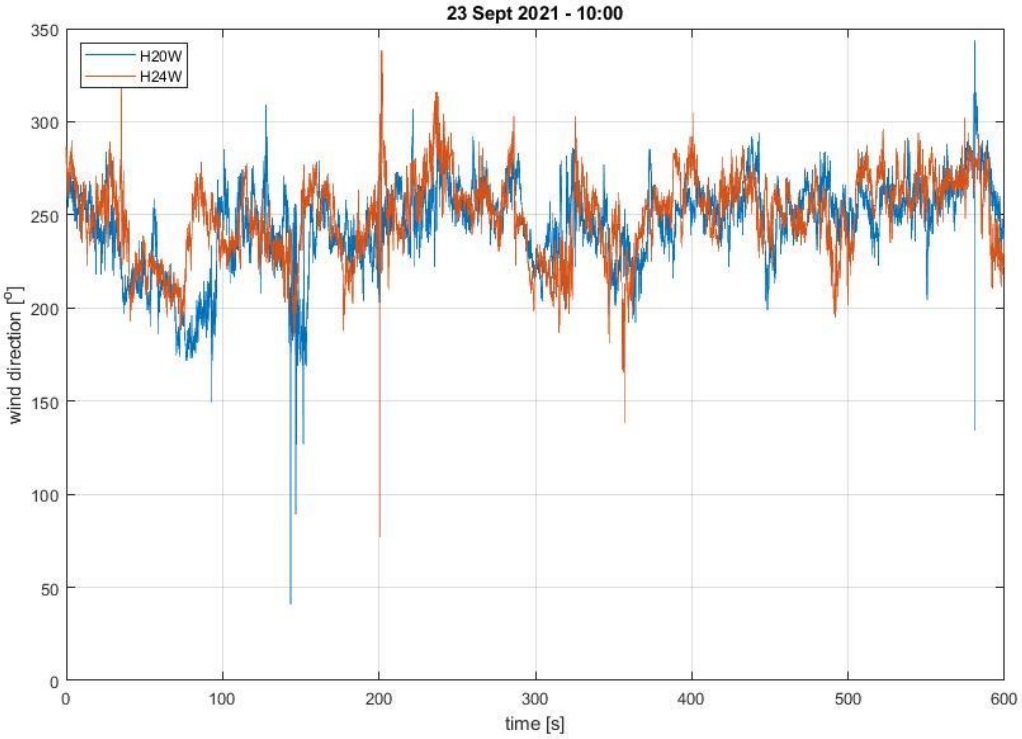
23 Sept 2021 - 10:00
H20W
H24W
wind direction [°]
time [s]
0
50
100
150
200
250
300
350
0
100
200
300
400
500
600

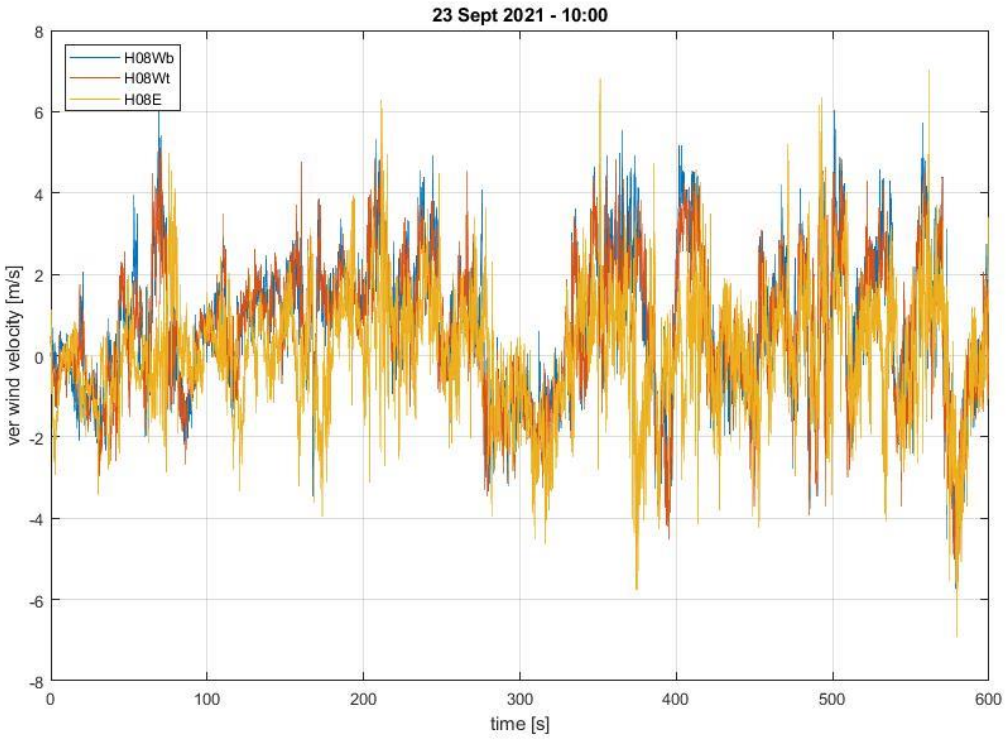
23 Sept 2021 - 10:00
H08Wb
H08Wt
H08E
ver wind velocity [m/s]
time [s]
-8
-6
-4
-2
0
2
4
6
8
0
100
200
300
400
500
600

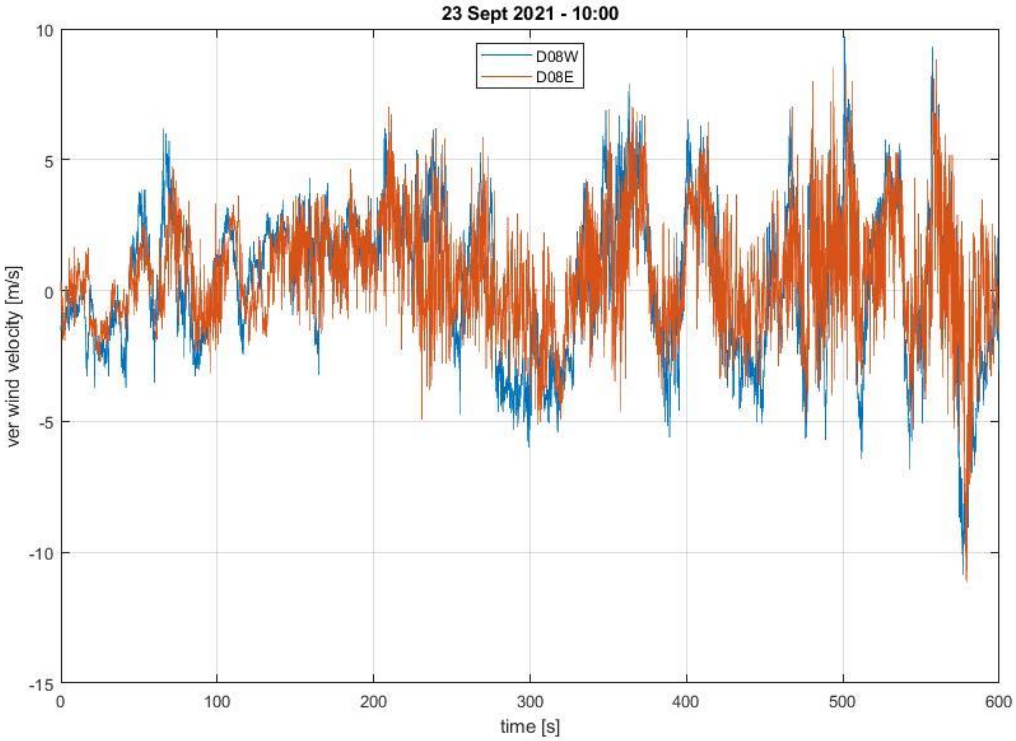
23 Sept 2021 - 10:00
D08W
D08E
ver wind velocity [m/s]
time [s]
10
5
0
-5
-10
-15
0
100
200
300
400
500
600

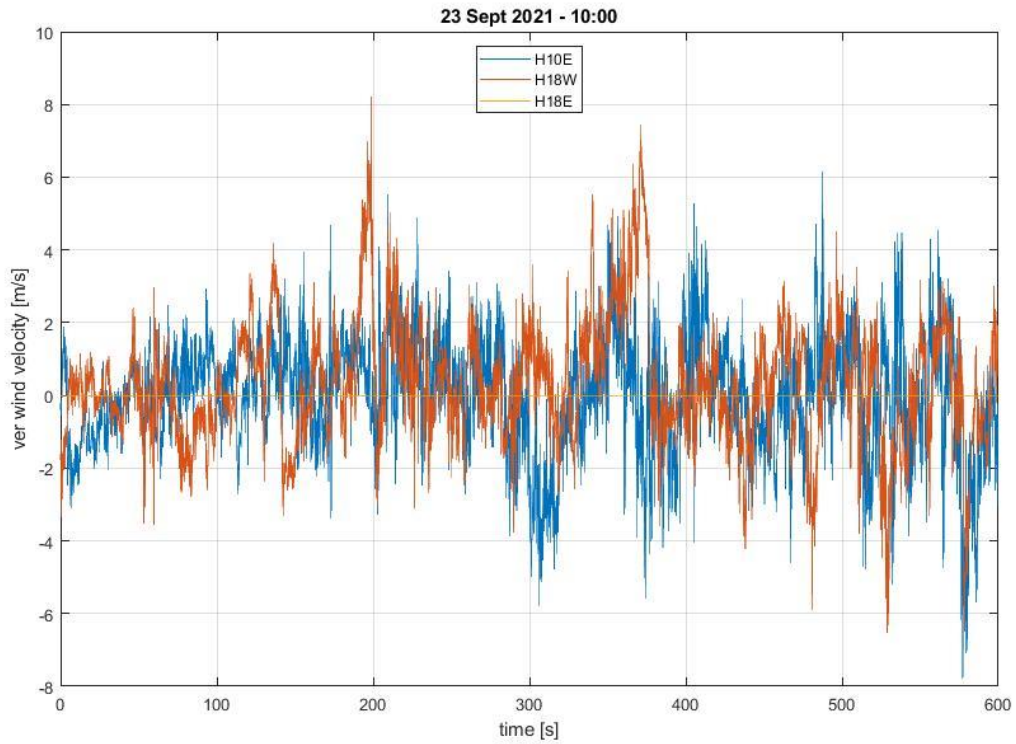
23 Sept 2021 - 10:00
H10E
H18W
H18E
ver wind velocity [m/s]
time [s]
10
8
6
4
2
0
-2
-4
-6
-8
0
100
200
300
400
500
600

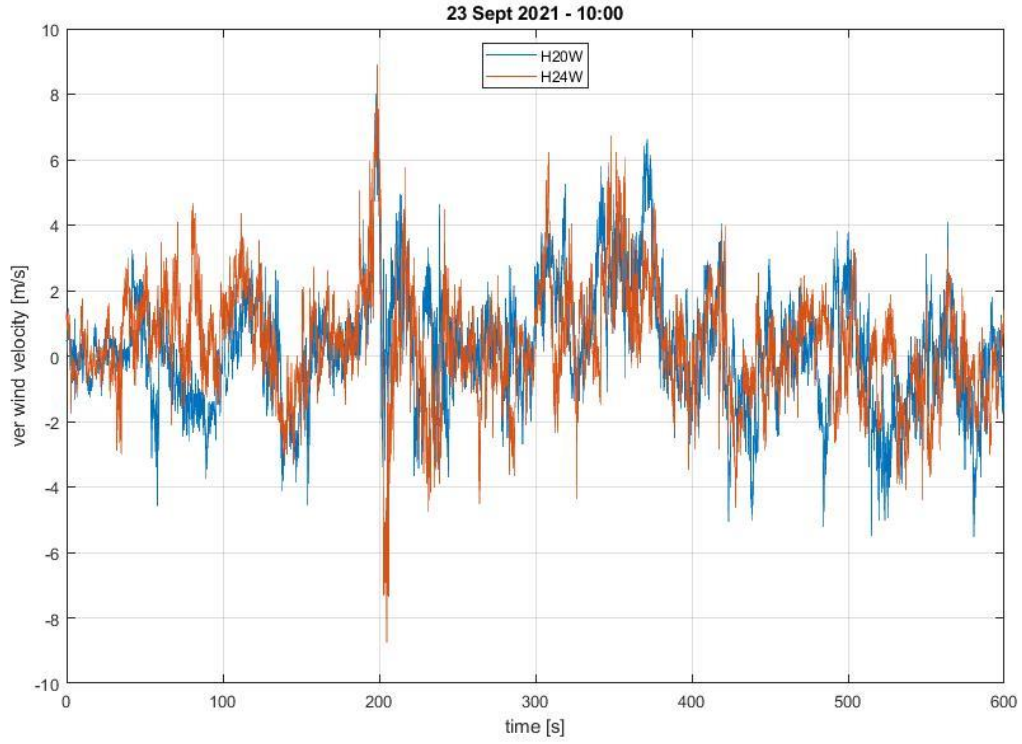
23 Sept 2021 - 10:00
H20W
H24W
ver wind velocity [m/s]
time [s]

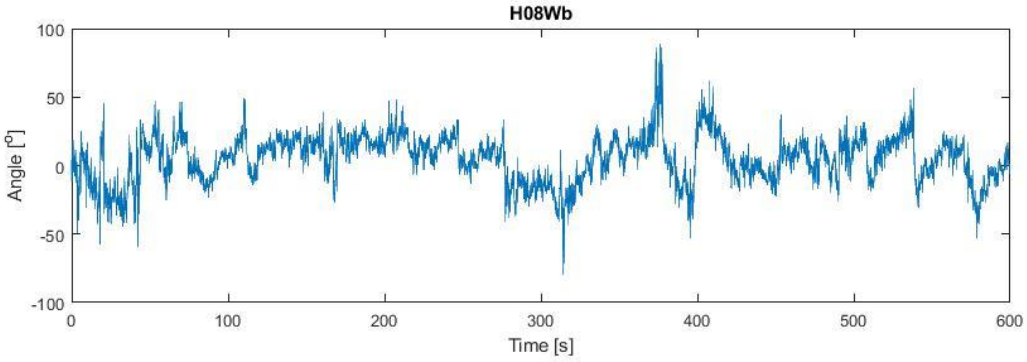
H08Wb
Angle [°]
Time [s]

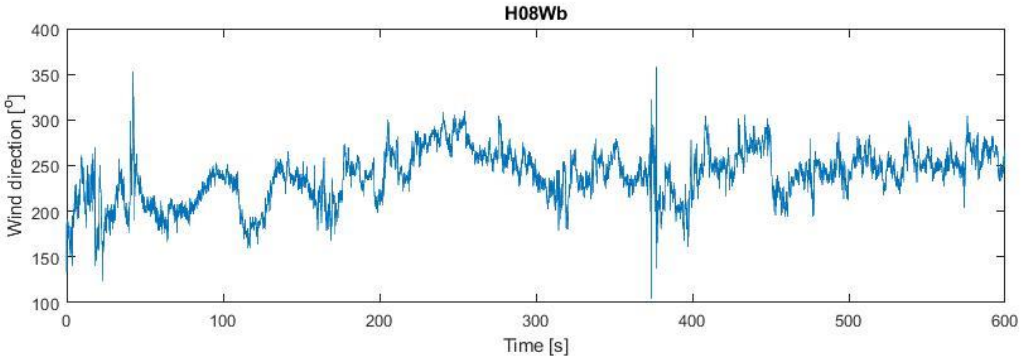
H08Wb
Wind direction [°]
Time [s]

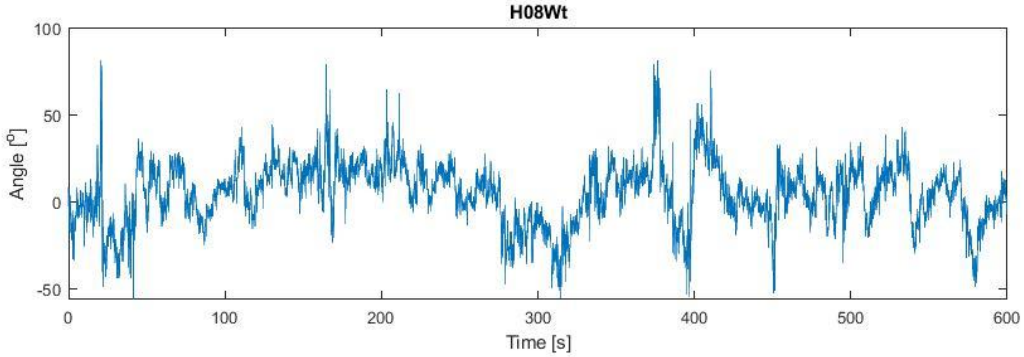
H08Wt
Angle [°]
Time [s]

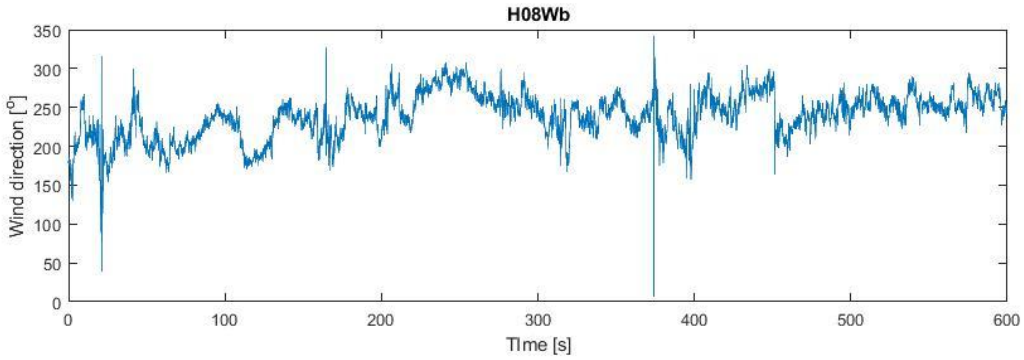
H08Wb
Wind direction [°]
Time [s]

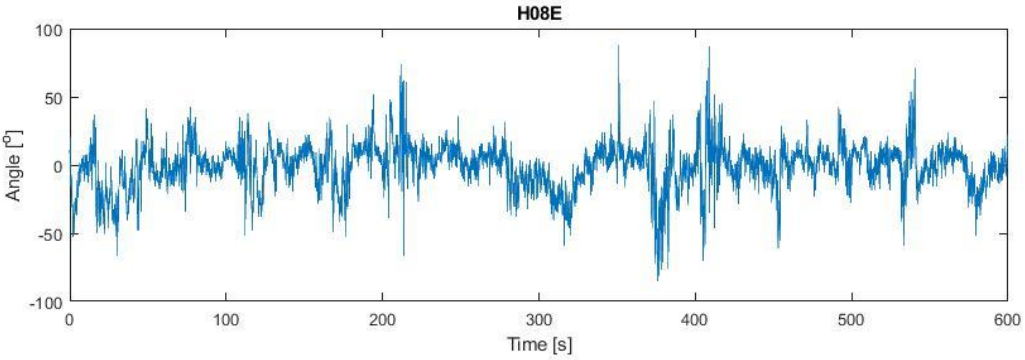
H08E
Angle [°]
Time [s]

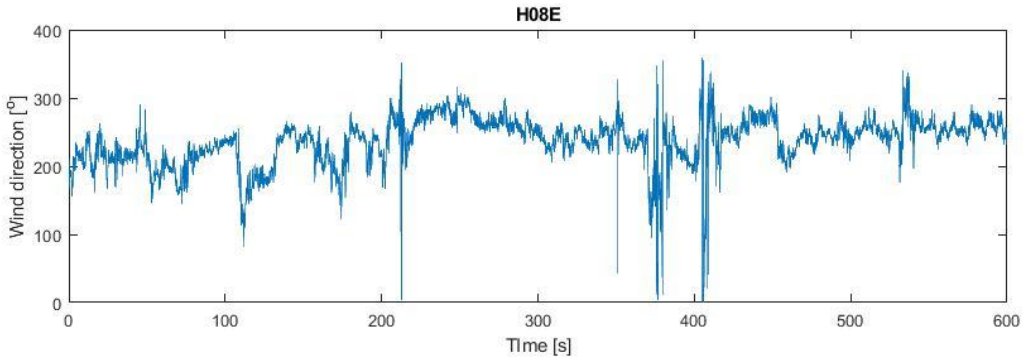
H08E
Wind direction [°]
Time [s]

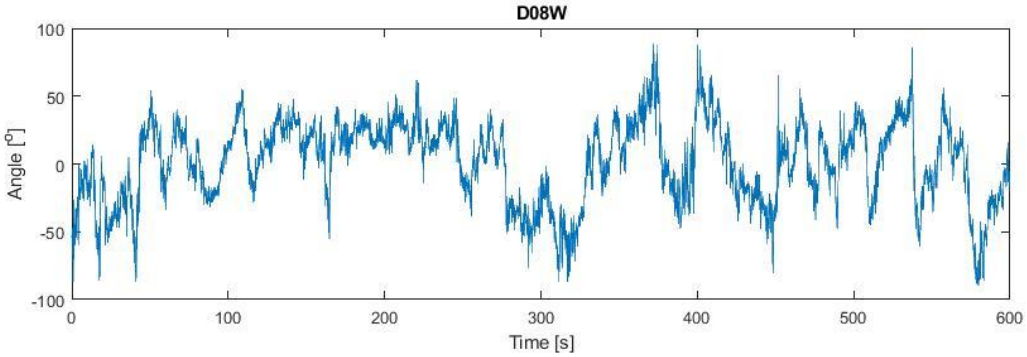
D08W
Angle [°]
Time [s]

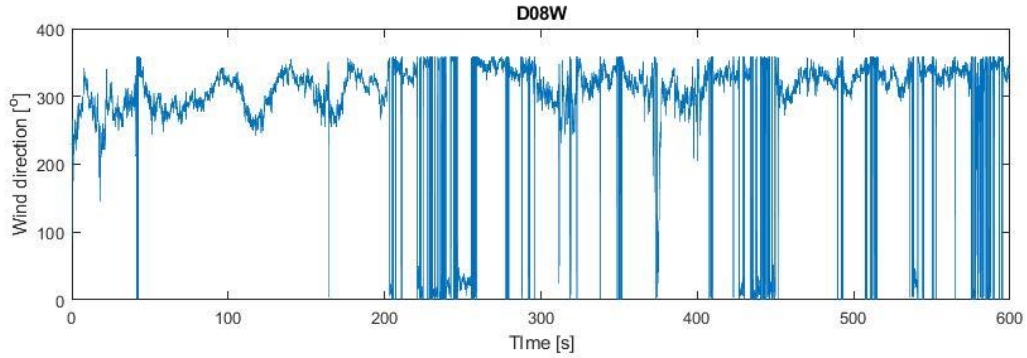
D08W
Wind direction [°]
Time [s]

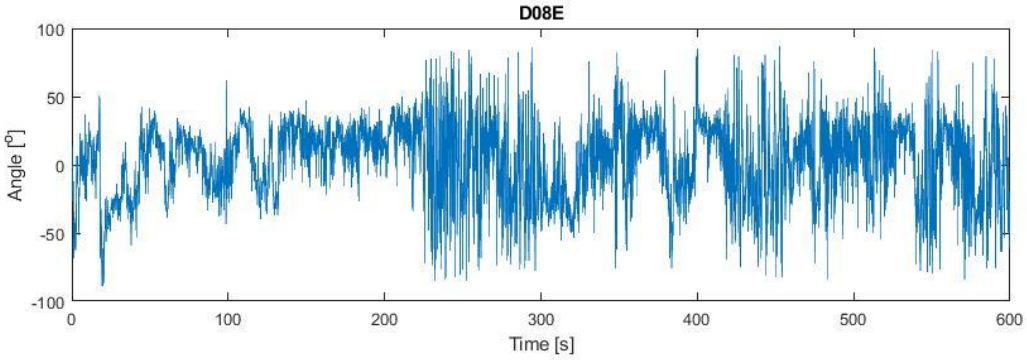
D08E
Angle [°]
Time [s]

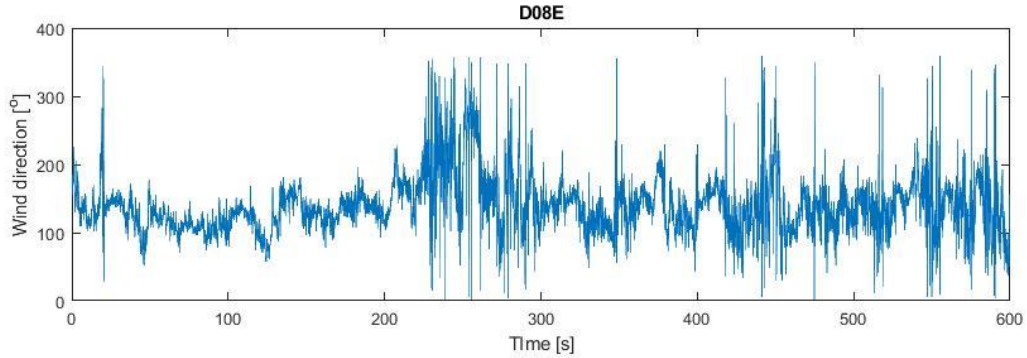
D08E
Wind direction [°]
Time [s]

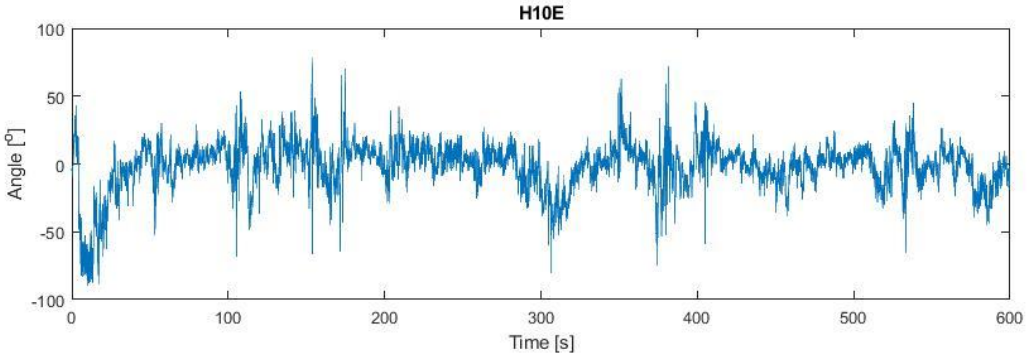
H10E
Angle [°]
Time [s]

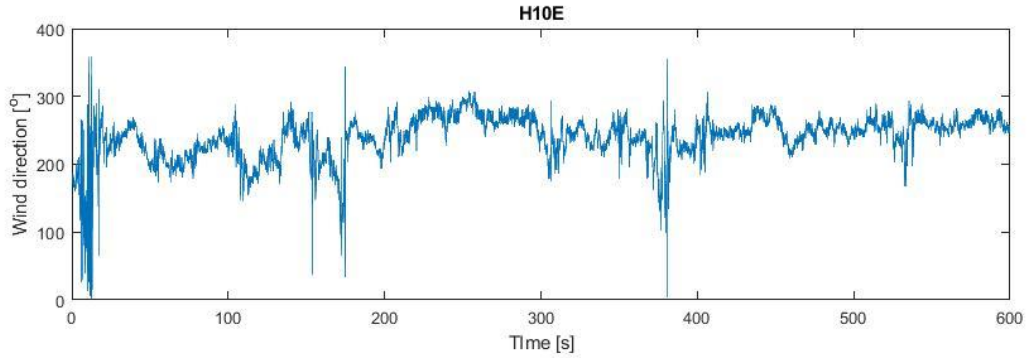
H10E
Wind direction [°]
TIme [s]

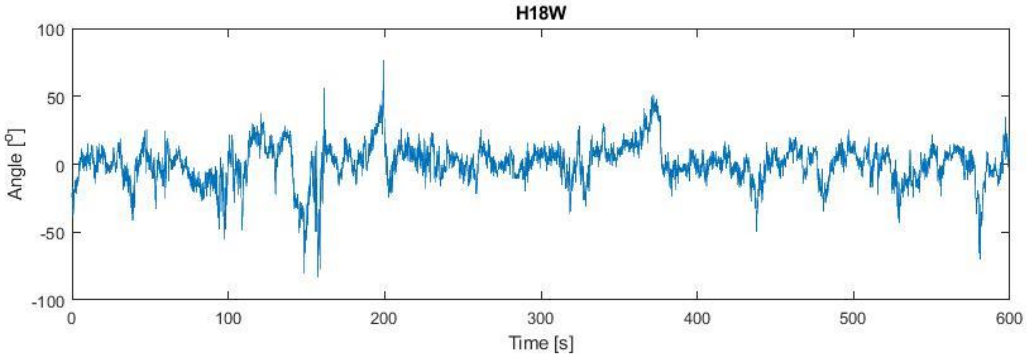
H18W
Angle [°]
Time [s]

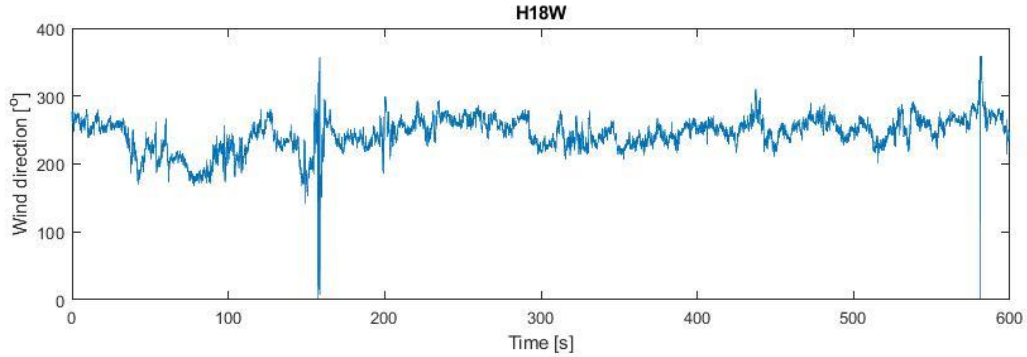
H18W
Wind direction [°]
Time [s]

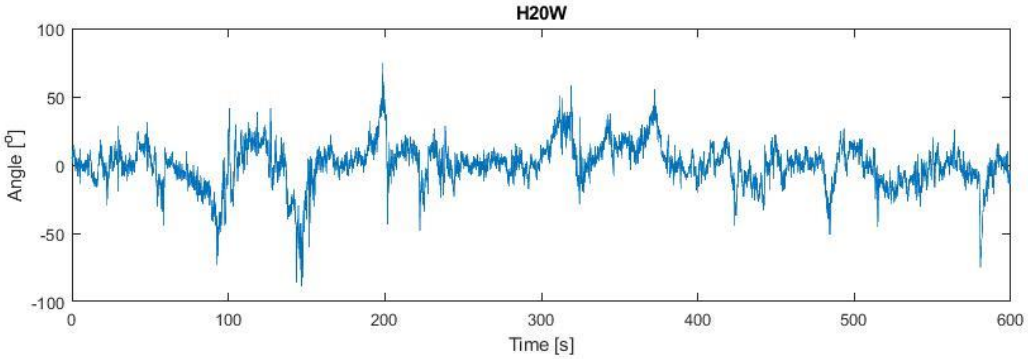
H20W
Angle [°]
Time [s]

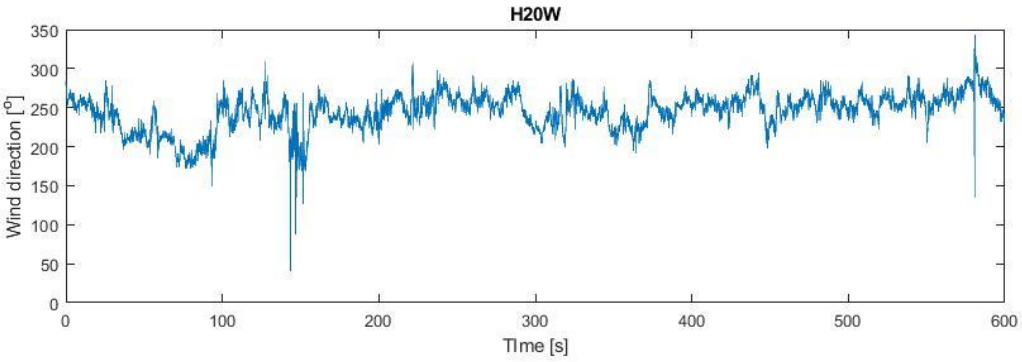
H20W
Wind direction [°]
TIme [s]

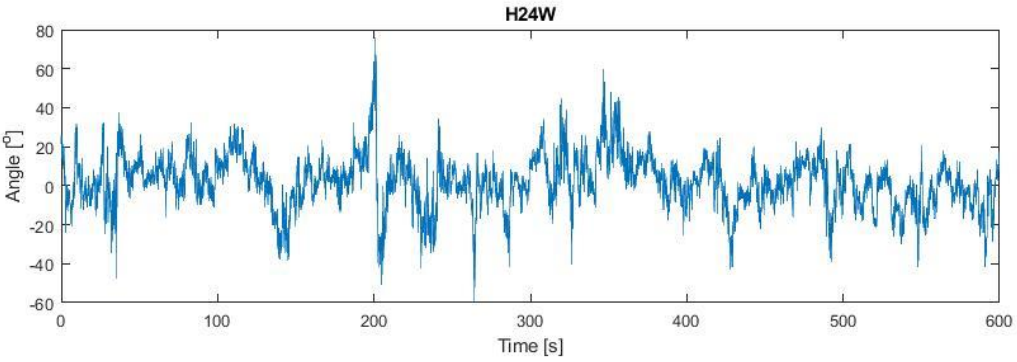
H24W
Angle [°]
Time [s]

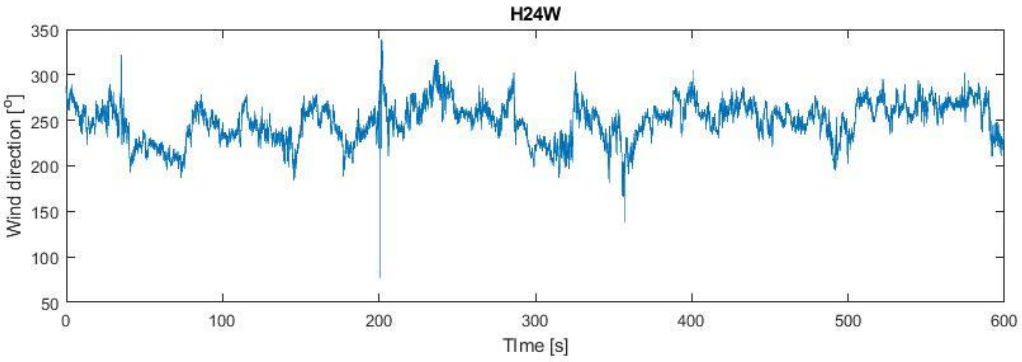
H24W
Wind direction [°]
TIme [s]

Appendix C: 18/10/21

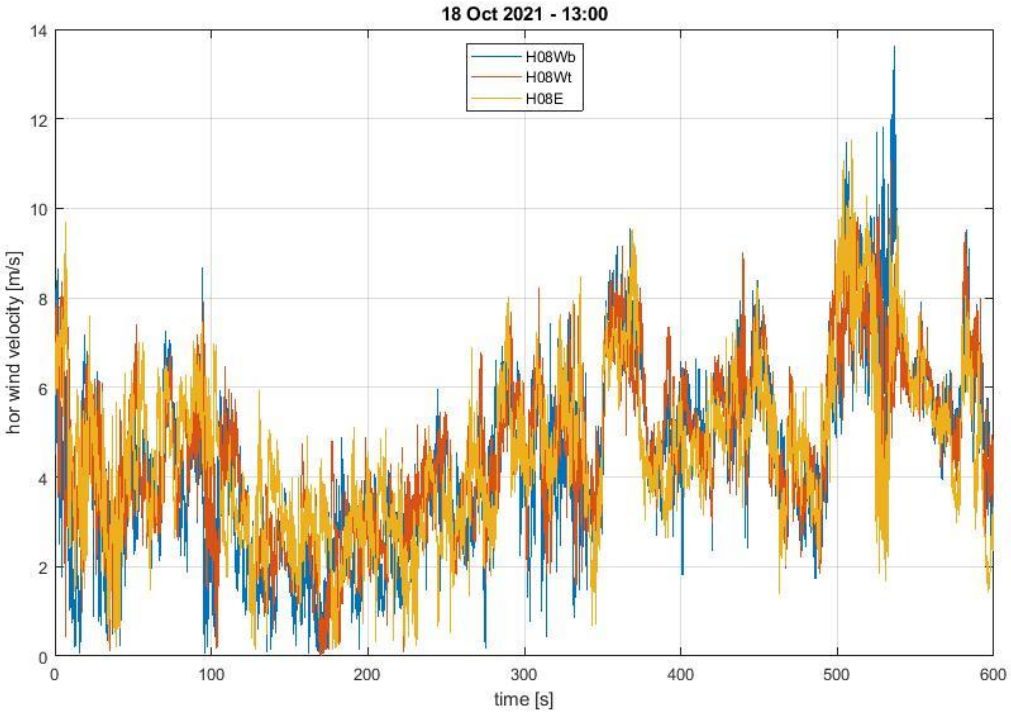

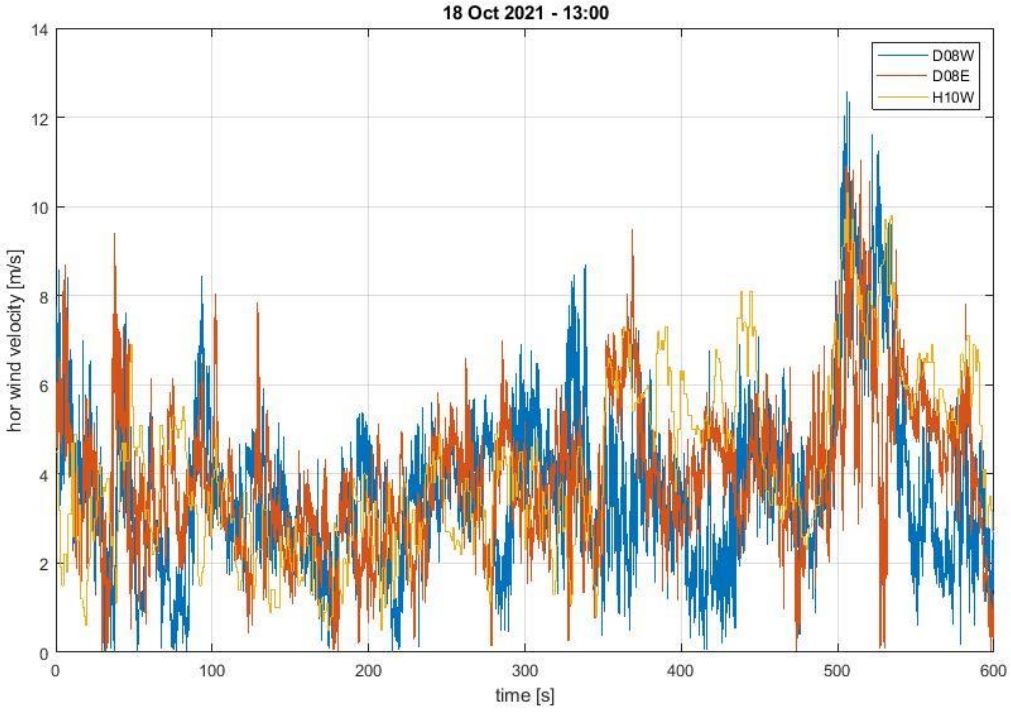

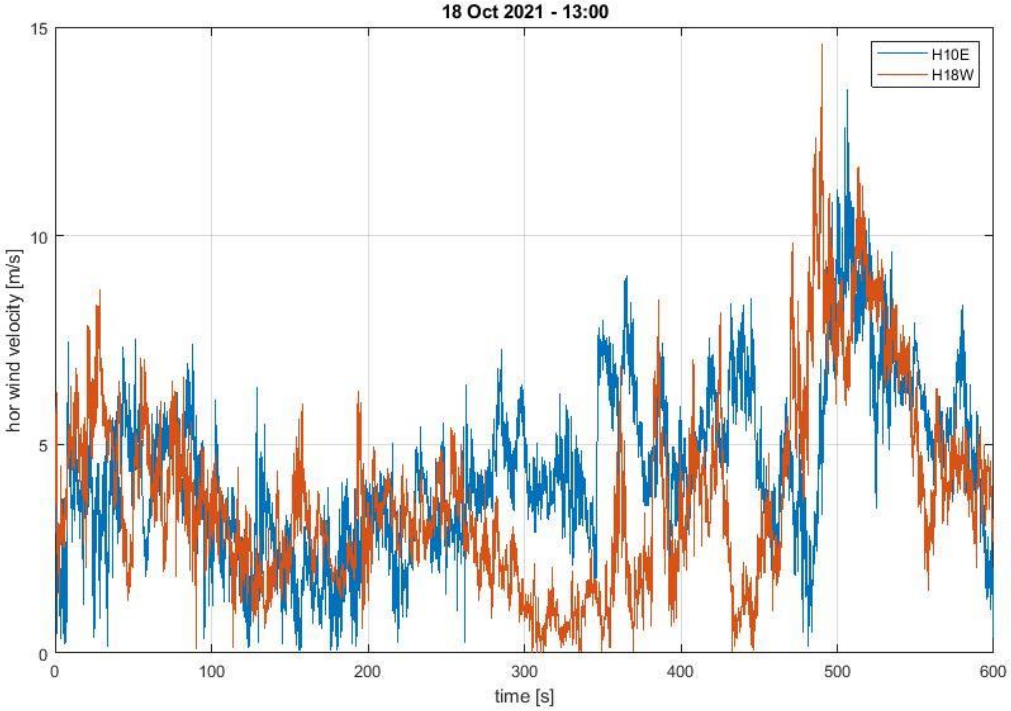
18 Oct 2021 - 13:00
H10E
H18W
hor wind velocity [m/s]
time [s]
0
5
10
15
0
100
200
300
400
500
600

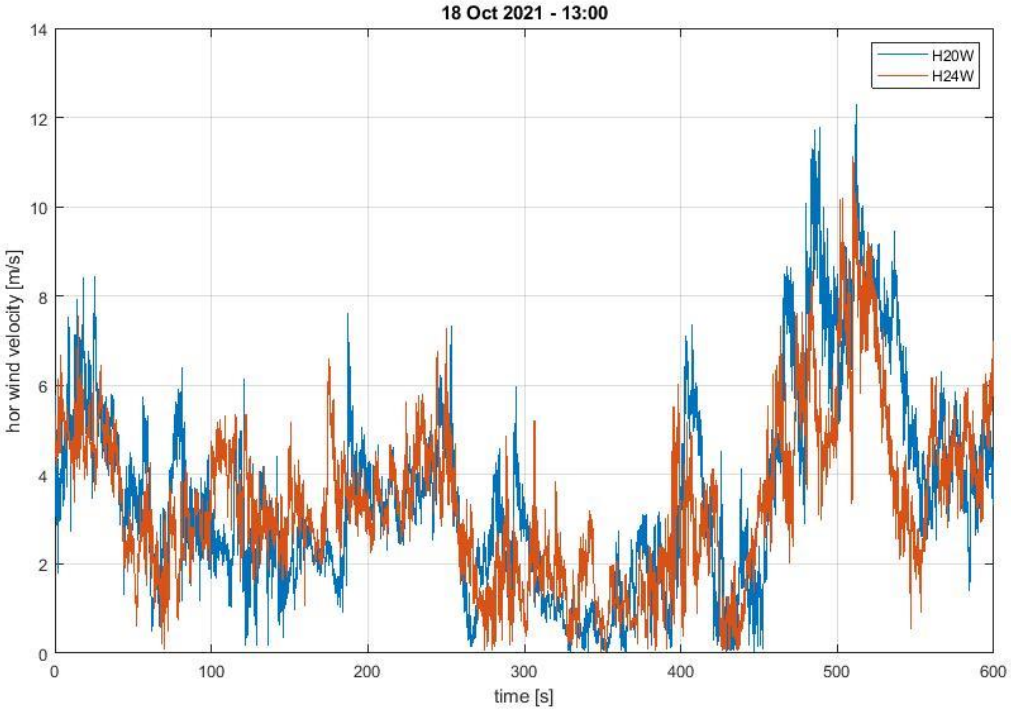
18 Oct 2021 - 13:00
H20W
H24W
hor wind velocity [m/s]
time [s]
0
2
4
6
8
10
12
14
0
100
200
300
400
500
600

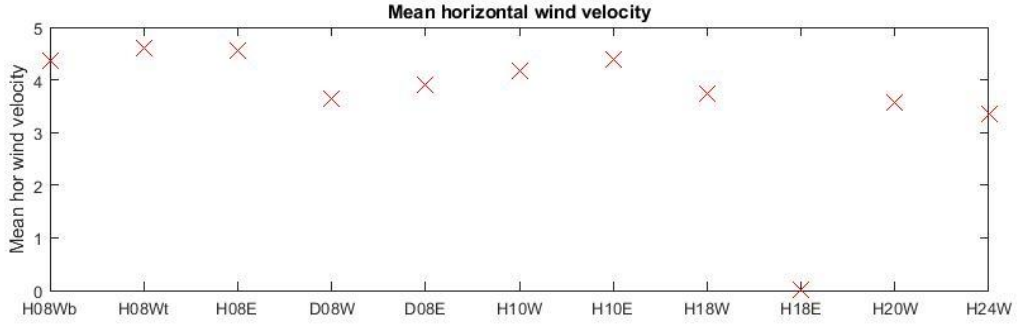
Mean horizontal wind velocity
Mean hor wind velocity
0
1
2
3
4
5
H08Wb
H08Wt
H08E
D08W
D08E
H10W
H10E
H18W
H18E
H20W
H24W

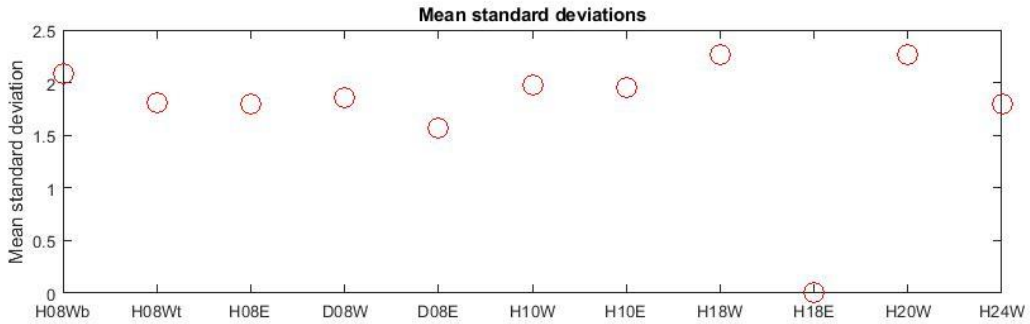
Mean standard deviations
Mean standard deviation
0
0.5
1
1.5
2
2.5
H08Wb
H08Wt
H08E
D08W
D08E
H10W
H10E
H18W
H18E
H20W
H24W

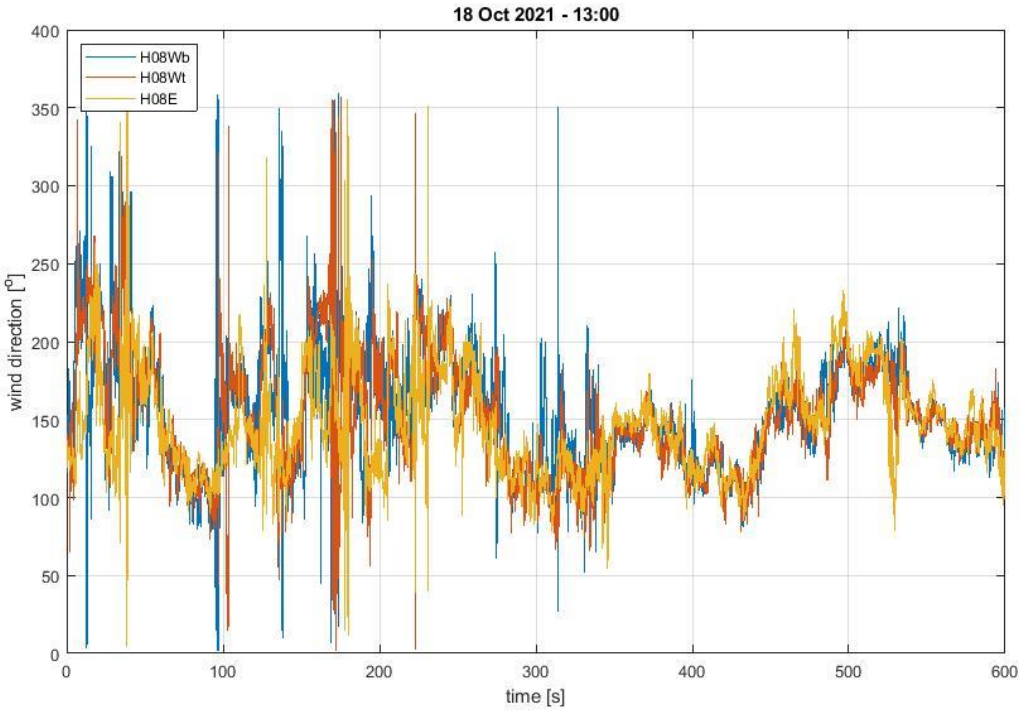
18 Oct 2021 - 13:00
H08Wb
H08Wt
H08E
wind direction [°]
0
50
100
150
200
250
300
350
400
0
100
200
300
400
500
600
time [s]

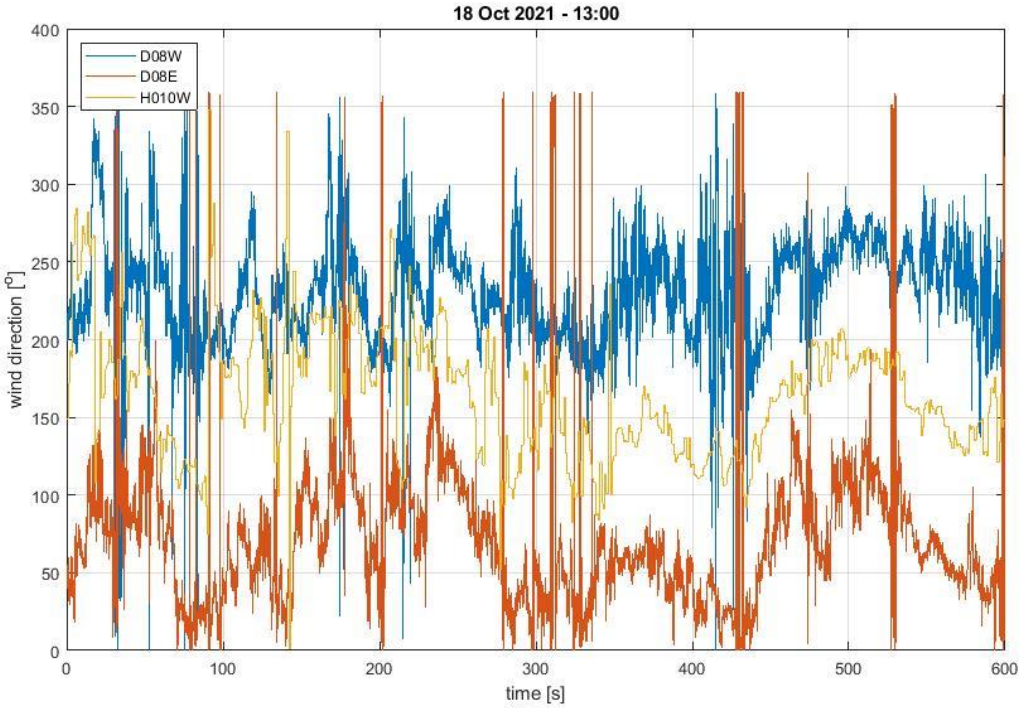
18 Oct 2021 - 13:00
D08W
D08E
H010W
wind direction [°]
time [s]
0
50
100
150
200
250
300
350
400
0
100
200
300
400
500
600

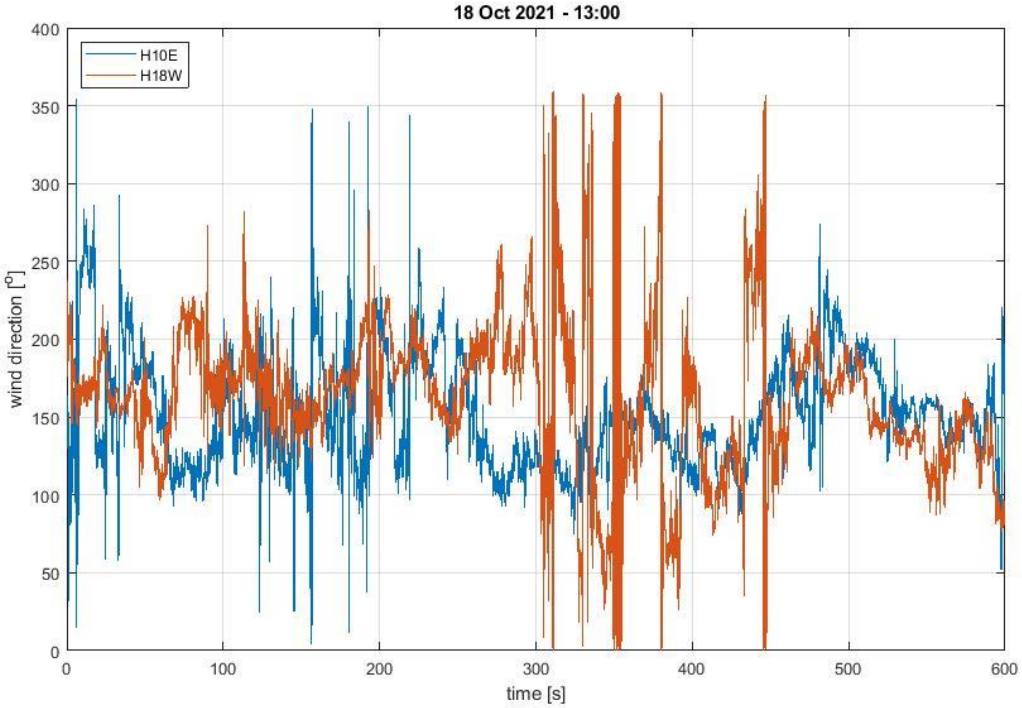
18 Oct 2021 - 13:00
H10E
H18W
wind direction [°]
time [s]
0
50
100
150
200
250
300
350
400
0
100
200
300
400
500
600

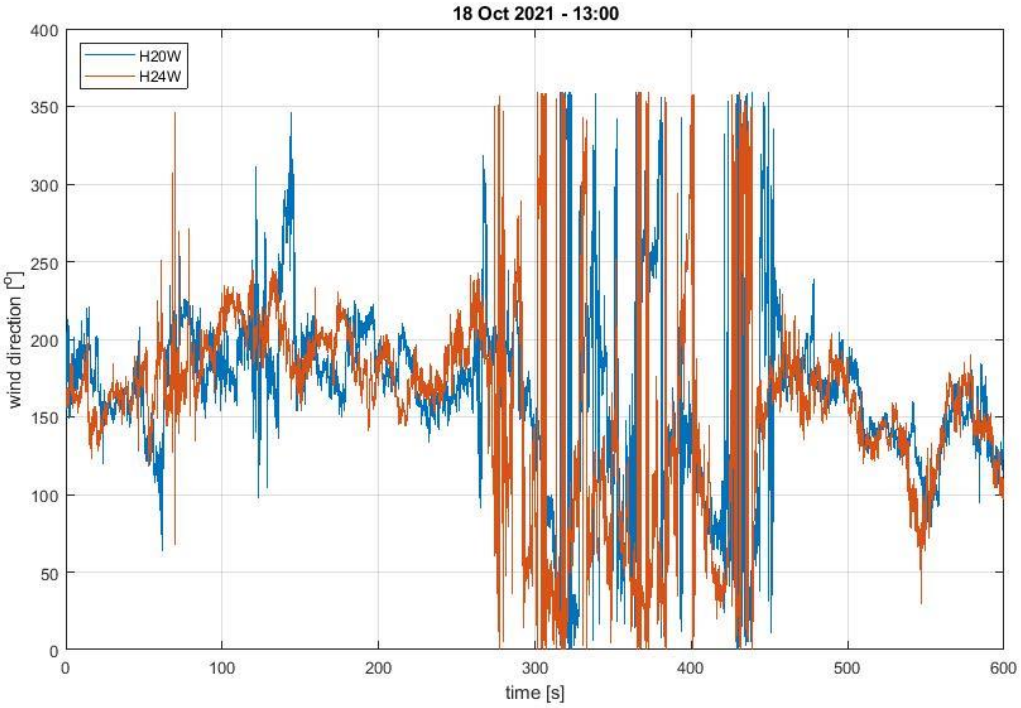
18 Oct 2021 - 13:00
H20W
H24W
wind direction [°]
time [s]
0
50
100
150
200
250
300
350
400
0
100
200
300
400
500
600

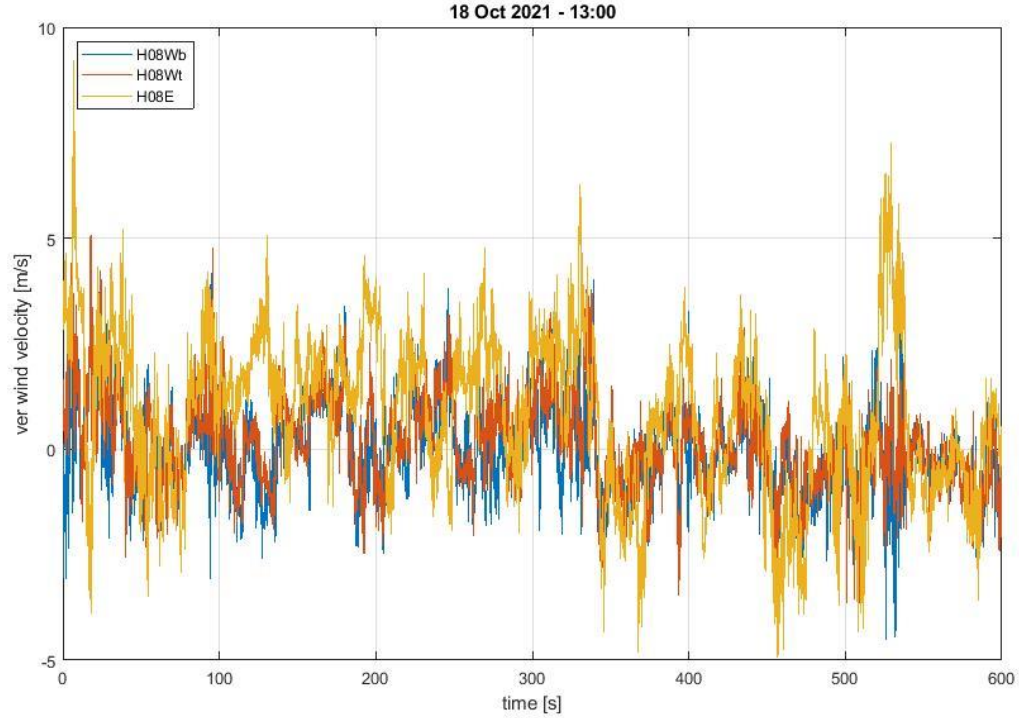
18 Oct 2021 - 13:00
H08Wb
H08Wt
H08E
ver wind velocity [m/s]
time [s]
-5
0
5
10
0
100
200
300
400
500
600

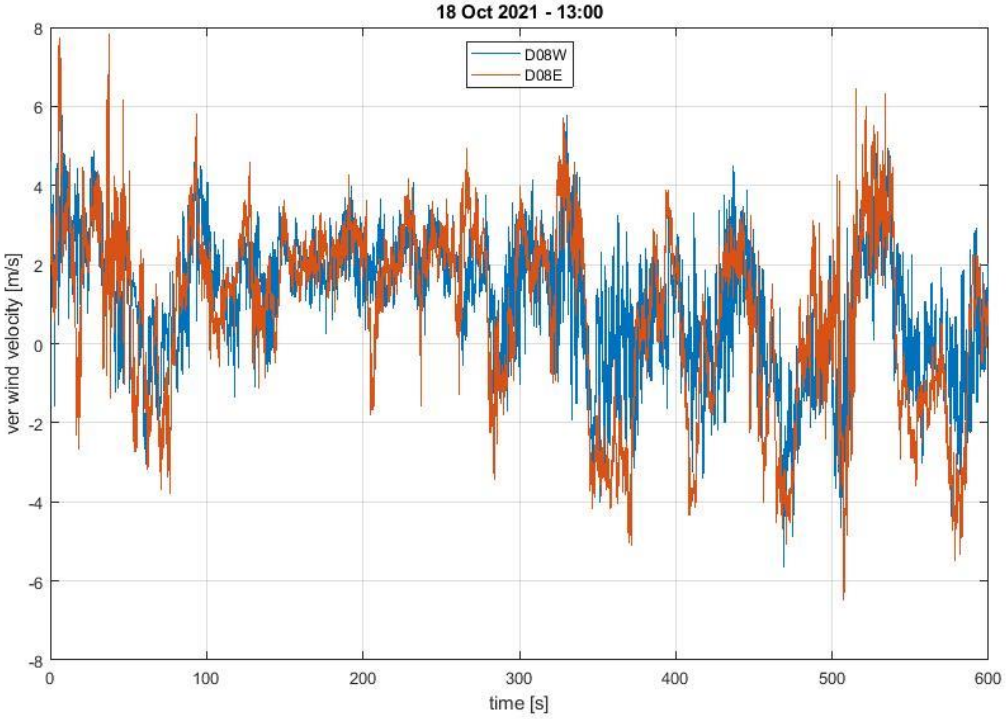
18 Oct 2021 - 13:00
D08W
D08E
ver wind velocity [m/s]
time [s]
8
6
4
2
0
-2
-4
-6
-8
0
100
200
300
400
500
600

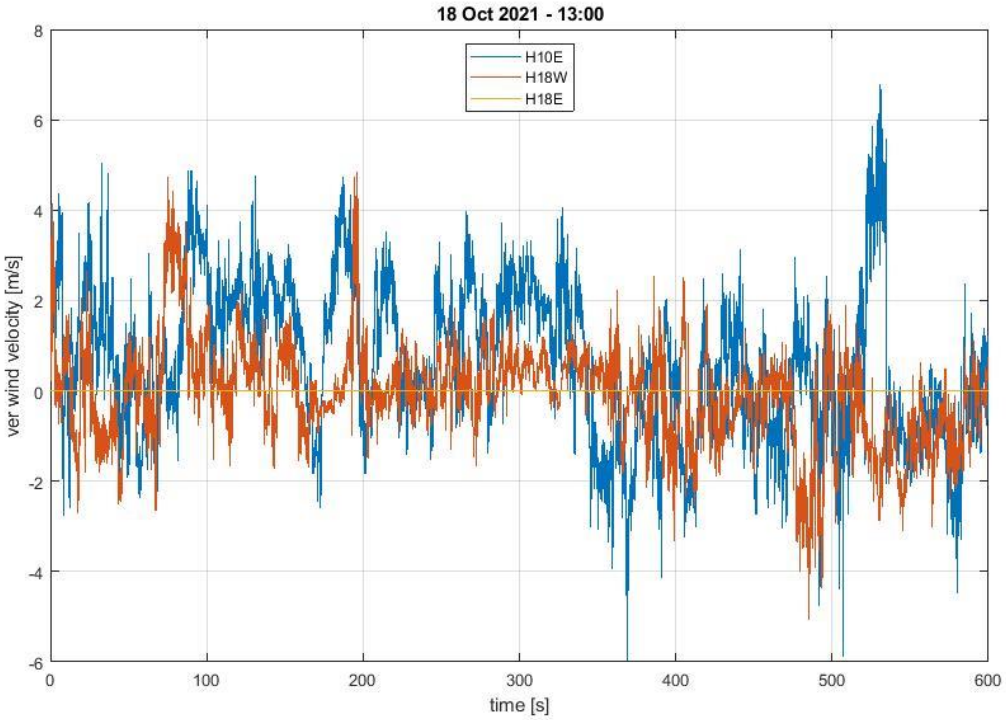
18 Oct 2021 - 13:00
H10E
H18W
H18E
ver wind velocity [m/s]
time [s]
8
6
4
2
0
-2
-4
-6
0
100
200
300
400
500
600

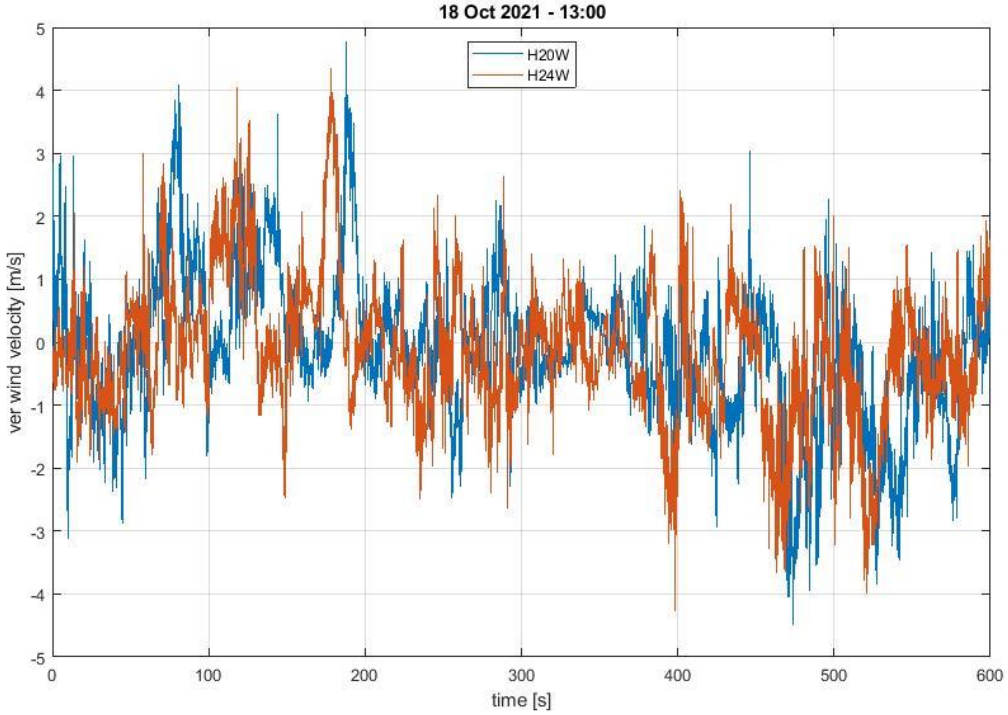
18 Oct 2021 - 13:00
H20W
H24W
ver wind velocity [m/s]
time [s]

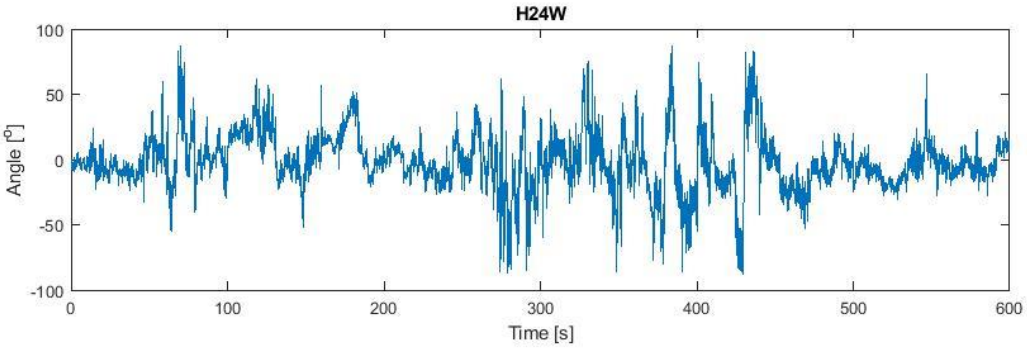
H24W
Angle [°]
Time [s]

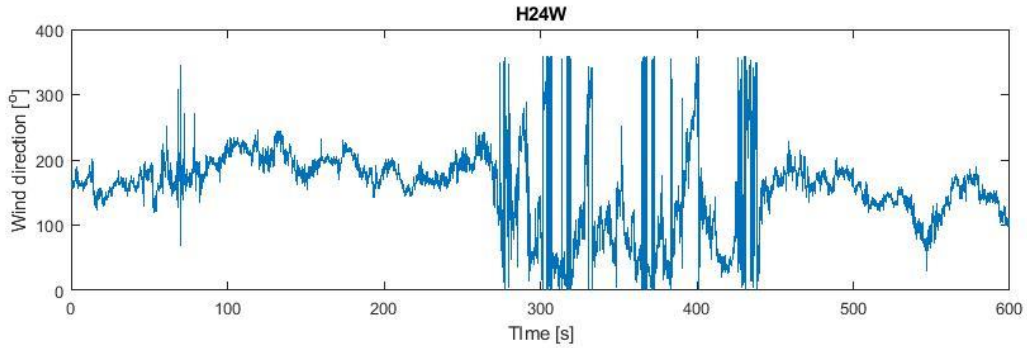
H24W
Wind direction [°]
TIme [s]

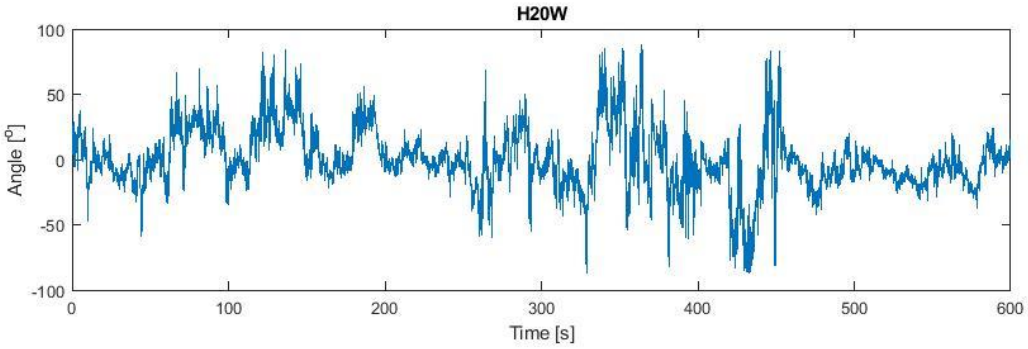
H20W
Angle [°]
Time [s]

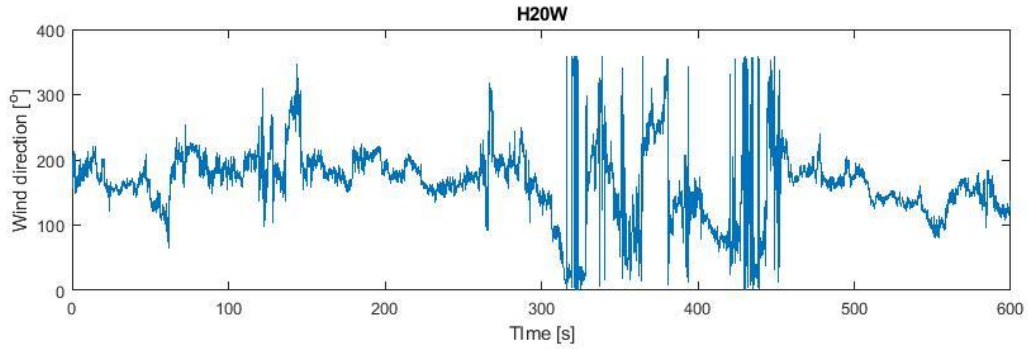
H20W
Wind direction [°]
TIme [s]

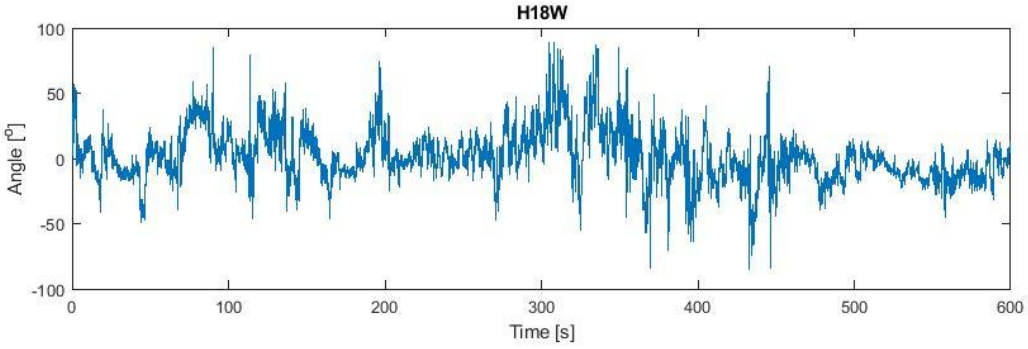
H18W
Angle [°]
Time [s]

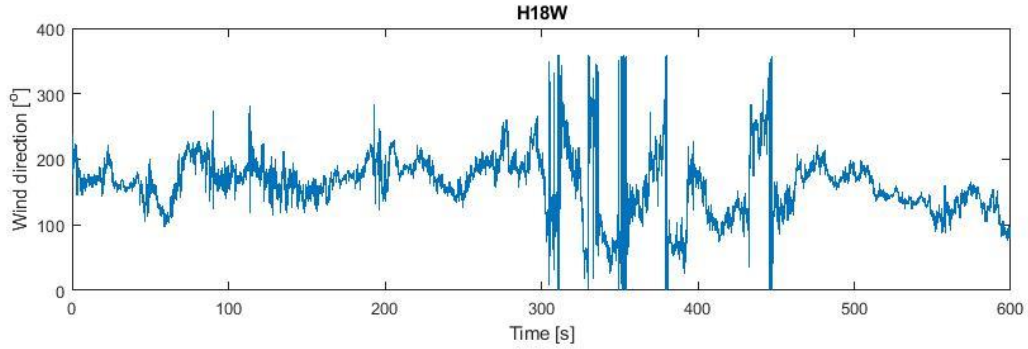
H18W
Wind direction [°]
Time [s]

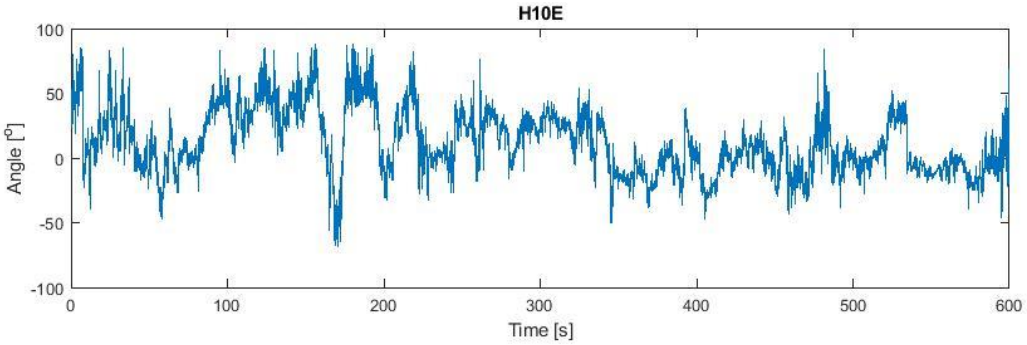
H10E
Angle [°]
Time [s]

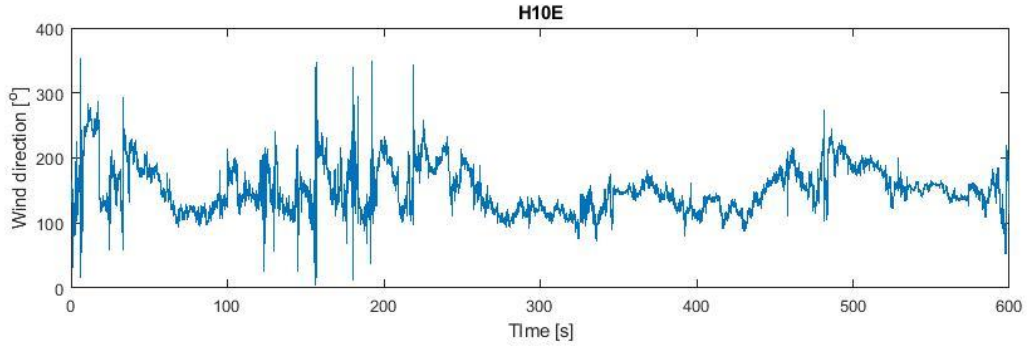
H10E
Wind direction [°]
Time [s]

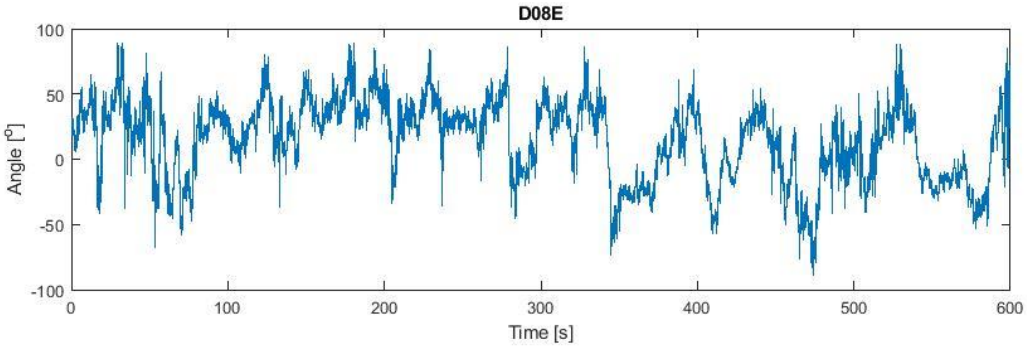
D08E
Angle [°]
Time [s]

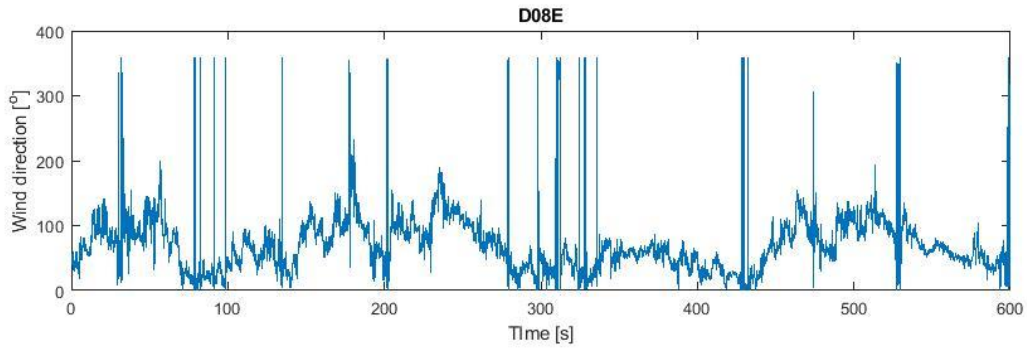
D08E
Wind direction [°]
Time [s]

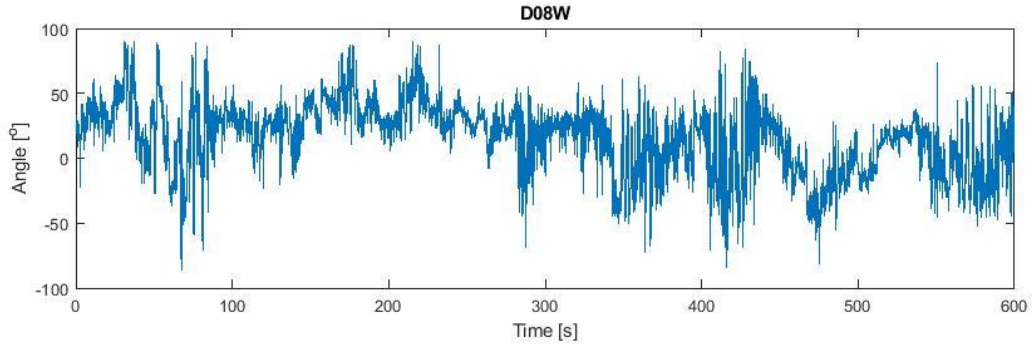
D08W
Angle [°]
Time [s]

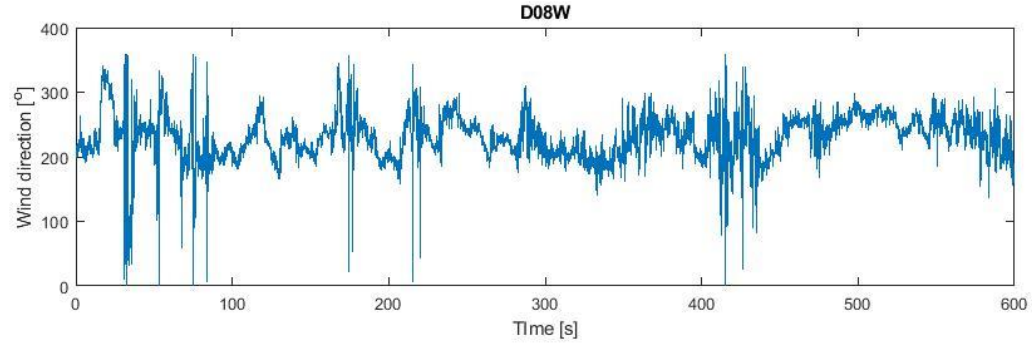
D08W
Wind direction [°]
TIme [s]

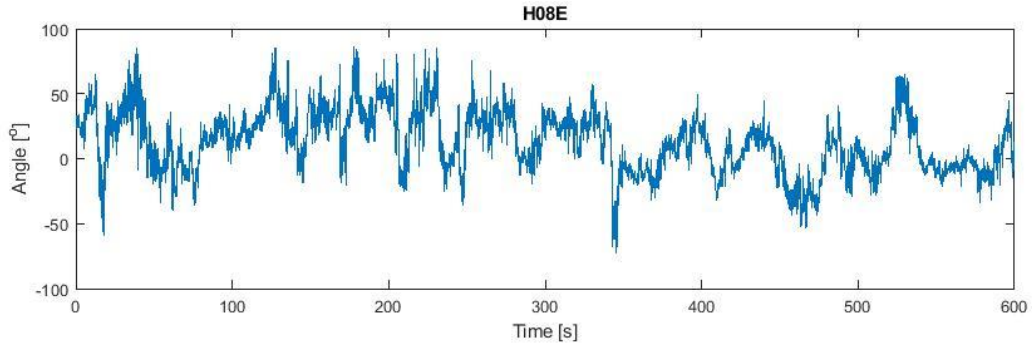
H08E
Angle [°]
Time [s]

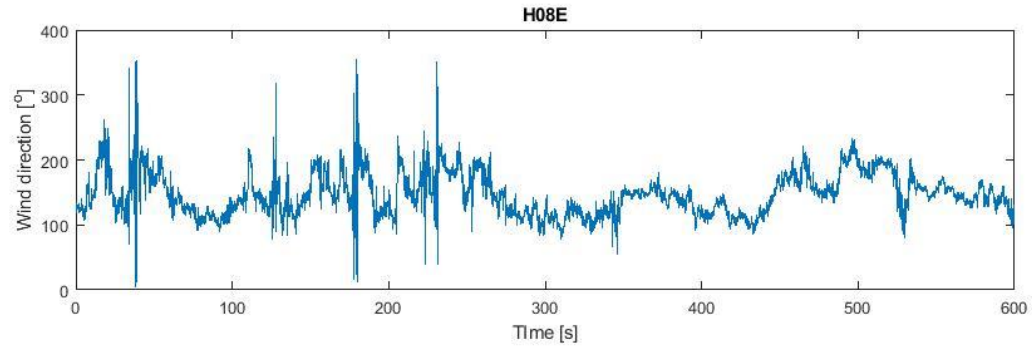
H08E
Wind direction [°]
TIme [s]

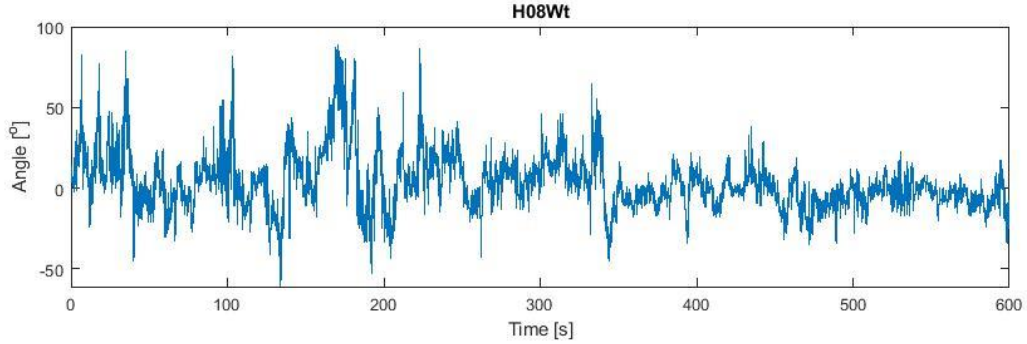
H08Wt
Angle [°]
Time [s]

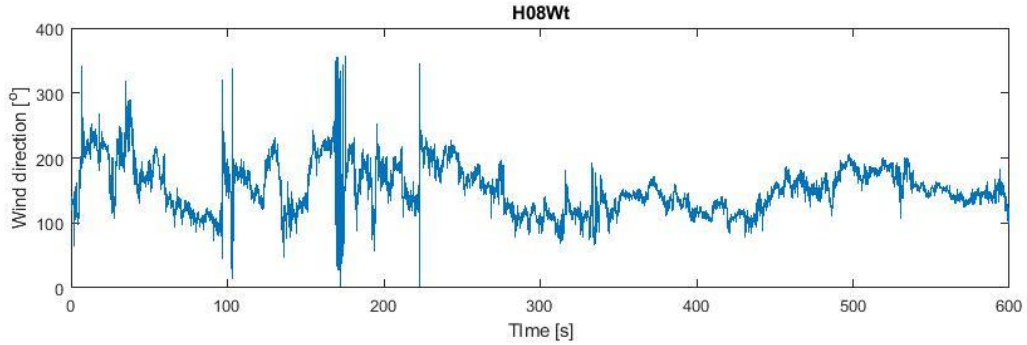
H08Wt
Wind direction [°]
TIme [s]

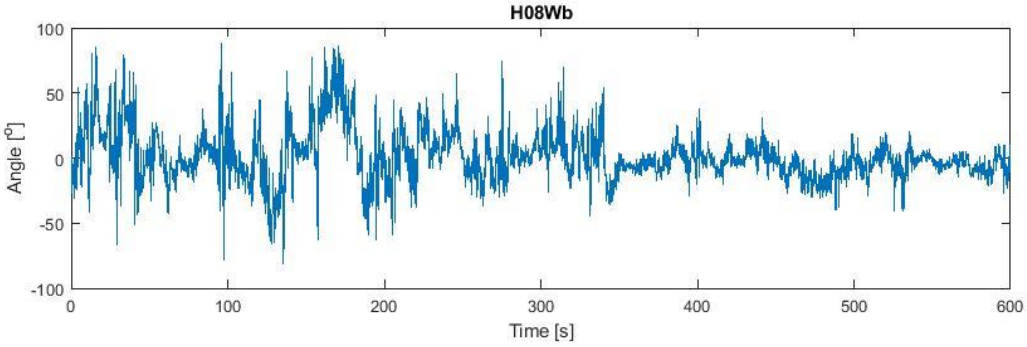
H08Wb
Angle [°]
Time [s]

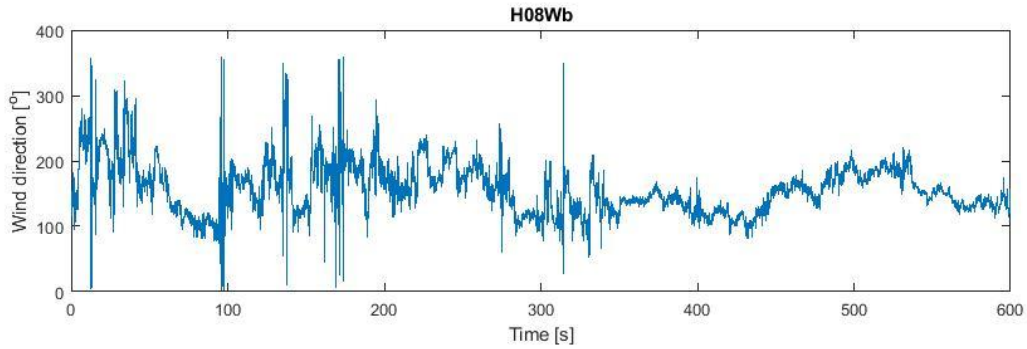
H08Wb
Wind direction [°]
Time [s]

Appendix D: 21/10/21

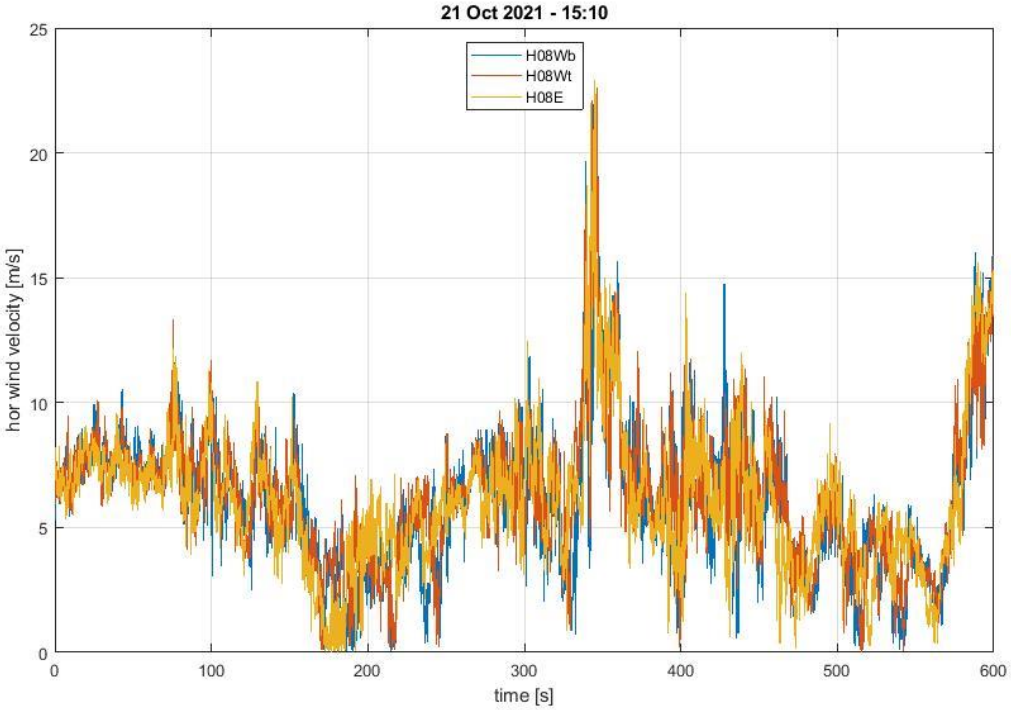

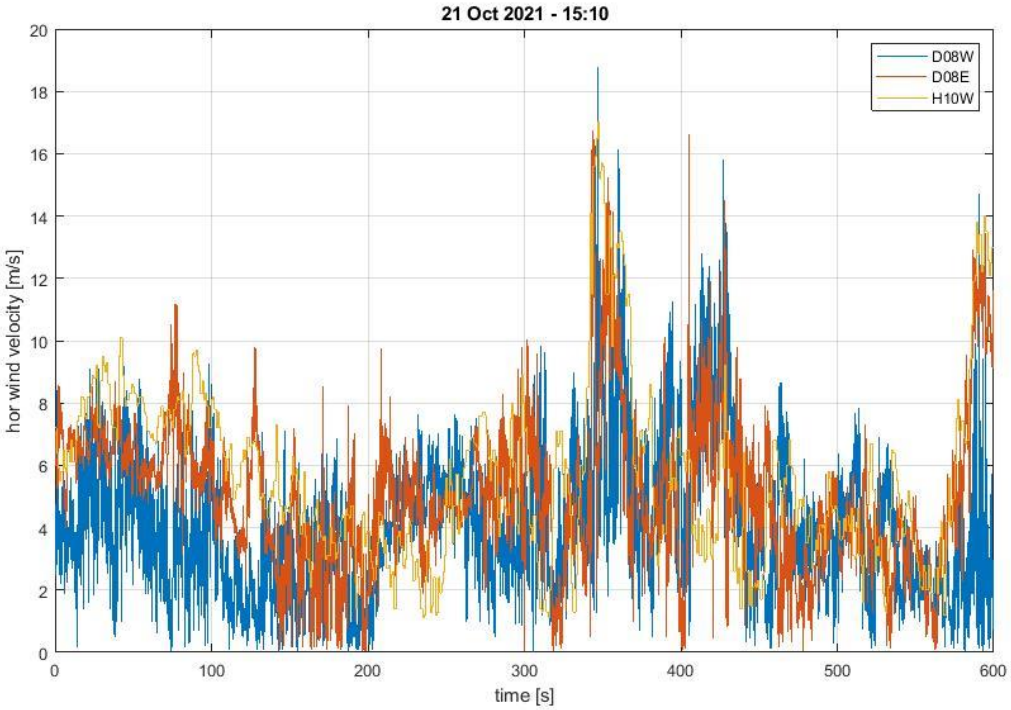

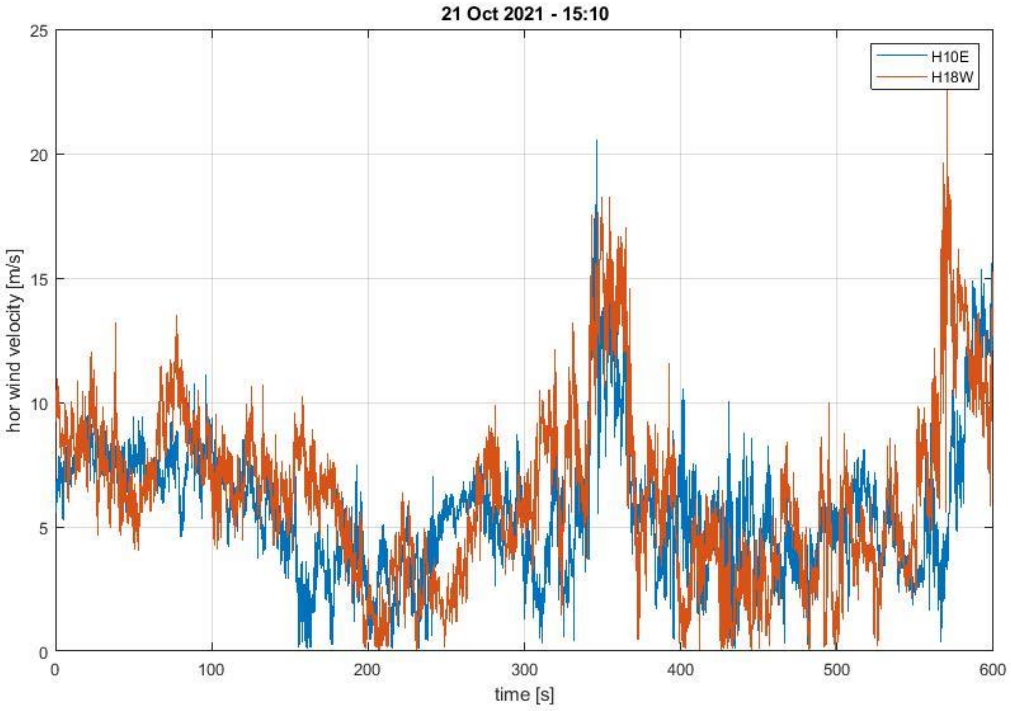
21 Oct 2021 - 15:10
H10E
H18W
hor wind velocity [m/s]
time [s]
0
5
10
15
20
25
0
100
200
300
400
500
600

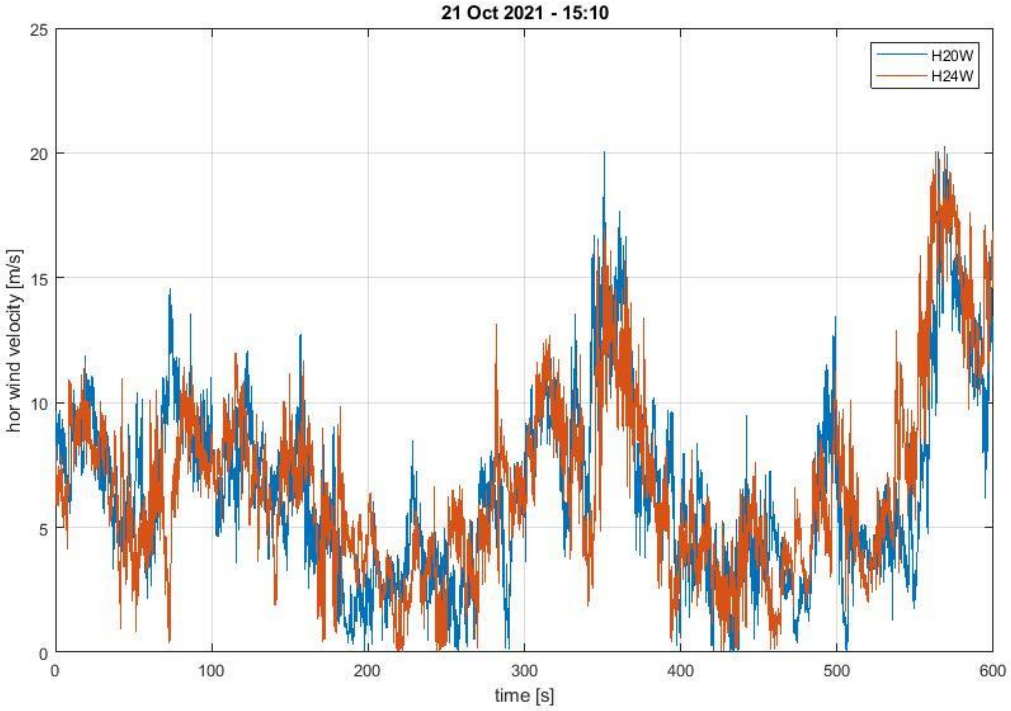
21 Oct 2021 - 15:10
H20W
H24W
hor wind velocity [m/s]
time [s]
0
5
10
15
20
25
0
100
200
300
400
500
600

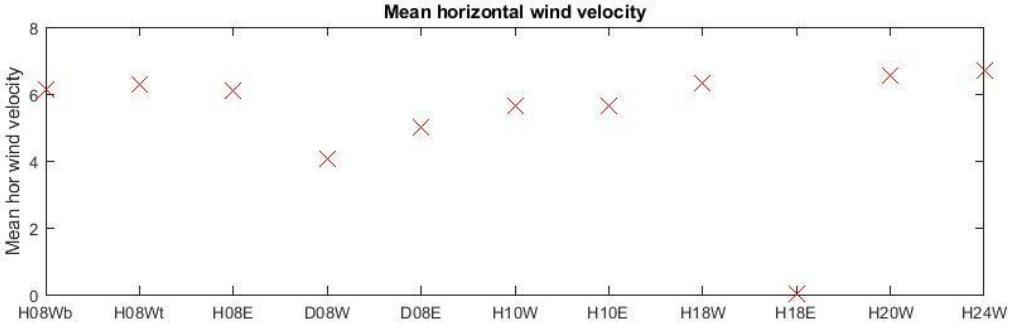
Mean horizontal wind velocity
Mean hor wind velocity
0
2
4
6
8
H08Wb
H08Wt
H08E
D08W
D08E
H10W
H10E
H18W
H18E
H20W
H24W

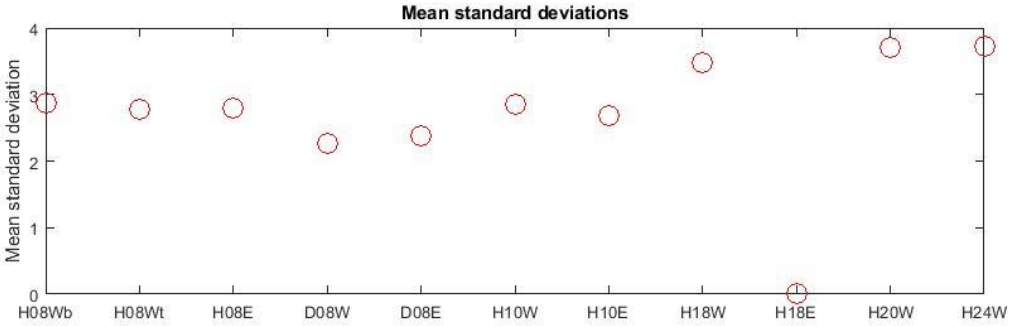
Mean standard deviations
Mean standard deviation
0
1
2
3
4
H08Wb
H08Wt
H08E
D08W
D08E
H10W
H10E
H18W
H18E
H20W
H24W

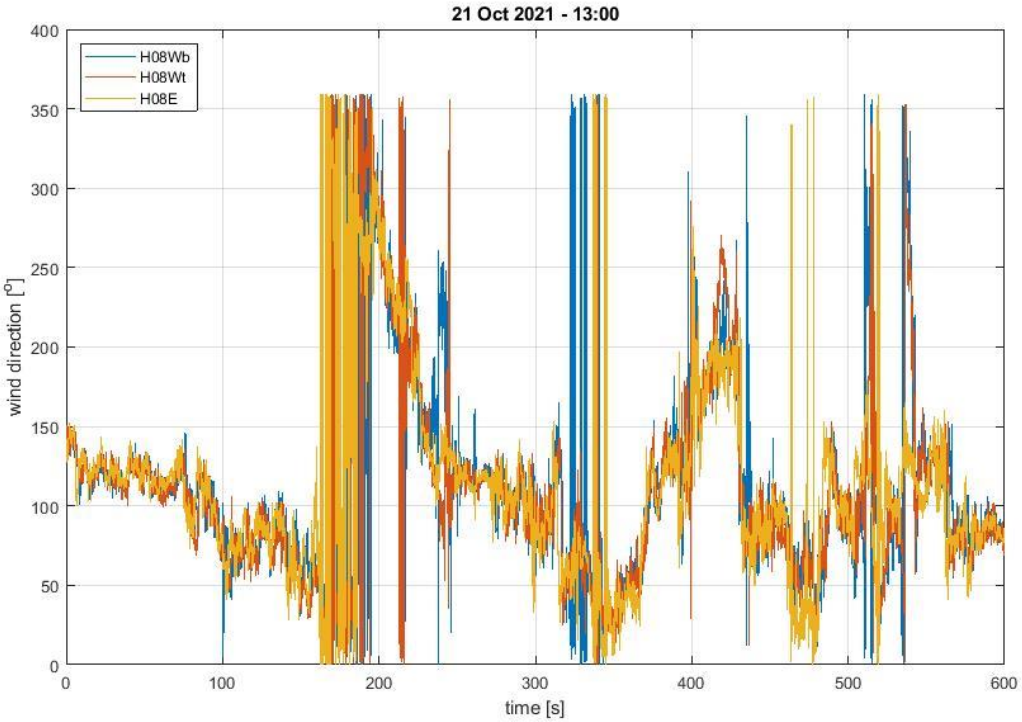
21 Oct 2021 - 13:00
H08Wb
H08Wt
H08E
wind direction [°]
0
50
100
150
200
250
300
350
400
0
100
200
300
400
500
600
time [s]

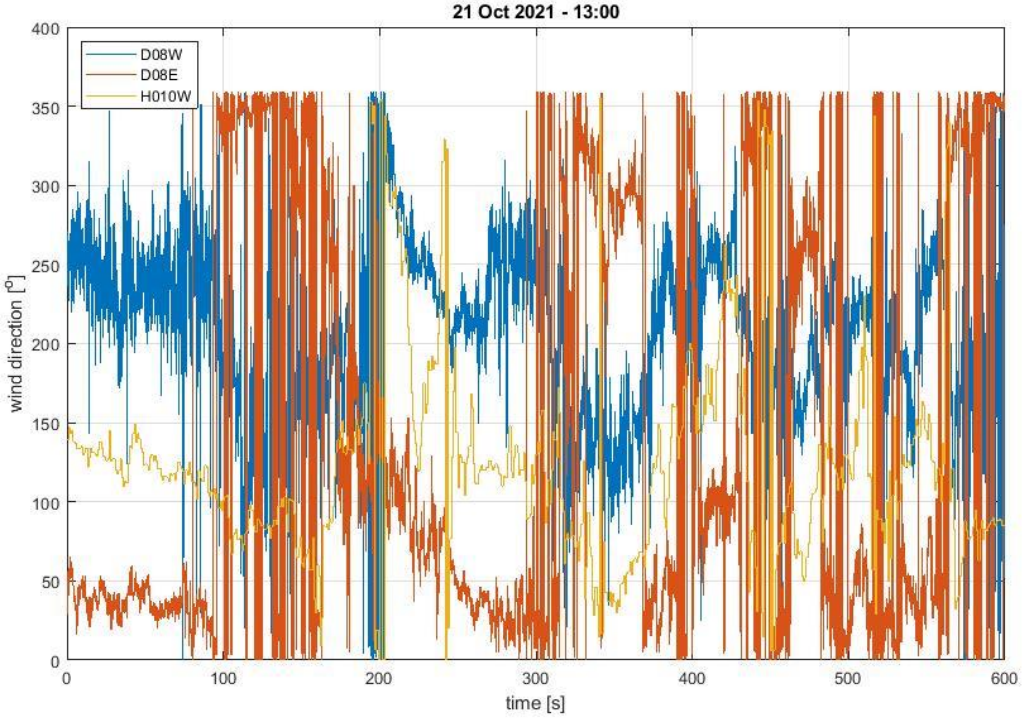
21 Oct 2021 - 13:00
D08W
D08E
H010W
wind direction [°]
time [s]
0
50
100
150
200
250
300
350
400
0
100
200
300
400
500
600

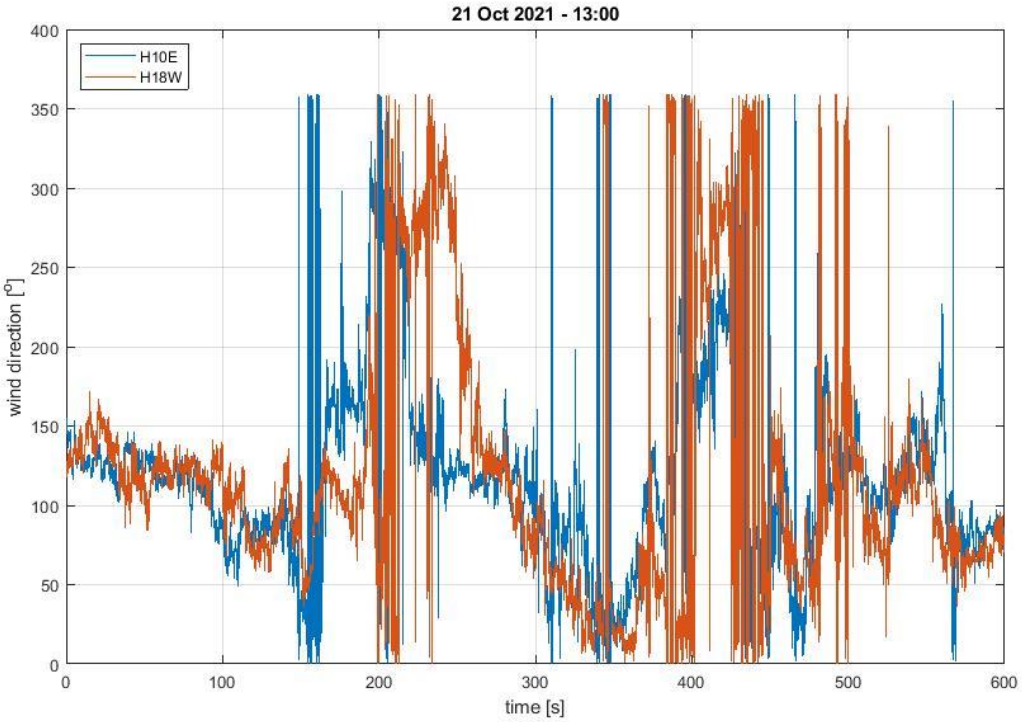
21 Oct 2021 - 13:00
H10E
H18W
wind direction [°]
time [s]
0
50
100
150
200
250
300
350
400
0
100
200
300
400
500
600

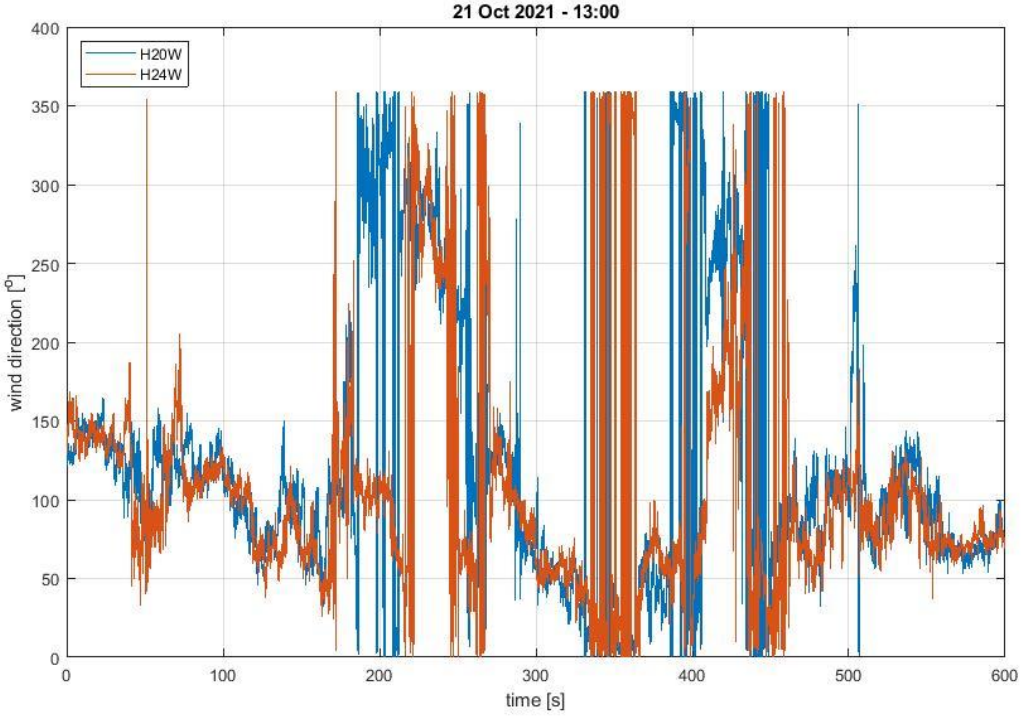
21 Oct 2021 - 13:00
H20W
H24W
wind direction [°]
time [s]
0
50
100
150
200
250
300
350
400
0
100
200
300
400
500
600

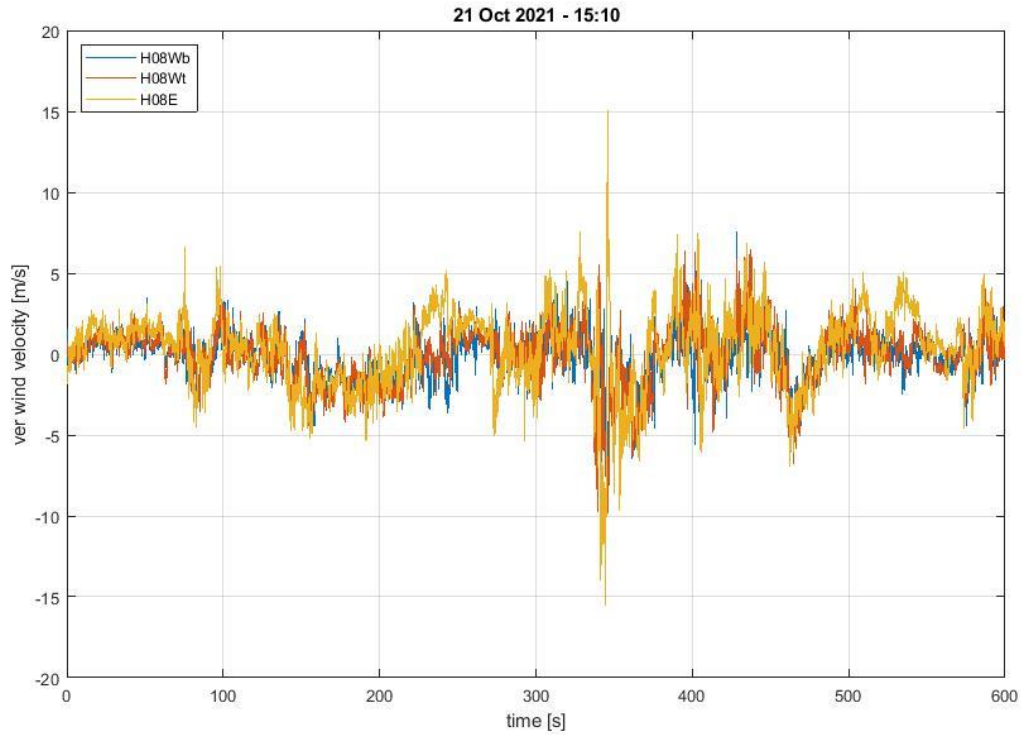
21 Oct 2021 - 15:10
H08Wb
H08Wt
H08E
ver wind velocity [m/s]
time [s]
-20
-15
-10
-5
0
5
10
15
20
0
100
200
300
400
500
600

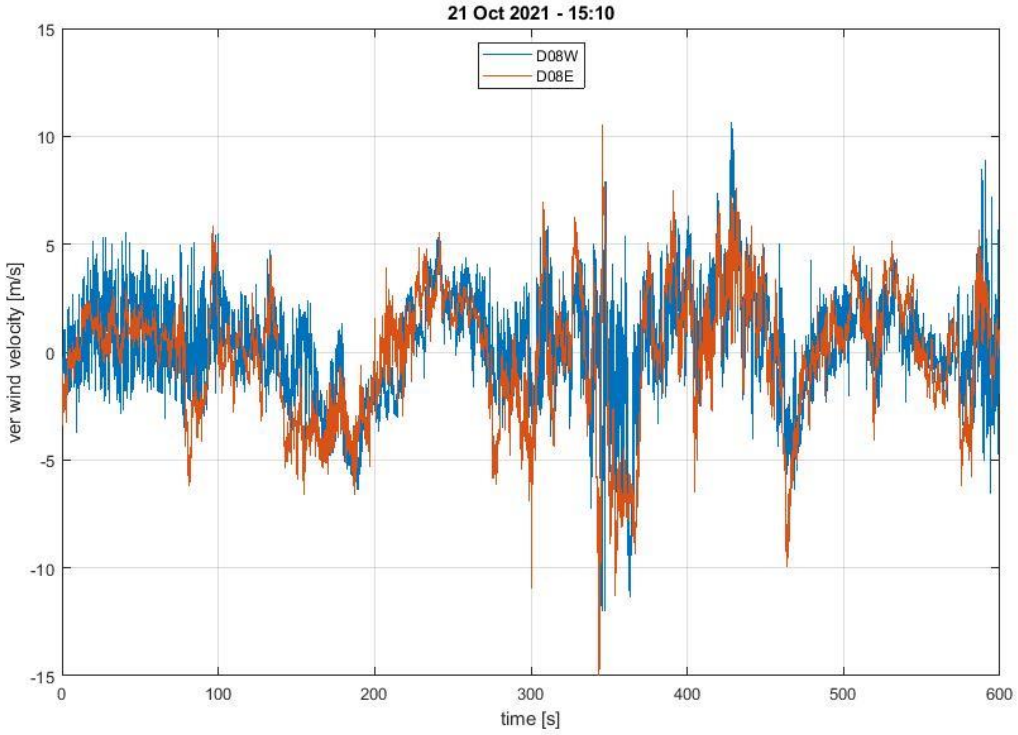
21 Oct 2021 - 15:10
D08W
D08E
ver wind velocity [m/s]
time [s]
15
10
5
0
-5
-10
-15
0
100
200
300
400
500
600

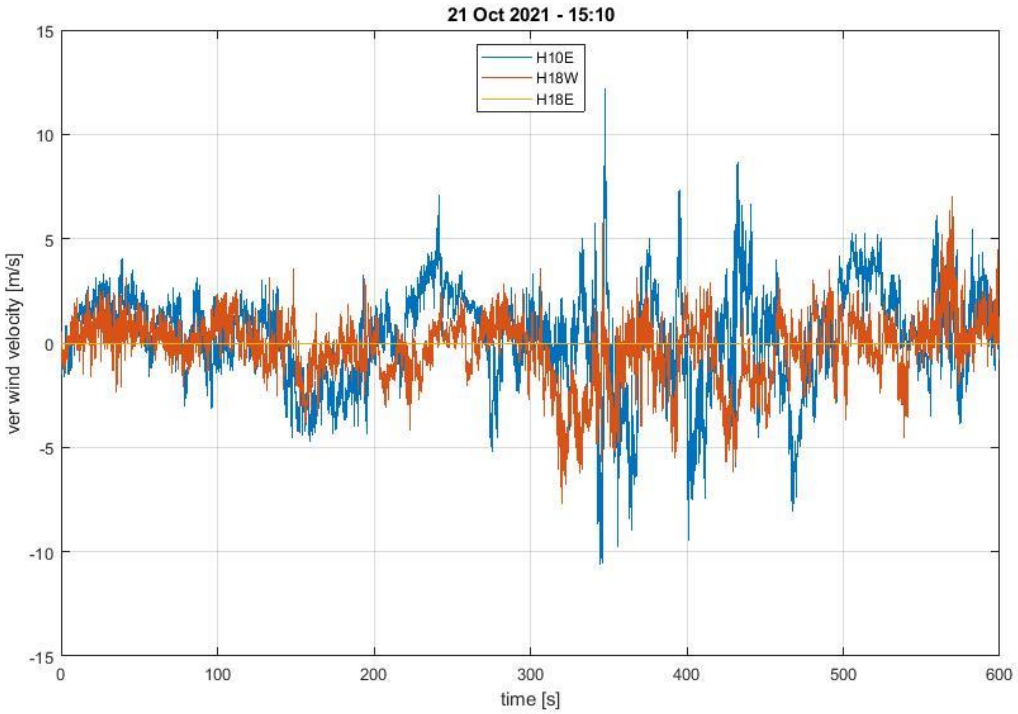
21 Oct 2021 - 15:10
H10E
H18W
H18E
ver wind velocity [m/s]
time [s]
15
10
5
0
-5
-10
-15
0
100
200
300
400
500
600

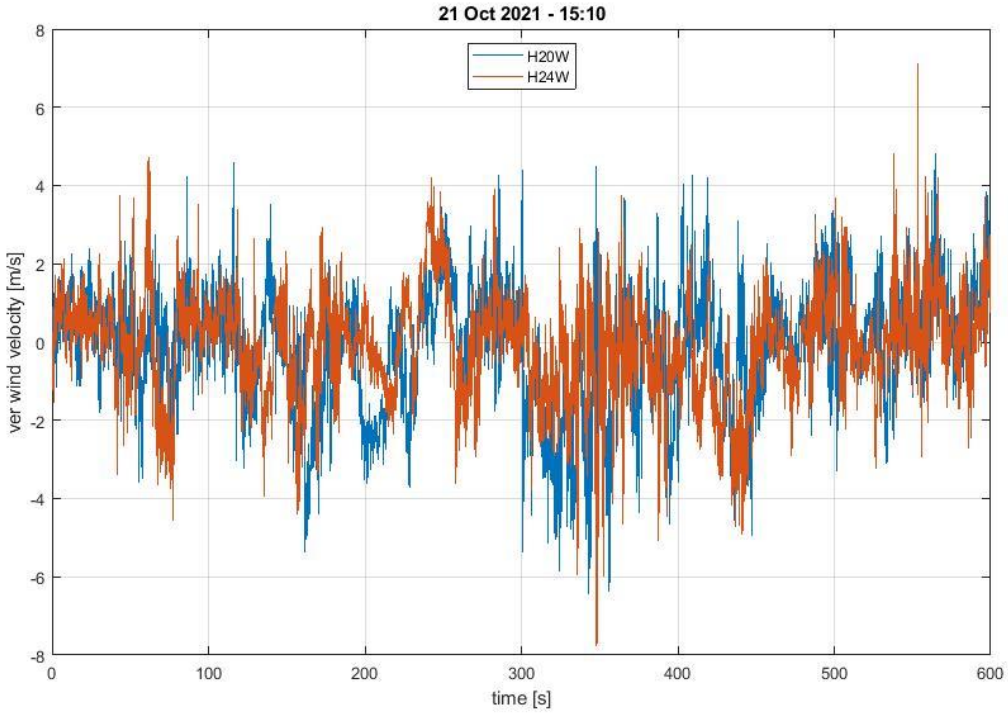
21 Oct 2021 - 15:10
H20W
H24W
ver wind velocity [m/s]
time [s]

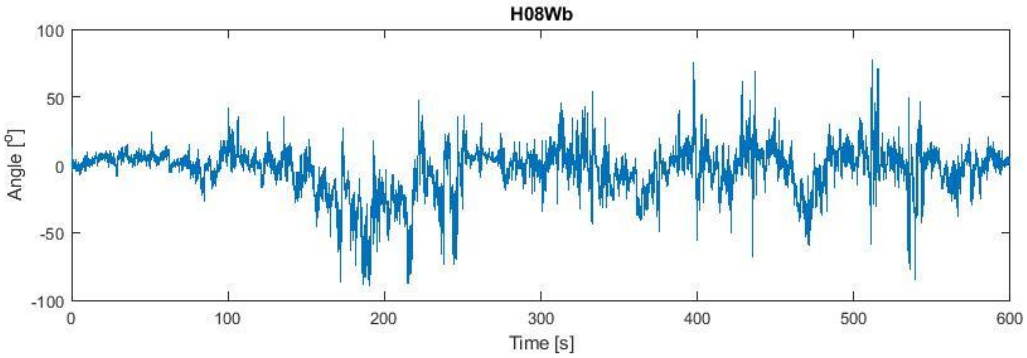
H08Wb
Angle [°]
Time [s]

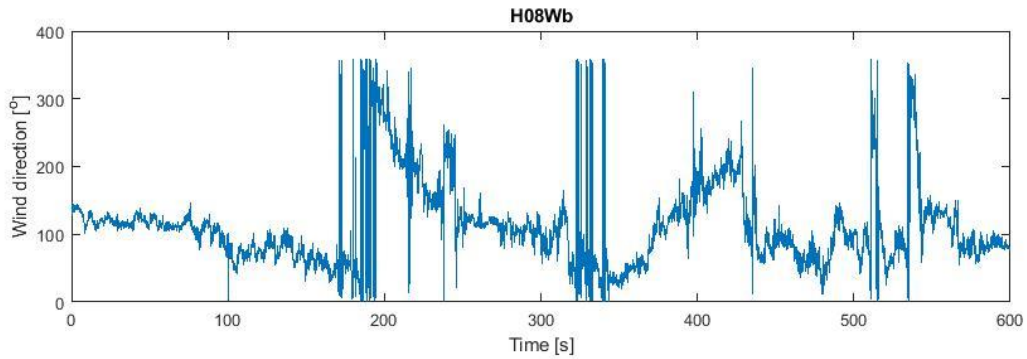
H08Wb
Wind direction [°]
Time [s]

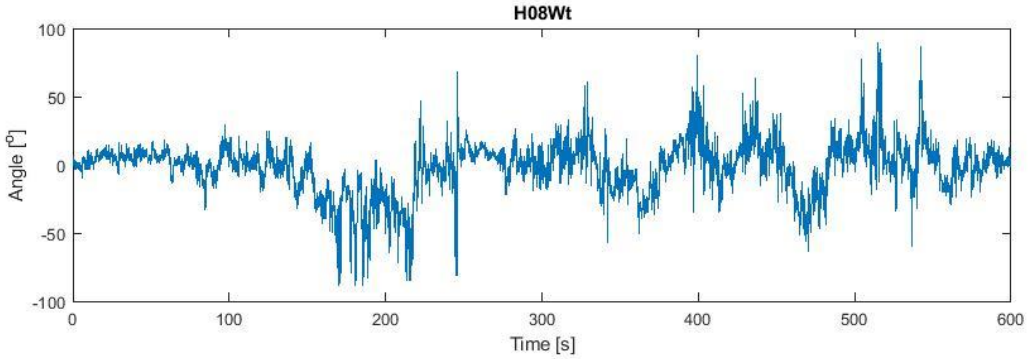
H08Wt
Angle [°]
Time [s]

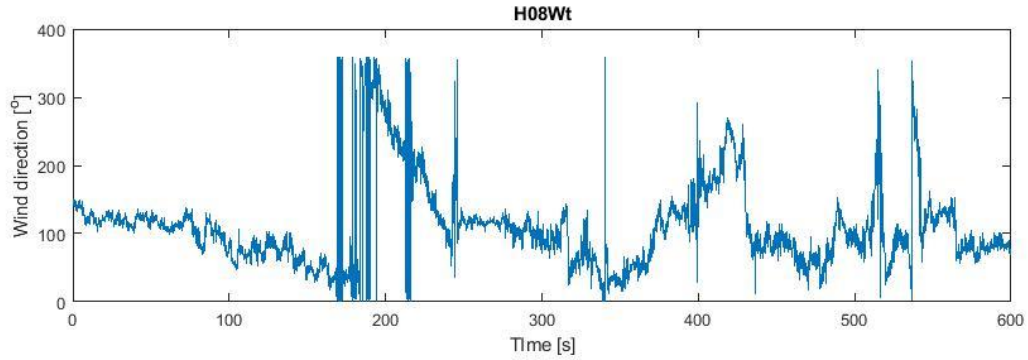
H08Wt
Wind direction [°]
TIme [s]

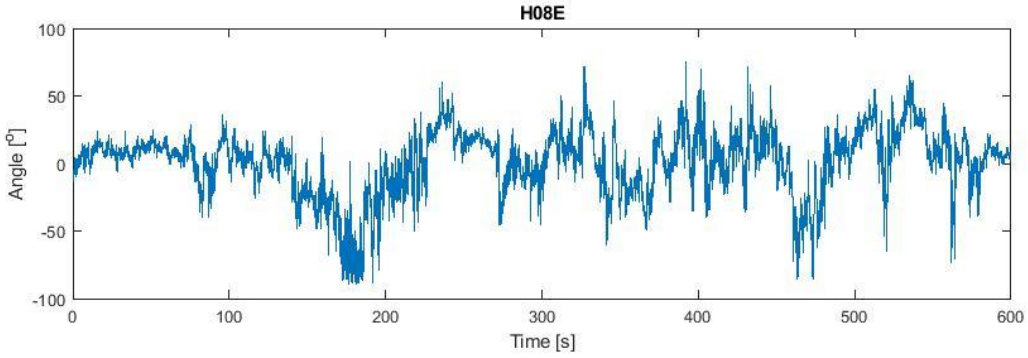
H08E
Angle [°]
Time [s]

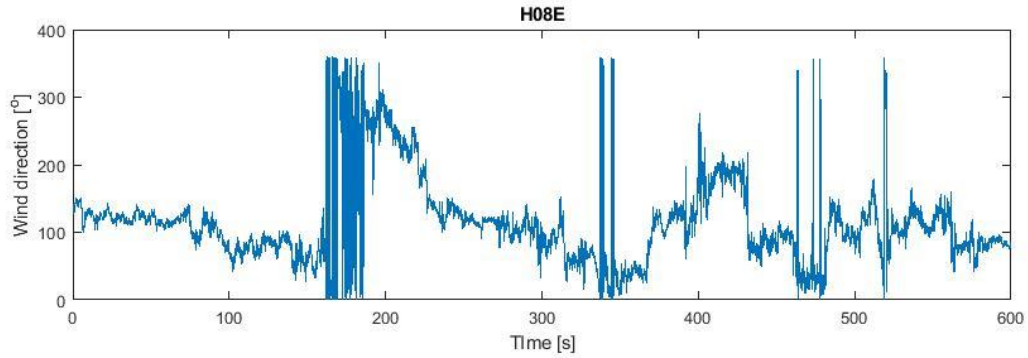
H08E
Wind direction [°]
TIme [s]

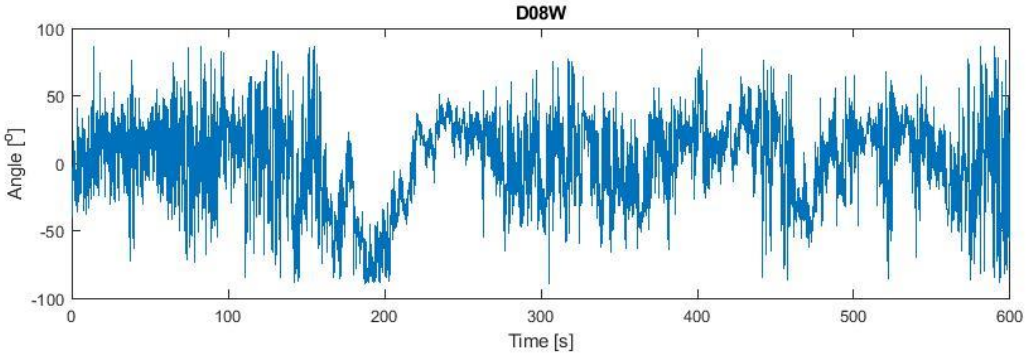
D08W
Angle [°]
Time [s]

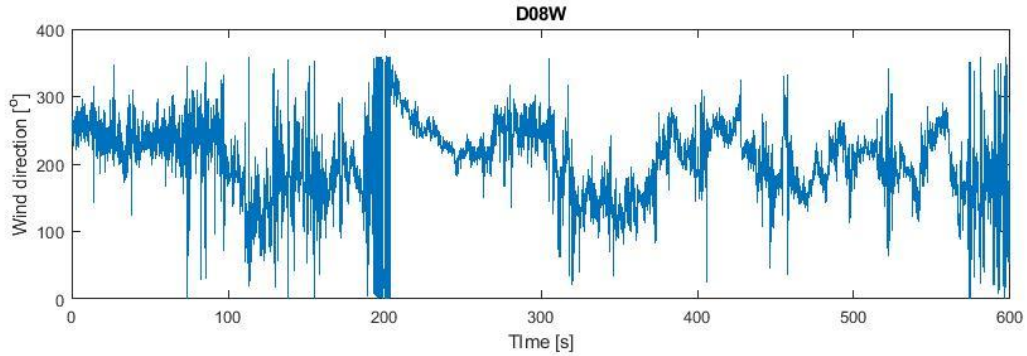
D08W
Wind direction [°]
TIme [s]

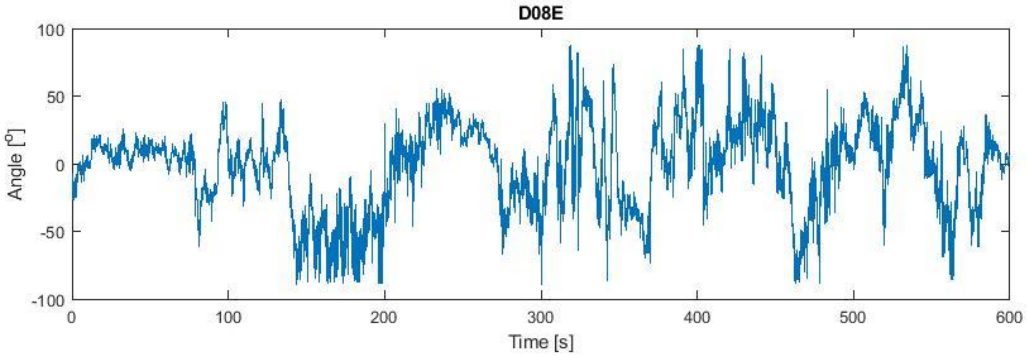
D08E
Angle [°]
Time [s]

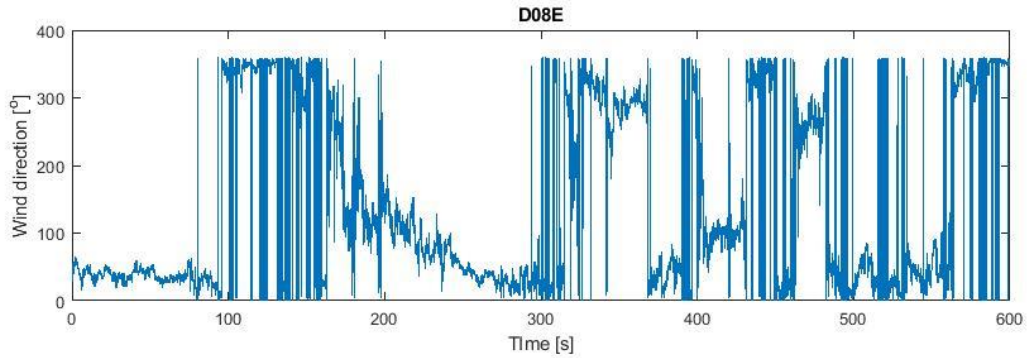
D08E
Wind direction [°]
TIme [s]

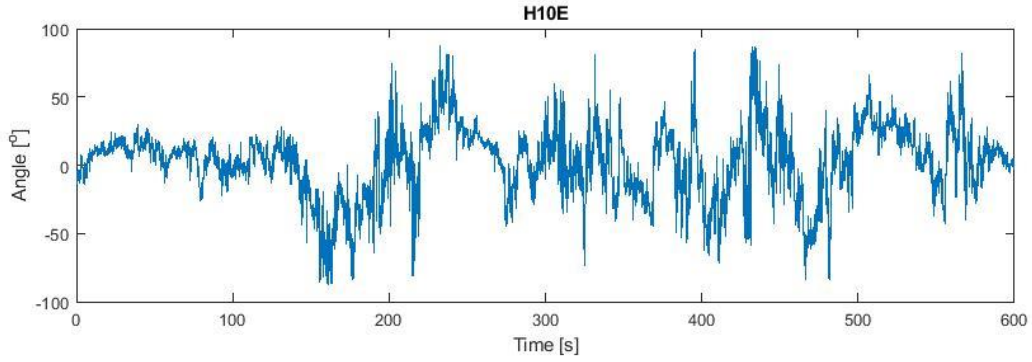
H10E
Angle [°]
Time [s]

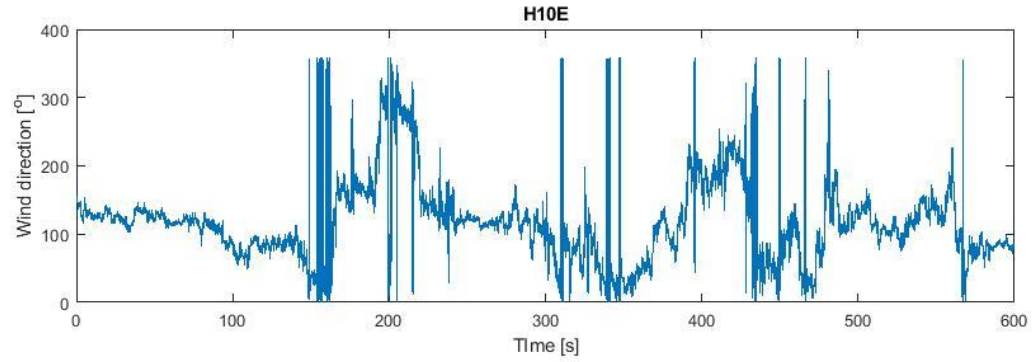
H10E
Wind direction [°]
Time [s]

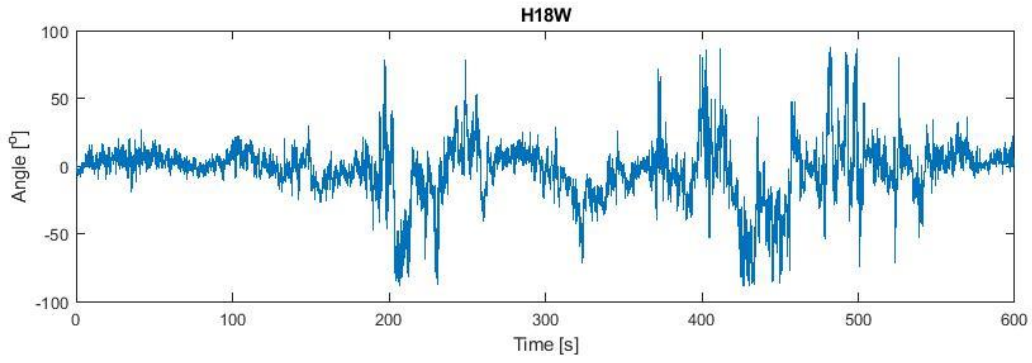
H18W
Angle [°]
Time [s]

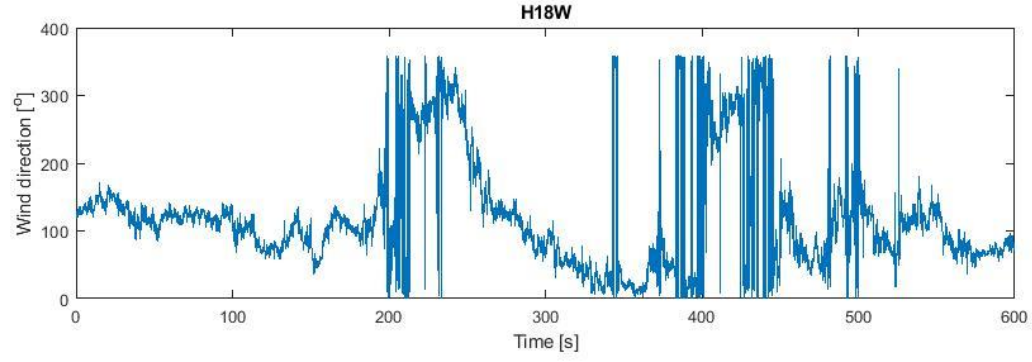
H18W
Wind direction [°]
Time [s]

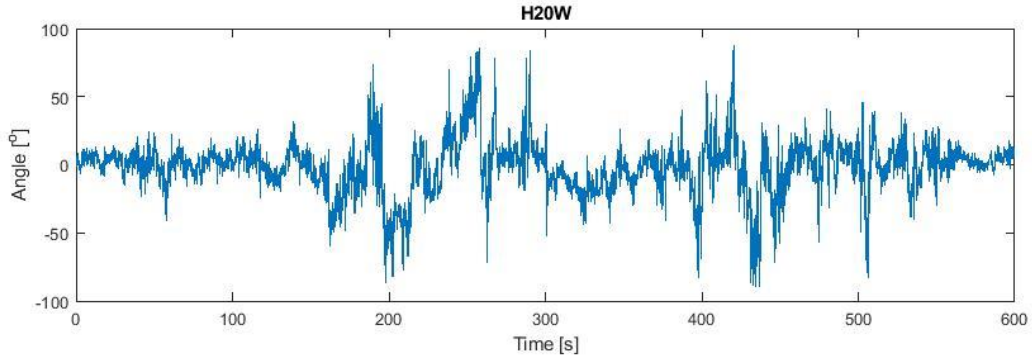
H20W
Angle [°]
Time [s]

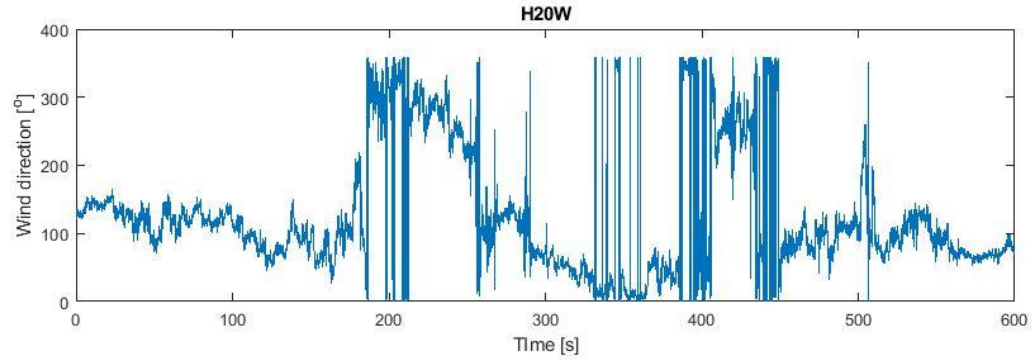
H20W
Wind direction [°]
TIme [s]

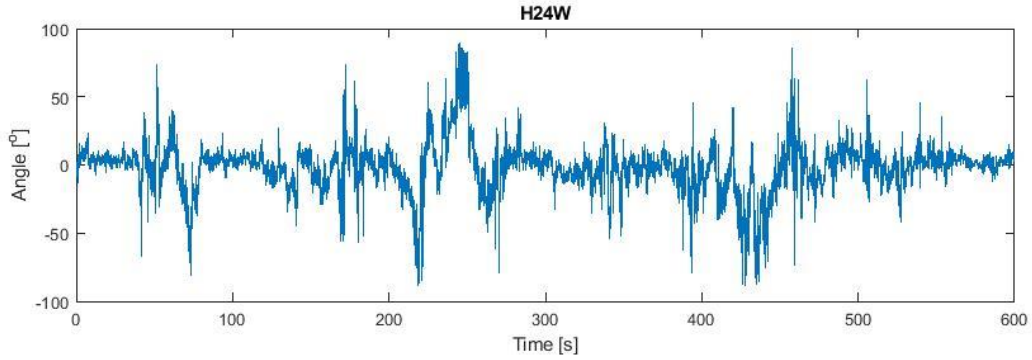
H24W
Angle [°]
Time [s]

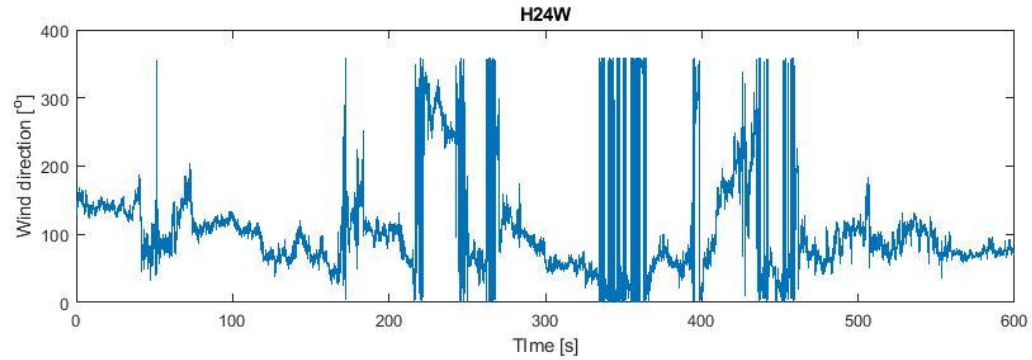
H24W
Wind direction [°]
TIme [s]